Density Functional Molecular Study on the Full Conformational Space of the *S*-4-(2-Hydroxypropoxy)carbazol Fragment of Carvedilol (1-(9H−Carbazol-4-yloxy)-3-[2-(2-methoxyphenoxy)ethylamino]-2-propanol) in Vacuum and in Different Solvent Media

David R. P. Almeida,*,† Luca F. Pisterzi,† Gregory A. Chass,‡ Ladislaus L. Torday,§ Andras Varro,§ Julius Gy. Papp,§,∥ and Imre G. Csizmadia†

Department of Chemistry, Lash Miller Laboratories, 80 St. George Street, University of Toronto, Toronto, Ontario, Canada M5S 3H6, Velocet Communications Inc., 210 Dundas St. West, Suite 810, Toronto, Ontario, Canada M5G 2E8, and Department of Pharmacology and Pharmacotherapy and Division of Cardiovascular Pharmacology (Hungarian Academy of Sciences and Szeged University), Szeged University, Dom ter12, Szeged, Hungary-6701

Received: May 21, 2002; In Final Form: August 2, 2002

Density functional theory (DFT) conformational analysis was carried out on the potential energy hypersurface (PEHS) of the carbazole-containing molecular fragment, *S*-4-(2-hydroxypropoxy)-carbazol, of the chiral cardiovascular drug molecule carvedilol, (1-(9H-carbazol-4-yloxy)-3-[2-(2-methoxyphenoxy)ethylamino]-2-propanol). The PEHS was computed in vacuum, chloroform, ethanol, DMSO, and water at the B3LYP/6-31G(d) level of theory. The carbazole ring system was confirmed to be planar, and the resultant PEHS in vacuum contained 19 converged minima, of which the global minima possessed a conformation with χ_1, χ_2, and χ_3 in the anti position and χ_{10} in the g position. Conformer stability for the *S*-4-(2-hydroxypropoxy)carbazol PEHS was influenced by intramolecular hydrogen bonding. Tomasi PCM reaction-field calculations revealed that the lowest SCF energies, relative conformer energies, and solvation free energies ($\Delta G^{solvation}$) for the *S*-4-(2-hydroxypropoxy)carbazol PEHS were in protic solvents, ethanol and water, because of the larger hydrogen bond donor values of these solvents, which aid in stabilization of the dipole moment created by the carbazole ring system and the oxygen and nitrogen atoms. However, solvent effects contributed most significantly to the stabilization of *S*-4-(2-hydroxypropoxy)carbazol conformers that contained no internal hydrogen bonding, whereas solvent effects were not as important for conformers that contained intramolecular hydrogen bonding.

1. Introduction

1.1. Biological Background. Carvedilol ($C_{24}H_{26}N_2O_4$) is a cardiovascular drug of proven efficiency in the treatment of mild-to-moderate congestive heart failure (CHF), essential hypertension, angina, and in the improvement of left ventricular function. Carvedilol is a lipophilic autonomic nervous system agent that acts as a multiple-action neurohormonal antagonist by producing nonselective beta blockage (β_1 and β_2) and selective alpha blockage (α_1) while also possessing myocardial-protective antioxidant properties.[1,2]

In dealing with chronic heart failure, angina, and hypertension, beta blockers block the activity of cardiac β-adrenergic receptors (both β_1 and β_2) to noradrenaline (NA), reducing cardiac output and oxygen consumption and therefore the total cardiac workload of the heart.[3,4] Carvedilol provides further positive effects by vasodilation (α_1-adrenergic blockage) at peripheral resistance vessels, which decreases preload and afterload, thereby further reducing cardiac work and wall tensions.[5] The U.S. Data and Safety Monitoring Board stopped, for ethical reasons, the clinical investigations of carvedilol before its completion because of greatly lowered mortality rates.[6,7]

A wide variety of different techniques and studies have indicated that the antioxidant activities of carvedilol reside in the carbazole moiety, which allows carvedilol to protect the myocardium and has an antiproliferative effect on intimal tissue, thereby reducing the major risk factor for stroke by cerebroprotection.[8−11] Carvedilol further provides protection against oxygen-containing free radicals generated during cerebral ischemia and stroke. Carvedilol appears to protect vascular function by scavenging these free radicals and protecting against free-radical-induced endothelial dysfunction. It is these reactive radicals that are implicated in the process of programmed cardiac cell death (apoptosis).[12] Moreover, oxygen-containing free radicals are believed to produce damage to many cellular elements such as lipids (for example, LDL particles), proteins, and nucleic acids. In comparison with other organs of the body, the nervous system may be especially vulnerable to oxygen-containing free radicals. The central nervous system (CNS) has a high rate of oxidative metabolic activity and high concentrations of readily oxidizable substrates. Also stemming from this antioxidant property, carvedilol may also prevent the development of nitrate tolerance in patients receiving continuous nitrate therapy.[7,13,14]

1.2. Chemical Background. Carvedilol, (1-(9H-carbazol-4-yloxy)-3-[2-(2-methoxyphenoxy)ethylamino]-2-propanol), is a chiral drug molecule commercially available as a racemic mixture of both its enantiomers (R[+] and S[−]). However,

* Corresponding author. E-mail: dalmeida@medscape.com.
† University of Toronto.
‡ Velocet Communications Inc.
§ Department of Pharmacology and Pharmacotherapy, Szeged University.
∥ Division of Cardiovascular Pharmacology, Hungarian Academy of Sciences and Szeged University.

10.1021/jp021253c CCC: $22.00
Published on Web 09/28/2002

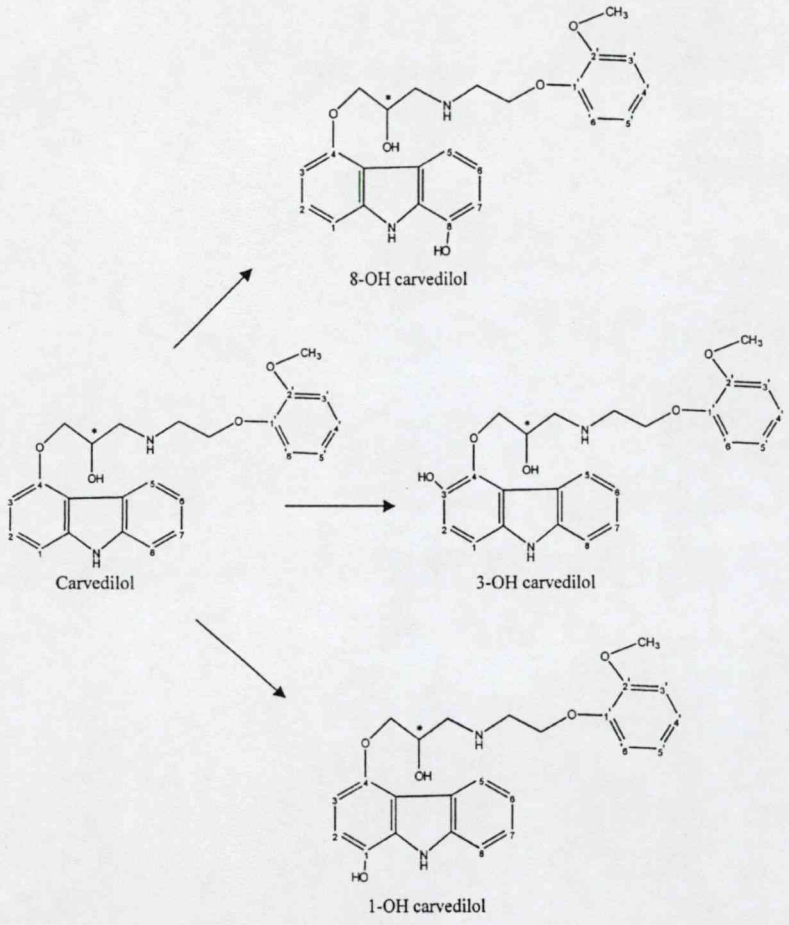

Figure 1. Structure of carvedilol and its antioxidant-marked metabolites. Note that the numbering used is by IUPAC convention (* indicates stereocenter).

the enantiomers of carvedilol show marked stereoselective properties. Both enantiomers have equal α_1 blocking activity and antioxidant activity, but only the S[−] enantiomer contains the nonselective β-adrenergic blocking activity.[10] This represents an unusual situation in which enantiomers of an optically active drug differ not only quantitatively in terms of potency but also qualitatively in that they possess distinct pharmacologic profiles.[15] As such, neither enantiomer alone has the same pharmacologic profile as the racemic mixture of carvedilol used clinically. This phenomena occurs even though the *R*- and *S*-4-(2-hydroxypropoxy)carbazol fragments of carvedilol contain enantiomeric PEHS.

Carvedilol, which is metabolized in the liver, produces antioxidant metabolites devoid of either α_1- or β-adrenergic blocking activity.[16,17] The antioxidant effect is due to the high reaction rates that the carbazole ring undergoes with hydroxyl and peroxide radicals. Carbazole's low redox potential gives carvedilol and its metabolites a powerful tendency to donate electrons more readily in order to "scavenge" the activities of oxygen-containing free radicals (electrons move spontaneously toward oxidant species with more positive redox potentials). However, the striking inhibitory effect of carbazole cannot be explained solely by its radical scavenging ability because its relatively high lipid solubility also provides antioxidant effects against lipid peroxidation.[18] Along with carvedilol, at least one of its three hydroxylated metabolites (cf. Figure 1) is known to have antioxidant properties that inhibit oxidation reactions promoted by the oxygen superoxide ion (O_2^-), hydrogen peroxide (H_2O_2), the hydroxyl radical (•OH), and peroxynitrite ($ONOO^-$) and therefore helps to protect the living body from the deleterious effects of free-radical damage.[19] Carvedilol's metabolites are more effective than vitamin E and in certain experimental setups are more effective than carvedilol itself.[7,12,20,21] The latter is due to the fact that a substitution by a hydroxyl group in a heterocyclic ring such as that of carbazole increases the molecular antioxidant action of that compound.[22]

2. Scope

Carvedilol was divided into three structural fragments according to its chemical activity: *R*- and *S*-4-(2-hydroxypropoxy)carbazol (fragment A) is the antioxidant and β-blocker portion of carvedilol (this analogue structure is similar to β blockers such as propranolol); *R*- and *S*-*N*-ethoxypropane-2-ol (fragment B), which connects the two ether oxygen of carvedilol; and aminoethoxy-2-methoxybenzene (fragment C), which is the chemical structure responsible for the α-blocker action of carvedilol (cf. Figure 2). This chemical fragmentation allows for a progressive study of carvedilol's complete conformational profile.

The objective of this computational study was to analyze the conformational character of *S*-4-(2-hydroxypropoxy)carbazol in different media (cf. Figure 3). A PEHS was first computed in vacuum with a dielectric constant (ϵ) of zero, and the PEHS converged conformers were then evaluated in subsequent protic and aprotic solvent media with higher dielectric constants: chloroform ($CHCl_3$, $\epsilon = 4.9$), ethanol (CH_3CH_2OH, $\epsilon = 24.55$), dimethyl sulfoxide (DMSO, $\epsilon = 46.7$), and water (H_2O, $\epsilon =$

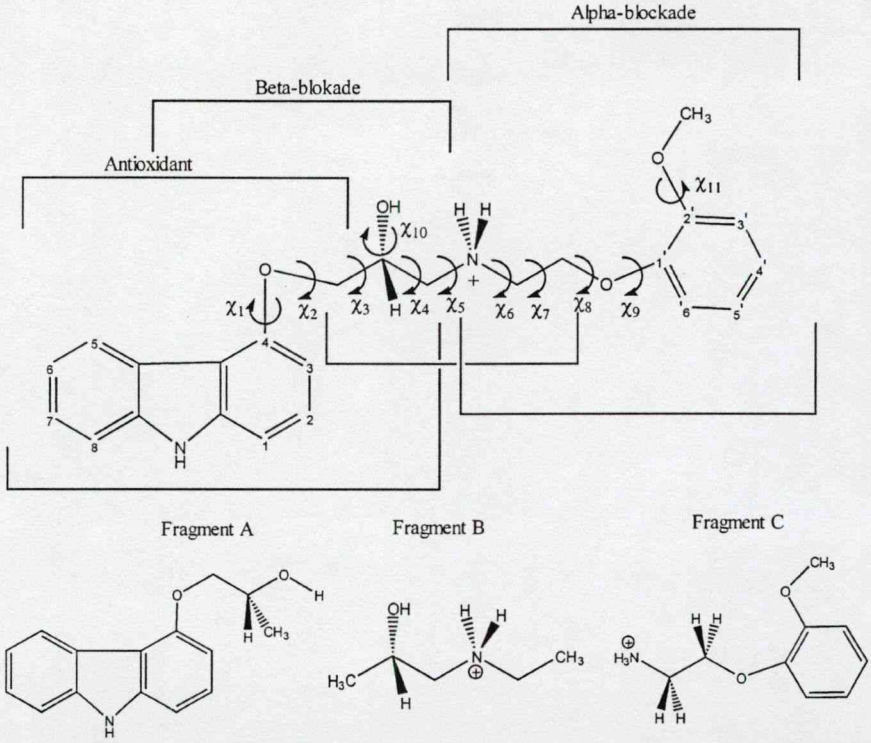

Figure 2. Complete molecular structure and function of *N*-protonated carvedilol indicating all 11 torsional angles (top) and its three characteristic fragments (A, B, and C).

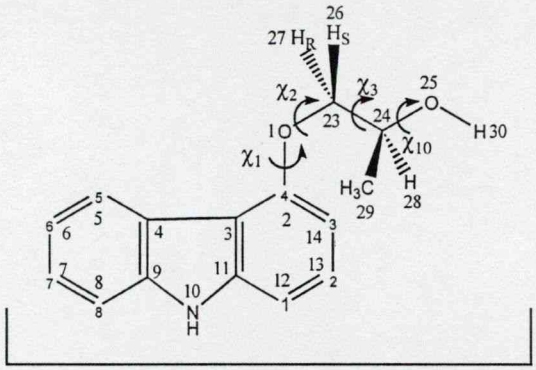

(*S*)-4-(2-hydroxypropoxy)carbazol

$\chi_1 = C^{23}-O^1-C^2-C^3$ $\chi_3 = C^{29}-C^{24}-C^{23}-O^1$

$\chi_2 = C^{24}-C^{23}-O^1-C^2$ $\chi_{10} = H^{30}-O^{25}-C^{24}-C^{23}$

Figure 3. Numbering and definition of torsional angles for *S*-4-(2-hydroxypropoxy)carbazol. Numbers placed on atoms indicate the IUPAC numbering system, and numbers placed beside atoms indicate the numbering used as *z*-matrix input for Gaussian 98.

78.39). *S*-4-(2-Hydroxypropoxy)carbazol contains a stereocenter (located at C24) with each of the *R*- and *S*-4-(2-hydroxypropoxy)carbazol enantiomers constituting the PEHS with torsional angles χ_1, χ_2, χ_3, and χ_{10} as such:

$$E_S = E_R$$

$$f_S(\chi_1, \chi_2, \chi_3, \chi_{10}) = f_R(-\chi_1, -\chi_2, -\chi_3, -\chi_{10}) \quad (1)$$

However, only the S enantiomer was studied in this work. Initially, 4-hydroxy carbazol was used to study the orientation of the hydroxyl group as well as the planarity of the carbazole ring structure.

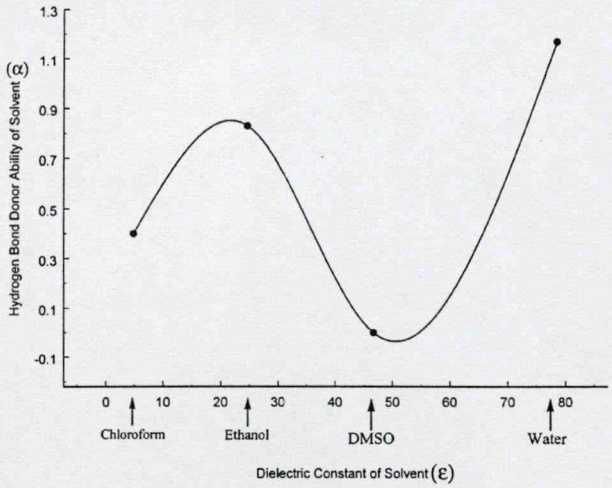

Figure 4. Hydrogen bond donor ability of the solvent (α) as a function of the dielectric constant (ε) according to the Abraham−Kamlet−Taff scale for the different solvent media in which the *S*-4-(2-hydroxypropoxy)carbazol was computed.

TABLE 1: Solvent Description According to the Dielectric Constant (ε) and Abraham−Kamlet−Taff Scale[a]

solvent	ε	π*	α	β
chloroform	4.9	0.58	0.4	0.00
ethanol	24.55	0.54	0.83	0.8
DMSO	46.7	1.00	0.00	0.76
water	78.39	1.09	1.17	0.2

[a] π* describes the index of dipolarity/polarizability, α describes the hydrogen bond donor ability, and β describes the hydrogen bond acceptor ability.[23,24]

Conformations of *S*-4-(2-hydroxypropoxy)carbazol are written in the form $\chi_1[\chi_2\,\chi_3]\chi_{10}$, for example, g+[g+g+]g+. Conformations are presented in this manner because of the fact that χ_1

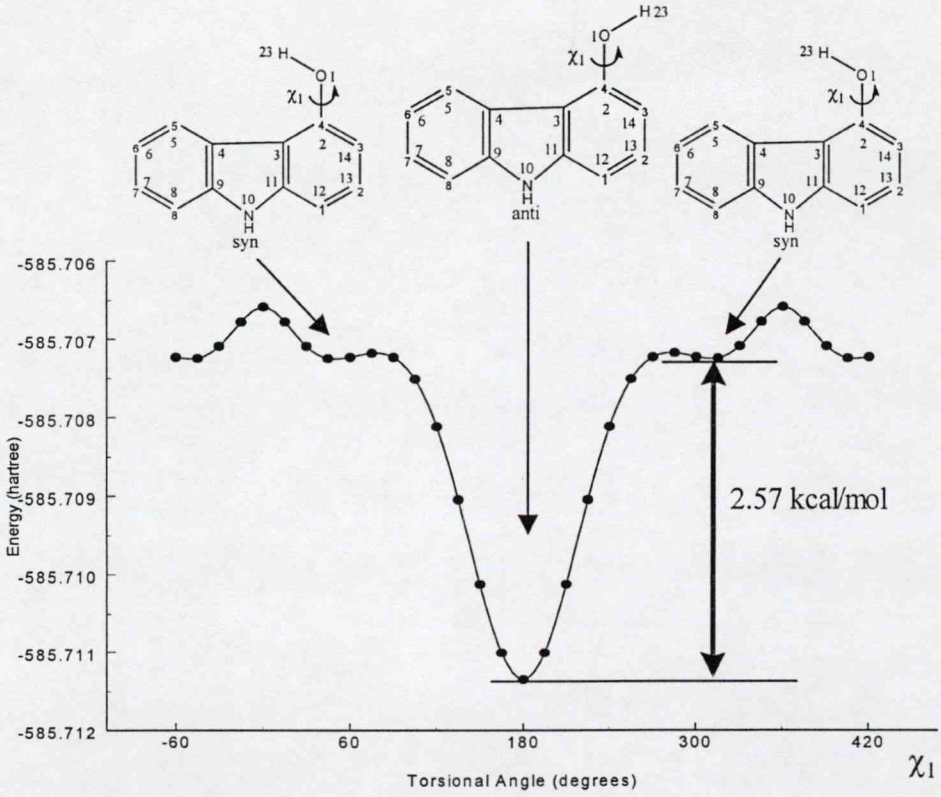

Figure 5. Conformational PEC for torsional angle χ_1 of 4-hydroxycarbazol computed at the RHF/3-21G level of theory.

and χ_{10} represent the torsional angles responsible for the activity of the carvedilol fragment, such as hydrogen bonding, whereas torsional angles χ_2 and χ_3 are responsible for the backbone orientation of *S*-4-(2-hydroxypropoxy)carbazol. Furthermore, each conformer was given a numeric code from 1 to 19, as shown in Table 4, for identification. Torsional angle χ_4, which is associated with the terminal methyl group, was not included because it comprises a symmetrical methyl rotation.

The four different solvents computed can be described according to dielectric constants and the Abraham−Kamlet−Taff scale (cf. Table 1). The Abraham−Kamlet−Taff scale equation (eq 2), first derived by Koppel and Palm, is a multiparametric approach and represents a linear solvation energy relationship (LSER).[23−25]

$$A = A_o + s(\pi^* + d\delta) + a\alpha + b\beta \qquad (2)$$

In the equation, A is the log of the rate or equilibrium constant (A_o is the same as the latter but in the reference solvent cyclohexane), π^* is the index of dipolarity/polarizability (often proportional to the dipole moment), δ is the polarizability correction, α is the hydrogen bond donor ability of the solvent, and β is the hydrogen bond acceptor ability of the solvent.[25]

Of interest to the carvedilol fragment is the ability of the solvent to be a hydrogen bond donor (α). It would be expected that protic solvents with hydrogen bond donor abilities would stabilize *S*-4-(2-hydroxypropoxy)carbazol by hydrogen bonding with the different oxygen and nitrogen atoms of the carvedilol fragment. In Figure 4, the dielectric constant (ϵ) is plotted against the ability of a solvent to be a hydrogen bond donor (α), and the resulting graph shows two peaks indicating the protic solvents ethanol and water, which have significant hydrogen bond donor abilities.

With regards to modeling the environment of *S*-4-(2-hydroxypropoxy)carbazol, one can make the analogy that hydrophobic environments such as cell membranes can be modeled with solvents with low dielectric constants, and hydrophilic environments, with solvents with high dielectric constants. On the basis of the latter, one aprotic (chloroform) and one protic (ethanol) solvent with low dielectric constants were computed along with one aprotic (DMSO) and one protic (water) solvent with high dielectric constants to further differentiate solvent−solute attributes.

3. Computational Method

S-4-(2-Hydroxypropoxy)carbazol was exclusively defined using the Gaussian 98 *z*-matrix internal coordinate system to define molecular structure, stereochemistry, and geometry.[26] Conformational assignments that yielded corresponding minima were selected and evaluated successively at the RHF/3-21G and RHF/6-31G(d) levels of theory (data not shown), and then full optimizations were carried out at the B3LYP/6-31G(d) level of theory in vacuum ($\epsilon = 0.00$). Vibrational frequency calculations were performed on all minima at the B3LYP/6-31G(d) level of theory to ensure that the optimized conformers were true minima and contained no imaginary frequencies. Potential energy curves (PEC) were calculated at the RHF/3-21G level of theory and were plotted using Axum 5.0.

The energies and solvation free energies ($\Delta G^{solvation}$) of the minima were then computed according to the polarized continuum (overlapping spheres) model (PCM) of Tomasi and coworkers with reaction-field calculations in different solvent media at the B3LYP/6-31G(d) level of theory.[27−29] Two aprotic (chloroform, DMSO) and two protic (ethanol, water) solvents were used to span a dielectric solvent range from 4.9 to 78.39 (cf. Scope). $\Delta G^{solvation}$ describes the free energy of dissolving a

TABLE 2: Optimized Minima for 4-Hydroxycarbazol

torsional angle χ_1 RHF/3-21G; B3LYP/6-31G(d) (degrees)	energy RHF/3-21G; B3LYP/6-31G(d) (hartrees)	relative energy RHF/3-21G; B3LYP/6-31G(d) (kcal mol^{-1})
49.95; 11.91	−585.707253023; −592.685596590	2.57; 1.47
−179.99; 180.00	**−585.711349552; −592.687846456**	**0.00; 0.00**
−50.03; −11.91	−585.707252997; −592.685596593	2.57; 1.47

TABLE 3: Summary of Density Functional Conformational PEHS for *S*-4-(2-Hydroxypropoxy)carbazol[a]

conformational assignment					conformational assignment					conformational assignment				
χ_1	χ_2	χ_3	χ_{10}		χ_1	χ_2	χ_3	χ_{10}		χ_1	χ_2	χ_3	χ_{10}	
g^+	g^+	g^+	g^+	**FOUND**	a	g^+	g^+	g^+	NOT FOUND	g^-	g^+	g^+	g^+	NOT FOUND
g^+	g^+	g^+	a	NOT FOUND	a	g^+	g^+	a	NOT FOUND	g^-	g^+	g^+	a	NOT FOUND
g^+	g^+	g^+	g^-	NOT FOUND	a	g^+	g^+	g^-	NOT FOUND	g^-	g^+	g^+	g^-	NOT FOUND
g^+	g^+	a	g^+	NOT FOUND	a	g^+	a	g^+	NOT FOUND	g^-	g^+	a	g^+	NOT FOUND
g^+	g^+	a	a	**FOUND**	a	g^+	a	a	**FOUND**	g^-	g^+	a	a	NOT FOUND
g^+	g^+	a	g^-	**FOUND**	a	g^+	a	g^-	**FOUND**	g^-	g^+	a	g^-	NOT FOUND
g^+	g^+	g^-	g^+	NOT FOUND	a	g^+	g^-	g^+	NOT FOUND	g^-	g^+	g^-	g^+	NOT FOUND
g^+	g^+	g^-	a	NOT FOUND	a	g^+	g^-	a	NOT FOUND	g^-	g^+	g^-	a	NOT FOUND
g^+	g^+	g^-	g^-	NOT FOUND	a	g^+	g^-	g^-	NOT FOUND	g^-	g^+	g^-	g^-	NOT FOUND
g^+	a	g^+	g^+	NOT FOUND	a	a	g^+	g^+	**FOUND**	g^-	a	g^+	g^+	**FOUND**
g^+	a	g^+	a	NOT FOUND	a	a	g^+	a	NOT FOUND	g^-	a	g^+	a	NOT FOUND
g^+	a	g^+	g^-	NOT FOUND	a	a	g^+	g^-	NOT FOUND	g^-	a	g^+	g^-	NOT FOUND
g^+	a	a	g^+	NOT FOUND	a	a	a	g^+	**FOUND**	g^-	a	a	g^+	NOT FOUND
g^+	a	a	a	NOT FOUND	a	a	a	a	NOT FOUND	g^-	a	a	a	NOT FOUND
g^+	a	a	g^-	**FOUND**	a	a	a	g^-	**FOUND**	g^-	a	a	g^-	NOT FOUND
g^+	a	g^-	g^+	NOT FOUND	a	a	g^-	g^+	**FOUND**	g^-	a	g^-	g^+	NOT FOUND
g^+	a	g^-	a	NOT FOUND	a	a	g^-	a	**FOUND**	g^-	a	g^-	a	NOT FOUND
g^+	a	g^-	g^-	NOT FOUND	a	a	g^-	g^-	**FOUND**	g^-	a	g^-	g^-	NOT FOUND
g^+	g^-	g^+	g^+	NOT FOUND	a	g^-	g^+	g^+	NOT FOUND	g^-	g^-	g^+	g^+	NOT FOUND
g^+	g^-	g^+	a	NOT FOUND	a	g^-	g^+	a	NOT FOUND	g^-	g^-	g^+	a	NOT FOUND
g^+	g^-	g^+	g^-	NOT FOUND	a	g^-	g^+	g^-	NOT FOUND	g^-	g^-	g^+	g^-	NOT FOUND
g^+	g^-	a	g^+	NOT FOUND	a	g^-	a	g^+	NOT FOUND	g^-	g^-	a	g^+	NOT FOUND
g^+	g^-	a	a	NOT FOUND	a	g^-	a	a	**FOUND (GM)**	g^-	g^-	a	a	NOT FOUND
g^+	g^-	a	g^-	NOT FOUND	a	g^-	a	g^-	NOT FOUND	g^-	g^-	a	g^-	**FOUND**
g^+	g^-	g^-	g^+	NOT FOUND	a	g^-	g^-	g^+	**FOUND**	g^-	g^-	g^-	g^+	NOT FOUND
g^+	g^-	g^-	a	NOT FOUND	a	g^-	g^-	a	**FOUND**	g^-	g^-	g^-	a	NOT FOUND
g^+	g^-	g^-	g^-	NOT FOUND	a	g^-	g^-	g^-	**FOUND**	g^-	g^-	g^-	g^-	**FOUND**

[a] **GM** = global minima.

TABLE 4: Optimized Minima for the PEHS of *S*-4-(2-Hydroxypropoxy)carbazol at the B3LYP/6-31G(d) Level of Theory in Vacuum (ϵ = 0.00)

conformational assignment										
χ_1	χ_2	χ_3	χ_{10}	code	χ_1	χ_2	χ_3	χ_{10}	E (hartrees)	rel E (kcal mol^{-1})
g^+	g^+	g^+	g^+	1	71.61	86.66	54.09	60.83	−785.829262611	5.82
g^+	a	g^+	a	2	85.32	66.14	179.21	−178.06	−785.827598267	6.86
g^+	g^-	g^+	a	3	86.84	84.20	171.19	−37.39	−785.832802691	3.60
g^+	g^-	a	a	4	83.69	−176.18	173.47	−50.51	−785.836021588	1.58
a	a	g^+	a	5	−177.94	80.97	−172.52	−168.69	−785.831134389	4.64
a	g^-	g^+	a	6	178.67	85.87	174.71	−49.02	−785.836186313	1.47
a	g^+	a	g^+	7	−177.32	176.06	65.92	50.13	−785.837144307	0.87
a	g^+	a	a	8	175.39	177.76	179.89	56.41	−785.833845516	2.94
a	**g^-**	**a**	**a**	**9**	**177.90**	**−174.47**	**178.47**	**−47.42**	**−785.838535810**	**0.00**
a	g^+	a	g^-	10	179.81	178.53	−62.41	75.42	−785.834879306	2.29
a	a	a	g^-	11	179.97	178.34	−65.51	176.80	−785.834840973	2.32
a	g^-	a	g^-	12	178.78	179.25	−66.90	−68.60	−785.834719233	2.40
a	a	g^-	a	13	−155.99	−105.18	−163.31	−167.56	−785.831784652	4.24
a	g^+	g^-	g^-	14	179.26	−81.79	−58.53	74.14	−785.833289249	3.29
a	a	g^-	g^-	15	179.66	−82.57	−62.65	175.70	−785.833158489	3.37
a	g^-	g^-	g^-	16	179.84	−82.40	−61.58	−68.66	−785.832614787	3.72
g^-	g^+	a	g^+	17	−84.52	176.61	68.94	53.44	−785.834927222	2.26
g^-	g^-	g^-	a	18	−74.55	−80.08	−166.17	−58.84	−785.830399507	5.11
g^-	g^-	g^-	g^-	19	−78.61	−85.32	−64.51	−66.57	−785.828425975	6.34

substance from vacuum and is a useful parameter when solvents are compared for a given solute.

4. Results and Discussion

4.1. Structural Analysis of the Carbazole Ring with 4-Hydroxycarbazol. The computational study began with 4-hydroxycarbazol. A PEC of torsional angle χ_1 was generated using the hydroxyl group to model the extending side chain of carvedilol and the orientation of the carbazole ring (cf. Figure 5). The PEC shows a global minimum at the anti orientation and two energetically equal enantiomeric local minima located at gauche$^+$ ($g+$) and gauche$^-$ ($g-$). Subsequent full optimizations at RHF/3-21G and B3LYP/6-31G(d) confirmed the carbazole ring system to be planar (cf. Table 2).

4.2. Conformational Analysis of the *S*-4-(2-Hydroxypropoxy)carbazol PEHS in Vacuum (Gas Phase). The PEHS of *S*-4-(2-hydroxypropoxy)carbazol was analyzed by optimizations of its minima. Conformational structural assignment for the conformational minima was made using the following conditions.

TABLE 5: PCM Energies of the *S*-4-(2-Hydroxypropoxy)carbazol PEHS Converged Minima at the B3LYP/6-31G(d) Level of Theory[a]

conformational assignment				*E* (hartrees) chloroform ($\epsilon = 4.9$)	*E* (hartrees) ethanol ($\epsilon = 24.55$)	*E* (hartrees) DMSO ($\epsilon = 46.7$)	*E* (hartrees) water ($\epsilon = 78.39$)	rel *E* (kcal mol^{-1}) chloroform; ethanol; DMSO; water
χ_1	χ_2	χ_3	χ_{10}					
g^+	g^+	g^+	g^+	−785.835452016	−785.847280815	−785.838105591	−785.848539067	5.71; 5.83; 5.75; 5.98
g^+	g^+	a	a	−785.835761703	−785.852014571	−785.839876218	−785.853562891	5.51; 2.86; 4.64; 2.82
g^+	g^+	a	g^-	−785.838938609	−785.851382704	−785.841626431	−785.852679025	3.52; 3.25; 3.54; 3.38
g^+	a	a	g^-	−785.841782502	−785.854792831	−785.844096606	−785.856067697	1.73; 1.11; 1.99; 1.25
a	g^+	a	a	−785.838922339	−785.854637440	−785.842460640	−785.856169766	3.53; 1.21; 3.02; 1.19
a	g^+	a	g^-	−785.842289029	−785.855924290	−785.845060186	−785.857127836	1.42; 0.40; 1.39; 0.59
a	a	g^+	g^+	−785.843247677	−785.855541580	−785.846006567	−785.857035590	0.81; 0.64; 0.79; 0.64
a	a	a	g^+	−785.841575633	−785.856360024	−785.845115549	−785.858035710	1.86; 0.13; 1.35; 0.02
a	**a**	**a**	**g^-**	**−785.844546250**	**−785.856564633**	**−785.847270577**	**−785.858062768**	**0.00; 0.00; 0.00; 0.00**
a	a	g^-	g^+	−785.841944548	−785.856262168	−785.845202712	−785.857767055	1.63; 0.19; 1.30; 0.19
a	a	g^-	a	−785.841847514	−785.856123578	−785.845024812	−785.857584251	1.69; 0.28; 1.41; 0.30
a	a	g^-	g^-	−785.842012425	−785.856238960	−785.845348877	−785.857757325	1.59; 0.20; 1.21; 0.19
a	g^-	a	a	−785.839191302	−785.853278143	−785.842532301	−785.854769318	3.36; 2.06; 2.97; 2.07
a	g^-	g^-	g^+	−785.840462811	−785.854751815	−785.843765296	−785.856185261	2.56; 1.14; 2.20; 1.18
a	g^-	g^-	a	−785.840011265	−785.853717388	−785.843115115	−785.855089322	2.85; 1.79; 2.61; 1.87
a	g^-	g^-	g^-	−785.840009467	−785.854576586	−785.843462962	−785.856168143	2.85; 1.25; 2.39; 1.19
g^-	a	g^+	g^+	−785.840819204	−785.853101302	−785.843407391	−785.854221604	2.34; 2.17; 2.42; 2.41
g^-	g^-	a	g^-	−785.836715823	−785.848459667	−785.839403800	−785.849810413	4.91; 5.09; 4.94; 5.18
g^-	g^-	g^-	g^-	−785.835724176	−785.849366072	−785.839007643	−785.850726739	5.54; 4.52; 5.19; 4.60

[a] Reaction-field calculations were done in chloroform ($\epsilon = 4.9$), ethanol ($\epsilon = 24.55$), DMSO ($\epsilon = 46.7$), and water ($\epsilon = 78.39$).

TABLE 6: PCM $\Delta G^{solvation}$ of the *S*-4-(2-Hydroxypropoxy)carbazol PEHS Converged Minima at the B3LYP/6-31G(d) Level of Theory in Chloroform, Ethanol, DMSO, and Water

conformational assignment				$\Delta G^{solvation}$ (kcal mol^{-1}) chloroform ($\epsilon = 4.9$)	$\Delta G^{solvation}$ (kcal mol^{-1}) ethanol ($\epsilon = 24.55$)	$\Delta G^{solvation}$ (kcal mol^{-1}) DMSO ($\epsilon = 46.7$)	$\Delta G^{solvation}$ (kcal mol^{-1}) water ($\epsilon = 78.39$)
χ_1	χ_2	χ_3	χ_{10}				
g^+	g^+	g^+	g^+	−1.83	−7.67	−3.21	−7.39
g^+	**g^+**	**a**	**a**	**−3.92**	**−12.51**	**−6.54**	**−12.84**
g^+	g^+	a	g^-	−2.12	−8.44	−3.75	−8.37
g^+	a	a	g^-	−2.08	−8.73	−3.49	−8.68
a	g^+	a	a	−3.73	−12.01	−6.00	−12.27
a	g^+	a	g^-	−2.67	−9.68	−4.49	−9.77
a	a	g^+	g^+	−2.53	−8.75	−4.33	−8.98
a	a	a	g^+	−3.89	−11.75	−6.20	−11.97
a	a	a	g^-	−2.81	−8.81	−4.68	−9.15
a	a	g^-	g^+	−3.37	−10.79	−5.50	−11.08
a	a	g^-	a	−3.35	−10.75	−5.44	−11.01
a	a	g^-	g^-	−3.59	−10.94	−5.78	−11.24
a	g^-	a	a	−3.75	−11.03	−6.02	−11.36
a	g^-	g^-	g^+	−3.11	−10.54	−5.20	−10.69
a	g^-	g^-	a	−3.00	−10.07	−4.99	−10.22
a	g^-	g^-	g^-	−3.32	−10.91	−5.51	−11.18
g^-	a	g^+	g^+	−2.03	−8.21	−3.57	−8.03
g^-	g^-	a	g^-	−1.91	−7.72	−3.37	−7.52
g^-	g^-	g^-	g^-	−3.12	−10.11	−5.13	−10.15

$$\text{gauche plus } (g+) = 60 \text{ (ideal)} \pm 50°$$

$$\text{anti } (a) = 180 \text{ (ideal)} \pm 50°$$

$$\text{gauche minus } (g-) = -60 \text{ (ideal)} \pm 50°$$

This is based on the general observation that if one were to rotate a tetrahedral carbon against another tetrahedral carbon the minima would generally fall within the above ranges. Conformers that were located by geometry optimization were termed **FOUND** and those that could not be located within the above thresholds were termed NOT FOUND (cf. Table 3). Conformations not found usually shifted to the nearest neighboring minima on the PEHS. However, if the nearest minima were also annihilated, as was the case for parts of the PEHS that did not contain stable structures, conformers shifted to a nearby stable geometry. For conformers that were found, fully optimized values are shown in Table 4. The PEHS of the *S*-configuration structure contained one global minima with χ_1, χ_2, and χ_3 in the anti position and χ_{10} in the $g-$ position. All minima contained respective enantiomeric pairs with regards to point and axis chirality (data not shown).

Conformer stability for the *S*-4-(2-hydroxypropoxy)carbazol PEHS was influenced by intramolecular hydrogen bonding between O1 and H30 (defined in Figure 3). Out of the four lowest-energy (i.e., with a relative energy of less than 2 kcal mol^{-1} in vacuum) *S*-4-(2-hydroxypropoxy)carbazol conformers, $g+[aa]g-$, $a[g+a]g-$, $a[ag+]g+$, and $a[aa]g-$, all contained a hydrogen bond between O1 and H30 with distances of 2.202, 2.325, 2.293, and 2.258 Å, respectively (cf. Figure 6). However, this is not to say that hydrogen bonding was not present in any other conformers; $g+[g+g+]g+$ (5.82 kcal mol^{-1}, 2.744 Å hydrogen bond), $g+[g+a]g-$ (3.60 kcal mol^{-1}, 2.189 Å hydrogen bond), $g-[ag+]g+$ (2.26 kcal mol^{-1}, 2.247 Å hydrogen bond), and $g-[g-a]g-$ (5.11 kcal mol^{-1}, 2.756 Å hydrogen bond) all contained hydrogen bonds with varying relative energies. Furthermore, the *S*-4-(2-hydroxypropoxy)-carbazol conformers with torsional angles χ_1 or χ_2 in the anti position were energetically aided by having the side chain extend away from the carbazole ring.

4.3. Analysis of the *S*-4-(2-Hydroxypropoxy)carbazol PEHS in Different Solvent Media. DFT was used to investigate

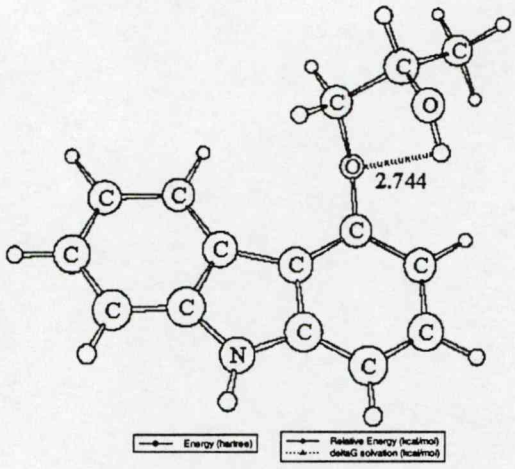

g+[g+g+]g+

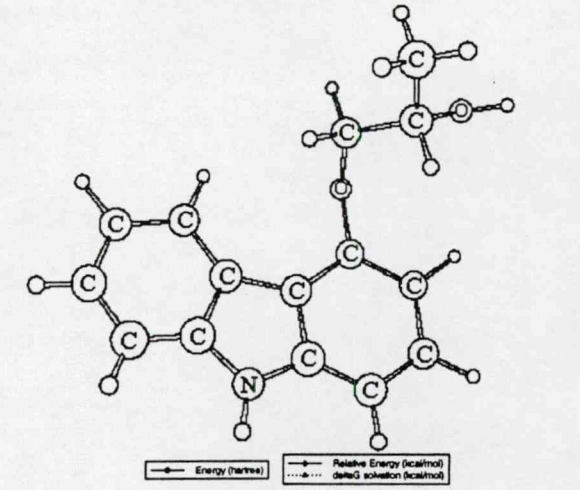

g+[g+a]a

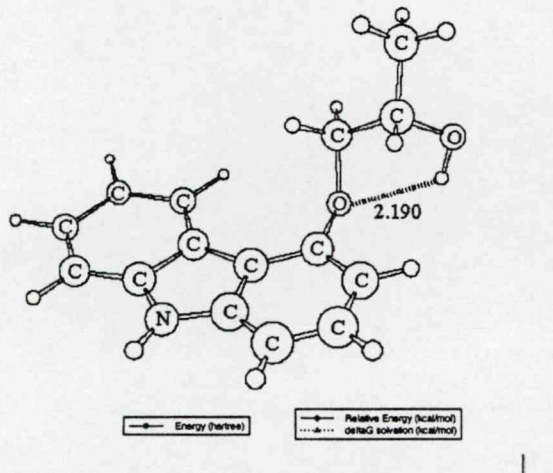

g+[g+a]g-

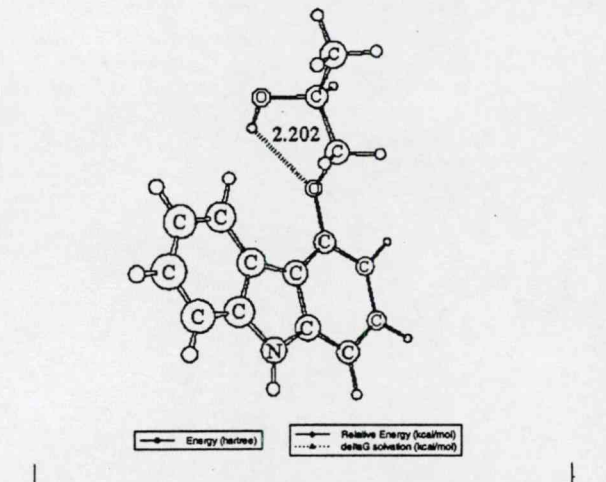

g+[aa]g-

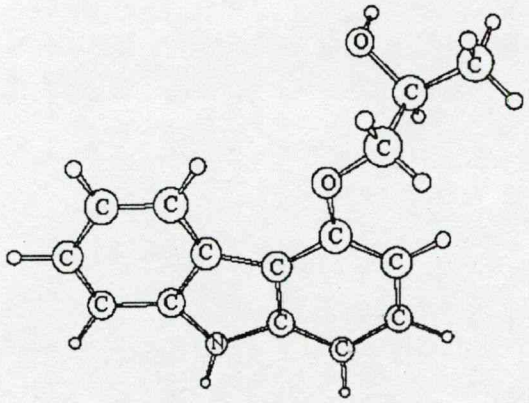

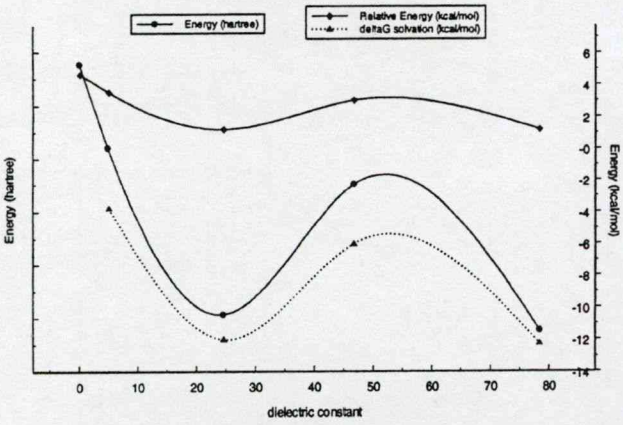

a[*g*+*a*]*a*

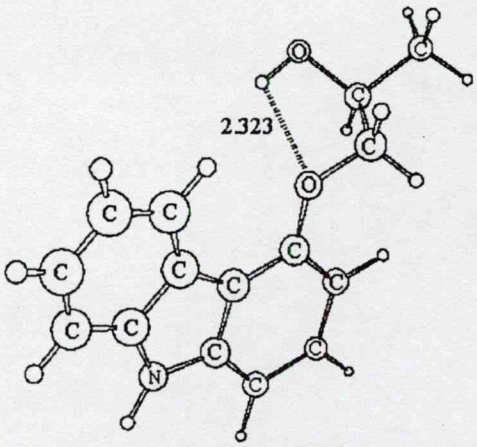

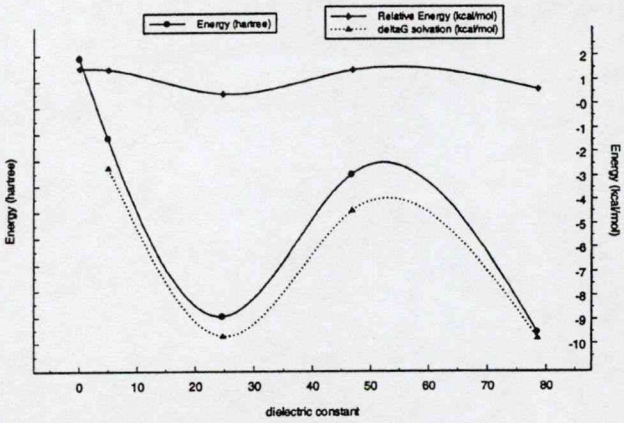

a[*g*+*a*]*g*-

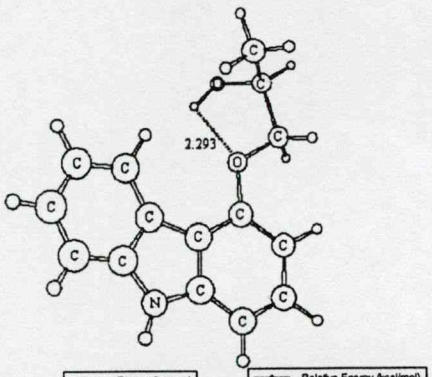

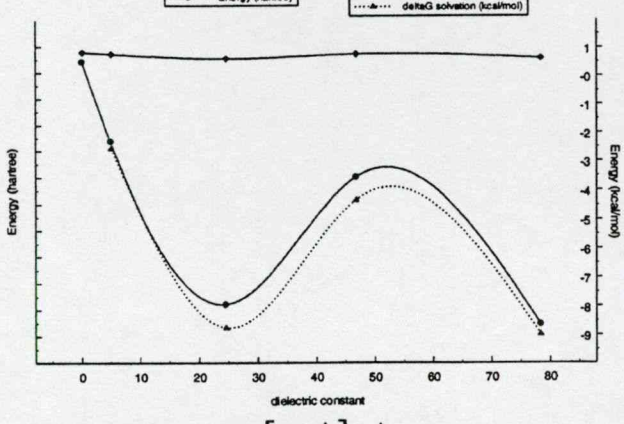

a[*ag*+]*g*+

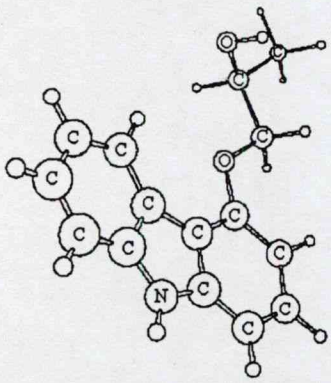

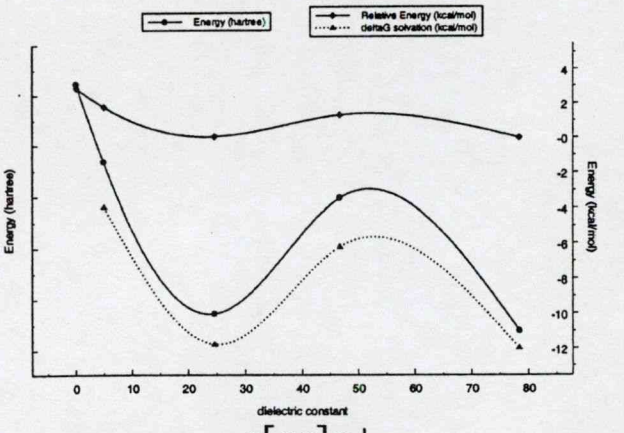

a[*aa*]*g*+

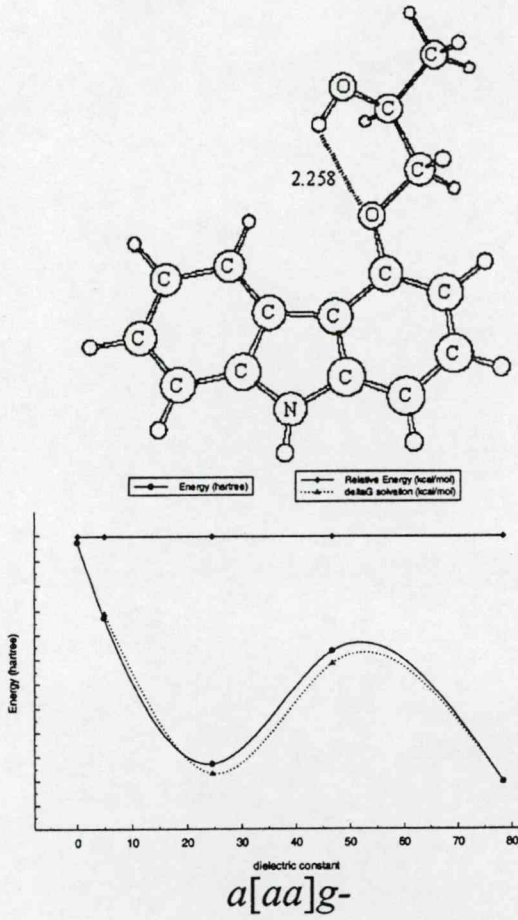

a[*aa*]*g*-

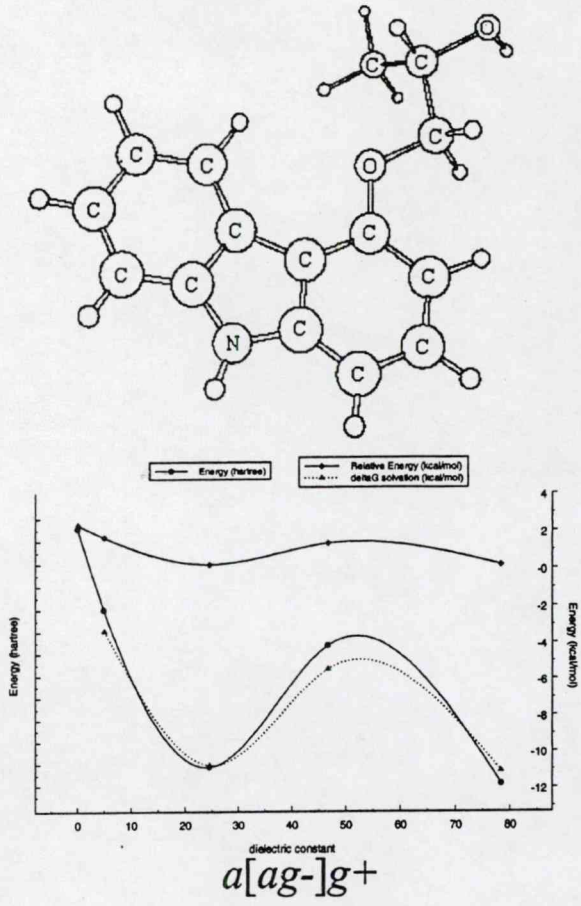

a[*ag*-]*g*+

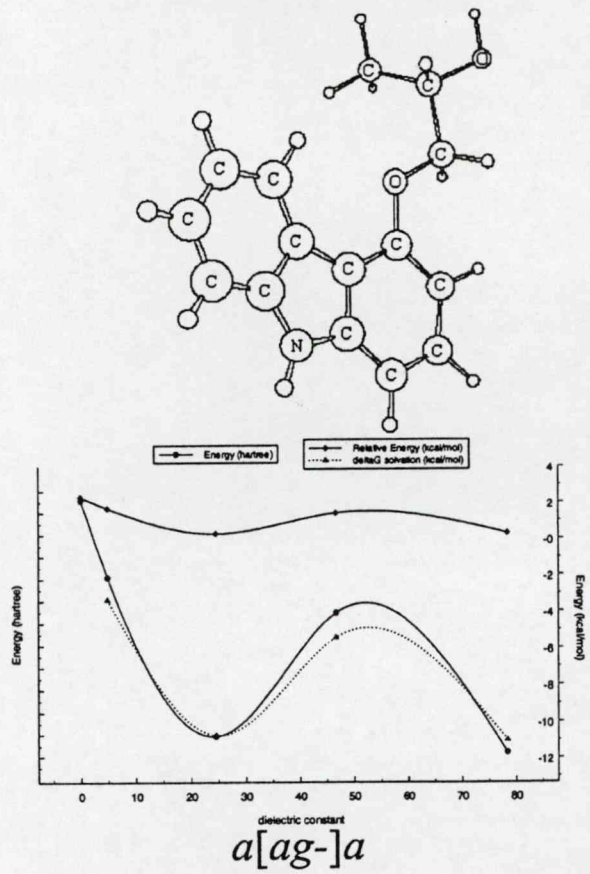

a[*ag*-]*a*

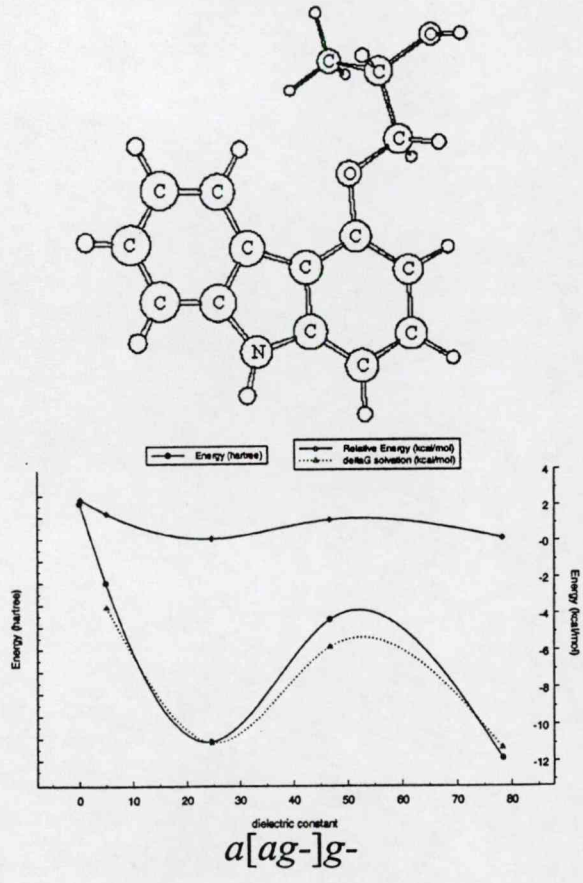

a[*ag*-]*g*-

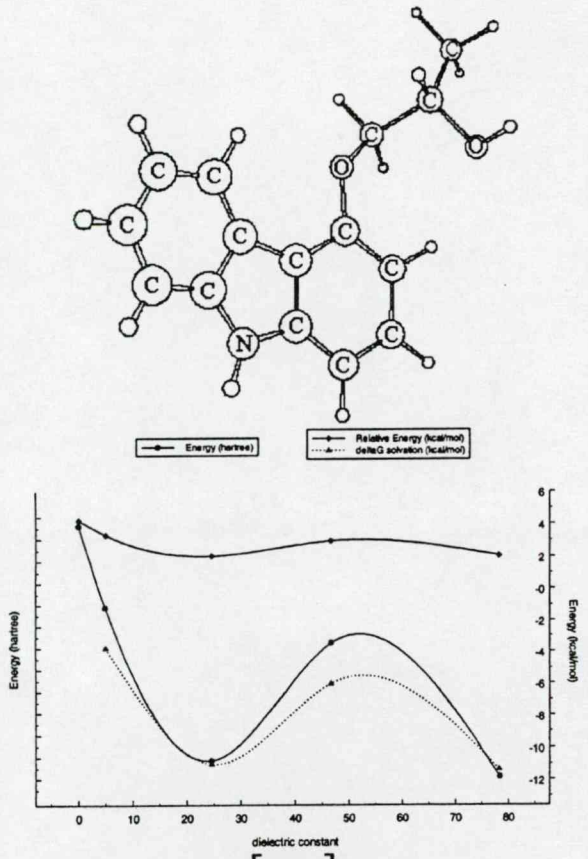

a[*g*-*a*]*a*

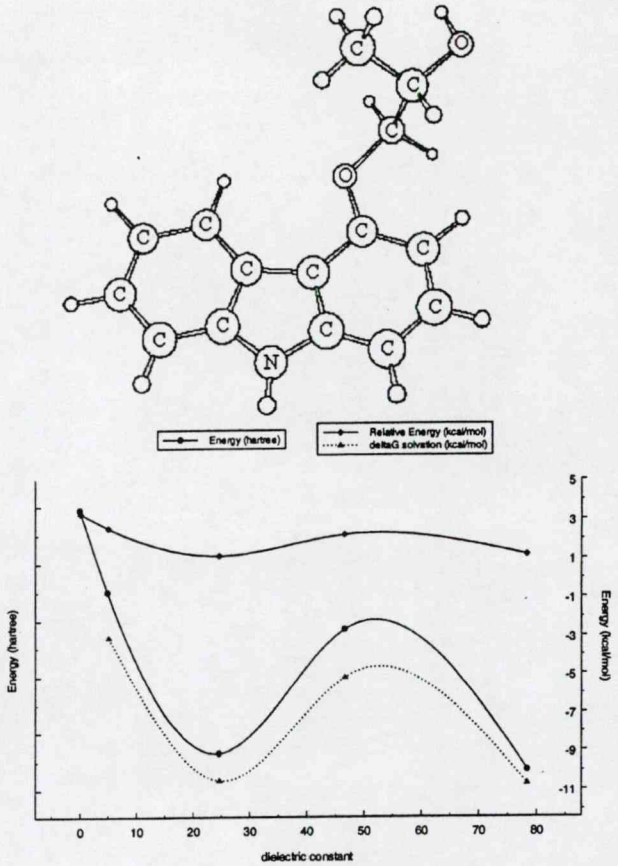

a[*g*-*g*-]*g*+

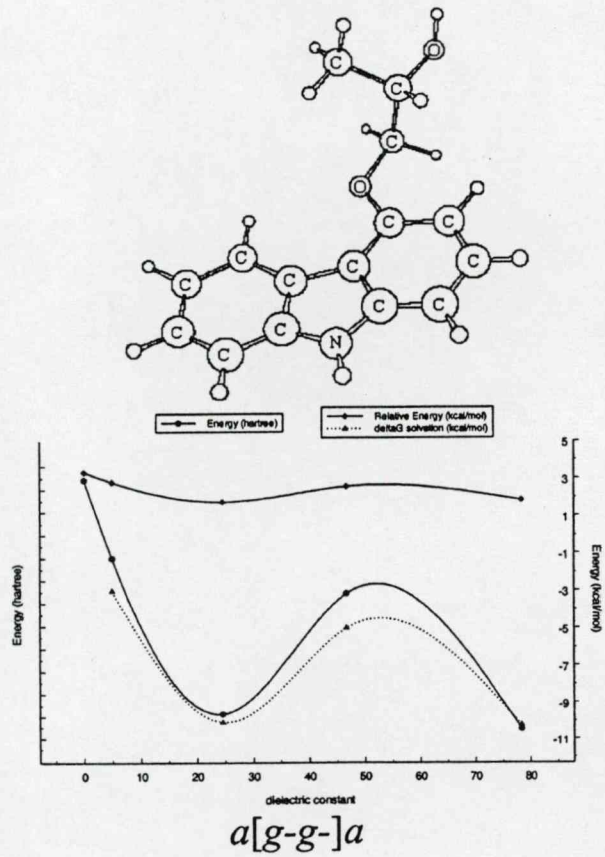

a[*g*-*g*-]*a*

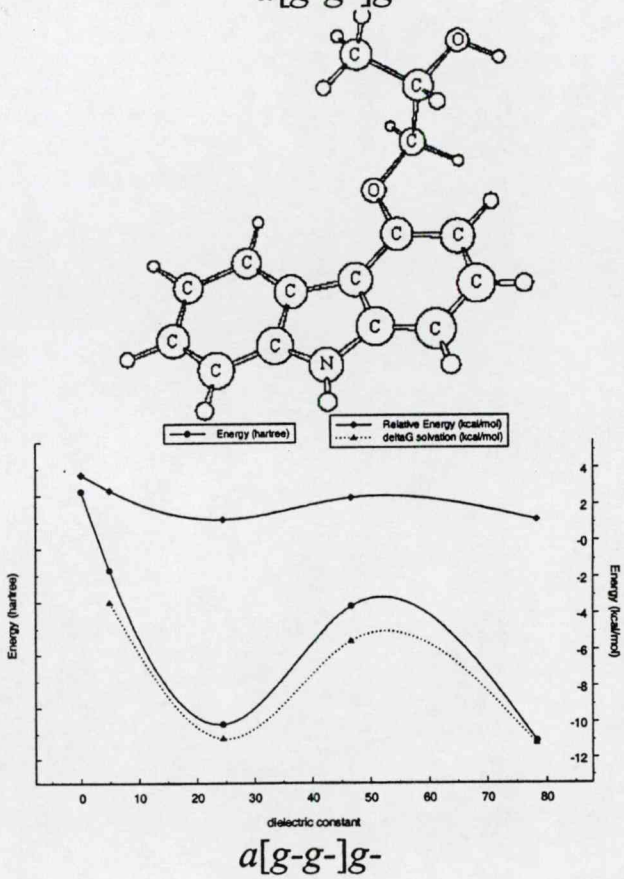

a[*g*-*g*-]*g*-

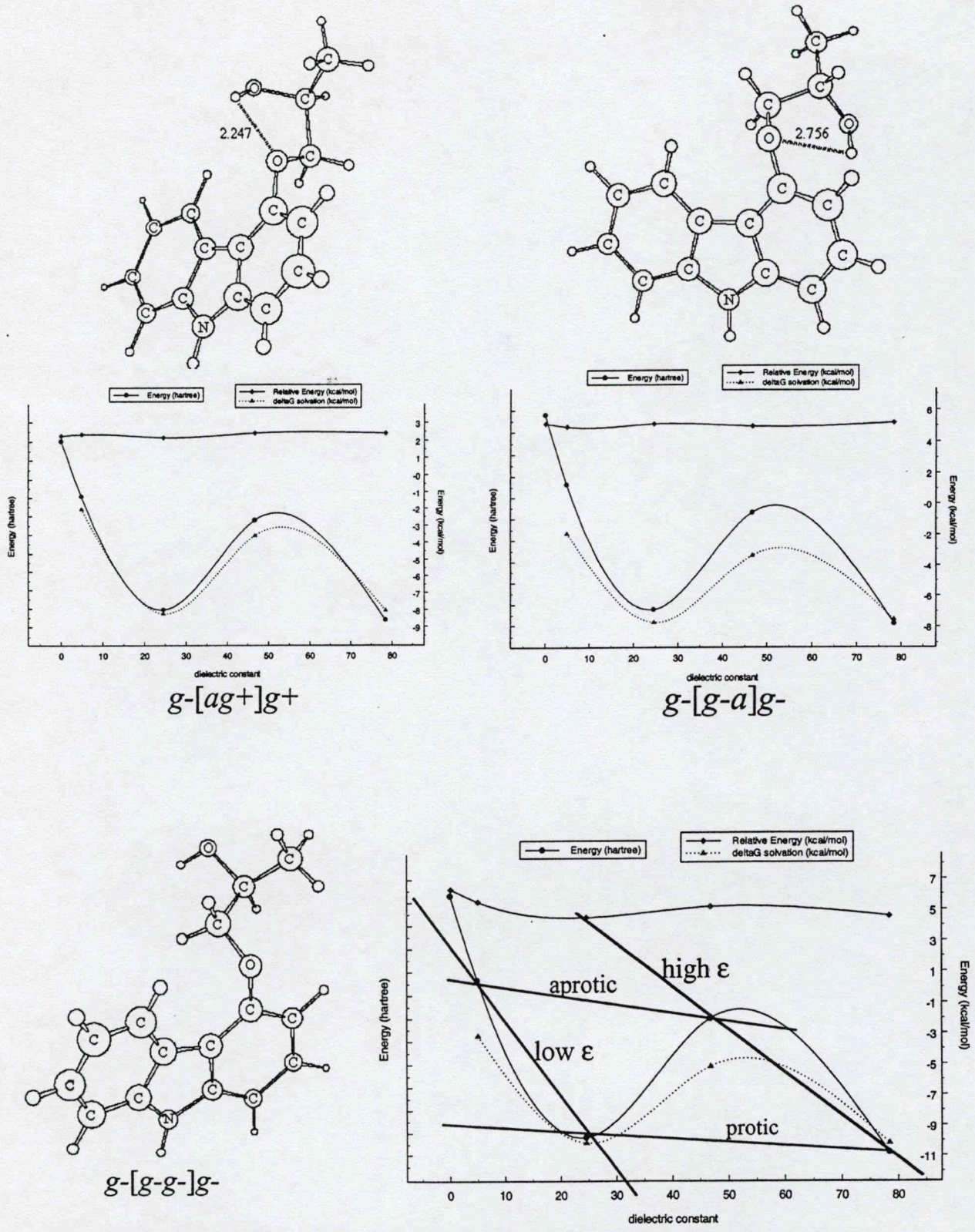

Figure 6. Structures of fully optimized *S*-4-(2-hydroxypropoxy)carbazol PEHS minima at the B3LYP/6-31G(d) level of theory in vacuum. The global conformer is *a*[*aa*]*g*−. Energetic relationships of the *S*-4-(2-hydroxypropoxy)carbazol PEHS converged minima; self-consistent field (SCF) energy (hartrees), relative conformer energy (kcal/mol), and $\Delta G^{\text{solvation}}$ (kcal/mol) as a function of the dielectric constant. Conformer *g*−[*g*−*g*−]*g*− was arbitrarily picked to illustrate the trends of the *S*-4-(2-hydroxypropoxy)carbazol PEHS in different solvent media (cf. Results and Discussion for explanation).

the solute−solvent interactions between *S*-4-(2-hydroxypropoxy)carbazol and various different solvents (chloroform, ethanol, DMSO, water) (cf. Figure 6). The computations were carried out using Tomasi's PCM reaction-field calculations by

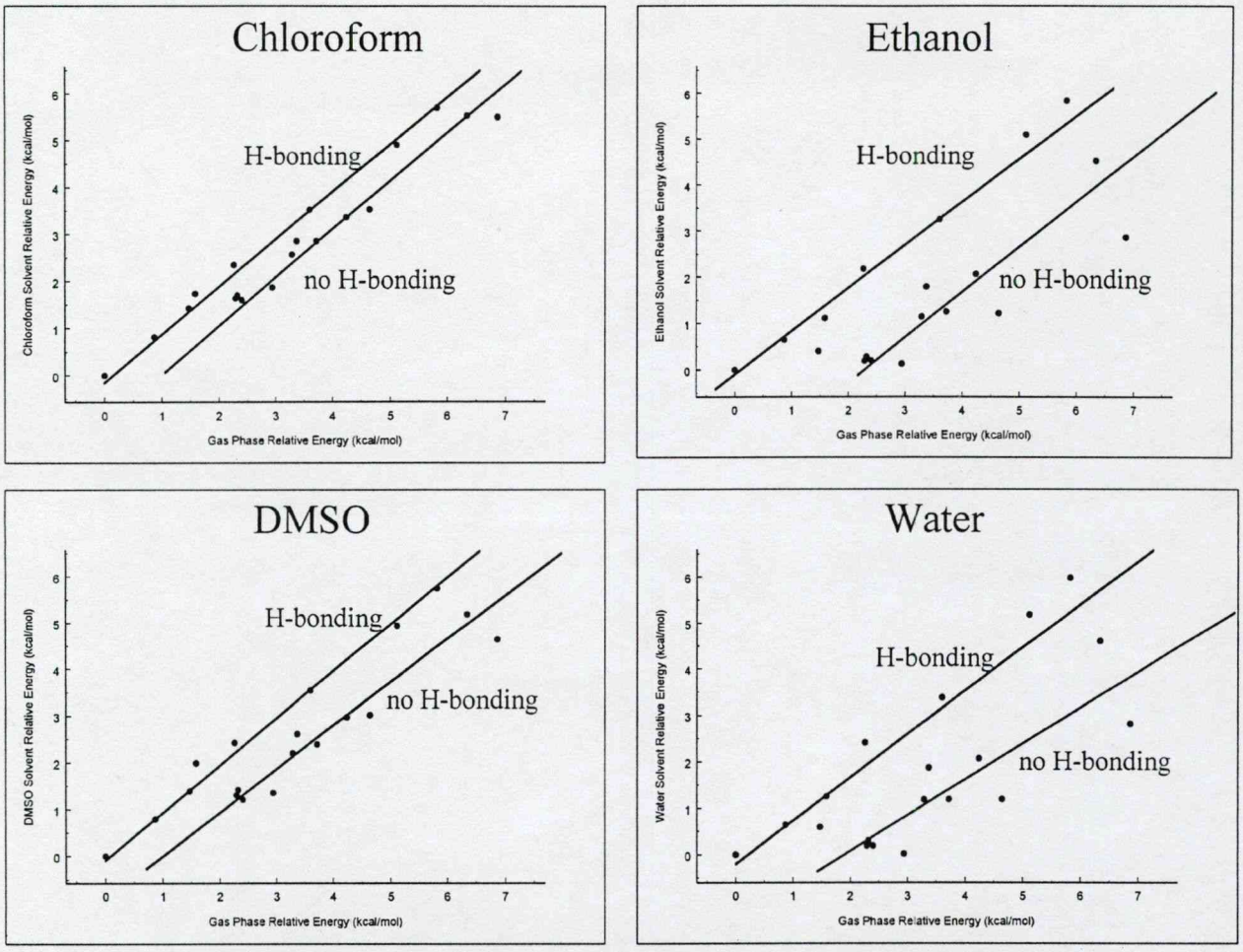

Figure 7. Correlation of relative energies of conformers in solvents with relative energies of conformers in the gas phase.

modeling the reaction field of the various solvents as a continuum of uniform dielectric constant (ϵ) and defining the solute cavity as the union of a series of interlocking atomic spheres.[30]

The trend seen for the *S*-4-(2-hydroxypropoxy)carbazol conformers is that SCF energies, relative energies, and $\Delta G^{\text{solvation}}$ values were all lower (i.e., more negative) in the protic solvents ethanol and water than in the aprotic solvents chloroform and DMSO (cf. Tables 5 and 6). The SCF energy for conformer $g-[g-g-]g-$ was arbitrarily picked to illustrate this trend (cf. last graph in Figure 6). The SCF energy was lower in the protic solvents for both low (ethanol) and high (water) dielectric constant solvents. This can be attributed to the larger hydrogen bond donor values of ethanol and water, which aid in the stabilization of the dipole moment created by the carbazole ring and the oxygen and nitrogen atoms. Moreover, the typical curves generated for SCF energy (hartrees), relative conformer energy (kcal/mol), and $\Delta G^{\text{solvation}}$ (kcal/mol) as a function of dielectric constant all reveal themselves to be similar to an "inverted" version of the curve found in Figure 4. This further emphasizes that the *S*-4-(2-hydroxypropoxy)carbazol conformers, when passing from the gas phase into solution, will be permitted to have the greatest charge separation (electronic polarization) by protic solvents that are able to provide hydrogen bond donor groups.

A further trend observed for all solvents tested is that solvation provides greater stabilization to conformers with no intramolecular hydrogen bonding, as these conformers have structures more accessible to the solvent molecules. *S*-4-(2-Hydroxypropoxy)carbazol conformers with intramolecular hydrogen bonding were stabilized mostly by the inherent hydrogen bonding, and solvation did not play a major role. This is illustrated in Figure 7, showing that conformers with intramolecular hydrogen bonding possess a line similar to $y = x$ of best fit, with a slope of 1. Conformers with no hydrogen bonding possess fitted lines shifted to the right by 1 kcal mol^{-1} in aprotic solvents such as DMSO and about 2 kcal mol^{-1} in protic solvents such as water, indicating greater stabilizing effects by solvation on the relative energies of those conformers with no hydrogen bonding.

Moreover, solvation free energies also correlate with the above trend (cf. Figure 8). The conformers with no internal hydrogen bonding all contained more negative $\Delta G^{\text{solvation}}$ values in all solvents compared with all conformers that possessed internal hydrogen bonding. The conformers with no intramolecular hydrogen bonding had fully extended conformations, enabling them to be fully solvated by the different solvent media, especially the protic solvents. Figure 8 also emphasizes that the effects of solvation on the *S*-4-(2-hydroxypropoxy)carbazol PEHS are similar for a given type of solvent—protic or aprotic—as discerned by the scatter of points. This indicates that conformer stability patterns will not vary widely within the types of either protic or aprotic solvents.

S-4-(2-Hydroxypropoxy)carbazol conformers with no internal hydrogen bonding showed higher relative energies in the gas phase; however, upon solvation with a protic solvent such as

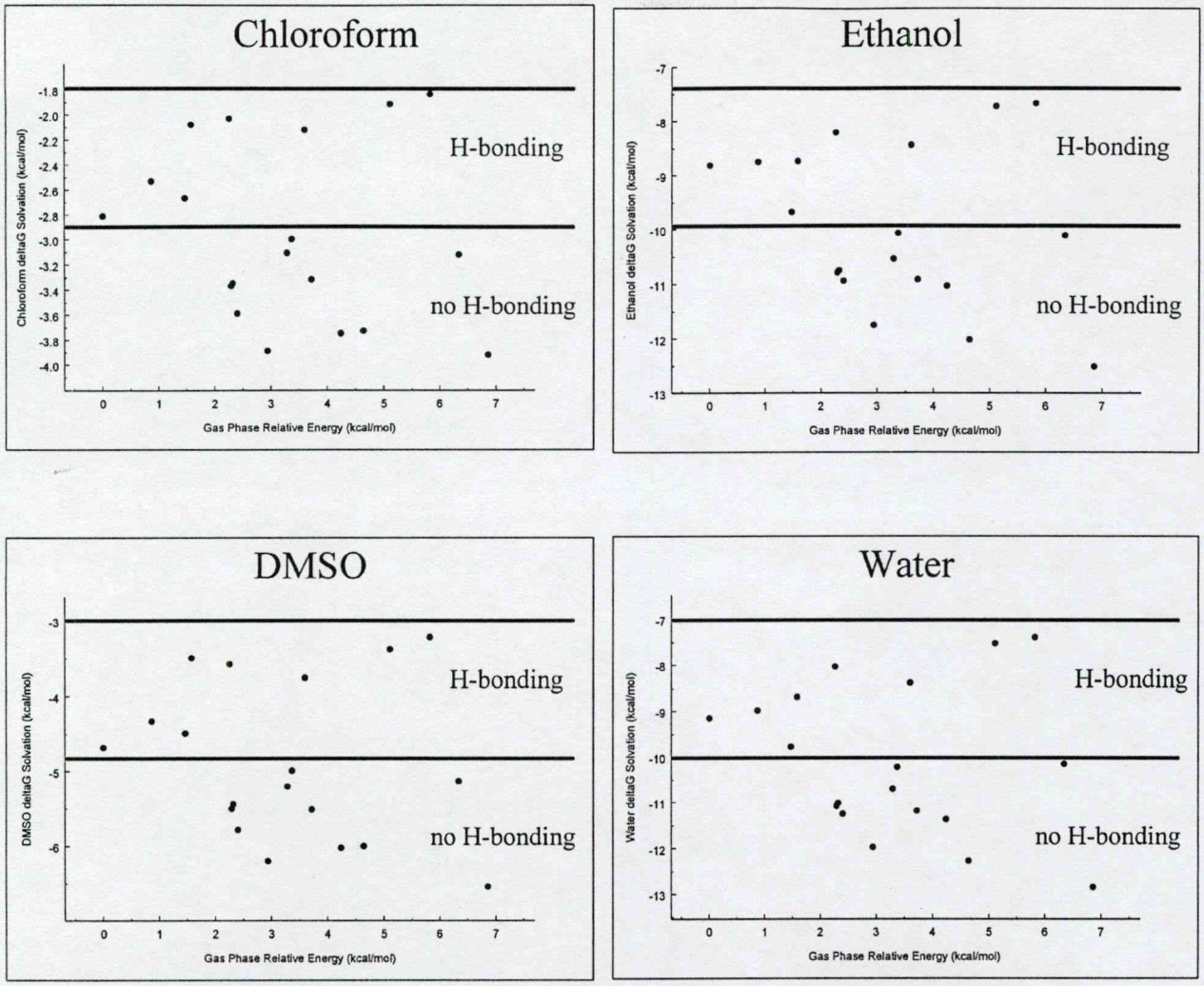

Figure 8. Correlation of $\Delta G^{solvation}$ of conformers in solvents with relative energies of conformers in the gas phase.

water, their relative energies dropped significantly. An example of the latter is conformer *a*[*aa*]*g*+, which had a relative energy of 2.94 kcal mol^{-1} in the gas phase but upon solvation in water had a solvation relative energy of 0.02 kcal mol^{-1}. This illustrates that internally hydrogen-bonded conformers are not solvated as well as those without hydrogen bonding, and therefore solvent effects are not as important as in cases where no internal hydrogen bonding occurs. Therefore, in molecular systems possessing internal hydrogen bonding, stability is conferred, in majority, by the hydrogen bonding, and these systems are not as influenced by solvent effects, whereas molecular systems with no internal hydrogen bonding will show a greater sensitivity to solvent stabilization effects.

5. Conclusions

For the *S*-4-(2-hydroxypropoxy)carbazol PEHS and, in general, for the two classifications for the media or environment that *S*-4-(2-hydroxypropoxy)carbazol (or another solute) may be in, (i) the environment may be classified as hydrophobic if the dielectric constant is less that 40 (example solvents are chloroform and ethanol) or hydrophilic if the dielectric constant is greater than 40 (example solvents are DMSO and water); and (ii) the media may be aprotic (chloroform and DMSO) or protic (ethanol and water). Resulting solute−solvent properties will be dependent accordingly on the inherent solute chemical properties (for example, stabilization forces) and their respective interactions with the biological environment in question. Finally, possible future work includes modeling the water solvent with explicit water molecules to further look at conformer stability.

References and Notes

(1) Carlson, W.; Oberg, K. *J. Cardiovasc. Pharmacol. Ther.* **1999**, *4*, 205.

(2) Capomolla, S.; Febo, O.; Gnemmi, M.; Riccardi, G.; Opasich, C.; Carporotondi, A.; Mortara, A.; Pinna, G.; Cobelli, F. *Am. Heart J.* **2000**, *139*, 596.

(3) Metra, M.; Nodari, S.; D'Aloia, A.; Bontempi, L.; Boldi, E.; Dei Cas, L. *Am. Heart J.* **2000**, *139*, 511.

(4) Feuerstein, G.; Ruffolo, R. R., Jr. *Adv. Pharmacol. (San Diego)* **1998**, *42*, 611.

(5) Saijonmaa, O.; Metsarinne, K.; Fyhrquist, F. *Blood Pressure* **1997**, *6*, 24.

(6) Packer, M.; Bristow, M. R.; Cohn, J. N.; Colucci, W. S.; Fowler, M. B.; Gilbert, E. M.; Shusterman, N. H. *N. Engl. J. Med.* **1996**, *334*, 1349.

(7) Berg, M. A.; Chasse, G. A.; Deretey, E.; Fuzery, A. K.; Fung, B. M.; Fung, D. Y. K.; Henry-Riyad, H.; Lin, A. C.; Mak, M. L.; Mantas, A.; Patel, M.; Repyakh, I. V.; Staikova, M.; Salpietro, S. J.; Tang, T.-H.; Vank, J. C.; Perczel, A.; Csonka, G. I.; Farkas, O.; Torday, L. L.; Szekely, Z.; Csizmadia, I. G. *J. Mol. Struct.: THEOCHEM* **2000**, *500*, 5.

(8) Hauf-Zachariou, U.; Blackwood, R. A.; Gunawardena, K. A.; O'Donnell, J. G.; Garnham, S.; Pfarr, E. *Eur. J. Clin. Pharmacol.* **1997**, *52*, 95.

(9) Noguchi, N.; Nishino, K.; Niki, E. *Biochem. Pharmacol.* **2000**, *159*, 1069.

(10) Yue, T. L.; Lysko, P. G.; Barone, F. C.; Gu, J. L.; Ruffolo, R. R., Jr.; Feuerstein, G. Z. *Ann. N.Y. Acad. Sci.* **1994**, *738*, 230.

(11) Guazzi, M.; Agostoni, P.; Matturri, M.; Pontone, G.; Guazzi, M. D. *Am. Heart. J.* **1999**, *138*, 460.

(12) Ruffollo, R. R., Jr.; Feuerstein, G. Z. *J. Cardiovasc. Pharmacol.* **1998**, *32* (Suppl. 1), S22.

(13) Yoshioka, T.; Iwamoto, N.; Tsukahara, F.; Iric, K.; Urakawa, I.; Muraki, T. *Br. J. Pharmacol.* **2000**, *129*, 1530.

(14) Watanabe, H.; Karihana, M.; Ohtsuka, S.; Sugishita, Y. *J. Am. Coll. Cardiol.* **1998**, *32*, 1194.

(15) Ruffolo, R. R., Jr.; Gellai, M.; Hieble, J. P.; Willette, R. N.; Nichols, A. J. *Eur. J. Clin. Pharmacol.* **1990**, *38*, S82.

(16) Gehr, T. W.; Tenero, D. M.; Boyle, D. A.; Qian, Y.; Sica, D. A.; Shusterman, N. H. *Eur. J. Clin. Pharmacol.* **1999**, *55*, 269.

(17) van der Does, R.; Hauf-Zachariou, U.; Pfarr, E.; Holtbrugge, W.; Konig, S.; Griffiths, M.; Lahiri, A. *Am. J. Cardiol.* **1999**, *83*, 643.

(18) Searlee, A. J. F.; Gree, C.; Wilson, R. L. Ellipticines and Carbazoles as Antioxidants. In *Oxygen Radicals and Biology*; Borns, W., Saran, M., Tait, D., Eds.; Walter de Gruyter & Co.: Berlin, 1984; pp 377−381.

(19) Feuerstein, G.; Yue, T. L.; Ma, X.; Ruffolo, R. R. *Prog. Cardiovasc. Dis.* **1998**, *41* (Suppl. 1), 17.

(20) Oldham, H. G.; Clarke, S. E. *Drug Metab. Dispos.* **1997**, *25*, 970.

(21) Feuerstein, R.; Yue, T. L. *Pharmacology* **1994**, *48*, 385.

(22) Yue, T. L.; Mckenna, P. J.; Lysko, P. G.; Gu, J. L.; Lysko, K. A.; Ruffolo, R. R., Jr.; Feuerstein, G. Z. *Eur. J. Pharmacol.* **1994**, *251*, 237.

(23) Abboud, J. L.; Kamlet, M. J.; Taft, R. W. *J. Am. Chem. Soc.* **1977**, *99*, 6027. Abboud, J. L.; Kamlet, M. J.; Taft, R. W. *J. Am. Chem. Soc.* **1977**, *99*, 8325.

(24) Abboud, J. L.; Kamlet, M. J.; Taft, R. W. *Prog. Phys. Org. Chem.* **1981**, *13*, 485.

(25) Bagno, A. Overview—Empirical and Thermodynamic Methods. *Solvation and Solvent Effects on Organic Reactivity*; Centro CNR Meccanismi Reazioni Organiche, Dipartimento di Chimica Organica: Padova, Italy, 2002; pp 20−22.

(26) Frisch, M. J.; Trucks, G. W.; Schlegel, H. B.; Scuseria, G. E.; Robb, M. A.; Cheeseman, J. R.; Zakrzewski, V. G.; Montgomery, J. A., Jr.; Stratmann, R. E.; Burant, J. C.; Dapprich, S.; Millam, J. M.; Daniels, A. D.; Kudin, K. N.; Strain, M. C.; Farkas, O.; Tomasi, J.; Barone, V.; Cossi, M.; Cammi, R.; Mennucci, B.; Pomelli, C.; Adamo, C.; Clifford, S.; Ochterski, J.; Petersson, G. A.; Ayala, P. Y.; Cui, Q.; Morokuma, K.; Malick, D. K.; Rabuck, A. D.; Raghavachari, K.; Foresman, J. B.; Cioslowski, J.; Ortiz, J. V.; Stefanov, B. B.; Liu, G.; Liashenko, A.; Piskorz, P.; Komaromi, I.; Gomperts, R.; Martin, R. L.; Fox, D. J.; Keith, T.; Al-Laham, M. A.; Peng, C. Y.; Nanayakkara, A.; Gonzalez, C.; Challacombe, M.; Gill, P. M. W.; Johnson, B. G.; Chen, W.; Wong, M. W.; Andres, J. L.; Head-Gordon, M.; Replogle, E. S.; Pople, J. A. *Gaussian 98*, revision A.9; Gaussian, Inc.: Pittsburgh, PA, 1998.

(27) Miertus, S.; Tomasi, J. *Chem. Phys.* **1982**, *65*, 239.

(28) Miertus, S.; Scrocco, E.; Tomasi, J. *Chem. Phys.* **1981**, *55*, 117.

(29) Cossi, M.; Barone, V.; Cammi, R.; Tomasi, J. *Chem. Phys. Lett.* **1996**, *255*, 327.

(30) Foresman, J. B.; Frish, A. Reaction Field Models of Solvation. *Exploring Chemistry with Electronic Structure Methods*, 2nd ed.; Gaussian Inc.: Pittsburgh, PA, 1996; pp 237−249.

ELSEVIER

Journal of Molecular Structure (Theochem) 631 (2003) 251–270

THEO CHEM

www.elsevier.com/locate/theochem

Gas phase conformational basicity of carvedilol Fragment B, 2(*S*)-1-(ethylamonium)propane-2-ol: An ab initio study on a protonophoretic of oxidative phosphorylation uncoupling

David R.P. Almeida[a,*], Donna M. Gasparro[a], Luca F. Pisterzi[a], Ladislaus L. Torday[b], Andras Varro[b], Julius Gy. Papp[b,c], Botond Penke[d,e]

[a]*Department of Chemistry, Lash Miller Laboratories, University of Toronto, 80 St. George Street, Toronto, Ont., Canada M5S 3H6*
[b]*Department of Pharmacology and Pharmacotherapy, Szeged University, Dom ter 12, Szeged 6701, Hungary*
[c]*Division of Cardiovascular Pharmacology, Hungarian Academy of Sciences and Szeged University, zDom ter 12, Szeged 6701, Hungary*
[d]*Institute of Medical Chemistry, Szeged University, Dom ter 8, Szeged 6720, Hungary*
[e]*Hungarian Academy of Sciences, Protein Chemistry Research Group, University of Szeged, Dom ter 8, Szeged 6720, Hungary*

Received 13 January 2003; accepted 31 March 2003

Abstract

Carvedilol is cardiovascular drug of proven efficacy. It is believed that carvedilol exerts cardio-protective effects by acting as a mild uncoupler of mitochondrial oxidative phosphorylation, thereby protecting mitochondria from oxidative stress and preserving proper bioenergetics and cardiac function. This uncoupling occurs via a proton-shuttling mechanism involving the amino group of carvedilol's side-chain. However, the molecular details of carvedilol's proton affinity have not yet been completely worked out, especially with regards to the attributes of molecular conformation. In the present study, the full conformational basicity of a fragment of carvedilol, 2(*S*)-1-(ethylamonium)propane-2-ol (Fragment B), is presented to illustrate the protonophoretic character of carvedilol. Full gas phase geometry optimizations were performed at the ab initio, RHF/3-21G, level of theory for the entire potential energy hypersurface (PEHS) of Fragment B. Subsequently, since deprotonation can occur via two different protons, a two-prong methodology was applied to calculate vertical and adiabatic energies of deprotonation. A total of 18 out of a possible 81 minima converged and the dominant characteristic in all protonated and deprotonated conformers was a *gauche* plus effect in the rotation about the C–OH bond at the Fragment B stereocentre. Optimized energies of deprotonation ranged from 245 to 262 kcal mol^{-1} while protons involved in internal hydrogen bonding required an extra 6–8 kcal mol^{-1} for deprotonation compared to protons that were oriented away from the backbone structure. The overall trend indicates that conformers devoid of significant stabilization interactions possessed lower energies of deprotonation; in other words, as the relative conformer energy increased, vertical and adiabatic energies of deprotonation tended to decrease. Thus, extrapolating to carvedilol and the proton transfer mechanism involved in oxidative phosphorylation uncoupling, events of deprotonation will favour molecular conformations with minimal intramolecular stabilization and with higher relative energies.

* Corresponding author.
E-mail addresses: dalmeida@medscape.com (D.R.P. Almeida), dgasparro@medscape.com (D.M. Gasparro), lpisterzi@medscape.com (L.F. Pisterzi), pyro@phcol.szote.u-szeged.hu (L.L. Torday), varro@phcol.szote.u-szeged.hu (A. Varro), papp@phcol.szote.u-szeged.hu (J.G. Papp).

0166-1280/03/$ - see front matter © 2003 Elsevier B.V. All rights reserved.
doi:10.1016/S0166-1280(03)00258-6

Keywords: Carvedilol; 2(*S*)-1-(ethylamonium)propane-2-ol; Basicity; Proton affinity; Ab initio

1. Introduction

1.1. Medical Background

The cardiovascular drug carvedilol, 1-(9H-Carbazol-4-yloxy)-3-[2-(2-methoxy-phenoxy)ethylamino]-2-propanol ($C_{24}H_{26}N_2O_4$), is used in the treatment of mild to moderate congestive heart failure (CHF), essential hypertension, angina, and in improvement of left ventricular function [1]. Indicative of carvedilol's efficacy is the fact that the US Data and Safety Monitoring Board stopped, for ethical reasons, the clinical trials of carvedilol before its completion due to greatly lowered morbidity and mortality rates [2,3].

Carvedilol is a lipophilic autonomic nervous system agent that acts as a multiple-action neurohormonal antagonist by producing nonselective beta-blockage (β_1 and β_2), selective alpha-blockage (α_1), while also possessing myocardial-protective antioxidant properties [1,4]. By blocking the activity of cardiac β-adrenergic receptors (β_1 and β_2) to noradrenaline, carvedilol reduces cardiac output and oxygen consumption, and therefore, total cardiac work-load of the heart [5,6]. Carvedilol also provides positive effects by vasodilation (α_1-adrenergic blockage) at peripheral resistance vessels, which decreases preload and after-load, thereby reducing cardiac work and wall tensions [7].

As an antioxidant, the carbazole ring gives carvedilol and its metabolites a powerful tendency to donate electrons to 'scavenge' the activities of reactive oxygen species (ROS) such as: oxygen superoxide ($O_2^{\cdot-}$), hydrogen peroxide (H_2O_2), hydroxyl radical ($^{\cdot}OH$), and peroxynitrite ($ONOO^-$), and therefore, helps to protect the living body from the deleterious effects of free radical damage [8]. The free radical scavenging ability of carbazole, such as that seen against lipid peroxidation, is enhanced by its high lipid solubility [9].

Carvedilol has been shown to act as a novel anti-fibrillar agent and may have uses in the prevention of Alzheimer's; a disease characterized by neuronal cell loss associated with fibril formation [10]. Fibril formation leading to neuritic plaques occurs due to the aggregation of β-amyloid peptide (Aβ, 39–43 residue peptide) and it is generally accepted that preventing the conversion of Aβ peptides into biologically active fibrils may provide a method for slowing Alzheimer's neurotoxicity and pathology. The effectiveness of carvedilol's inhibition of Aβ fibril formation is due to three factors: (1) one central basic amino pharmacophore, (2) two cyclic hydrophobic ring centroids, and (3) the molecular flexibility to adopt a specific three-dimensional pharmacophore conformation [10]. However, it is currently not known if fibril inhibition occurs via carvedilol binding directly to Aβ monomers or to small oligomers [10].

1.2. Biological background

One of the cardio-protective effects of carvedilol resides in its ability to protect mitochondria from oxidative stress. This occurs by mild uncoupling of oxidative phosphorylation via the protonable amino group of carvedilol's side-chain [11]. Mitochondrial bioenergetics are involved in both physiological and pathological conditions since cardiac function is closely related to mitochondrial output. Due to the high demand of ATP from working cardiac muscles, a constant mitochondrial input is required. A compromise of mitochondrial bioenergetics leads to adverse consequences such as a failure to maintain calcium homeostasis which triggers apoptotic and necrotic pathways of cell death and suppresses delivery of ATP to heart muscles [12]. Uncouplers of oxidative phosphorylation are defined as chemical agents that selectively prevent the utilization of chemical energy derived from respiratory electron transport for the net phosphorylation of ATP from ADP [13]. These agents decrease the moles of inorganic phosphate (P_i) used (into organically bound form) per atom of oxygen consumed, and therefore, decrease the P/O ratio to zero in the presence of substrate. However, respiration in the mitochondria continues, i.e. respiration-dependent ATP synthesis is eliminated but respiration itself is not inhibited [13].

Characteristics of uncouplers in isolated mitochondria include increased respiration, inhibition of mitochondria-catalyzed exchange reactions, greatly increased apparent ATPase activity, and osmotic swelling [13].

It has been proposed that carvedilol's amino group ($pK_a = 7.9$) decreases the mitochondrial electric potential via a weak protonophoretic mechanism and uncouples oxidative phosphorylation by picking up a proton in the low pH cytosolic leaflet of the inner mitochondrial membrane (mitochondrial intermembrane space) and then crosses the membrane in the positively-charged protonated form into the relatively higher pH mitochondrial matrix [11]. It is postulated that carvedilol is able to cross the membrane as a positively charged species because of its high lipid solubility and driven by the electric potential which is negative in the matrix with regards to the intermembrane space [11]. Carvedilol then releases the proton in the matrix and returns to the cytosolic leaflet in the deprotonated neutral from [11]. The antioxidant activity of carvedilol in mitochondria may be due in part to this phenomenon known as 'mild uncoupling' in which a small decrease in mitochondrial electric potential induces a reduction in the ROS produced by the mitochondrial respiratory chain [11,14,15].

Thus, as described above, a proton-transfer process is ultimately responsible for the uncoupling in mitochondria by carvedilol. As such, it is necessary to explicitly define the molecular details of carvedilol's protonophoretic character. In this work, the intrinsic conformational basicity of 2(*S*)-1-(ethylamonium)propane-2-ol (Fragment B) will be analyzed because the function of proton affinity (basicity) and the willingness to give up a proton will correlate with the uncoupling effect on mitochondrial oxidative phosphorylation. Using a smaller model, possessing the same amino group in carvedilol's side-chain, the current investigators will illustrate the influence that carvedilol's molecular conformation exerts on its protonophoretics. An analysis of the entire conformational surface of Fragment B will be carried out because the diversity of effects in uncoupling found between carvedilol and its metabolite 3-hydroxyl carvedilol have been attributed to differences in molecular conformation [11], and therefore, it is essential to survey the entire conformational space.

1.3. Chemical background

Carvedilol contains one strereocentre and is commercially available as a racemic mixture of both its enantiomers (R[+] and S[−]) (c.f. Fig. 1). However, the enantiomers of carvedilol show marked stereoselective properties; both enantiomers have equal α_1 blocking activity and antioxidant activity but only the S[−] enantiomer contains the nonselective β-adrenergic blocking activity [16,17]. As such, neither enantiomer alone has the same pharmacologic profile as the racemic mixture of carvedilol used clinically. Moreover, carvedilol's metabolites (1-hydroxyl, 3-hydroxyl, and 8-hydroxyl carvedilol; c.f. Fig. 1) are potent antioxidants since a hydroxyl group substitution in a heterocyclic ring (such as carbazole) increases the molecular antioxidant action of a given compound [3, 16,18,19]. Metabolites 1-hydroxyl and 3-hydroxyl carvedilol (c.f. Fig. 1) are also able to act as novel anti-fibrillar agents because they retain the needed pharmacophores and conformational flexibility [10]. This implicates that the conformational profile and intrinsic characteristics of carvedilol can be extrapolated to the structurally-analogous metabolites of carvedilol.

Carvedilol possesses three distinct pharmacophores, and therefore, was deconstructed into three structural fragments: *R*- and *S*-4-(2-hydroxypropoxy)carbazol (Fragment A) is responsible for the carbazole-related antioxidant effects of carvedilol, 2(*R* and *S*)-1-(ethylamonium)propane-2-ol (Fragment B) contains the protonophoretic amino group which connects the two oxygen-containing fragments of carvedilol, and aminoethoxy-2-methoxy-benzene (Fragment C) is responsible for the α-blocker action of carvedilol (c.f. Fig. 1). Beta-blockage is exerted by the composite of both Fragment A and B. While *R*- and *S*-4-(2-hydroxypropoxy)carbazol (Fragment A) has been studied [20], the current objective is the investigation of Fragment B.

2. Computational method

Fragment B was constructed with four torsional angles and the conformers of its potential energy hypersurface (PEHS) can be described according to Eq. (1) (c.f. Fig. 2). Newman projections display possible conformations of H12 (χ_{10} torsional angle) at

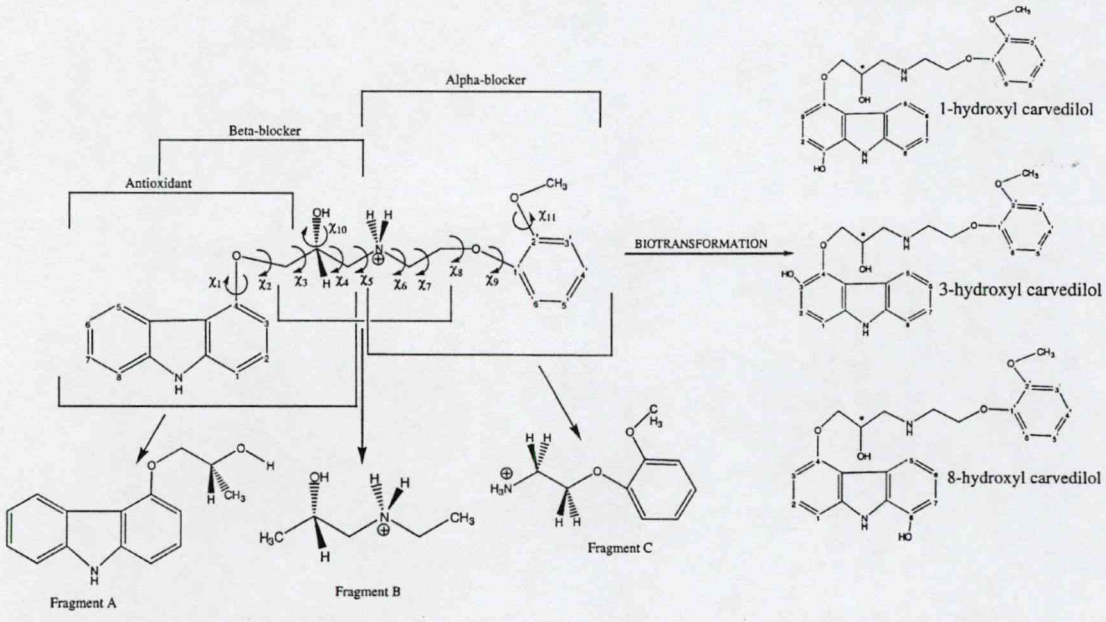

Fig. 1. The complete molecular structure and function of *N*-protonated carvedilol indicating all eleven torsional angles (top) and its three pharmocophoric fragments: *R*- and *S*-4-(2-hydroxypropoxy)carbazol (Fragment A), 2(*R* and *S*)-1-(ethylamonium)propane-2-ol (Fragment B), and aminoethoxy-2-methoxy-benzene (Fragment C). Upon biotransformation, three hydroxylated metabolites of carvedilol still possessing activity are formed: 1-hydroxyl, 3-hydroxyl, and 8-hydroxyl carvedilol (right).

the Fragment B stereocentre (c.f. Fig. 2).

$$E = f(\chi_4, \chi_5, \chi_6, \chi_{10}) \quad (1)$$

The structure of Fragment B indicates that carvedilol can be deprotonated via two protons. The latter is evident when either of the two protons is replaced by deuterium which leads to a nitrogen centre with either an *S*- or *R*-configuration, depending on which proton is replaced with deuterium. The protons are denoted as H_S (H16) and H_R (H21) in Fig. 2. This designation

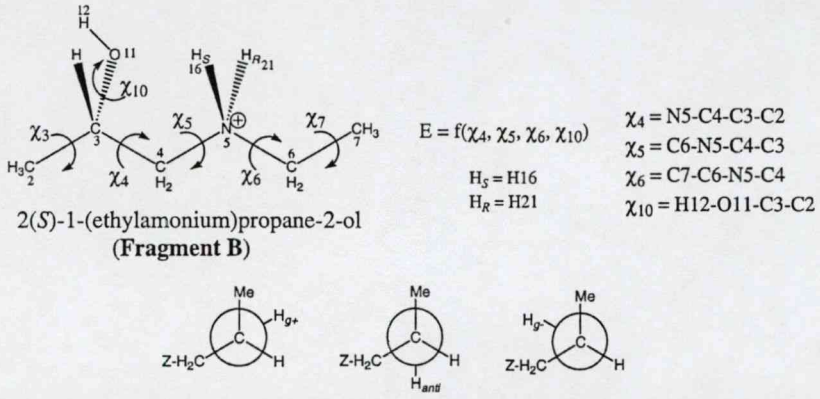

Fig. 2. Numbering and definition of torsional angles for 2(*S*)-1-(ethylamonium)propane-2-ol (Fragment B) (top). Newman projections along the C3-O11 bond (C3 front and O11 rear) display the g^+ (left), *anti* (middle), and g^- (right) conformations of torsional angle χ_{10} at the stereocentre of Fragment B and carvedilol. (Numbers placed beside atoms indicates numbering used as *z*-matrix input for GAUSSIAN 98.)

may also be applied to deprotonation scheme; for example, deprotonation of H_S would leave the nitrogen centre with H_R bonded and possessing an *R*-configuration. Therefore, dependent on the conformations adopted by Fragment B (and carvedilol accordingly), H_S and H_R will require different energies of deprotonation. Previous proton affinity studies on carvedilol and the amino group do not discriminate the different protons and reveal energies of deprotonation between 234 and 238 kcal mol^{-1} [11]. Multi-dimensional conformational analysis (MDCA) was performed on Fragment B to analyze the different energies of deprotonation associated with its full conformational space.

It is expected that, as it was shown for Fragment A, Fragment B will exhibit axis chirality as well as point chirality (from the *R*- and *S*-configurations) [20]. As such, the conformers present in the *R*-configuration PEHS can be predicted from the computed *S*-configuration of Fragment B according to Eq. (2). Eq. (2) states that stereoisomers, *S* and *R*, posses both point chirality and axis chirality and are exactly enantiomeric. Thus, a true enantiomeric pair requires not only the switching of point chirality from the *R*- to *S*-stereoisomer, but also the switching of all torsional angles from clockwise (CW) to counter-clockwise (CCW) rotation as demanded by Eq. (2). Consequently, the PEHS minima must all have an energetically equal enantiomer while all other pairs have diastereomeric relationships.

$$E_S = E_R \tag{2}$$

$$f_S(\chi_4, \chi_5, \chi_6, \chi_{10}) = f_R(-\chi_4, -\chi_5, -\chi_6, -\chi_{10}).$$

All computations were performed using the GAUSSIAN 98 software program [21]. Fragment B was exclusively defined using the GAUSSIAN 98 *z*-matrix internal coordinate system, to specify molecular structure, stereochemistry, and geometry. All calculations were performed at the Hartree–Fock, RHF/3-21G, level of theory.

Structural analysis of Fragment B was computed by MDCA of the Fragment B PEHS with optimizations of the conformational minima. With four torsional angles (χ_4, χ_5, χ_6, χ_{10}), and three possible minima for each torsional angle (*gauche plus*, g^+; *anti*, *a*; *gauche minus*, g^-), there are expected a grand total of 81 ($=3^4$) possible minima for each configuration of Fragment B. Only the *S*-configuration was computed because all structures are expected to be enantiomeric according to Eq. (2). Potential energy curves (PECs) were composed of either 12 or 24 points computed at 30° and 15° increments, respectively, according to Eq. (3) at the RHF/3-21G level of theory and plotted using Axum 5.0.

$$E = f(\chi_{10}) \tag{3}$$

After the PEHS was calculated, a separate two prong conformational methodology was applied to analyze the intrinsic basicity of the amino group of Fragment B. For each unique converged conformation of the PEHS, protonated Fragment B (BH^+) was deprotonated of protons H_S and H_R, independently of each other. Initially, vertical proton affinities were calculated with single-point energy (SPE) calculations and these energy values are denoted as $\Delta E_{vert}(S)$ and $\Delta E_{vert}(R)$ for H_S and H_R deprotonation, respectively (c.f. Eqs. (4) and (5)). The H_S and H_R deprotonated Fragment B (B) structures were then geometrically optimized and the respective adiabatic proton affinities (process in which the geometries are relaxed) were calculated based on fully optimized values. These values, denoted as $\Delta E_{opt}(S)$ and $\Delta E_{opt}(R)$ represent H_S and H_R optimized energies of deprotonation, respectively (c.f. Eqs. (6) and (7)). A third value, denoted as $\Delta\Delta E(S)$ and $\Delta\Delta E(R)$, represents the difference between the SPE [$\Delta E_{vert}(S)$ and $\Delta E_{vert}(R)$] and the optimized [$\Delta E_{opt}(S)$ and $\Delta E_{opt}(R)$] values for the energies of deprotonation for each conformer (c.f. Eqs. (8) and (9)]. This latter set of values can be interpreted as the stabilization experienced by Fragment B conformers as they adopted an optimized conformation after deprotonation. The above methodology is illustrated in Fig. 3. (A positive value for the energy of deprotonation appears because bond-breaking is always an endothermic process.)

$$\Delta E_{vert}(S) = |E_{opt}[BH^+] - E_{SP}[B]| \tag{4}$$

(H_S deprotonation)

$$\Delta E_{vert}(R) = |E_{opt}[BH^+] - E_{SP}[B]| \tag{5}$$

(H_R deprotonation)

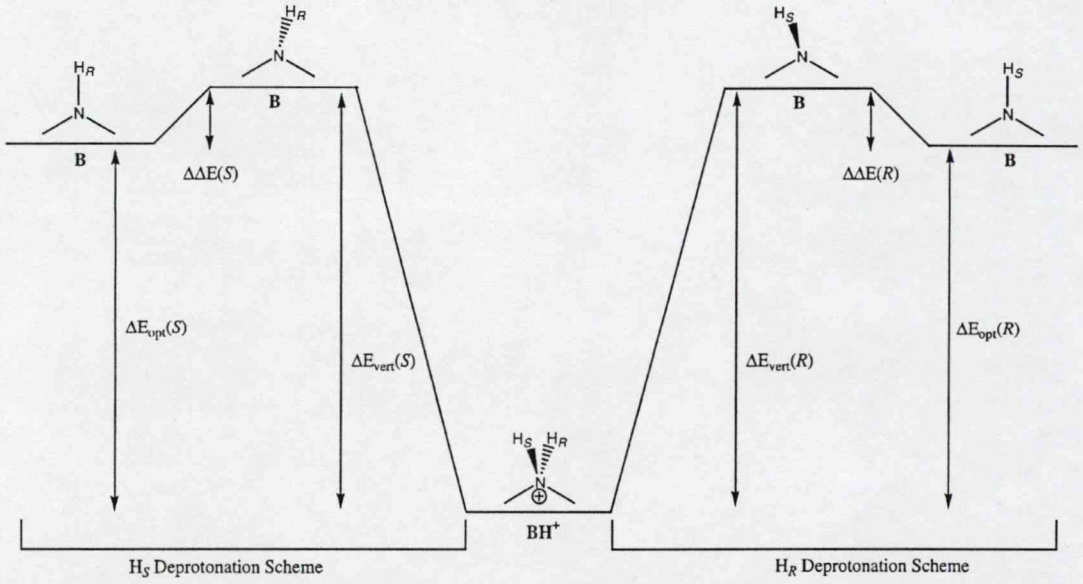

Fig. 3. Methodology employed to analyze the basicity of the amino group of Fragment B. Each converged minima of the protonated Fragment B PEHS was subject to independent deprotonation of the H_S (H16) and H_R (H21) protons (see Computational Method for explanation).

$$\Delta E_{opt}(S) = |E_{opt}[BH^+] - E_{opt}[B]| \quad (6)$$

(H_S deprotonation)

$$\Delta E_{opt}(R) = |E_{opt}[BH^+] - E_{opt}[B]| \quad (7)$$

(H_R deprotonation)

$$\Delta\Delta E(S) = \Delta E_{vert}(S) - \Delta E_{opt}(S) \quad (8)$$

(H_S deprotonation)

$$\Delta\Delta E(R) = \Delta E_{vert}(R) - \Delta E_{opt}(R) \quad (9)$$

(H_R deprotonation)

3. Results and discussion

3.1. MDCA and basicity of 2(S)-1-(ethylamonium)propane-2-ol (Fragment B)

The full PEHS of protonated Fragment B was investigated by geometry optimizations of the minima. All structures that converged were deprotonated of H_S and H_R, independently of each other, and then subject to further geometry optimizations. A full glossary (c.f. Table 1) and graphical representation (c.f. Fig. 4) of all converged protonated, H_S deprotonated, and H_R deprotonated minima is presented. Structural assignments for the conformational minima were made according to the conditions in Eq. (10).

gauche plus (g^+) = 60 (ideal) ± 60°

anti (a) = 180 (ideal) ± 60° (10)

gauche minus (g^-) = −60 (ideal) ± 60°.

This is based on the general observation that, if one were to rotate a tetrahedral carbon against another tetrahedral carbon, the minima would generally fall within the above ranges.

A total of 18 minima converged out of a possible 81 (22.2%) for the protonated PEHS of Fragment B (c.f. Table 2). As is clearly evident from the distribution of minima in Fig. 4, the dominant characteristic of all converged minima (protonated and deprotonated) was that all contained torsional angle χ_{10} (hydroxyl stereocentre) in the g^+ position. This was favoured because it

Table 1
Summary of converged conformational minima for the PEHS of 2(*S*)-1-(ethylamonium)propane-2-ol (Fragment B) at the RHF/3-21G level of theory for protonated (A), H_S (H16) deprotonated (B), and H_R (H21) deprotonated conformers (C) (F, Found; NF, Not Found; GM, Global Minima)

Conformational assignment				A	B	C	Conformational assignment				A	B	C	Conformational assignment				A	B	C
χ_4	χ_5	χ_6	χ_{10}				χ_4	χ_5	χ_6	χ_{10}				χ_4	χ_5	χ_6	χ_{10}			
g^+	g^+	g^+	g^+	F	F	F	a	g^+	g^+	g^+	F	NF	F	g^-	g^+	g^+	g^+	NF	NF	NF
g^+	g^+	g^+	a	NF	NF	NF	a	g^+	g^+	a	NF	NF	NF	g^-	g^+	g^+	a	NF	NF	NF
g^+	g^+	g^+	g^-	NF	NF	NF	a	g^+	g^+	g^-	NF	NF	NF	g^-	g^+	g^+	g^-	NF	NF	NF
g^+	g^+	a	g^+	NF	F	NF	a	g^+	a	g^+	F	NF	F	g^-	g^+	a	g^+	NF	NF	NF
g^+	g^+	a	a	NF	NF	NF	a	g^+	a	a	NF	NF	NF	g^-	g^+	a	a	NF	NF	NF
g^+	g^+	a	g^-	NF	NF	NF	a	g^+	a	g^-	NF	NF	NF	g^-	g^+	a	g^-	NF	NF	NF
g^+	g^+	g^-	g^+	NF	F	NF	a	g^+	g^-	g^+	F	NF	F	g^-	g^+	g^-	g^+	NF	NF	NF
g^+	g^+	g^-	a	NF	NF	NF	a	g^+	g^-	a	NF	NF	NF	g^-	g^+	g^-	a	NF	NF	NF
g^+	g^+	g^-	g^-	NF	NF	NF	a	g^+	g^-	g^-	NF	NF	NF	g^-	g^+	g^-	g^-	NF	NF	NF
g^+	a	g^+	g^+	F	NF	NF	a	a	g^+	g^+	F	F	F	g^-	a	g^+	g^+	F	F	NF
g^+	a	g^+	a	NF	NF	NF	a	a	g^+	a	NF	NF	NF	g^-	a	g^+	a	NF	NF	NF
g^+	a	g^+	g^-	NF	NF	NF	a	a	g^+	g^-	NF	NF	NF	g^-	a	g^+	g^-	NF	NF	NF
g^+	a	a	g^+	F	NF	F_{GM}	a	a	a	g^+	F_{GM}	F_{GM}	F	g^-	a	a	g^+	F	F	F
g^+	a	a	a	NF	NF	NF	a	a	a	a	NF	NF	NF	g^-	a	a	a	NF	NF	NF
g^+	a	a	g^-	NF	NF	NF	a	a	a	g^-	NF	NF	NF	g^-	a	a	g^-	NF	NF	NF
g^+	a	g^-	g^+	F	NF	F	a	a	g^-	g^+	F	F	NF	g^-	a	g^-	g^+	F	F	F
g^+	a	g^-	a	NF	NF	NF	a	a	g^-	a	NF	NF	NF	g^-	a	g^-	a	NF	NF	NF
g^+	a	g^-	g^-	NF	NF	NF	a	a	g^-	g^-	NF	NF	NF	g^-	a	g^-	g^-	NF	NF	NF
g^+	g^-	g^+	g^+	NF	NF	NF	a	g^-	g^+	g^+	NF	NF	NF	g^-	g^-	g^+	g^+	NF	NF	F
g^+	g^-	g^+	a	NF	NF	NF	a	g^-	g^+	a	NF	NF	NF	g^-	g^-	g^+	a	NF	NF	NF
g^+	g^-	g^+	g^-	NF	NF	NF	a	g^-	g^+	g^-	NF	NF	NF	g^-	g^-	g^+	g^-	NF	NF	NF
g^+	g^-	a	g^+	F	F	NF	a	g^-	a	g^+	NF	NF	NF	g^-	g^-	a	g^+	F	F	F
g^+	g^-	a	a	NF	NF	NF	a	g^-	a	a	NF	NF	NF	g^-	g^-	a	a	NF	NF	NF
g^+	g^-	a	g^-	NF	NF	NF	a	g^-	a	g^-	NF	NF	NF	g^-	g^-	a	g^-	NF	NF	NF
g^+	g^-	g^-	g^+	F	F	NF	a	g^-	g^-	g^+	F	F	F	g^-	g^-	g^-	g^+	F	F	F
g^+	g^-	g^-	a	NF	NF	NF	a	g^-	g^-	a	NF	NF	NF	g^-	g^-	g^-	a	NF	NF	NF
g^+	g^-	g^-	g^-	NF	NF	NF	a	g^-	g^-	g^-	NF	NF	NF	g^-	g^-	g^-	g^-	NF	NF	NF

allows the lone pairs of the oxygen atom (O11) to act as hydrogen bond acceptors towards the nitrogen proton(s). As such, conformers were stabilized by internal hydrogen bonds between O11 and either the H_S or H_R proton. The significance of this intramolecular hydrogen bonding is evident in the relative energies of the protonated conformers; all conformers with hydrogen bonding possesses relative energies below 4 kcal mol^{-1} while protonated conformers that lack the internal hydrogen bonding have relative energies between 6 and 13 kcal mol^{-1}. The hydrogen bond results in the formation of a five-membered ring as seen for the global minima of the protonated PEHS, $aaag^+$ (c.f. Fig. 5). Further, as indicated by the Newman projections in Fig. 2, the smallest steric hindrance occurs when the stereocentre χ_{10} is in the g^+ conformation, therefore, this stabilizing force adds to the prevalence of the g^+ conformation for torsional angle χ_{10}. The structural features of all converged protonated conformers are found in Table 3, Section 1.

Once the protonated PEHS of Fragment B was computed, the H_S and H_R protons were deprotonated as shown in Fig. 3. Upon deprotonation, SPE calculations were performed for each type of proton for each converged conformer and the non-optimized energy of deprotonation calculated (c.f. $\Delta E_{vert}(S)$ and $\Delta E_{vert}(R)$ in Table 2). It was found that conformers

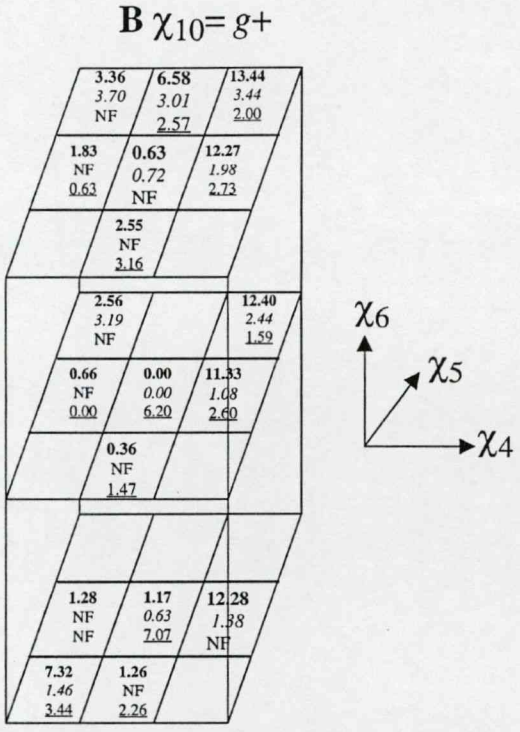

Fig. 4. Graphical summary of all converged conformational minima for the PEHS of 2(*S*)-1-(ethylamonium)propane-2-ol (Fragment B) at the RHF/3-21G level of theory. Relative energies are indicated as follows: bold values for converged protonated conformers, *italicized values* for converged H_S (H16) deprotonated conformers, and *underlined values* for converged H_R (H21) deprotonated conformers. Conformers which were not originally or subsequently found within a respective conformational assignment where at least one other minima converged are indicated with NF (Not Found). Blank spaces indicate conformational assignments that lacked any converged conformers. Note that all converged conformational minima possessed torsional angle χ_{10} in the g^+ conformation.

showed the greatest difference in the $\Delta E_{vert}(S)$ and $\Delta E_{vert}(R)$ energies of deprotonation when the conformers possessed hydrogen bonding between O11 with either of these two protons. In these instances, the proton not involved in hydrogen bonding was relatively easily deprotonated. However, the proton involved in hydrogen bonding possessed a larger energy of deprotonation because of its involvement in intramolecular stabilization. The latter trend was present for all protonated conformers possessing internal hydrogen bonding (c.f. 3.2 relative basicity of the H_S and H_R protons below).

After all non-optimized energies of deprotonation had been calculated, all H_S (c.f. Table 4) and H_R (c.f. Table 5) deprotonated conformers were subject to full geometry optimizations. Not every unique protonated conformed converged to a unique deprotonated conformer upon optimization (i.e. some deprotonated conformers converged to the same molecular conformation upon optimization). Of the H_S deprotonated conformers (c.f. Table 4), the global minima $aaag^+$ retained the intramolecular hydrogen bond, albeit a longer and weaker hydrogen bond (2.28 Å), between O11 and H_R found in the protonated global minima having the same conformation (c.f. Fig. 5). Of the H_R deprotonated conformers (c.f. Table 5), the global minima was found to be g^+aag^+. This conformer possessed a five-membered ring with a 2.27 Å hydrogen bond very similar to the H_S deprotonated global minima. Structural features of converged H_S and H_R deprotonated conformers are found in Table 3, Sections 2 and 3, respectively.

With regards to the structural features present in the deprotonated conformers, hydrogen bonding was not as dominant a stabilization force as that found for the protonated conformers. This was due to the fact that the lone pair now exposed on the nitrogen atom repelled the hydrogen bond donor lone pairs of O11. When the nitrogen was protonated and positively charged, an ion–dipole interaction was present between the nitrogen and oxygen atoms. Upon deprotonation, this interaction was removed. The repulsion experienced between the two heteroatoms is evident based on the much longer hydrogen bond distances in the optimized deprotonated conformers.

All deprotonated conformers, like the protonated PEHS conformers, possessed torsional angle χ_{10} in the g^+ position. To further investigate the persistence of this *gauche effect* on the conformational identity of Fragment B, PECs were computed according to Eq. (3). For both protonated and deprotonated Fragment B, PECs were generated with torsional angles χ_4, χ_5, and χ_6 in the *anti* position; however, for completeness, one PEC was generated with χ_4, χ_5, and χ_6 at optimized *anti* values (based on the $aaag^+$ conformation) and one PEC was generated with these three torsional angles frozen in the *anti* position at 180.00° (c.f. Fig. 6).

Table 2
Optimized minima for the PEHS of 2(*S*)-1-(ethylamonium)propane-2-ol (Fragment B) computed at the RHF/3-21G level of theory. Optimizations were followed by SPE calculations for independent deprotonation of H_S (H16) and H_R (H21) protons, denoted as $\Delta E_{vert}(S)$ and $\Delta E_{vert}(R)$, respectively

Conformational assignment				χ_4 degrees	χ_5 degrees	χ_6 degrees	χ_{10} degrees	E (hartree) protonated; deprotonated H_S; deprotonated H_R	Relative E; $\Delta E_{vert}(S)$; $\Delta E_{vert}(R)$ (kcal mol^{-1})
χ_4	χ_5	χ_6	χ_{10}						
g^+	g^+	g^+	g^+	57.38	66.37	58.14	70.70	−324.793727316; −324.383143312; −324.381925633	7.32; 257.65; 258.41
g^+	g^+	g^+	a					NOT FOUND MOVED TO $g^+ag^+g^+$	
g^+	g^+	g^+	g^-					NOT FOUND MOVED TO $g^+g^+g^+g^+$	
g^+	g^+	a	g^+					NOT FOUND MOVED TO g^+aag^+	
g^+	g^+	a	a					NOT FOUND MOVED TO g^+aag^+	
g^+	g^+	a	g^-					NOT FOUND MOVED TO g^+aag^+	
g^+	g^+	g^-	g^+					NOT FOUND MOVED TO g^+aag^+	
g^+	g^+	g^-	a					NOT FOUND MOVED TO g^+aag^+	
g^+	g^+	g^-	g^-					NOT FOUND MOVED TO $g^+ag^-g^+$	
g^+	a	g^+	g^+	77.45	155.53	66.95	66.96	−324.803348723; −324.370422703; −324.382241913	1.28; 271.67; 264.25
g^+	a	g^+	a					NOT FOUND MOVED TO $g^+ag^+g^+$	
g^+	a	g^+	g^-					NOT FOUND MOVED TO $g^+ag^+g^+$	
g^+	a	a	g^+	77.04	157.33	−179.56	67.45	−324.804338872; −324.370793410; −324.383547600	0.66; 272.05; 264.05
g^+	a	a	a					NOT FOUND MOVED TO g^+aag^+	
g^+	a	a	g^-					NOT FOUND MOVED TO g^+aag^+	
g^+	a	g^-	g^+	77.04	158.06	−75.46	67.12	−324.802468298; −324.369387191; −324.382362342	1.83; 271.76; 263.62
g^+	a	g^-	a					NOT FOUND MOVED TO $g^+ag^-g^+$	
g^+	a	g^-	g^-					NOT FOUND MOVED TO $g^+ag^-g^+$	
g^+	g^-	g^+	g^+					NOT FOUND MOVED TO aag^+g^+	
g^+	g^-	g^+	a					NOT FOUND MOVED TO aag^+g^+	
g^+	g^-	g^+	g^-					NOT FOUND MOVED TO aag^+g^+	
g^+	g^-	a	g^+	89.94	−98.15	179.17	65.87	−324.801304451; −324.376716678; −324.365840488	2.56; 266.43; 273.26
g^+	g^-	a	a					NOT FOUND MOVED TO $g^+g^-ag^+$	
g^+	g^-	a	g^-					NOT FOUND MOVED TO $g^+g^-ag^+$	
g^+	g^-	g^-	g^+	88.01	−100.37	−75.18	65.30	−324.800033440; −324.375899954; −324.365661207	3.36; 266.15; 272.57
g^+	g^-	g^-	a					NOT FOUND MOVED TO $g^+g^-g^-g^+$	
g^+	g^-	g^-	g^-					NOT FOUND MOVED TO $g^+g^-g^-g^+$	
a	g^+	g^+	g^+	160.44	84.73	75.97	51.78	−324.803380654; −324.370295100; −324.380697015	1.26; 271.77; 265.24
a	g^+	g^+	a					NOT FOUND MOVED TO $ag^+g^+g^+$	
a	g^+	g^+	g^-					NOT FOUND MOVED TO $ag^+g^+g^+$	
a	g^+	a	g^+	159.67	82.59	−178.21	50.43	−324.804820840; −324.371180064; −324.382020238	0.36; 272.11; 265.31
a	g^+	a	a					NOT FOUND MOVED TO ag^+ag^+	
a	g^+	a	g^-					NOT FOUND MOVED TO ag^+ag^+	
a	g^+	g^-	g^+	151.31	95.77	−64.00	50.51	−324.801332654; −324.366403815; −324.378430764	2.55; 272.92; 265.37
a	g^+	g^-	a					NOT FOUND MOVED TO $ag^+g^-g^+$	
a	g^+	g^-	g^-					NOT FOUND MOVED TO $ag^+g^-g^+$	

(*continued on next page*)

Table 2 (*continued*)

Conformational assignment				χ_4 degrees	χ_5 degrees	χ_6 degrees	χ_{10} degrees
χ_4	χ_5	χ_6	χ_{10}				
a	*a*	g^+	g^+	163.82	−160.12	74.88	52.72
a	*a*	g^+	*a*				
a	*a*	g^+	g^-				
a	*a*	*a*	g^+	163.43	−158.84	179.48	52.99
a	*a*	*a*	*a*				
a	*a*	*a*	g^-				
a	*a*	g^-	g^+	163.01	−157.12	−67.28	53.23
a	*a*	g^-	*a*				
a	*a*	g^-	g^-				
a	g^-	g^+	g^+				
a	g^-	g^+	*a*				
a	g^-	g^+	g^-				
a	g^-	*a*	g^+				
a	g^-	*a*	*a*				
a	g^-	*a*	g^-				
a	g^-	g^-	g^+	−175.68	−67.90	−56.89	47.87
a	g^-	g^-	*a*				
a	g^-	g^-	g^-				
g^-	g^+	g^+	g^+				
g^-	g^+	g^+	*a*				
g^-	g^+	g^+	g^-				
g^-	g^+	*a*	g^+				
g^-	g^+	*a*	*a*				
g^-	g^+	*a*	g^-				
g^-	g^+	g^-	g^+				
g^-	g^+	g^-	*a*				
g^-	g^+	g^-	g^-				
g^-	*a*	g^+	g^+	−65.71	179.45	71.69	61.00
g^-	*a*	g^+	*a*				
g^-	*a*	g^+	g^-				
g^-	*a*	*a*	g^+	−65.08	−178.48	−179.82	61.68
g^-	*a*	*a*	*a*				
g^-	*a*	*a*	g^-				
g^-	*a*	g^-	g^+	−64.62	−175.20	−70.01	62.22
g^-	*a*	g^-	*a*				
g^-	*a*	g^-	g^-				
g^-	g^-	g^+	g^+				
g^-	g^-	g^+	*a*				
g^-	g^-	g^+	g^-				

E (hartree) protonated; deprotonated H_S; deprotonated H_R	Relative E; $\Delta E_{ven}(S)$; $\Delta E_{ven}(R)$ (kcal mol^{-1})
−324.803518745; −324.382647073; −324.370596945	1.17; 264.10; 271.66
NOT FOUND MOVED TO aag^+g^+	
NOT FOUND MOVED TO aag^+g^+	
−324.805389226; −324.383705631; −324.371916613	0.00; 264.61; 272.01
NOT FOUND MOVED TO $aaag^+$	
NOT FOUND MOVED TO $aaag^+$	
−324.804392810; −324.382419825; −324.371475806	0.63; 264.79; 271.66
NOT FOUND MOVED TO aag^-g^+	
NOT FOUND MOVED TO aag^-g^+	
NOT FOUND MOVED TO aaag$^+$	
NOT FOUND MOVED TO $aaag^+$	
NOT FOUND MOVED TO $aaag^+$	
NOT FOUND MOVED TO aaag$^+$	
NOT FOUND MOVED TO $aaag^+$	
NOT FOUND MOVED TO $aaag^+$	
−324.794908573; −324.382377089; −324.382826135	6.58; 258.87; 258.59
NOT FOUND MOVED TO $ag^-g^-g^+$	
NOT FOUND MOVED TO aag^-g^+	
NOT FOUND MOVED TO $g^-ag^+g^+$	
NOT FOUND MOVED TO $g^-ag^+g^+$	
NOT FOUND MOVED TO $g^-ag^+g^+$	
NOT FOUND MOVED TO g^-aag^+	
NOT FOUND MOVED TO g^-aag^+	
NOT FOUND MOVED TO g^-aag^+	
NOT FOUND MOVED TO $g^-ag^-g^+$	
NOT FOUND MOVED TO g^-aag^+	
NOT FOUND MOVED TO $g^-ag^-g^+$	
−324.785812572; −324.384528756; −324.382471731	12.28; 251.81; 253.10
NOT FOUND MOVED TO $g^-ag^+g^+$	
NOT FOUND MOVED TO $g^-ag^+g^+$	
−324.787326426; −324.385190901; −324.384040306	11.33; 252.34; 253.07
NOT FOUND MOVED TO g^-aag^+	
NOT FOUND MOVED TO g^-aag^+	
−324.785836750; −324.383589352; −324.383583730	12.27; 252.41; 252.42
NOT FOUND MOVED TO $g^-ag^-g^+$	
NOT FOUND MOVED TO $g^-ag^-g^+$	
NOT FOUND MOVED TO $g^-ag^+g^+$	
NOT FOUND MOVED TO $g^-ag^+g^+$	
NOT FOUND MOVED TO $g^-ag^+g^+$	

g^-	g^-	a	g^+	−60.25	−69.11	−175.71	65.39	−324.785622305; −324.383378864; −324.384106841	12.40; 252.41; 251.95
g^-	g^-	g^-	a					NOT FOUND MOVED TO $g^-g^-ag^+$	
g^-	g^-	a	g^-					NOT FOUND MOVED TO $g^-g^-ag^+$	
g^-	g^-	g^-	g^+	−60.25	−67.59	−67.79	64.38	−324.783970218; −324.381707969; −324.383073438	13.44; 252.42; 251.57
g^-	g^-	g^-	a					NOT FOUND MOVED TO $g^-g^-g^+g^+$	
g^-	g^-	g^-	g^-					NOT FOUND MOVED TO $g^-g^-g^-g^+$	

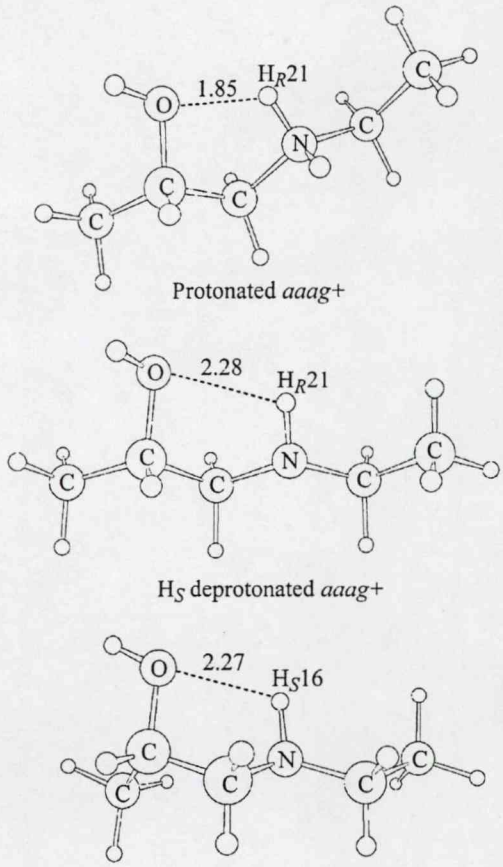

Fig. 5. Optimized global minima of the protonated Fragment B PEHS ($aaag^+$), H_S deprotonated Fragment B PEHS ($aaag^+$), and H_R deprotonated Fragment B PEHS (g^+aag^+).

For protonated Fragment B, one can see a profound *gauche effect* in both the χ_4-χ_5-χ_6-optimized and χ_4-χ_5-χ_6-frozen PECs. The χ_4-χ_5-χ_6-optimized PEC contains a deep minima about g^+, a very small minima at the *anti* conformation, and a very large barrier of rotation about the g^- position. The *gauche effect* is due to the hydrogen bonding prevalent in stable conformers between O11 and either nitrogen protons while the large barrier of rotation may be attributed to the repulsion between H12 and the positive nitrogen centre along with the steric hindrance between H12 and the Fragment B backbone. The *gauche effect* is exaggerated in

Table 3
Structural features of the converged protonated and deprotonated conformers of the 2(*S*)-1-(ethylamonium)propane-2-ol (Fragment B) PEHS. (All structures presented in this table were subject to full geometry optimizations at the RHF/3-21G level of theory)

Conformational assignment				#	Structural features	Relative E (kcal mol^{-1})
χ_4	χ_5	χ_6	χ_{10}			
I. Protonated conformers (BH^+)						
g^+	g^+	g^+	g^+	1	–	7.32
g^+	a	g^+	g^+	2	1.81 Å O11···H16 H-bond forming a 5-membered ring	1.28
g^+	a	a	g^+	3	1.83 Å O11···H16 H-bond forming a 5-membered ring	0.66
g^+	a	g^-	g^+	4	1.83 Å O11···H16 H-bond forming a 5-membered ring	1.83
g^+	g^-	a	g^+	5	1.74 Å O11···H21 H-bond forming a 5-membered ring	2.56
g^+	g^-	g^-	g^+	6	1.74 Å O11···H21 H-bond forming a 5-membered ring	3.36
a	g^+	g^+	g^+	7	1.80 Å O11···H16 H-bond forming a 5-membered ring	1.26
a	g^+	a	g^+	8	1.82 Å O11···H16 H-bond forming a 5-membered ring	0.36
a	g^+	g^-	g^+	9	1.75 Å O11···H16 H-bond forming a 5-membered ring	2.55
a	a	g^+	g^+	10	1.85 Å O11···H21 H-bond forming a 5-membered ring	1.17
a	a	a	g^+	11	1.85 Å O11···H21 H-bond forming a 5-membered ring	0.00
a	a	g^-	g^+	12	1.83 Å O11···H21 H-bond forming a 5-membered ring	0.63
a	g^-	g^-	g^+	13	–	6.58
g^-	a	g^+	g^+	14	–	12.28
g^-	a	a	g^+	15	–	11.33
g^-	a	g^-	g^+	16	–	12.27
g^-	g^-	a	g^+	17	–	12.4
g^-	g^-	g^-	g^+	18	–	13.44
II. H_S Deprotonated conformers (B)						
g^+	g^+	g^+	g^+		–	1.46
g^+	g^+	a	g^+		–	1.16
g^+	g^+	g^-	g^+		–	2.65
g^+	g^-	a	g^+		2.36 Å O11···H21 H-bond forming a 5-membered ring	3.19
g^+	g^-	g^-	g^+		2.32 Å O11···H21 H-bond forming a 5-membered ring	3.70
a	a	g^+	g^+		2.30 Å O11···H21 H-bond forming a 5-membered ring	0.63
a	a	a	g^+		2.28 Å O11···H21 H-bond forming a 5-membered ring	0.00
a	a	g^-	g^+		2.25 Å O11···H21 H-bond forming a 5-membered ring	0.72
a	g^-	g^-	g^+		–	3.01
g^-	a	g^+	g^+		–	1.38
g^-	a	a	g^+		–	1.08
g^-	a	g^-	g^+		–	1.98
g^-	g^-	a	g^+		–	2.44
g^-	g^-	g^-	g^+		–	3.44
III. H_R Deprotonated conformers (B)						
g^+	g^+	g^+	g^+		–	3.44
g^+	a	g^+	g^+		2.24 Å O11···H16 H-bond forming a 5-membered ring	0.74
g^+	a	a	g^+		2.27 Å O11...H16 H-bond forming a 5-membered ring	0.00
g^+	a	g^-	g^+		2.29 Å O11···H16 H-bond forming a 5-membered ring	0.63
a	g^+	g^+	g^+		2.36 Å O11···H16 H-bond forming a 5-membered ring	2.26
a	g^+	a	g^+		2.39 Å O11···H16 H-bond forming a 5-membered ring	1.47
a	g^+	g^-	g^+		2.34 Å O11···H16 H-bond forming a 5-membered ring	3.16
a	a	g^+	g^+		–	7.07
a	a	a	g^+		–	6.20
a	g^-	g^-	g^+		–	2.57
g^-	g^-	g^+	g^+		–	2.95
g^-	a	a	g^+		–	2.60
g^-	a	g^-	g^+		–	2.73
g^-	g^-	a	g^+		–	1.59
g^-	g^-	g^-	g^+		–	2.00

Table 4
Optimized conformational minima for the H_S (H16) deprotonated PEHS of 2(*S*)-1-(ethylamonium)propane-2-ol (Fragment B) at the RHF/3-21G level of theory

Optimized protonated conformation				Optimized deprotonated conformation				χ_4 degrees	χ_5 degrees	χ_6 degrees	χ_{10} degrees	*E* (hartree)	Relative *E* (kcal mol^{-1})	$\Delta E_{opt}(S)$ (kcal mol^{-1})	$\Delta\Delta E(S)$ (kcal mol^{-1})
χ_4	χ_5	χ_6	χ_{10}	χ_4	χ_5	χ_6	χ_{10}								
g^+	g^+	g^+	g^+	g^+	g^+	g^+	g^+	50.43	83.64	77.22	49.67	−324.394428616	1.46	250.56	7.09
g^+	*a*	g^+	g^+	g^+	g^+	g^+	g^+						1.46	256.60	15.07
g^+	*a*	*a*	g^+	g^+	g^+	*a*	g^+	50.95	84.16	−172.11	51.08	−324.394908988	1.16	256.92	15.13
g^+	*a*	g^-	g^+	g^+	g^+	g^-	g^+	56.57	83.85	−119.59	53.43	−324.392530627	2.65	257.24	14.52
g^+	g^-	*a*	g^+	g^+	g^-	*a*	g^+	64.42	−97.94	−165.27	56.27	−324.391676422	3.19	257.05	9.38
g^+	g^-	g^-	g^+	g^+	g^-	g^-	g^+	64.05	−104.16	−79.37	56.73	−324.390858084	3.70	256.76	9.39
a	g^+	g^+	g^+	*a*	*a*	g^+	g^+						0.63	255.78	15.99
a	g^+	*a*	g^+	*a*	*a*	*a*	g^+						0.00	256.06	16.05
a	g^+	g^-	g^+	*a*	*a*	g^-	g^+						0.72	254.60	18.32
a	*a*	g^+	g^+	*a*	*a*	g^+	g^+	−179.70	176.35	68.11	68.85	−324.395761426	0.63	255.87	8.23
a	*a*	*a*	g^+	*a*	*a*	*a*	g^+	179.76	−178.55	−178.61	68.55	−324.396758432	0.00	256.42	8.19
a	*a*	g^-	g^+	*a*	*a*	g^-	g^+	179.09	−176.55	−76.04	68.61	−324.395608581	0.72	256.52	8.27
a	g^-	g^-	g^+	*a*	g^-	g^-	g^+	−169.50	−62.51	−52.24	63.94	−324.391953903	3.01	252.86	6.01
g^-	*a*	g^+	g^+	g^-	*a*	g^+	g^+	−63.77	158.80	67.41	55.51	−324.394564704	1.38	245.51	6.30
g^-	*a*	*a*	g^+	g^-	*a*	*a*	g^+	−63.66	165.72	−176.33	55.45	−324.395037053	1.08	246.17	6.17
g^-	*a*	g^-	g^+	g^-	*a*	g^-	g^+	−63.79	165.45	−78.14	55.38	−324.393598336	1.98	246.13	6.28
g^-	g^-	*a*	g^+	g^-	g^-	*a*	g^+	−61.45	−67.54	−167.25	61.43	−324.392871990	2.44	246.45	5.96
g^-	g^-	g^-	g^+	g^-	g^-	g^-	g^+	−62.03	−70.31	−74.28	61.11	−324.391281427	3.44	246.42	6.00

Table 5
Optimized conformational minima for the H_R (H21) deprotonated PEHS of 2(*S*)-1-(ethylamonium)propane-2-ol (Fragment B) at the RHF/3-21G level of theory

Optimized protonated conformation				Optimized deprotonated conformation				χ_4 degrees	χ_5 degrees	χ_6 degrees	χ_{10} degrees	*E* (hartree)	Relative *E* (kcal mol^{-1})	$\Delta E_{opt}(R)$ (kcal mol^{-1})	$\Delta\Delta E(R)$ (kcal mol^{-1})
χ_4	χ_5	χ_6	χ_{10}	χ_4	χ_5	χ_6	χ_{10}								
g^+	g^+	g^+	g^+	g^+	g^+	g^+	g^+	51.28	62.71	57.55	56.22	−324.391921532	3.44	252.14	6.27
g^+	a	g^+	g^+	g^+	a	g^+	g^+	62.16	178.29	76.43	51.71	−324.396225633	0.74	255.47	8.78
g^+	a	a	g^+	g^+	a	a	g^+	61.53	−179.94	178.63	51.76	−324.397398012	0.00	255.36	8.69
g^+	a	g^-	g^+	g^+	a	g^-	g^+	61.10	−174.77	−67.91	51.53	−324.396390104	0.63	254.82	8.80
g^+	g^-	a	g^+	g^+	a	a	g^+						0.00	253.46	19.80
g^+	g^-	g^-	g^+	g^+	a	g^-	g^+						0.63	253.29	19.28
a	g^+	g^+	g^+	a	g^+	g^+	g^+	176.20	79.56	79.77	63.77	−324.393799336	2.26	257.02	8.22
a	g^+	a	g^+	a	g^+	a	g^+	175.64	75.73	174.34	63.35	−324.395057646	1.47	257.13	8.18
a	g^+	g^-	g^+	a	g^+	g^-	g^+	173.28	94.91	−71.86	63.65	−324.392355344	3.16	256.64	8.73
a	a	g^+	g^+	a	a	g^+	g^+	−166.91	−164.54	77.40	70.40	−324.386129069	7.07	261.92	9.74
a	a	a	g^+	a	a	a	g^+	−167.45	−165.09	175.81	70.54	−324.387523460	6.20	262.21	9.8
a	a	g^-	g^+	a	g^-	g^-	g^+						2.57	257.96	13.7
a	g^-	g^-	g^+	a	g^-	g^-	g^+	−168.04	−82.94	−77.07	70.83	−324.393306541	2.57	252.01	6.58
g^-	a	g^+	g^+	g^-	g^-	g^+	g^+	−61.38	−110.00	73.08	57.70	−324.392689804	2.95	246.69	6.41
g^-	a	a	g^+	g^-	a	a	g^+	−64.05	−156.73	176.23	60.89	−324.393253702	2.60	247.28	5.79
g^-	a	g^-	g^+	g^-	a	g^-	g^+	−63.12	−144.51	−68.17	60.18	−324.393040514	2.73	246.48	5.94
g^-	g^-	a	g^+	g^-	g^-	a	g^+	−62.99	−86.60	176.93	56.92	−324.394864360	1.59	245.20	6.75
g^-	g^-	g^-	g^+	g^-	g^-	g^-	g^+	−63.66	−89.52	−75.03	56.64	−324.394212001	2.00	244.58	6.99

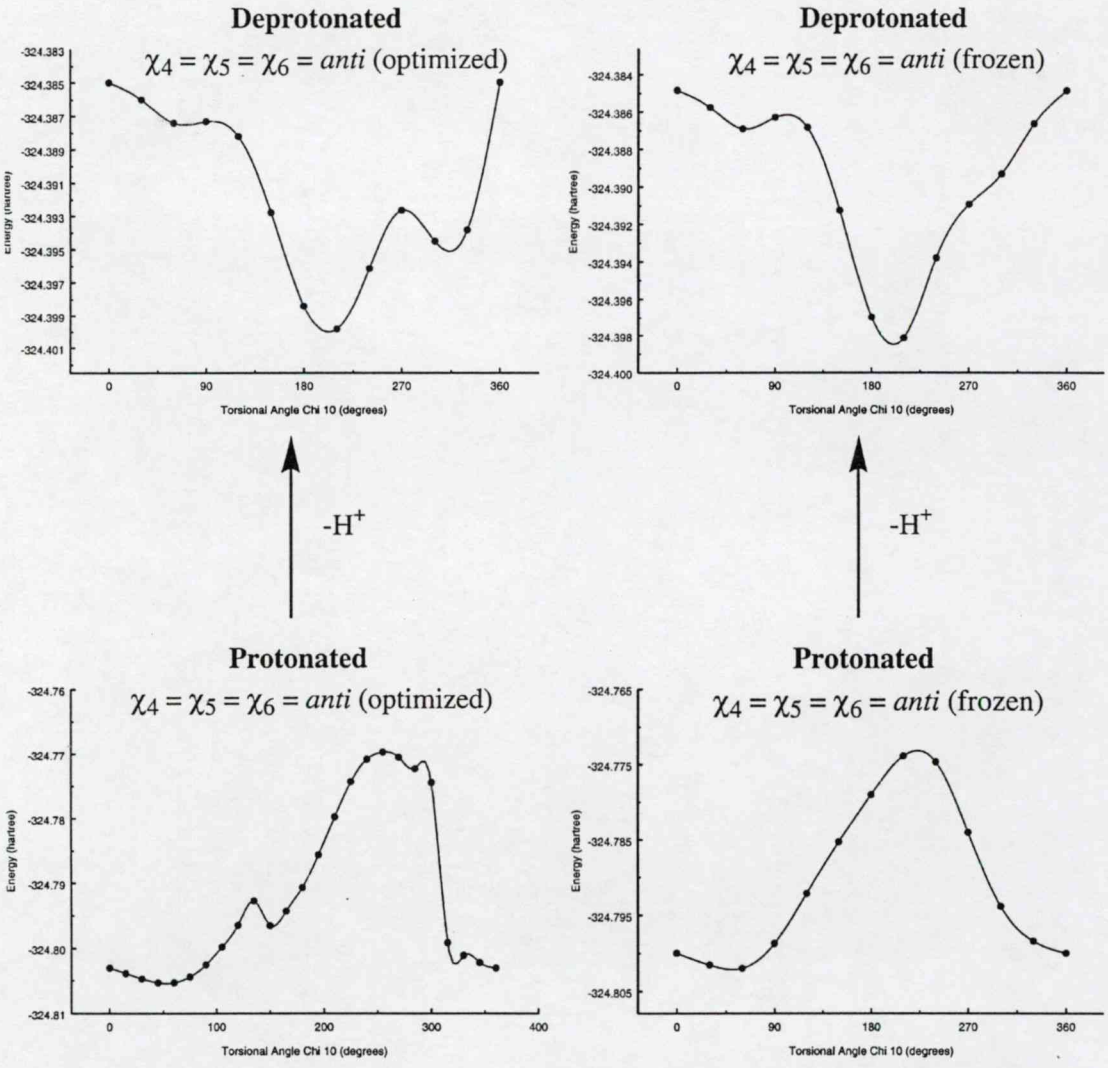

Fig. 6. PECs of torsional angle χ_{10} computed at the RHF/3-21G level of theory. PECs of protonated and deprotonated Fragment B with χ_4, χ_5, and χ_6 optimized and frozen in the *anti* conformation are shown.

the χ_4-χ_5-χ_6-frozen PEC, which lacks the subtle *anti* minima. This amplified *gauche effect* may be attributed to the inability of the H12, H_S, H_R, and $-CH_2-Z$ groups to avoid each other during the g^- rotation due to the freezing of the χ_4, χ_5, and χ_6 torsional angles.

Although only 22% of the possible protonated PEHS minima converged, this value may be revised in light of the *gauche effect* seen at the g^+ position for torsional angle χ_{10}. When one considers only the 27 conformational minima where χ_{10} is in the g^+ position, then 66.7% of conformers converged and were found for the protonated PEHS. Contrasting, zero minima converged for conformational assignments where torsional angle χ_{10} was either in

the *anti* or g^- position. This illustrates the dominant *gauche effect* in the conformational identity of Fragment B.

With regards to deprotonated Fragment B, a very different topological behaviour is depicted in the generated PECs (c.f. Fig. 6). The χ_4-χ_5-χ_6-optimized PEC possesses an *anti effect* and the significant g^+ *gauche effect* has been almost completely abolished and the large barrier of rotation in the g^- position has been replaced by a local minima. The χ_4-χ_5-χ_6-frozen PEC illustrates the same *anti effect*, however, the g^- local minima is absent from the PEC. The *anti effect* arises from the probable hydrogen bonding between H12 and the nitrogen lone pair when χ_{10} is in the *anti* position. The *anti* position also allows for hydrogen bonding between either nitrogen proton and O11.

Interestingly, although the PECs show this *anti effect*, it is completely absent from the geometrical optimizations of the deprotonated Fragment B minima (c.f. Table 4 and 5). This may be due in part to torsional angles χ_4, χ_5, and χ_6, which have a greater effect on the overall conformation than is evident from the PECs. Also, prevalence of the χ_{10} torsional angle in the g^+ conformation in protonated PEHS conformers (due to the *gauche effect* in the protonated structure), may largely determine the conformation that torsional angle χ_{10} assumes in the deprotonated state. This is said because hydrogen bonding alone is not deterministic of the g^+ conformation; the barrier of rotation (as indicated by the Newman projections) must also be taken into account. In other words, although hydrogen bonding seems to act as the dominant intramolecular stabilization force (as exemplified by the relative energies of hydrogen bonded conformers versus conformers that lack internal hydrogen bonding), it is not only in hydrogen bonded conformers that torsional angle χ_{10} adopts the g^+ conformation. Instead, all protonated and deprotonated conformers that do not possess internal hydrogen bonding still have the χ_{10} torsional angle oriented in the g^+ position. The latter further emphasizes the significance of the barrier of rotation that is deterministic of the conformational character of Fragment B and carvedilol's backbone. Therefore, the *gauche effect* in protonated Fragment B may influence the conformational identity of deprotonated Fragment B such that the *gauche effect* is still seen on the geometrically optimized minima of the deprotonated structures, although the PECs display an *anti effect* for torsional angle χ_{10}.

3.2. Relative basicity of the H_S and H_R protons

Carvedilol, with a pK_a of 7.9, is expected to be involved in a large number of protonophoretic pathways. At a physiological pH of 7.4, about two-thirds of the amino group is in its protonated form. To further study the basicity of the amino group, the relative basicity of the different protons, H_S and H_R, was investigated.

Initially, non-optimized energies of deprotonation ($\Delta E_{vert}(S)$ and $\Delta E_{vert}(R)$) revealed that conformers were subject to variable deprotonation energies dependent on whether or not one of the protons was involved in internal hydrogen bonding (c.f. Table 2). Upon comparing the differences in $\Delta E_{vert}(S)$ and $\Delta E_{vert}(R)$, it was found that conformers with no hydrogen bonding contained comparable energies of deprotonation for H_S and H_R, usually less that than 1 kcal mol^{-1} difference between the two protons (c.f. $|\Delta E_{vert}(S) - \Delta E_{vert}(R)|$ in Table 6). However, for conformers with internal hydrogen bonding, the hydrogen bonded proton usually required an additional 6–8 kcal mol^{-1} for deprotonation (c.f. Table 6). The latter trends are displayed in Fig. 7 (top) indicating that conformers with internal hydrogen bonding varied in $\Delta E_{vert}(S)$ and $\Delta E_{vert}(R)$ values, depending on which proton was involved in hydrogen bonding. However, conformers with no internal hydrogen bonding present displayed no such differences in their respective $\Delta E_{vert}(S)$ and $\Delta E_{vert}(R)$ energies of deprotonation since either proton could be abstracted with roughly the same investment of energy.

Upon optimization of deprotonated conformers, optimized energies of deprotonation were calculated for each H_S and H_R deprotonated conformer in Table 4 and 5, respectively, and in Table 6. As expected, geometry optimizations of the deprotonated conformers reduced the majority of differences between the H_S and H_R protons found in the non-optimized energies of deprotonation (c.f. Table 6). However, for the conformers aag^+g^+ and $aaag^+$, the H_R proton required an addition 6.05 and 5.79 kcal mol^{-1}, respectively, for deprotonation compared to the H_S proton (c.f. Fig. 7, middle). In

Table 6
Summary of energies of deprotonation and the differences found between H_S (H16) and H_R (H21) deprotonation for each converged conformation of 2(*S*)-1-(ethylamonium)propane-2-ol (Fragment B) at the RHF/3-21G level of theory

Protonated conformation				$\Delta E_{vert}(S)$ (kcal mol^{-1})	$\Delta E_{vert}(R)$ (kcal mol^{-1})	$\lvert\Delta E_{vert}(S) - \Delta E_{vert}(R)\rvert$ (kcal mol^{-1})	$\Delta E_{opt}(S)$ (kcal mol^{-1})	$\Delta E_{opt}(R)$ (kcal mol^{-1})	$\lvert\Delta E_{opt}(S) - \Delta E_{opt}(R)\rvert$ (kcal mol^{-1})	$\Delta\Delta E(S)$ (kcal mol^{-1})	$\Delta\Delta E(R)$ (kcal mol^{-1})	$\lvert\Delta\Delta E(S) - \Delta\Delta E(R)\rvert$ (kcal mol^{-1})
χ_4	χ_5	χ_6	χ_{10}									
g^+	g^+	g^+	g^+	257.65	258.41	0.76	250.56	252.14	1.58	7.09	6.27	0.82
g^+	a	g^+	g^+	271.67	264.25	7.42	256.60	255.47	1.13	15.07	8.78	6.29
g^+	a	a	g^+	272.05	264.05	8.00	256.92	255.36	1.56	15.13	8.69	6.44
g^+	a	g^-	g^+	271.76	263.62	8.14	257.24	254.82	2.42	14.52	8.80	5.72
g^+	g^-	a	g^+	266.43	273.26	6.83	257.05	253.46	3.59	9.38	19.80	10.42
g^+	g^-	g^-	g^+	266.15	272.57	6.42	256.76	253.29	3.47	9.39	19.28	9.89
a	g^+	g^+	g^+	271.77	265.24	6.53	255.78	257.02	1.24	15.99	8.22	7.77
a	g^+	a	g^+	272.11	265.31	6.80	256.06	257.13	1.07	16.05	8.18	7.87
a	g^+	g^-	g^+	272.92	265.37	7.55	254.60	256.64	2.04	18.32	8.73	9.59
a	a	g^+	g^+	264.10	271.66	7.56	255.87	261.92	6.05	8.23	9.74	1.51
a	a	a	g^+	264.61	272.01	7.40	256.42	262.21	5.79	8.19	9.8	1.61
a	a	g^-	g^+	264.79	271.66	6.87	256.52	257.96	1.44	8.27	13.7	5.43
a	g^-	g^-	g^+	258.87	258.59	0.28	252.86	252.01	0.85	6.01	6.58	0.57
g^-	a	g^+	g^+	251.81	253.10	1.29	245.51	246.69	1.18	6.30	6.41	0.11
g^-	a	a	g^+	252.34	253.07	0.73	246.17	247.28	1.11	6.17	5.79	0.38
g^-	a	g^-	g^+	252.41	252.42	0.01	246.13	246.48	0.35	6.28	5.94	0.34
g^-	g^-	a	g^+	252.41	251.95	0.46	246.45	245.20	1.25	5.96	6.75	0.79
g^-	g^-	g^-	g^+	252.42	251.57	0.85	246.42	244.58	1.84	6.00	6.99	0.99

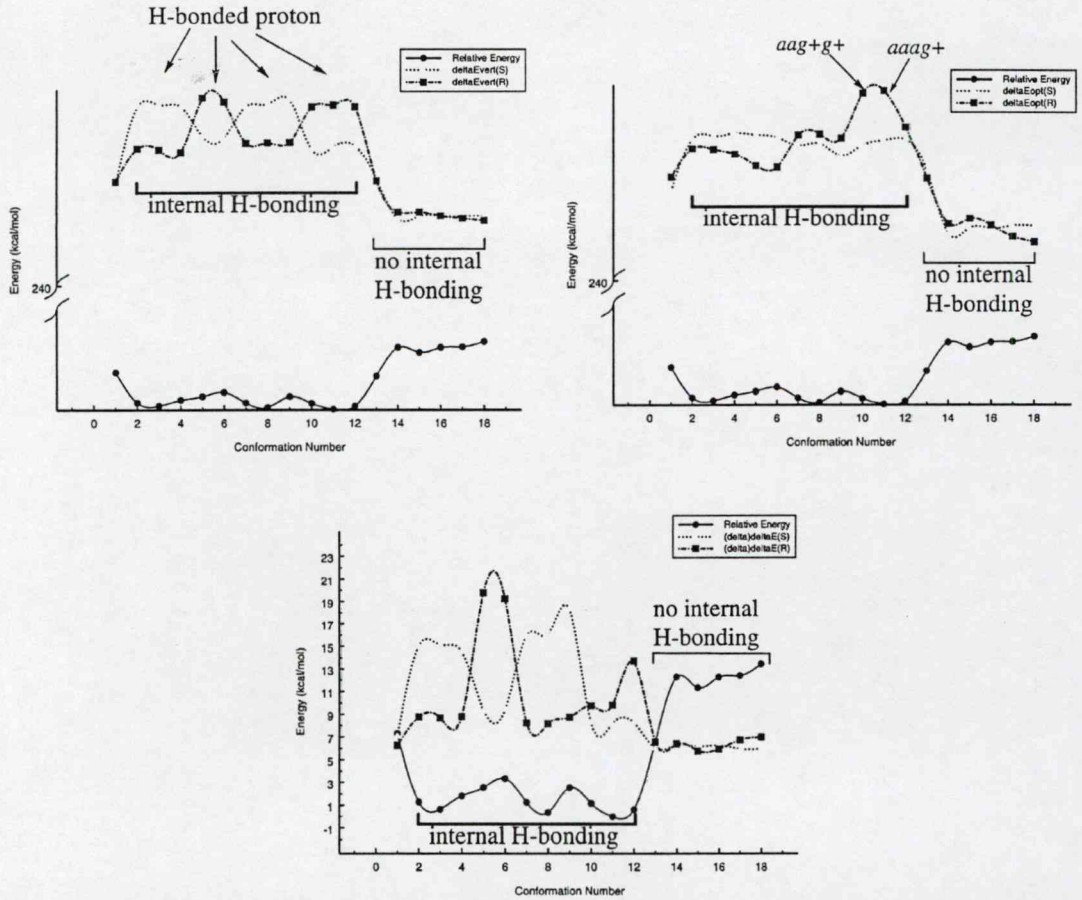

Fig. 7. Trends in $\Delta E_{vert}(S)$ and $\Delta E_{vert}(R)$ (top), $\Delta E_{opt}(S)$ and $\Delta E_{opt}(R)$ (middle), $\Delta\Delta E(S)$ and $\Delta\Delta E(R)$ (bottom) as compared to the relative energy of converged Fragment B conformational minima. (Conformation numbers are defined in Table 3.)

these conformers, the favoured formation of a five-membered ring due to hydrogen bonding between O11 and H_R made the deprotonation of H_R a more energetically demanding task. Deprotonation of these protons from Fragment B would require more energy to overcome the stabilization gained by the five-membered ring.

When analyzing the differences between non-optimized and optimized energies of deprotonation for the conformers, values denoted as $\Delta\Delta E(S)$ and $\Delta\Delta E(R)$ were used to compare the stabilization gained by a respective deprotonated conformer upon optimization (c.f. Table 6). H_S deprotonated conformers: $g^+ag^+g^+$, g^+aag^+, $ag^+g^+g^+$, ag^+ag^+, and $ag^+g^-g^+$; as well as H_R deprotonated conformers: $g^+g^-ag^+$ and $g^+g^-g^-g^+$ all had $\Delta\Delta E$ values greater than 15 kcal mol^{-1} (c.f. Table 6). These high $\Delta\Delta E$ values indicate that the optimized molecular conformation adopted conferred stability to the deprotonated fragment. This trend is similar to the vertical energies of deprotonation. Thus, if the proton abstracted is involved in intramolecular stabilization, then the $\Delta\Delta E$ values would be larger because a more significant molecular geometry rearrangement is necessary. This is opposed to the deprotonation of protons not involved in intramolecular interactions which would

not require major alterations in geometry (c.f. Fig. 7, bottom).

The overall trend shows that conformers devoid of large stabilization interaction had lower energies of deprotonation. This is to say, as the relative conformer energy increased, the SPE and optimized energies of deprotonation decreased (c.f. Fig. 7). Further, conformers with hydrogen bonding had an antagonistic behaviour present for the nitrogen protons; if the H_S proton was involved in hydrogen bonding, then the H_R proton was easily deprotonated and vice versa. Graphically, the latter is displayed as mirror-like increases and decreases in energies of deprotonation for different protons in hydrogen bonded conformers (c.f. conformations 2–12 in Fig. 7, top). However, no such behaviour was evident when no internal hydrogen bonding was present, causing both protons to have comparable energies of deprotonation (c.f. conformations 1, 13–18 in Fig. 7, top).

Calculated (optimized) energies of deprotonation for Fragment B range from the lowest of 244.58 kcal mol^{-1} for the H_R deprotonation of $g^-g^-g^-g^+$ to the highest of 262.21 kcal mol^{-1} for the H_R deprotonation of $aaag^+$. Previous work done on carvedilol has revealed energies of deprotonation of 234 and 238 kcal mol^{-1} for only two conformations of carvedilol, irrespective of the protons deprotonated, at the RHF/6-31G(d) level of theory [11]. These values, given the different basis sets and the fact that two are for whole carvedilol and the rest are for Fragment B, are comparable.

In considering the data, the route with the lowest energy of deprotonation is via the H_R deprotonation of conformer $g^-g^-g^-g^+$ (c.f. Fig. 8). This conformer possessed the highest relative energy of the protonated Fragment B PEHS (13.44 kcal mol^{-1}), lacking internal hydrogen bonding and minimizing the stabilization effect of the ion–dipole interaction

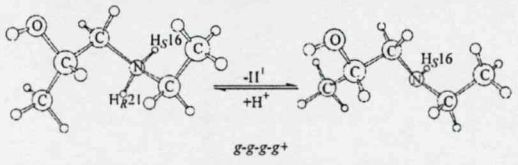

Fig. 8. Route of lowest energy of deprotonation (optimized) is via the H_R deprotonation of conformer $g^-g^-g^-g^+$ (244.58 kcal mol^{-1}).

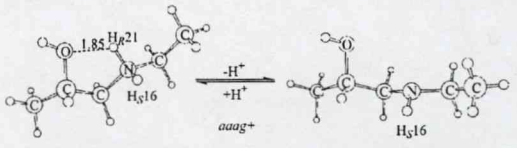

Fig. 9. Route of largest energy of deprotonation (optimized) is via the H_R deprotonation of conformer $aaag^+$ (262.21 kcal mol^{-1}).

between O11 and N5 by having the nitrogen atom and its protons pointing away from the hydroxyl group. As such, deprotonation of either protons was relatively easy

$$|\Delta E_{opt}(S) - \Delta E_{opt}(R)| = 246.42 - 244.58 = 1.84$$

kcal mol^{-1}) because the molecular conformation did not significantly bias any proton. Further, the $\Delta\Delta E$ values indicate that the stabilization gained by the molecular conformation adopted was not substantially large, about 6–7 kcal mol^{-1}.

Contrasting, the $aaag^+$ molecular conformation possessed the largest energy of deprotonation for the deprotonation of its H_R proton ($\Delta E_{opt}(R)$ value of 262.21 kcal mol^{-1}). This conformer also possessed a large difference in energy of deprotonation between the two protons with the H_R proton requiring an additional 5.79 kcal mol^{-1} for deprotonation. The $aaag^+$ conformation was the global minima of the protonated PEHS, possessing a 1.85 Å O11-H_R hydrogen bond forming a five-membered ring (c.f. Fig. 5). As illustrated in Fig. 9, this molecular conformation possesses an inherently difficult H_R deprotonation. Substantial stability was conferred by optimization of the deprotonated conformer as seen with the $\Delta\Delta E$ values (c.f. Table 6).

4. Conclusions

The data therefore indicates that for Fragment B, and extrapolating to carvedilol, events of deprotonation will favour conformations with minimal intramolecular stabilization, and therefore, larger relative energies. This includes minimizing hydrogen bonding and ion-dipole interactions between the positive nitrogen centre and electron lone pairs. Further, it may be expected that abstracted protons will be the ones oriented maximally away from the backbone of

carvedilol and Fragment B as seen with the H_R deprotonation of $g^-g^-g^-g^+$.

This may at first seem somewhat counter-intuitive because the usual emphasis is on finding very stable minima (with low relative energies) as the dominant representatives of PEHS. However, it is imperative that structures with large relative energies are not neglected because the data presented here suggests that different mechanisms will favour different structures. In the carvedilol protonophoretic pathway implicated in the uncoupling of oxidative phosphorylation, molecular conformations with high relative energies will be the best candidates for deprotonation. The latter would be expected especially when once considers that the uncoupling mechanism of proton shuttling requires carvedilol not only to be protonated, but also to be deprotonated upon crossing back into the matrix of the mitochondria. A very stable structure that takes up a proton in the intermembrane space would not be favoured for deprotonation in the matrix. Rather, a structure with minimal stabilization and a decreased basic character would be most accessible to enzymes, substrates, and favoured in protonophoretic pathways as that postulated for carvedilol in the uncoupling of oxidative phosphorylation in the mitochondria.

References

[1] W. Carlson, K.J. Oberg, Cardiovasc. Pharmacol. Ther. 4 (1999) 205.

[2] M. Packer, M.R. Bristow, J.N. Cohn, W.S. Colucci, M.B. Fowler, E.M. Gilbert, N.H Shusterman, N. Engl. J. Med. 334 (1996) 1349.

[3] M.A. Berg, G.A. Chasse, E. Deretey, A.K. Fuzery, B.M. Fung, D.Y.K. Fung, H. Henry-Riyad, A.C. Lin, M.L. Mak, A. Mantas, M. Patel, I.V. Repyakh, M. Staikova, S.J. Salpietro, Ting-Hua Tang, J.C. Vank, A. Perczel, G.I. Csonka, O. Farkas, L.L. Torday, Z. Szekely, I.G. Csizmadia, J. Mol. Struct. (THEOCHEM) 500 (2000) 5.

[4] S. Capomolla, O. Febo, M. Gnemmi, G. Riccardi, C. Opasich, A. Carporotondi, A. Mortara, G. Pinna, F. Cobelli, Am. Heart J. 139 (2000) 596.

[5] M. Metra, S. Nodari, A. D'Aloia, L. Bontempi, E. Boldi, L. Dei Cas, Am. Heart J. 139 (2000) 511.

[6] G. Feuerstein, R.R. Ruffolo Jr., Adv. Pharmacol. 42 (1998) 611.

[7] O. Saijonmaa, K. Metsarinne, F. Fyhrquist, Blood Press. 6 (1997) 24.

[8] G. Feuerstein, T.L. Yue, X. Ma, R.R. Ruffolo, Prog. Cardiovasc. Dis. 41 (1 Suppl 1) (1998) 17.

[9] A.J.F. Searlee, C. Gree, R.L. Wilson, Ellipticines and carbazoles as antioxidants, in: W. Borns, M. Saran, D. Tait (Eds.), Oxygen Radicals and Biology, Walter de Gruyter & Co, Berlin, 1984, pp. 377–381.

[10] D.R. Howlett, A.R. George, D.E. Owen, R.V. Ward, R.E. Markwell, Biochemical Journal 343 (1999) 419.

[11] P.J. Oliveira, M.P. Marques, L.A.E. Batista de Carvalho, A.J.M. Moreno, Biochemical and Biophysical Research Communications 276 (2000) 82.

[12] R.J. Ferrari, Cardiovasc. Pharmacol. 28 (1996) S1.

[13] P.G. Heytler, Uncouplers of Oxidative Phosphorylation, Methods in Enzymology, LV, Academic Press, New York, 1979, pp. 462-472.

[14] A. Tzagoloff, Mitochondria, Plenum Press, New York, 1982.

[15] S.S. Korshunov, V.P. Skulachev, A.A. Starkov, FEBS Lett. 416 (1997) 15.

[16] H.G. Oldham, S.E. Clarke, Drug Metab. Dispos. 25 (1997) 970.

[17] R.R. Ruffolo Jr., M. Gellai, J.P. Hieble, R.N. Willette, A.J. Nichols, Eur. J. Clin. Pharmacol. 38 (1990) S82.

[18] R. Feuerstein, T.L. Yue, Pharmacology 48 (1994) 385.

[19] T.L. Yue, P.J. Mckenna, P.G. Lysko, J.L. Gu, K.A. Lysko, R.R. Ruffolo Jr., G.Z. Feuerstein, Eur. J. Pharmacol. 251 (1994) 237.

[20] D.R.P. Almeida, L.F. Pisterzi, G.A. Chass, L.L. Torday, A. Varro, J. Gy. Papp, I.G.J. Csizmadia, Phys. Chem. A 106 (43) (2002) 10423.

[21] M.J. Frisch, G.W. Trucks, H.B. Schlegel, G.E. Scuseria, M.A. Robb, J.R. Cheeseman, V.G. Zakrzewski, J.A. Montgomery, Jr., R.E. Stratmann, J.C. Burant, S. Dapprich, J.M. Millam, A.D. Daniels, K.N. Kudin, M.C. Strain, O. Farkas, J. Tomasi, V. Barone, M. Cossi, R. Cammi, B. Mennucci, C.Pomelli, C. Adamo, S. Clifford, J. Ochterski, G.A. Petersson, P.Y. Ayala, Q. Cui, K. Morokuma, D.K. Malick, A.D. Rabuck, K. Raghavachari, J.B. Foresman, J. Cioslowski, J.V. Ortiz, A.G. Baboul, B.B. Stefanov, G. Liu, A. Liashenko, P. Piskorz, I. Komaromi, R. Gomperts, R.L. Martin, D.J. Fox, T. Keith, M.A. Al-Laham, C.Y. Peng, A. Nanayakkara, C. Gonzalez, M. Challacombe, P.M.W. Gill, B.G. Johnson, W. Chen, M.W. Wong, J.L. Andres, M. Head-Gordon, E.S. Replogle, J.A. Pople, GAUSSIAN 98 (Revision A.9), Gaussian, Inc., Pittsburgh PA, 1998.

Molecular Study on the Enantiomeric Relationships of Carvedilol Fragment A, 4-(2-Hydroxypropoxy)carbazol, along with Selected Analogues

David R. P. Almeida,*,†,‡ Donna M. Gasparro,†,‡ Luca F. Pisterzi,† Ladislaus L. Torday,§ Andras Varro,§ Julius Gy. Papp,§,∥ Botond Penke,⊥ and Imre G. Csizmadia†

Department of Chemistry, Lash Miller Laboratories, 80 Saint George Street, University of Toronto, Toronto, Ontario, Canada M5S 3H6, Department of Pharmacology and Toxicology, Faculty of Medicine, Medical Sciences Building, University of Toronto, Toronto, Ontario, Canada M5S 1A8, Department of Pharmacology and Pharmacotherapy, Szeged University, Dom ter 12, Szeged, Hungary-6701, Division of Cardiovascular Pharmacology, Hungarian Academy of Sciences and Szeged University, Dom ter 12, Szeged, Hungary-6701, and Institute of Medical Chemistry, Szeged University, Dom ter 8, Szeged, Hungary-6720

Received: January 15, 2003; In Final Form: May 15, 2003

Chirality and activity relationships are paramount to pharmaceutical design and synthesis. Generally, point chirality (enantiomeric *R* and *S* configurations) is emphasized most in molecules and drugs; however, axis chirality (present when structures adopt conformations with asymmetrical distributions of electron density) must also be considered as a stereogenic unit of interest. Together, stereogenic units and optical isomerism describe the chiral disposition of electron density about nuclei. In this essence, different components of chirality are always present in molecular systems. In assessing the different chiral parameters of pharmaceuticals, the cardiovascular drug carvedilol serves as an ideal example because both enantiomers produce different physiological effects. In the current study, *R*- and *S*-4-(2-hydroxypropoxy)carbazol (carvedilol fragment A), along with prochiral and chiral analogues, are studied to investigate the chiral components of carvedilol. Further, the effects of substituent variation about a stereocenter are investigated and discussed using conformational energy as a surrogate of structure (based on the fact that energy is a function of molecular spatial orientation) to determine the energetic equivalency of prochiral and chiral structures. Multidimensional conformational analysis (MDCA) was performed on selected structures using restricted Hartree−Fock (RHF) and density functional theory (DFT with the Becke 3LYP hybrid exchange-correlation functional) molecular orbital computations to elucidate the structural and energetic basis of chirality. The analogues had the following prochiral and chiral structures: R−CH_2−OH, [*R*] and [*S*] R−CHMe−OH, and R−CMe_2−OH, with substituent R being either $MeCH_2$- or $ArCH_2$-, where Ar is the carbazole moiety. Potential energy curves (PECs) of torsional angles χ_1, χ_2, χ_3, and χ_{10} for *R*- and *S*-4-(2-hydroxypropoxy)carbazol verified that all torsional angles are indeed enantiomeric. Correspondingly, the potential energy hypersurfaces (PEHSs) of *R*- and *S*-4-(2-hydroxypropoxy)carbazol were also enantiomeric, as illustrated with optimizations of conformational minima; converged minima occurred in equivalent point chiral and axis chiral pairs. Similarly to *R*- and *S*-4-(2-hydroxypropoxy)carbazol, achiral and chiral analogues analyzed by MDCA displayed axis chirality while chiral structures displayed both axis and point chirality. As such, the presence of point and axis chirality in molecular systems allows predictions to be made concerning the orientations of viable conformations of a respective PEHS. Further, the data indicate that chirality induced by an asymmetric distribution of electron density (axis chirality) is always present whenever a structure adopts asymmetric conformations. Like enantiomers of point chirality, axis chiral conformers also occur in pairs. Potential energy surfaces (PESs) were generated about the prochiral and chiral centers for all structures at the RHF/3-21G level of theory and used to test the equivalency of conformational energy between sufficiently constructed achiral and chiral structures. It is hypothesized that, with regard to conformational energy, the addition of two chiral enantiomers minus the addition of two achiral structures will give a zero result (assuming the only structural differences occur at the stereocenters). The combination of prochiral and chiral potential energy surfaces, according to an equation describing two consecutive and concerted methyl substitutions, gave a practically flat, virtually zero surface, indicating that sufficiently constructed achiral structures are energetically equivalent to chiral enantiomers. Thus, solely on the basis of molecular structure, chiral properties such as energy, number of converged conformers in a PEHS, conformations of corresponding point chiral and axis chiral pairs, and intramolecular interactions can be predicted from achiral structures. It remains to be seen how this can be utilized in drug research and development.

1. Introduction

1.1. Chirality in Pharmaceutical Agents: The Thalidomide Disaster. Thalidomide, prescribed from 1957 to 1962 as an exceptionally safe sedative/hypnotic in adults for morning sickness, was later found to be a teratogen (capable of creating malformations in embryos). Thalidomide was blamed for having caused serious birth defects such as phocomelia (infants born without normal arms and legs) in more than 10 000 babies. Retrospective studies linked these birth defects with the mother's ingestion of thalidomide during the third to eighth week of pregnancy.

Thalidomide has one carbon stereocenter and exists as two optically active enantiomers (*R* and *S*). Tests with mice in 1961

* Corresponding author. E-mail: dalmeida@medscape.com.
† Department of Chemistry, University of Toronto.
‡ Department of Pharmacology and Toxicology, University of Toronto.
§ Department of Pharmacology and Pharmacotherapy, Szeged University.
∥ Division of Cardiovascular Pharmacology, Hungarian Academy of Sciences and Szeged University.
⊥ Institute of Medical Chemistry, Szeged University.

10.1021/jp030057i CCC: $25.00
Published on Web 07/01/2003

suggested that only one enantiomer was teratogenic while the other possessed the desired therapeutic activity. However, subsequent tests on rabbits showed that both enantiomers had the same physiological activities. This is initially counterintuitive because one would expect enantiomers to interact quite differently with the various chiral molecules of nature. It was later verified that the enantiomers of thalidomide interconvert (racemize) under physiological conditions, causing both enantiomers to appear in the blood in roughly equal quantities.[1] Therefore, an optically or enantiomerically pure sample (containing only one enantiomer) of thalidomide versus a racemic mixture (of both enantiomers) would still produce teratogenic effects. As such, not approving thalidomide, as was done in the U.S., was the only method to prevent the thalidomide disaster.

Thalidomide is a dramatic example that chirality and activity relationships are significant to drug designers and the pharmaceutical industry, as many drug molecules synthesized exert pharmacological and physiological activities via enantiomeric-selective routes. The Food and Drug Administration (FDA) policy, published in 1992, strongly urges companies to evaluate racemates and enantiomers for new drugs for the purposes of finding the safest, most effective pharmaceuticals.[2] Methods such as computerized predictions use computational tools to predict single-enantiomer activities before separating a racemate.[3] This saves time in pharmaceutical research and helps identify the active enantiomer, leading to safer drugs. It is thus of interest to the pharmaceutical industry, and to drug research in general, to evaluate chirality exhaustively as a means to design drugs with the largest possible safety profiles.

1.2. Stereogenic Units. The importance of a point chiral stereogenic unit, as illustrated with the right-handed (*R*) or left-handed (*S*) stereocenter, is widely accepted in bio-organic chemistry. Point chiral *R* and *S* enantiomers have the same physical properties but can produce different biological and physiological effects in a molecular environment with an asymmetrical disposition (e.g., nonselective β-adrenergic receptor antagonism by *S*[−] carvedilol). Contrasting, enantiomers may also produce the same biological effects when they interact with a symmetrical molecular environment (e.g. both enantiomers of carvedilol have equal α_1-adrenergic antagonist capabilities and antioxidant activity).

However, an asymmetric center can act not only as a stereogenic unit but also as an axis as well. Axis chirality, resulting from a clockwise [to *g*+ or plus (P)] or counterclockwise [to *g*− or minus (M)] conformational twist, is an important phenomenon in the field of chirality. The presence of axis chirality occurs when molecular structures adopt conformations with asymmetrical electron distributions; for a given prochiral or point chiral (*R* and *S*) structure, an asymmetric molecular formation (e.g. *g*+) will have an energetically equivalent conformation with the corresponding axis chirality (e.g. *g*−). Axis chirality may play a significant role in molecular recognition or in docking at chiral active sites of enzymes or receptors. In assuming a unified viewpoint, one might say that optical isomerism provides evidence about the chiral disposition of electron density in space around the nuclei. The chirality of the electron density is always there irrespective of whether it is associated with a carbon carrying four different substituents (i.e. point chirality) or it is associated with the asymmetric electron distribution caused by a conformation twist (i.e. axis chirality).

In dealing with these two types of chirality, we may acknowledge the following convention for conformational twist:[4−6]

$$g+ \text{ or } \mathrm{P} \rightarrow S$$
$$g- \text{ or } \mathrm{M} \rightarrow R$$

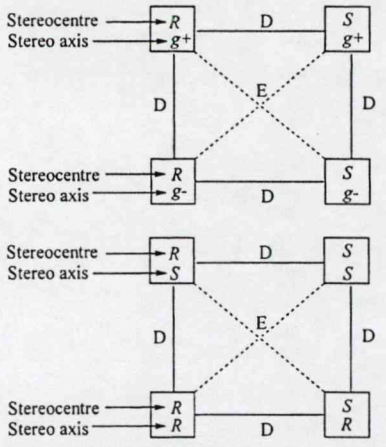

Figure 1. Schematic illustration of enantiomeric (E) and diastereomeric (D) relationships for a system with one point chiral stereocenter and one stereo axis of rotation (i.e. axis chiral plane about an adjacent C−C bond) as stereogenic units.

In view of that, having one stereocenter and one rotation about an adjacent C−C bond, we may recognize four stereoisomers with enantiomeric (E) and diastereomeric (D) relationships, as shown in Figure 1.

It is then evident that, in the case of multiple rotors, the enantiomeric and diastereomeric relations are not always obvious at first sight. In the present work, we wish to report such relationships for a key fragment of the drug molecule carvedilol, 1-(9H-carbazol-4-yloxy)-3-[2-(2-methoxyphenoxy)ethylamino]-2-propanol. Fragment A of carvedilol has one stereocenter (point chiral *R* and *S* forms) and four torsional modes of motion (torsional angles) which determine the conformation of the molecular structure and the associated axis chiral parameters. Thus, fragment A has a total of five stereogenic units. It is relevant to study the characteristics of the different chiral forms of carvedilol because of its unique pharmacological profile (i.e. the two enantiomers of carvedilol possess different biological effects). The objectives of the current work are twofold: first, decompose and quantify the different chiral components of carvedilol fragment A to illustrate its full chiral profile; second, address the effects of substituent variation about a stereocenter and the basis of energetic equivalency between prochiral and chiral compounds. Conformational energy will be used as a surrogate for molecular structure because changes in structure, such as alterations in the substituents at a stereocenter, can be quantified by changes in energy. The relative effects can then be compared for given sets of compounds.

1.3. Biological and Medical Background. Carvedilol ($C_{24}H_{26}N_2O_4$) is a cardiovascular drug of proven efficacy in the treatment of mild to moderate congestive heart failure (CHF), essential hypertension, and angina and in improvement of left ventricular function. Carvedilol is a lipophilic autonomic nervous system agent that acts as a multiple-action neurohormonal antagonist by producing nonselective β-blockage (β_1 and β_2) and selective α-blockage (α_1), while also possessing myocardial-protective antioxidant properties.[7,8]

In dealing with chronic heart failure and hypertension, β-blockers block the activity of cardiac β-adrenergic receptors (both β_1 and β_2) to noradrenaline reducing the total cardiac workload of the heart.[9,10] Carvedilol provides further positive effects by vasodilation (α_1-adrenergic blockage) at peripheral resistance vessels, which decreases preload and after-load, thereby further reducing cardiac work and wall tensions.[11,12]

The US Data and Safety Monitoring Board (US DSMB) stopped, for ethical reasons, the clinical investigation of carvedilol before its completion due to greatly lowered mortality rates.[13]

As an antioxidant, the carbazole ring of carvedilol is highly reactive with oxygen-containing radicals. Carbazole possesses a low redox potential which gives carvedilol and its metabolites a powerful tendency to donate electrons more readily in order to "scavenge" the activities of reactive oxygen species (ROS) such as oxygen superoxide ($O_2^{\bullet -}$), hydrogen peroxide (H_2O_2), hydroxyl radical ($^{\bullet}OH$), and peroxynitrite ($ONOO^-$), and as a result, it helps to protect the living body from the deleterious effects of free radical damage.[14] Carvedilol's free-radical scavenging ability against lipid peroxidation is enhanced by its relatively high lipid solubility.[15] Of interest, some of carvedilol's metabolites are more effective than carvedilol itself as antioxidants due to the fact that a hydroxyl group substitution in a heterocyclic ring, such as that of carbazole, increases the molecular antioxidant action of a compound.[13,16,17,18]

1.4. Chemical Background. Carvedilol is a chiral drug molecule (with 1 point chiral strereocenter and 11 torsional modes) commercially available as a racemic mixture of both its enantiomers (*R*[+] and *S*[−]) (cf. Figure 2). The enantiomers of carvedilol show marked stereoselective properties in that both enantiomers have equal α_1 blocking activity and antioxidant activity but only the *S*[−] enantiomer contains the nonselective β-adrenergic blocking activity.[16] Further, along with carvedilol, three of its hydroxylated metabolites have marked antioxidant properties while being devoid of either α_1- or β-adrenergic blocking activity (cf. Figure 2).[19,20] This represents a situation in which both enantiomers of an optically active drug offer different beneficial effects to the patient. As such, the enantiomers differ not only quantitatively in terms of potency but also qualitatively in that they possess distinct pharmacologic profiles and neither enantiomer alone has the same pharmacologic profile as the racemic mixture of carvedilol used clinically.[21]

Carvedilol was divided into three structural fragments according to its chemical activity: *R*- and *S*-4-(2-hydroxypropoxy)-carbazol (fragment A) is the antioxidant and β-blocker portion of carvedilol, 2(*R* and *S*)-1-(ethylamonium)propane-2-ol (fragment B) connects the two ether oxygens of carvedilol and possesses the protonophoretic amino group involved in the uncoupling of oxidative phosphorylation in the mitochondria,[22] and aminoethoxy-2-methoxy-benzene (fragment C) is the structure responsible for the α-blocker action of carvedilol (cf. Figure 3).

This study focuses on the chiral interactions and relationships of carvedilol by analyzing fragment A (structures **I-*R*** and **I-*S***; cf. Figure 4), because this fragment contains the antioxidant carbazole ring system and the same point chiral stereocenter of carvedilol. Analysis was also carried out on prochiral and chiral variations of fragment A and its noncarbazole analogue. The stereocenter of fragment A is found at C24, and each of the enantiomers constitute the potential energy hypersurface (PEHS) with torsional angles χ_1, χ_2, χ_3, and χ_{10} as described by eq 1 (cf. Figure 4). The torsional angle χ_4, which is associated with the terminal methyl group, was not included because it comprises a symmetrical methyl rotation.

$$E = f(\chi_1, \chi_2, \chi_3, \chi_{10}) \tag{1}$$

The six structures—2-methoxyethan-1-ol (analogue **IV-H$_2$**), 1-methoxy-2-methylpropane-2-ol (analogue **IV-Me$_2$**), (2*S*)-1-methoxypropan-2-ol (analogue **III-[H,Me]-*S***), (2*R*)-1-methoxypropan-2-ol (analogue **III-[H,Me]-*R***), (2-hydroxyethoxy)-carbazol (analogue **II-H$_2$**), and (2-hydroxy-2-methylethoxy)carbazol (analogue **II-Me$_2$**)—are presented and defined in Figure 4. The respective PEHSs of the four carbazole-containing structures can all be described by eq 1 while the remaining four structures can be described by eq 2.

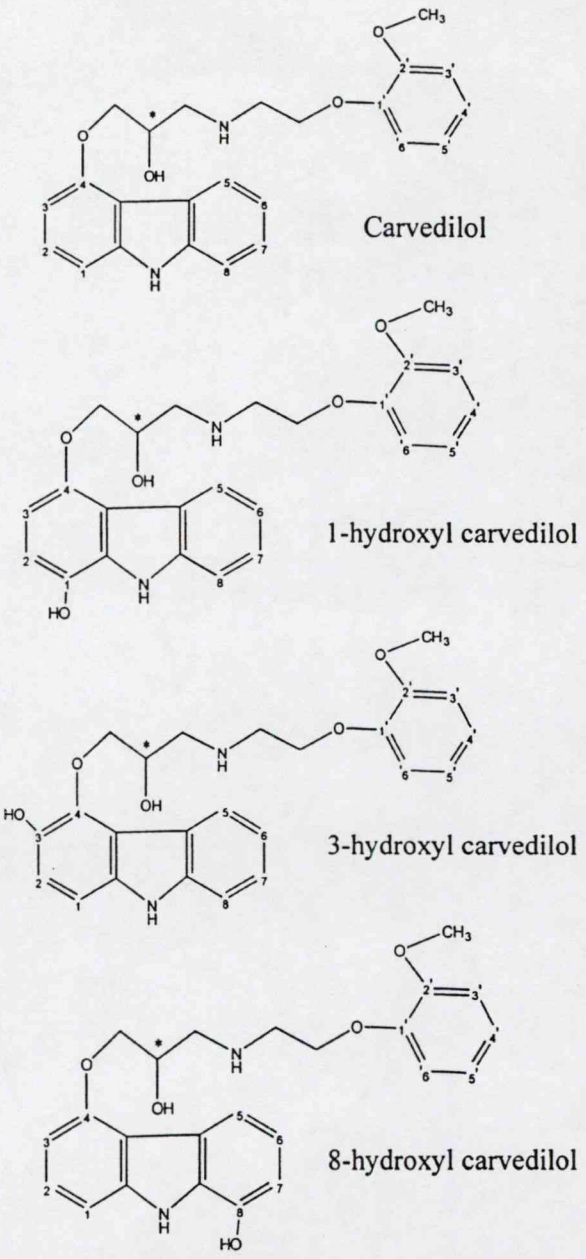

Figure 2. Structure of carvedilol and its antioxidant metabolites (IUPAC numbering used and stereocenter indicated by *).

$$E = f(\chi_2, \chi_3, \chi_{10}) \tag{2}$$

Structures **IV-H$_2$**, **IV-Me$_2$**, **III-[H,Me]-*S***, and **III-[H,Me]-*R*** were constructed by replacing the bulky carbazole ring system with the simplest alkyl group, a methyl substituent. The backbone present in carvedilol, and in **I-*R*** and **I-*S***, remained in all structures with the exceptions that **IV-H$_2$** was devoid of the methyl group formerly present at the chiral center while **IV-Me$_2$** was constructed with two methyl groups at the former chiral center, and consequently, both of these analogues are achiral. Structures **III-[H,Me]-*R*** and **III-[H,Me]-*S*** retained the chirality present in carvedilol. Analogues **II-H$_2$** and **II-Me$_2$** were con-

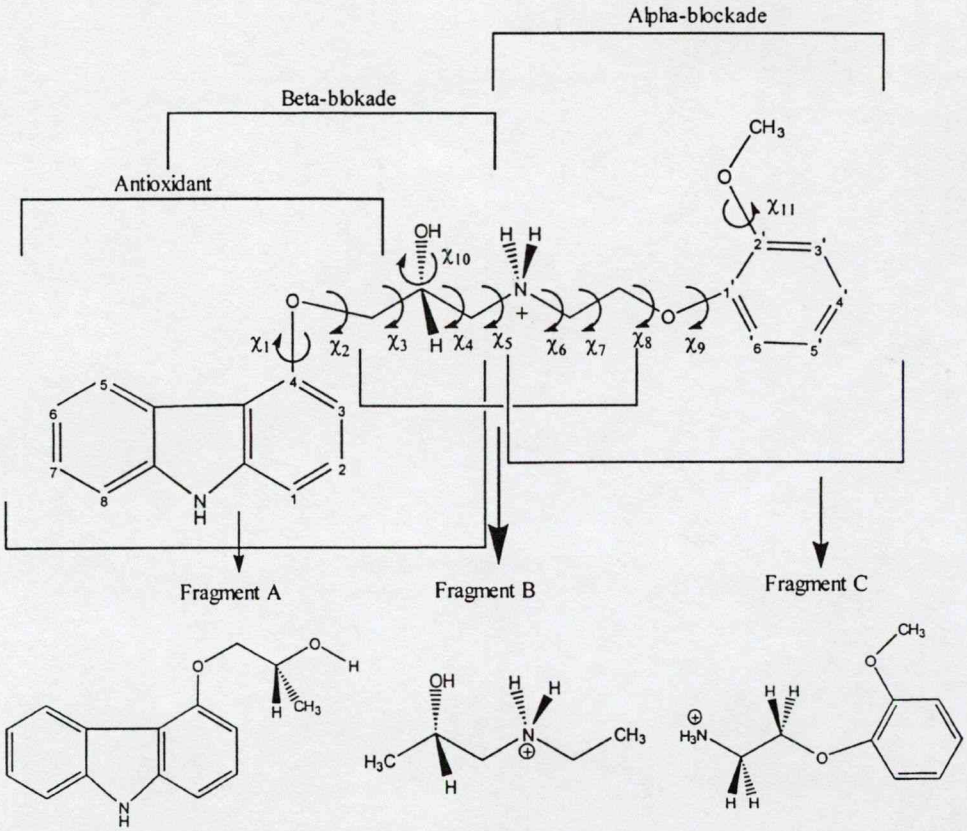

Figure 3. Complete molecular structure and function of N-protonated carvedilol indicating all 11 torsional angles (top) and its three characteristic fragments: *R*- and *S*-4-(2-hydroxypropoxy)carbazol (fragment A), *R*- and *S*-*N*-ethylpropane (fragment B), and *N*-ethoxy-2-methoxybenzene (fragment C).

structed in the same manner as **IV-H_2** and **IV-Me_2** with the exception that the carbazole ring was maintained. As such, **II-H_2** and **II-Me_2** are achiral representative structures of **I-*R*** and **I-*S***.

It is stated above that both enantiomers of carvedilol have equal α_1-adrenergic antagonist and antioxidant activities. Given the prochiral and chiral structures in Figure 4, it is of interest to ask the question, if two enantiomers produce the same biological activity (as with carvedilol), would it be possible to construct prochiral analogues of these enantiomers that could produce the same biological effects? That is, could achiral structures by synthesized that in some way could "mimic" the effects of chiral structures in a biological environment? Here, we explore such an idea with the structures presented in Figure 4.

In analyzing the various achiral and chiral structures, it is hypothesized that, with regard to conformational energies, the addition of two chiral structures, minus the addition of two achiral structures, would give a result of zero. That is, the sum of the enantiomeric *R* and *S* conformational energies would be negated by the sum of the conformational energies of the corresponding prochiral structures. This process is shown in Figure 5. How such a summation or comparison of analogous prochiral and chiral structures relates to mode of action is not fully clear (cf. Results and Discussion). However, because the complete conformational energies of a PEHS (instead of just selected conformations) comprise all structural and chiral features for a given structure, it allows us to investigate how conformational energy varies with respect to stereocenter molecular architecture. Such effects may be useful to investigate possible situations where, given the right type of molecular environment, achiral drugs could be used to "mimic" chiral compounds.

2. Computational Method

All computations were performed using the Gaussian 98 software program,[23] and all structures were exclusively defined using the Gaussian 98 z-matrix internal coordinate system to specify molecular structure, stereochemistry, and geometry. Structural analysis was done on optimized conformational minima for the respective **IV-H_2**, **IV-Me_2**, **III-[H,Me]-*S***, **III-[H,Me]-*R***, **I-*R***, and **I-*S*** PEHSs. PEHSs were selected and evaluated successively at the RHF/3-21G and RHF/6-31G(d) levels of theory, and then full optimizations were carried out using the Becke 3LYP hybrid functional at the B3LYP/6-31G-(d) level of theory.[24] Separate vibrational frequency calculations were performed on all converged minima at the B3LYP/6-31G-(d) level of theory to ensure that the optimized conformers were true minima and contained no imaginary frequencies. Potential energy surfaces (PESs) were constructed according to eq 3 for **IV-H_2**, **IV-Me_2**, **III-[H,Me]-*S***, **III-[H,Me]-*R***, **II-H_2**, **II-Me_2**, **I-*R***, and **I-*S*** from potential energy curve (PEC) cross sections calculated at the RHF/3-21G level of theory and plotted using Axum 5.0.[25]

$$E = f(\chi_3, \chi_{10}) \tag{3}$$

3. Results and Discussion

3.1. Enantiomeric Analysis of the I-*R* and I-*S* Torsional Angles. PEC cross sections for each torsional angle of **I-*R*** and **I-*S*** (χ_1, χ_2, χ_3, and χ_{10}) were computed using the RHF/3-21G level of theory. Given that these two structures are enantiomeric, it would be expected that each torsional mode of rotation is also enantiomeric. The latter was verified; the PECs generated

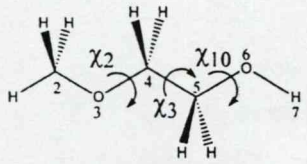

2-methoxyethan-1-ol
(analogue **IV-H$_2$**)

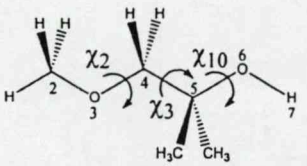

1-methoxy-2-methyl-propane-2-ol
(analogue **IV-Me$_2$**)

χ_2 = C5-C4-O3-C2
χ_3 = O6-C5-C4-O3
χ_{10} = H7-O6-C5-C4

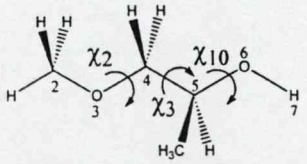

(2*S*)-1-methoxypropan-2-ol
(analogue **III-[H,Me]-*S***)

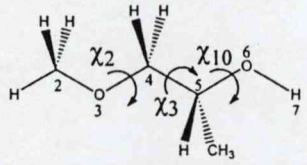

(2*R*)-1-methoxypropan-2-ol
(analogue **III-[H,Me]-*R***)

E = f(χ_2, χ_3, χ_{10},)

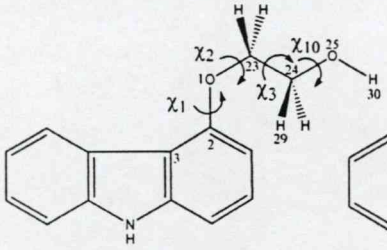

(2-hydroxyethoxy)carbazol
(analogue **II-H$_2$**)

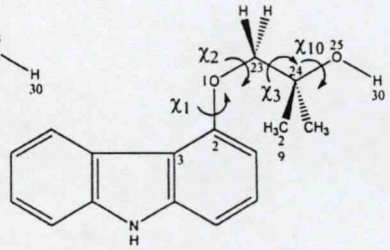

(2-hydroxy-2-methyl-ethoxy)carbazol
(analogue **II-Me$_2$**)

χ_1 = C23-O1-C2-C3
χ_2 = C24-C23-O1-C2
χ_3 = C29-C24-C23-O1
χ_{10} = H30-O25-C24-C23

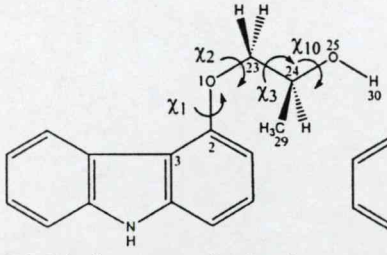

S-4-(2-hydroxypropoxy)carbazol
(Fragment A, **I-*S***)

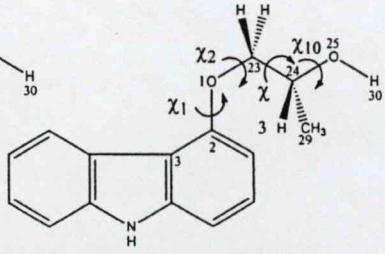

R-4-(2-hydroxypropoxy)carbazol
(Fragment A, **I-*R***)

E = f(χ_1, χ_2, χ_3, χ_{10},)

Figure 4. Numbering and definition of torsional angles for analogues **IV-H$_2$**, **IV-Me$_2$**, **III-[H,Me]-*S***, **III-[H,Me]-*R***, **II-H$_2$**, **II-Me$_2$**, **I-*R***, and **I-*S***. Numbers placed beside atoms indicate numbering used as the z-matrix input for Gaussian 98.

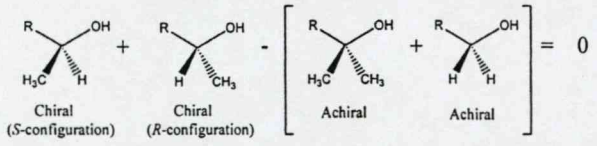

Figure 5. Calculation of the energetic equivalence of two consecutive and concerted methyl substitutions as described by $\Delta E = \{[E_R(>\text{CHMe}) + E_S(>\text{CMeH})] - [E(>\text{CMe}_2) + E(>\text{CH}_2)]\}$.

for the specified torsional angles produced topological representations of the fragment's conformational identity showing that the two structures are truly enantiomeric (cf. Figure 6). Symmetry symbols are used to identify identical points for a given torsional angle PEC. Each PEC was produced with the other three torsional angles frozen in the anti position (180.00°) to ensure no confounding factors (such as sterics) were present for any of the torsional angles and that a controlled scan of the torsional angle was obtained. As such, the only variable in each PEC is the torsional angle being scanned because all other torsional parameters are kept rigid.

From the evaluated PECs one could estimate that the global minima for the 4-(2-hydroxypropoxy)carbazol carvedilol fragment would occur at the conformation with the torsional angles χ_1, χ_2, χ_3, and χ_{10} in the anti, anti, $g+$, $g+$ and anti, anti, $g-$, $g-$ for the *R*- and *S*-configurations, respectively. This was inferred by examining the location of the global minimum for each torsional angle (χ_1, χ_2, χ_3, and χ_{10}) from each individual generated PEC.

3.2. Enantiomeric Analysis of the I-*R* and I-*S* Conformational PEHSs. After verifying that each torsional angle of the carvedilol fragment was enantiomeric, the entire PEHS described by eq 1 was analyzed by optimizations of conformational

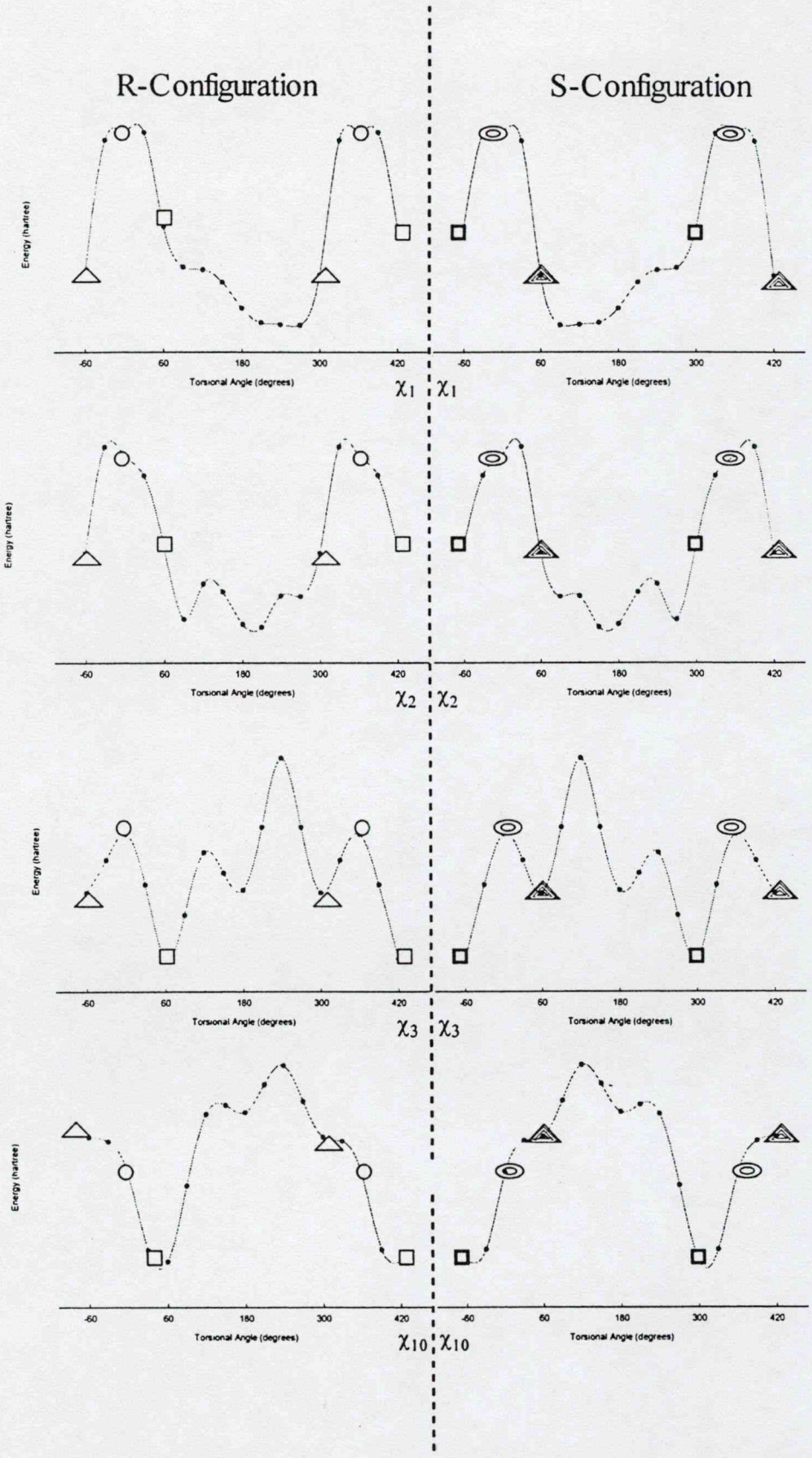

Figure 6. Enantiomeric PECs for *R*- and *S*-4-(2-hydroxypropoxy)carbazol computed at the RHF/3-21G level of theory. PECs generated for scanned torsional angles were produced with the other three torsional angles rigid at the anti position. PEC symmetry identification points are depicted by △ = gauche minus ($g-$), ○ = zero point, and □ = gauche plus ($g+$) for the *R*-configuration and □ = gauche minus ($g-$), circle in a circle = zero point, and triangle in a triangle = gauche plus ($g+$) for the *S*-configuration.

TABLE 1: Summary of Converged Conformational Minima for the PEHS of *S*-4-(2-Hydroxypropoxy)carbazol (Fragment A, I-*S*) at the RHF/3-21G [A], RHF/6-31G(d) [B], and B3LYP/6-31G(d) [C][26] Levels of Theory[a]

conformational assignment				level of theory			conformational assignment				level of theory			conformational assignment				level of theory		
χ_1	χ_2	χ_3	χ_{10}	A	B	C	χ_1	χ_2	χ_3	χ_{10}	A	B	C	χ_1	χ_2	χ_3	χ_{10}	A	B	C
g^+	g^+	g^+	g^+	F	F	F	a	g^+	g^+	g^+	F	NF	NF	g^-	g^+	g^+	g^+	NF	NF	NF
g^+	g^+	g^+	a	NF	NF	NF	a	g^+	g^+	a	NF	NF	NF	g^-	g^+	g^+	a	NF	NF	NF
g^+	g^+	g^+	g^-	NF	NF	NF	a	g^+	g^+	g^-	F	NF	NF	g^-	g^+	g^+	g^-	NF	NF	NF
g^+	g^+	a	g^+	NF	NF	NF	a	g^+	a	g^+	NF	NF	NF	g^-	g^+	a	g^+	NF	NF	NF
g^+	g^+	a	a	F	F	F	a	g^+	a	a	F	F	F	g^-	g^+	a	a	F	NF	NF
g^+	g^+	a	g^-	F	F	F	a	g^+	a	g^-	F	F	F	g^-	g^+	a	g^-	NF	NF	NF
g^+	g^+	g^-	g^+	NF	NF	NF	a	g^+	g^-	g^+	NF	NF	NF	g^-	g^+	g^-	g^+	NF	NF	NF
g^+	g^+	g^-	a	NF	NF	NF	a	g^+	g^-	a	NF	NF	NF	g^-	g^+	g^-	a	NF	NF	NF
g^+	g^+	g^-	g^-	NF	NF	NF	a	g^+	g^-	g^-	NF	NF	NF	g^-	g^+	g^-	g^-	NF	NF	NF
g^+	a	g^+	g^+	F	F	NF	a	a	g^+	g^+	F	F	F	g^-	a	g^+	g^+	F GM	F	F
g^+	a	g^+	a	NF	NF	NF	a	a	g^+	a	NF	NF	NF	g^-	a	g^+	a	F	F	NF
g^+	a	g^+	g^-	NF	NF	NF	a	a	g^+	g^-	NF	NF	NF	g^-	a	g^+	g^-	F	NF	NF
g^+	a	a	g^+	F	NF	NF	a	a	a	g^+	F	F	F	g^-	a	a	g^+	F	F	NF
g^+	a	a	a	NF	NF	NF	a	a	a	a	NF	NF	NF	g^-	a	a	a	NF	NF	NF
g^+	a	a	g^-	F	F	F	a	a	a	g^-	F	F GM	F GM	g^-	a	a	g^-	F	F	NF
g^+	a	g^-	g^+	F	F	NF	a	a	g^-	g^+	F	F	F	g^-	a	g^-	g^+	F	F	NF
g^+	a	g^-	a	NF	NF	NF	a	a	g^-	a	F	F	F	g^-	a	g^-	a	F	F	NF
g^+	a	g^-	g^-	NF	NF	NF	a	a	g^-	g^-	F	F	F	g^-	a	g^-	g^-	F	F	NF
g^+	g^-	g^+	g^+	NF	NF	NF	a	g^-	g^+	g^+	NF	NF	NF	g^-	g^-	g^+	g^+	NF	NF	NF
g^+	g^-	g^+	a	NF	NF	NF	a	g^-	g^+	a	F	NF	NF	g^-	g^-	g^+	a	F	NF	NF
g^+	g^-	g^+	g^-	NF	NF	NF	a	g^-	g^+	g^-	NF	NF	NF	g^-	g^-	g^+	g^-	NF	NF	NF
g^+	g^-	a	g^+	NF	NF	NF	a	g^-	a	g^+	F	NF	NF	g^-	g^-	a	g^+	NF	NF	NF
g^+	g^-	a	a	NF	NF	NF	a	g^-	a	a	F	F	F	g^-	g^-	a	a	NF	NF	NF
g^+	g^-	a	g^-	NF	NF	NF	a	g^-	a	g^-	F	NF	NF	g^-	g^-	a	g^-	F	F	F
g^+	g^-	g^-	g^+	NF	NF	NF	a	g^-	g^-	g^+	F	F	F	g^-	g^-	g^-	g^+	NF	NF	NF
g^+	g^-	g^-	a	NF	NF	NF	a	g^-	g^-	a	F	F	F	g^-	g^-	g^-	a	NF	NF	NF
g^+	g^-	g^-	g^-	NF	NF	NF	a	g^-	g^-	g^-	F	F	F	g^-	g^-	g^-	g^-	F	F	F

[a] F = found; NF = not found; GM = global minimum.

minima. With four torsional angles (χ_1, χ_2, χ_3, χ_{10}) and three possible minima for each torsional angle ($g+$, a, $g-$), there are a grand total of 81 ($=3^4$) possible minima for each configuration. Minima are indicated as either $\chi_1[\chi_2\chi_3]\chi_{10}$ or $[\chi_2\chi_3]\chi_{10}$ because the torsional angles χ_2 and χ_3 are reflective of the backbone conformation assumed by carvedilol fragment A.

Conformational structural assignments for the conformational minima were made using the following conditions:

$$\text{gauche plus (g+)} = 60 \text{ (ideal)} \pm 60°$$
$$\text{anti (a)} = 180 \text{ (ideal)} \pm 60°$$
$$\text{gauche minus (g−)} = -60 \text{ (ideal)} \pm 60°$$

This is based on the general observation that, if one were to rotate a tetrahedral carbon against another tetrahedral carbon, the minima would generally fall within the above ranges. All possible minima were computed at noncorrelated Hartree−Fock RHF/3-21G, subsequent minima at RHF/6-31G(d), and then using the density functional hybrid B3LYP/6-31G(d). Minima were then sorted according to the above conformational assignments and were either termed found (F) if they converged or not found (NF) if the structure shifted to nearby minima or was annihilated due to lack of stability at a specific conformation. Tables 1 and 2 show a summary of all the converged PEHS conformers at all levels of theory for **I-*S*** and **I-*R***, respectively. The B3LYP/6-31G(d) results in column C of Table 1 are adapted from ref 26.

The number of minima found for **I-*S*** and **I-*R*** are, respectively, 36 minima converged (the global minima were the $g-[ag+]g+$ and $g+[ag-]g-$ conformations) at RHF/3-21G (cf. Supporting Information Tables S1 and S2), 27 minima ($a[aa]g-$ and $a[aa]g+$) at RHF/6-31G(d) (cf. Supporting Information Tables S3 and S4), and 19 minima ($a[aa]g-$ and $a[aa]g+$) at B3LYP/6-31G(d) (cf. ref 26 for **I-*S*** and Table 3 for **I-*R***). Minima were stabilized by intramolecular hydrogen bonding between O1 and H30.[26]

All converged minima at the B3LYP/6-31G(d) level of theory that were concluded to be authentic minima (i.e. possessed no imaginary frequencies) were used to construct a topological representation of the PEHS for **I-*S*** and **I-*R*** (cf. Figure 7). From this schematic diagram, it is evident that all minima occurred in corresponding enantiomeric pairs. Further, the PEHS generated for both stereoisomers illustrates that both the *R*- and *S*-configurations possess both point chirality and axis chirality and are exactly enantiomeric, as described by eq 4.

$$E_R = E_S \tag{4}$$
$$f_R(\chi_1,\chi_2,\chi_3,\chi_{10}) = f_S(-\chi_1,-\chi_2,-\chi_3,-\chi_{10})$$

It is therefore evident that in the present molecular system we are witnessing the combination of both point chirality and axis chirality. Consequently, a true enantiomeric pair requires not only the switching of point chirality from the *R*- to the *S*-stereoisomer but also the switching of all torsional angles from clockwise (CW) to counterclockwise (CCW) rotation, as demanded by eq 4. Consequently, the graphical representation of the computed PEHS shows that all minima must have an energetically equal enantiomer (as described in eq 4). All other pairs have diastereomeric relationships. This observation is valid for all three levels of theory employed for all conformational optimizations. The above is also schematically illustrated in Figure 1.

DFT global minima, $a[aa]g-$ and $a[aa]g+$ for the *S*- and *R*-configurations, respectively, reveal that the initial guesses of $a[ag-]g-$ and $a[ag+]g+$ for global minima obtained from the RHF/3-21G PECs were quite close to the final DFT converged global minima. In fact, these PEC-based predictions were closer

TABLE 2: Summary of Converged Conformational Minima for the PEHS of *R*-4-(2-Hydroxypropoxy)carbazol (Fragment A, I-*R*) at the RHF/3-21G [A], RHF/6-31G(d) [B], and B3LYP/6-31G(d) [C] Levels of Theory[a]

conformational assignment				level of theory			conformational assignment				level of theory			conformational assignment				level of theory		
χ_1	χ_2	χ_3	χ_{10}	A	B	C	χ_1	χ_2	χ_3	χ_{10}	A	B	C	χ_1	χ_2	χ_3	χ_{10}	A	B	C
g^+	g^+	g^+	g^+	F	F	F	a	g^+	g^+	g^+	F	F	F	g^-	g^+	g^+	g^+	NF	NF	NF
g^+	g^+	g^+	a	NF	NF	NF	a	g^+	g^+	a	F	F	F	g^-	g^+	g^+	a	NF	NF	NF
g^+	g^+	g^+	g^-	NF	NF	NF	a	g^+	g^+	g^-	F	F	F	g^-	g^+	g^+	g^-	NF	NF	NF
g^+	g^+	a	g^+	F	F	F	a	g^+	a	g^+	F	NF	NF	g^-	g^+	a	g^+	NF	NF	NF
g^+	g^+	a	a	NF	NF	NF	a	g^+	a	a	F	F	F	g^-	g^+	a	a	NF	NF	NF
g^+	g^+	a	g^-	NF	NF	NF	a	g^+	a	g^-	F	NF	NF	g^-	g^+	a	g^-	NF	NF	NF
g^+	g^+	g^-	g^+	NF	NF	NF	a	g^+	g^-	g^+	NF	NF	NF	g^-	g^+	g^-	g^+	NF	NF	NF
g^+	g^+	g^-	a	F	NF	NF	a	g^+	g^-	a	F	NF	NF	g^-	g^+	g^-	a	NF	NF	NF
g^+	g^+	g^-	g^-	NF	NF	NF	a	g^+	g^-	g^-	NF	NF	NF	g^-	g^+	g^-	g^-	NF	NF	NF
g^+	a	g^+	g^+	F	F	NF	a	a	g^+	g^+	F	F	F	g^-	a	g^+	g^+	NF	NF	NF
g^+	a	g^+	a	F	F	NF	a	a	g^+	a	F	F	F	g^-	a	g^+	a	NF	NF	NF
g^+	a	g^+	g^-	F	F	NF	a	a	g^+	g^-	F	F	F	g^-	a	g^+	g^-	F	F	NF
g^+	a	a	g^+	F	F	NF	a	a	a	g^+	F	F GM	F GM	g^-	a	a	g^+	F	F	F
g^+	a	a	a	NF	NF	NF	a	a	a	a	NF	NF	NF	g^-	a	a	a	NF	NF	NF
g^+	a	a	g^-	F	F	NF	a	a	a	g^-	F	F	F	g^-	a	a	g^-	F	NF	NF
g^+	a	g^-	g^+	F	NF	NF	a	a	g^-	g^+	NF	NF	NF	g^-	a	g^-	g^+	NF	NF	NF
g^+	a	g^-	a	F	F	NF	a	a	g^-	a	NF	NF	NF	g^-	a	g^-	a	NF	NF	NF
g^+	a	g^-	g^-	F GM	F	F	a	a	g^-	g^-	F	F	F	g^-	a	g^-	g^-	F	F	NF
g^+	g^-	g^+	g^+	NF	NF	NF	a	g^-	g^+	g^+	NF	NF	NF	g^-	g^-	g^+	g^+	NF	NF	NF
g^+	g^-	g^+	a	NF	NF	NF	a	g^-	g^+	a	NF	NF	NF	g^-	g^-	g^+	a	NF	NF	NF
g^+	g^-	g^+	g^-	NF	NF	NF	a	g^-	g^+	g^-	NF	NF	NF	g^-	g^-	g^+	g^-	NF	NF	NF
g^+	g^-	a	g^+	NF	NF	NF	a	g^-	a	g^+	F	F	F	g^-	g^-	a	g^+	F	F	F
g^+	g^-	a	a	F	NF	NF	a	g^-	a	a	F	F	F	g^-	g^-	a	a	F	F	F
g^+	g^-	a	g^-	NF	NF	NF	a	g^-	a	g^-	NF	NF	NF	g^-	g^-	a	g^-	NF	NF	NF
g^+	g^-	g^-	g^+	NF	NF	NF	a	g^-	g^-	g^+	F	NF	NF	g^-	g^-	g^-	g^+	NF	NF	NF
g^+	g^-	g^-	a	NF	NF	NF	a	g^-	g^-	a	NF	NF	NF	g^-	g^-	g^-	a	NF	NF	NF
g^+	g^-	g^-	g^-	NF	NF	NF	a	g^-	g^-	g^-	F	NF	NF	g^-	g^-	g^-	g^-	F	F	F

[a] F = found; NF = not found; GM = global minimum.

TABLE 3: Optimized Minima for the PEHS of *R*-4-(2-Hydroxypropoxy)carbazol (Fragment A, I-*R*) at the B3LYP/6-31G(d) Level of Theory

conformational assignment									
χ_1	χ_2	χ_3	χ_{10}	χ_1	χ_2	χ_3	χ_{10}	E (hartree)	rel E (kcal·mol^{-1})
g^+	g^+	g^+	g^+	78.66	85.51	64.48	66.64	−785.828 425 897	6.34
g^+	g^+	a	g^+	74.44	80.27	166.22	58.86	−785.830 399 472	5.11
g^+	a	g^-	g^-	84.56	−176.64	−68.86	−53.52	−785.834 927 568	2.26
a	g^+	g^+	g^+	−179.82	82.40	61.44	68.99	−785.832 614 704	3.72
a	g^+	g^+	a	−179.85	82.74	62.70	−175.60	−785.833 159 064	3.37
a	g^+	g^+	g^-	−179.33	81.90	58.61	−74.35	−785.833 289 337	3.29
a	g^+	a	a	156.09	105.16	163.35	167.64	−785.831 784 831	4.24
a	a	g^+	g^+	−178.82	−179.20	66.89	68.63	−785.834 719 251	2.40
a	a	g^+	a	179.99	−178.34	65.45	−176.78	−785.834 841 115	2.32
a	a	g^+	g^-	−179.64	−178.70	62.36	−75.51	−785.834 880 226	2.29
a	a	a	g^+	−178.53	175.39	−178.18	47.53	−785.838 535 919	0.00
a	a	a	g^-	−175.20	−177.94	−179.89	−56.46	−785.833 846 146	2.94
a	a	g^-	g^-	177.68	−176.27	−65.84	−50.64	−785.837 142 473	0.87
a	g^-	a	g^+	−178.26	−86.25	−174.77	49.15	−785.836 187 425	1.47
a	g^-	a	a	177.86	−80.88	172.56	168.92	−785.831 134 398	4.64
g^-	a	a	g^+	−83.67	176.13	−173.69	50.76	−785.836 021 086	1.58
g^-	g^-	a	g^+	−87.09	−84.22	−171.18	37.39	−785.832 806 928	3.60
g^-	g^-	a	a	−85.33	−66.15	−179.25	177.98	−785.827 602 283	6.86
g^-	g^-	g^-	g^-	−71.75	−86.37	−54.09	−60.91	−785.829 262 278	5.82

to the DFT global minima than to the global minima from the RHF/3-21G conformational optimizations. This is likely due to the fact that the PECs were constructed with the three other torsional angles rigid, allowing good topological profiles to be generated for each torsional angle without confounding factors from the other torsional angles.

3.3. PEHS Conformational Analysis of IV-H_2, IV-Me_2, III-[H,Me]-*S*, and III-[H,Me]-*R*. Selected analogues were subject to the same conformational structural assignments and optimization methods as described above for **I-*S*** and **I-*R***. A summary of the converged minima for **IV-H_2** is found in Table 4. This analogue contains two equivalent global minima at [*ag*+]*g*− and [*ag*−]*g*+ (cf. Figure 8 and Table 5) that converged at all three levels of theory (cf. Supporting Information Tables S5 and S6). **I-*S*** and **I-*R***, which were strained by the large carbazole ring substituent, had fewer numbers of minima converge at each level of theory. The simple methyl substituent, along with only two hydrogen atoms present at carbon center C5, produced a PEHS with 21 converged minima out of a possible 27 for each different level of theory. Due to the latter, although a larger basis set and the DFT level of theory produced better energies, the PEHS remained relatively unchanged for the three levels of geometry optimizations.

The other noncarbazole achiral analogue, **IV-Me_2**, was also analyzed with geometry optimizations (cf. Table 6). This analogue was identical to **IV-H_2** with the exception that C5

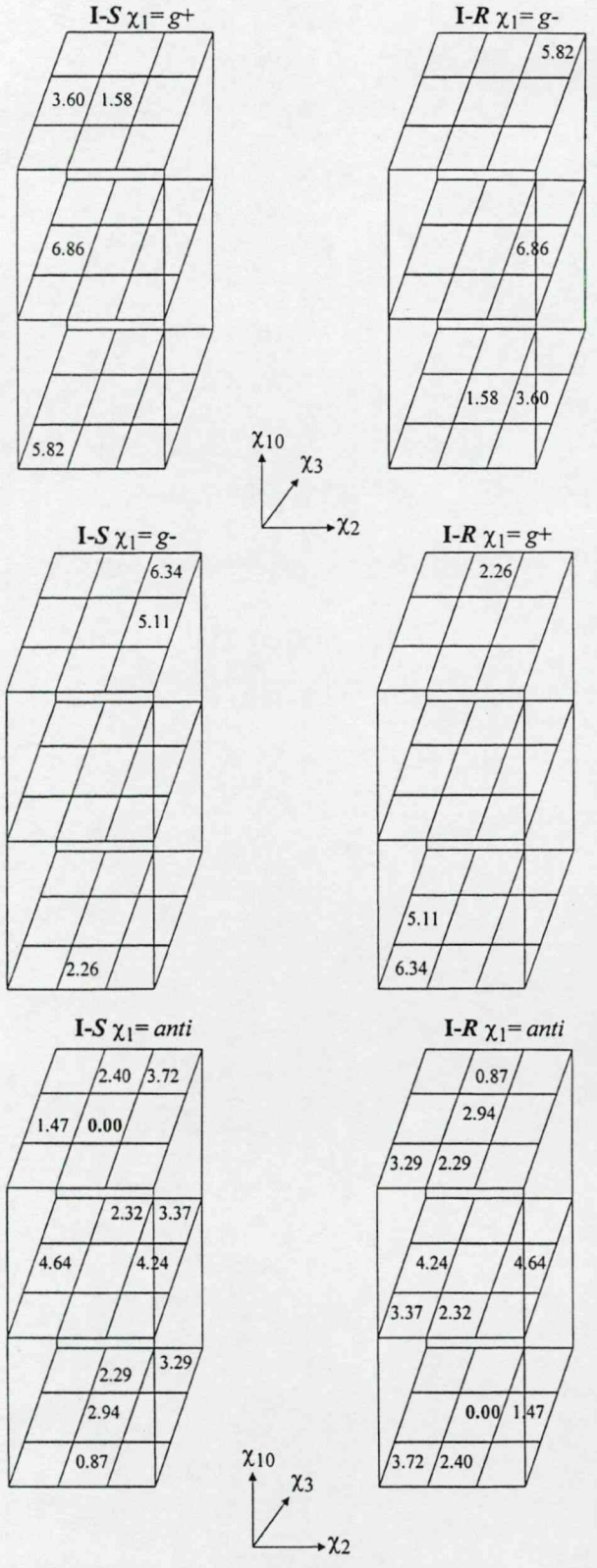

Figure 7. Graphical representation of the density functional computed PEHSs for *R*- and *S*-4-(2-hydroxypropoxy)carbazol (**I-*R*** and **I-*S***) indicating all minima found and the associated relative energy in kcal·mol^{-1}. Minima that were not found have a blank space.

contained two methyl substituents as opposed to two hydrogen atoms. Like the case of **IV-H$_2$**, two energetically identical global minima occurred at the conformations [*ag*+]*g*− and [*ag*−]*g*+

TABLE 4: Summary of Converged Conformational Minima for the PEHS of 2-Methoxyethan-1-ol (IV-H$_2$) at the RHF/3-21G [A], RHF/6-31G(d) [B], and B3LYP/6-31G(d) [C] Levels of Theory[a]

conformational assignment					
χ_2	χ_3	χ_{10}	A	B	C
g^+	g^+	g^+	NF	NF	NF
g^+	g^+	a	F	F	F
g^+	g^+	g^-	F	F	F
g^+	a	g^+	F	F	F
g^+	a	a	F	F	F
g^+	a	g^-	F	F	F
g^+	g^-	g^+	NF	NF	NF
g^+	g^-	a	F	F	F
g^+	g^-	g^-	F	F	F
a	g^+	g^+	F	F	F
a	g^+	a	NF	NF	NF
a	g^+	g^-	F (GM)	F (GM)	F (GM)
a	a	g^+	F	F	F
a	a	a	F	F	F
a	a	g^-	F	F	F
a	g^-	g^+	F (GM)	F (GM)	F (GM)
a	g^-	a	NF	NF	NF
a	g^-	g^-	F	F	F
g^-	g^+	g^+	F	F	F
g^-	g^+	a	F	F	F
g^-	g^+	g^-	NF	NF	NF
g^-	a	g^+	F	F	F
g^-	a	a	F	F	F
g^-	a	g^-	F	F	F
g^-	g^-	g^+	F	F	F
g^-	g^-	a	F	F	F
g^-	g^-	g^-	NF	NF	NF

[a] F = found; NF = not found; GM = global minimum.

for all three different levels of theory (cf. Figure 9 and Table 7). However, due to the steric restrictions imposed by the somewhat larger methyl groups at C5, only 11 out of the possible 27 minima converged at the different levels of optimization (cf. Supporting Information Tables S7 and S8). The presence of the methyl groups prevented most of the conformations with the torsional angle χ_2 in the *g*+ or *g*− position from converging.

Here too we witness the presence of axis chirality in these achiral (with regards to point chirality) structures. Therefore, although these achiral structures will not rotate plane-polarized light as point chiral structures do, they possess axis chirality which occurs when the structures adopt conformations with asymmetric electron density planes. The only exception to this is the [*aa*]*a* conformation. This conformation separates all minima for a given structure because it is the only conformation with a symmetric electron density plane, and therefore, axis chirality is not present—consequently, it does not have an axis chiral pair. However, conformations above and below the [*aa*]*a* conformation are influenced by axis chirality and are paired according to eq 5. Equation 5 states that for an achiral structure with two energetically equivalent minima, P and M, all torsional angles for those minima are switched from clockwise (CW) to counterclockwise (CCW) rotation. This axis chirality is the same as that demanded by eq 4 for the two enantiomeric minima.

$$E_P = E_M \tag{5}$$

$$f_P(\chi_2,\chi_3,\chi_{10}) = f_M(-\chi_2,-\chi_3,-\chi_{10})$$

It must be regarded that, as stated earlier, irrespective of the presence of a point chiral stereocenter with four different

TABLE 5: Optimized Minima for the PEHS of 2-Methoxyethan-1-ol (IV-H_2) at the B3LYP/6-31G(d) Level of Theory

conformational assignment							
χ_2	χ_3	χ_{10}	χ_2	χ_3	χ_{10}	E (hartree)	rel E (kcal·mol^{-1})
g^+	g^+	a	74.84	64.71	−176.35	−269.542 422 374	5.34
g^+	g^+	g^-	84.22	55.17	−43.31	−269.548 526 782	1.51
g^+	a	g^+	82.10	176.20	67.87	−269.543 841 268	4.45
g^+	a	a	83.07	178.41	−177.30	−269.543 541 796	4.63
g^+	a	g^-	81.30	178.57	−67.44	−269.544 279 753	4.17
g^+	g^-	a	81.32	−75.42	173.05	−269.545 157 695	3.62
g^+	g^-	g^-	78.24	−71.37	−63.90	−269.545 185 796	3.60
a	g^+	g^+	−178.77	64.47	58.69	−269.544 928 112	3.76
a	g^+	g^-	−173.81	59.60	−49.85	−269.550 927 094	0.00
a	a	g^+	−178.30	179.68	69.45	−269.546 263 161	2.93
a	a	a	180.00	180.00	180.00	−269.545 824 036	3.20
a	a	g^-	178.30	−179.67	−69.48	−269.546 263 144	2.93
a	g^-	g^+	173.81	−59.60	49.85	−269.550 927 095	0.00
a	g^-	g^-	178.77	−64.47	−58.69	−269.544 928 111	3.76
g^-	g^+	g^+	−78.24	71.37	63.90	−269.545 185 796	3.60
g^-	g^+	a	−81.32	75.42	−173.04	−269.545 157 695	3.62
g^-	a	g^+	−81.30	−178.57	67.44	−269.544 279 753	4.17
g^-	a	a	−83.07	−178.41	177.30	−269.543 541 796	4.63
g^-	a	g^-	−82.10	−176.20	−67.87	−269.543 841 268	4.45
g^-	g^-	g^+	−84.23	−55.18	43.31	−269.548 526 783	1.51
g^-	g^-	a	−74.84	−64.71	176.35	−269.542 422 374	5.34

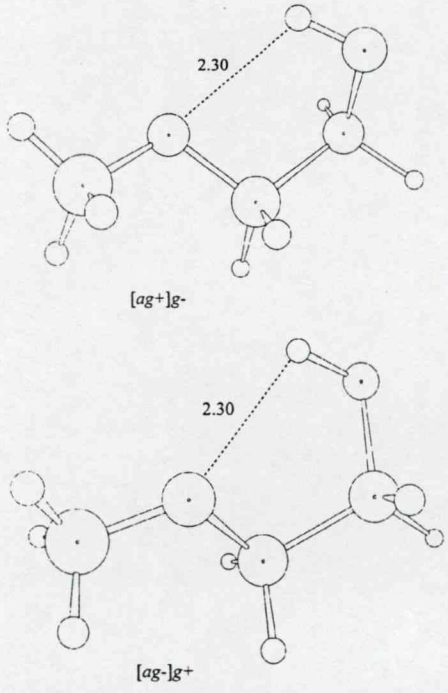

Figure 8. Global minima conformers of the 2-methoxyethan-1-ol (**IV-H_2**) PEHS. Conformers [*ag*+]*g*− (top) and [*ag*−]*g*+ (bottom) are axis chiral pairs computed at the B3LYP/6-31G(d) level of theory and possess an intramolecular hydrogen bond as the dominant stabilization feature.

substituents, the chirality induced by an asymmetric distribution of electron density—axis chirality—is always present whenever the structure adopts asymmetric conformations. Further, like enantiomers of point chirality, axis chiral conformers come in pairs.

If one were to differently combine the two achiral analogues, **IV-H_2** and **IV-Me_2** at C5, one would acquire two enantiomers: **III-[H,Me]-*S*** and **III-[H,Me]-*R*** (cf. Figure 4). These two enantiomers were each evaluated with geometry optimizations of converged minima as above (cf. Tables 8 and 9). Given that

TABLE 6: Summary of Converged Conformational Minima for the PEHS of 1-Methoxy-2-methyl-propane-2-ol (IV-Me_2) at the RHF/3-21G [A], RHF/6-31G(d) [B], and B3LYP/6-31G(d) [C] Levels of Theory[a]

conformational assignment					
χ_2	χ_3	χ_{10}	A	B	C
g^+	g^+	g^+	NF	NF	NF
g^+	g^+	a	NF	NF	NF
g^+	g^+	g^-	NF	NF	NF
g^+	a	g^+	NF	NF	NF
g^+	a	a	NF	NF	NF
g^+	a	g^-	NF	NF	NF
g^+	g^-	g^+	NF	NF	NF
g^+	g^-	a	F	F	F
g^+	g^-	g^-	F	F	F
a	g^+	g^+	NF	NF	NF
a	g^+	a	F	F	F
a	g^+	g^-	F (GM)	F (GM)	F (GM)
a	a	g^+	F	F	F
a	a	a	F	F	F
a	a	g^-	F	F	F
a	g^-	g^+	F (GM)	F (GM)	F (GM)
a	g^-	a	F	F	F
a	g^-	g^-	NF	NF	NF
g^-	g^+	g^+	F	F	F
g^-	g^+	a	F	F	F
g^-	g^+	g^-	NF	NF	NF
g^-	a	g^+	NF	NF	NF
g^-	a	a	NF	NF	NF
g^-	a	g^-	NF	NF	NF
g^-	g^-	g^+	NF	NF	NF
g^-	g^-	a	NF	NF	NF
g^-	g^-	g^-	NF	NF	NF

[a] F = found; NF = not found; GM = global minimum.

21 and 11 minima converged for the **IV-H_2** and **IV-Me_2** PEHSs, respectively, it would be expected that, with one hydrogen and one methyl group at C5, the number halfway between 11 and 21 would converge for the enantiomeric structures (i.e. (11 + 21)/2 = 16). This is exactly what occurred, with each configuration and level of theory having 16 out of a possible 27 minima converge for each enantiomer. Further, given that the global minima occurred at the [*ag*+]*g*− and [*ag*−]*g*+ conformations for the achiral structures, it would be expected that the

TABLE 7: Optimized Minima for the PEHS of 1-Methoxy-2-methyl-propane-2-ol (IV-Me_2) at the B3LYP/6-31G(d) Level of Theory

conformational assignment							
χ_2	χ_3	χ_{10}	χ_2	χ_3	χ_{10}	E (hartree)	Rel E (kcal·mol^{-1})
g^+	g^-	a	χ_2	χ_3	χ_{10}	−348.182 592 886	3.36
g^+	g^-	g^-	81.08	−67.14	−63.97	−348.182 032 926	3.71
a	g^+	a	−177.62	69.32	−174.14	−348.181 677 861	3.94
a	g^+	g^-	−174.24	55.90	−46.46	−348.187 950 829	0.00
a	a	g^+	−178.29	179.67	70.72	−348.184 592 291	2.11
a	a	a	180.00	−179.98	−179.95	−348.184 521 481	2.15
a	a	g^-	178.29	−179.67	−70.72	−348.184 592 292	2.11
a	g^-	g^+	174.24	−55.90	46.46	−348.187 950 829	0.00
a	g^-	a	177.62	−69.32	174.15	−348.181 677 884	3.94
g^-	g^+	g^+	−81.08	67.13	63.97	−348.182 032 924	3.71
g^-	g^+	a	−86.20	71.30	−174.64	−348.182 592 888	3.36

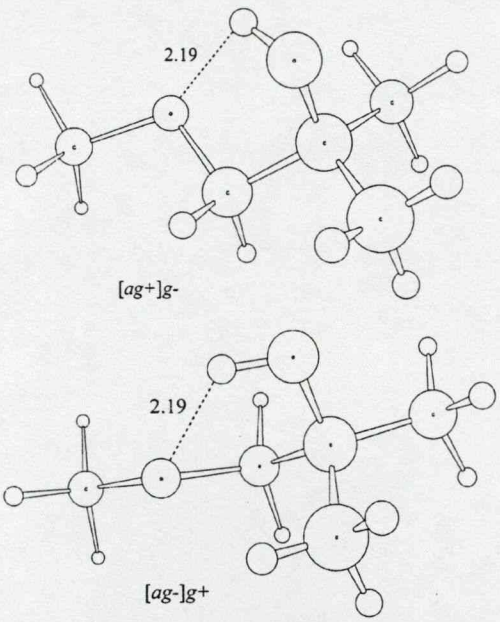

Figure 9. Global minima conformers of the 1-methoxy-2-methyl-propane-2-ol (**IV-Me_2**) PEHSs computed at the B3LYP/6-31G(d) level of theory. Similarly to the **IV-H_2** PEHS, conformers [*ag*+]*g*− (top) and [*ag*−]*g*+ (bottom) are axis chiral pairs with the same intramolecular hydrogen bond as the dominant stabilization feature.

chiral enantiomers would have global minima at either of these conformations. This also occurred. However, the enantiomers varied their global minima at the RHF/3-21G and RHF/6-31G-(d) levels of theory (cf. Figure 10 and Tables 8 and 9). Also, like the cases of the achiral analogues, the PEHSs of **III-[H,-Me]-*S*** and **III-[H,Me]-*R*** stayed constant at the different levels of theory. This was contrary to the cases of the PEHSs of **I-*S*** and **I-*R***, where the number of converged minima decreased at successive levels of theory.

Conformational analysis of **III-[H,Me]-*S*** and **III-[H,Me]-*R*** (cf. Tables 10 and 11) revealed that their respective PEHSs can be described by eq 4 and Figure 1, illustrating the presence of point and axis chirality in these enantiomers (cf. Supporting Information Tables S9−S12). Topological representations of the PEHSs were also constructed for these analogues to illustrate the above trend (cf. Figure 11). In comparing the PEHSs of **III-[H,Me]-*S*** and **III-[H,Me]-*R*** with those of **I-*S*** and **I-*R***, one can see that the presence of the bulky carbazole ring system limits the possible conformations the carvedilol fragment can adopt. Also, like **I-*S*** and **I-*R***, all four methyl-substituted analogues were stabilized by intramolecular hydrogen bonding

TABLE 8: Summary of Converged Conformational Minima for the PEHS of (2*S*)-1-Methoxypropan-2-ol (III-[H,Me]-*S*) at the RHF/3-21G [A], RHF/6-31G(d) [B], and B3LYP/6-31G(d) [C] Levels of Theory[a]

conformational assignment					
χ_2	χ_3	χ_{10}	A	B	C
g^+	g^+	g^+	NF	NF	NF
g^+	g^+	a	F	F	F
g^+	g^+	g^-	F	F	F
g^+	a	g^+	NF	NF	NF
g^+	a	a	NF	NF	NF
g^+	a	g^-	NF	NF	NF
g^+	g^-	g^+	NF	NF	NF
g^+	g^-	a	F	F	F
g^+	g^-	g^-	F	F	F
a	g^+	g^+	NF	NF	NF
a	g^+	a	F	F	F
a	g^+	g^-	F	F (GM)	F (GM)
a	a	g^+	F	F	F
a	a	a	F	F	F
a	a	g^-	F	F	F
a	g^-	g^+	F (GM)	F	F
a	g^-	a	F	F	F
a	g^-	g^-	NF	NF	NF
g^-	g^+	g^+	F	F	F
g^-	g^+	a	F	F	F
g^-	g^+	g^-	NF	NF	NF
g^-	a	g^+	F	F	F
g^-	a	a	F	F	F
g^-	a	g^-	F	F	F
g^-	g^-	g^+	NF	NF	NF
g^-	g^-	a	NF	NF	NF
g^-	g^-	g^-	NF	NF	NF

[a] F = found; NF = not found; GM = global minimum.

between the ether oxygen (O3) and the terminal hydroxyl hydrogen (H7) (cf. Figures 8−10).

The above discussion illustrates that the properties of achiral and chiral structures are not completely distinct (given that the only differences occur at the chiral center) and that deductions about chiral structures can be made from achiral analysis and vice versa. Also, the presence of axis chirality in an achiral system ensures that not all conformations will be unique but rather can be predicted from eq 5.

3.4. PES Analysis of the Chiral and Achiral Centers of I-*R*, I-*S*, II-H_2, II-Me_2, III-[H,Me]-*S*, III-[H,Me]-*R*, IV-H_2, and IV-Me_2. To further study the chiral and achiral centers of the carvedilol analogues, 169-point PESs were constructed from PEC cross sections of torsional angles χ_3 and χ_{10} according to eq 3 at the RHF/3-21G level of theory (cf. Computational Method). These surfaces were constructed using these two torsional angles because they directly surround the chiral and

TABLE 9: Summary of Converged Conformational Minima for the PEHS of (2*R*)-1-Methoxypropan-2-ol (III-[H,Me]-*R*) at the RHF/3-21G [A], RHF/6-31G(d) [B], and B3LYP/6-31G(d) [C] Levels of Theory[a]

conformational assignment					
χ_2	χ_3	χ_{10}	A	B	C
g^+	g^+	g^+	NF	NF	NF
g^+	g^+	a	NF	NF	NF
g^+	g^+	g^-	NF	NF	NF
g^+	a	g^+	F	F	F
g^+	a	a	F	F	F
g^+	a	g^-	F	F	F
g^+	g^-	g^+	NF	NF	NF
g^+	g^-	a	F	F	F
g^+	g^-	g^-	F	F	F
a	g^+	g^+	NF	NF	NF
a	g^+	a	F	F	F
a	g^+	g^-	F (GM)	F	F
a	a	g^+	F	F	F
a	a	a	F	F	F
a	a	g^-	F	F	F
a	g^-	g^+	F	F (GM)	F (GM)
a	g^-	a	F	F	F
a	g^-	g^-	NF	NF	NF
g^-	g^+	g^+	F	F	F
g^-	g^+	a	F	F	F
g^-	g^+	g^-	NF	NF	NF
g^-	a	g^+	NF	NF	NF
g^-	a	a	NF	NF	NF
g^-	a	g^-	NF	NF	NF
g^-	g^-	g^+	F	F	F
g^-	g^-	a	F	F	F
g^-	g^-	g^-	NF	NF	NF

[a] F = found; NF = not found; GM = global minimum.

achiral centers and therefore provide the best representation of the behavior about these centers. Given that the rest of the structures are identical, these will allow for valid interpretations of what is occurring at C5 and C24.

All four methyl-substituted analogues were computed (cf. Figure 12). The PESs of **IV-H_2** and **IV-Me_2** illustrate the effects of having two methyl groups bonded at C5 (for the latter) versus two hydrogen atoms (for the former). The barriers of rotation for **IV-Me_2** are larger than that of **IV-H_2**, as expected. The PESs of **III-[H,Me]-*S*** and **III-[H,Me]-*R*** reveal intermediate barriers of rotation. Upon analysis of their respective contour maps, the presence of both point and axis chirality is evident, similar to the graphical representation in Figure 11.

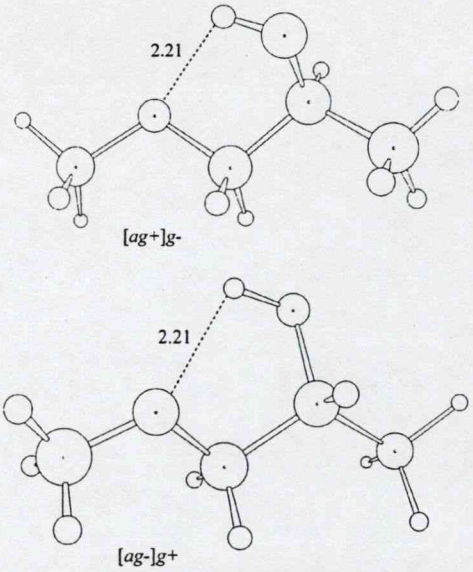

Figure 10. Global minima conformers of the (2*S*)-1-methoxypropan-2-ol (**III-[H,Me]-*S***) and (2*R*)-1-methoxypropan-2-ol (**III-[H,Me]-*R***) PEHSs computed at the B3LYP/6-31G(d) level of theory. Conformer [*ag*+]*g*− (top) represents the **III-[H,Me]-*S*** global minimum while conformer [*ag*−]*g*+ (bottom) represents the **III-[H,Me]-*R*** global minimum. Both conformers are enantiomeric and axis chiral pairs and possess intramolecular hydrogen bonding as the dominant feature.

The same methodology was applied to **II-H_2** and **II-Me_2**, which are the achiral analogues of the carbazole-containing enantiomers (cf. Figure 13). The effects of the carbazole ring substituent are seen as large maxima indicating large barriers of rotation present in all four PEHS. The double-methyl achiral structure also has larger barriers of rotation while the enantiomers have intermediate barriers due to the presence of only a single methyl at C24. Like the cases of **III-[H,Me]-*S*** and **III-[H,Me]-*R***, analysis of the contour maps for **I-*R*** and **I-*S*** reveals both point and axis chirality.

Upon construction of the PESs, the question put forth by Figure 5 was addressed: given the summation in eq 6, with two enantiomers with one stereocenter (denoted as >CHMe and >CMeH) and two corresponding achiral structures (denoted as $>CMe_2$ and $>CH_2$), would the summation of the two chiral structures cancel out the summation of the two achiral structures? In other words, would ΔE equal zero? This was tested

TABLE 10: Optimized Minima for the PEHS of (2*S*)-1-Methoxypropan-2-ol (III-[H,Me]-*S*) at the B3LYP/6-31G(d) Level of Theory

conformational assignment							
χ_2	χ_3	χ_{10}	χ_2	χ_3	χ_{10}	E (hartree)	rel E (kcal·mol^{-1})
g^+	g^+	a	77.95	63.78	−176.82	−308.861 759 588	5.58
g^+	g^+	g^-	84.85	52.21	−39.81	−308.868 518 645	1.33
g^+	g^-	a	83.72	−74.52	175.99	−308.864 709 683	3.72
g^+	g^-	g^-	79.25	−71.11	−59.35	−308.864 078 627	4.12
a	g^+	a	−175.69	71.27	−171.49	−308.863 878 357	4.25
a	g^+	g^-	−174.20	56.59	−45.91	−308.870 644 238	0.00
a	a	g^+	−178.25	174.71	72.56	−308.866 380 432	2.68
a	a	a	179.74	174.65	177.60	−308.866 211 574	2.78
a	a	g^-	179.01	176.00	−66.05	−308.866 106 215	2.85
a	g^-	g^+	174.72	−58.47	48.62	−308.869 488 916	0.72
a	g^-	a	177.81	−72.18	174.53	−308.863 889 500	4.24
g^-	g^+	g^+	−79.71	68.49	66.38	−308.864 165 391	4.07
g^-	g^+	a	−83.12	73.27	−173.44	−308.864 450 066	3.89
g^-	a	g^+	−81.44	176.91	70.61	−308.864 404 100	3.92
g^-	a	a	−83.98	176.50	175.83	−308.864 066 200	4.13
g^-	a	g^-	−80.81	179.85	−63.76	−308.863 793 580	4.30

TABLE 11: Optimized Minima for the PEHS of (2*R*)-1-Methoxypropan-2-ol (III-[H,Me]-*R*) at the B3LYP/6-31G(d) Level of Theory

conformational assignment							
χ_2	χ_3	χ_{10}	χ_2	χ_3	χ_{10}	E (hartree)	rel E (kcal·mol^{-1})
g^+	a	g^+	80.81	−179.85	63.76	−308.863 793 580	4.30
g^+	a	a	83.98	−176.50	−175.83	−308.864 066 200	4.13
g^+	a	g^-	81.44	−176.91	−70.61	−308.864 404 100	3.92
g^+	g^-	a	83.12	−73.27	173.44	−308.864 450 067	3.89
g^+	g^-	g^-	79.71	−68.49	−66.38	−308.864 165 391	4.07
a	g^+	a	−177.81	72.18	−174.53	−308.863 889 500	4.24
a	g^+	g^-	−174.72	58.47	−48.62	−308.869 488 917	0.72
a	a	g^+	−179.01	−176.00	66.05	−308.866 106 219	2.85
a	a	a	−179.73	−174.65	−177.60	−308.866 211 567	2.78
a	a	g^-	178.26	−174.71	−72.56	−308.866 380 447	2.68
a	g^-	g^+	174.20	−56.59	45.91	−308.870 644 238	0.00
a	g^-	a	175.69	−71.27	171.50	−308.863 878 355	4.25
g^-	g^+	g^+	−79.25	71.11	59.35	−308.864 078 622	4.12
g^-	g^+	a	−83.72	74.52	−175.99	−308.864 709 683	3.72
g^-	g^-	g^+	−84.85	−52.21	39.81	−308.868 518 645	1.33
g^-	g^-	a	−77.95	−63.78	176.82	−308.861 759 588	5.58

by using the constructed PESs described above because they covered all the conformational space about the stereocenters.

$$\Delta E = \{[E_R(>\mathrm{CHMe}) + E_S(>\mathrm{CMeH})] - [E(>\mathrm{CMe_2}) + E(>\mathrm{CH_2})]\} \quad (6)$$

According to Figure 5 and eq 6, the PESs of the four methyl-substituted analogues (cf. Figure 12) were added. The resulting values were used to produce another PES with ΔE energy values of about 0.0001 to 0.0007 hartree (~0.06−0.4 kcal·mol^{-1}). When the energy axis (z-axis) was calibrated to 1.0×10^{-3} hartree, which was the calibration used to produce the full PESs for analogues **IV-H$_2$**, **IV-Me$_2$**, **III-[H,Me]-*S***, and **III-[H,Me]-*R***, a resultant flat surface was produced (cf. Figure 14).

The same summation was performed on the four carbazole-substituted analogues from Figure 13, and the resulting values were plotted. The ΔE energy values produced from the summation were about 0.0005−0.009 hartree (~0.3−5.6 kcal·mol^{-1}), or about a factor of 10 larger than the PES produced for the methyl-substituted analogues. A flat surface was also produced when the calibration energy was reduced to 1.0×10^{-2} hartree (cf. Figure 15). (The raw data for Figures 12−15 are given in Supporting Information Tables S13 and S14.)

Given the above, the conformational energies of two prochiral structures can combine with the conformational energies of two enantiomers to produce a ΔE very close to zero. Although the ΔE energy values were not exactly zero, it would be expected that tight or very tight convergence threshold values would increase the number of zero significant digits for ΔE. With this is mind, it is of interest to ask the question, if the energetics of chiral compounds can be reproduced with achiral structures, would the administration of a mixture of two achiral structures have the same physiological effects as a racemic mixture of two enantiomers?

To the above question, the initial answer would seem to be no if one considers an asymmetrical molecular environment. In an asymmetrical environment, it is likely that only a chiral compound would have biological effects because nature would require a specific orientation for a biological effect. The latter statement is exemplified by the carvedilol β-adrenergic antagonist action; it is not expected that a mixture of two achiral compounds would have any β-adrenergic effects because only the *S*[-] configuration of carvedilol exerts action. This biological action would suggest an asymmetrical environment in which only a compound with a specific orientation (a chiral compound) could exert effects. However, if one considers symmetrical environments where enantiomers have equal activity, for

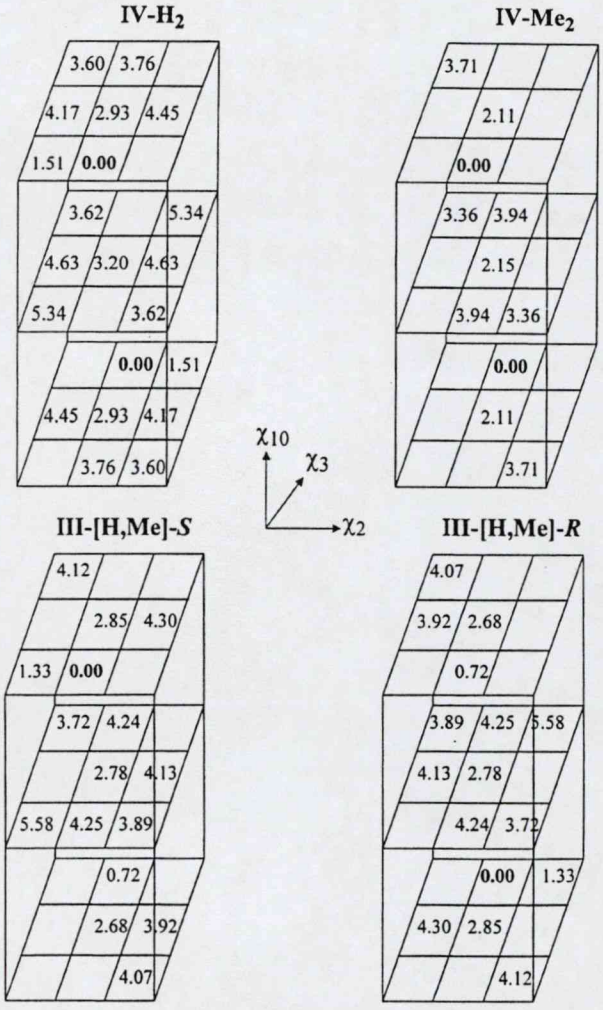

Figure 11. Graphical representation of the density functional computed PEHSs for **IV-H$_2$**, **IV-Me$_2$**, **III-[H,Me]-*S***, and **III-[H,Me]-*R*** indicating all minima found and the associated relative energy in kcal·mol^{-1}. Minima that were not found have a blank space.

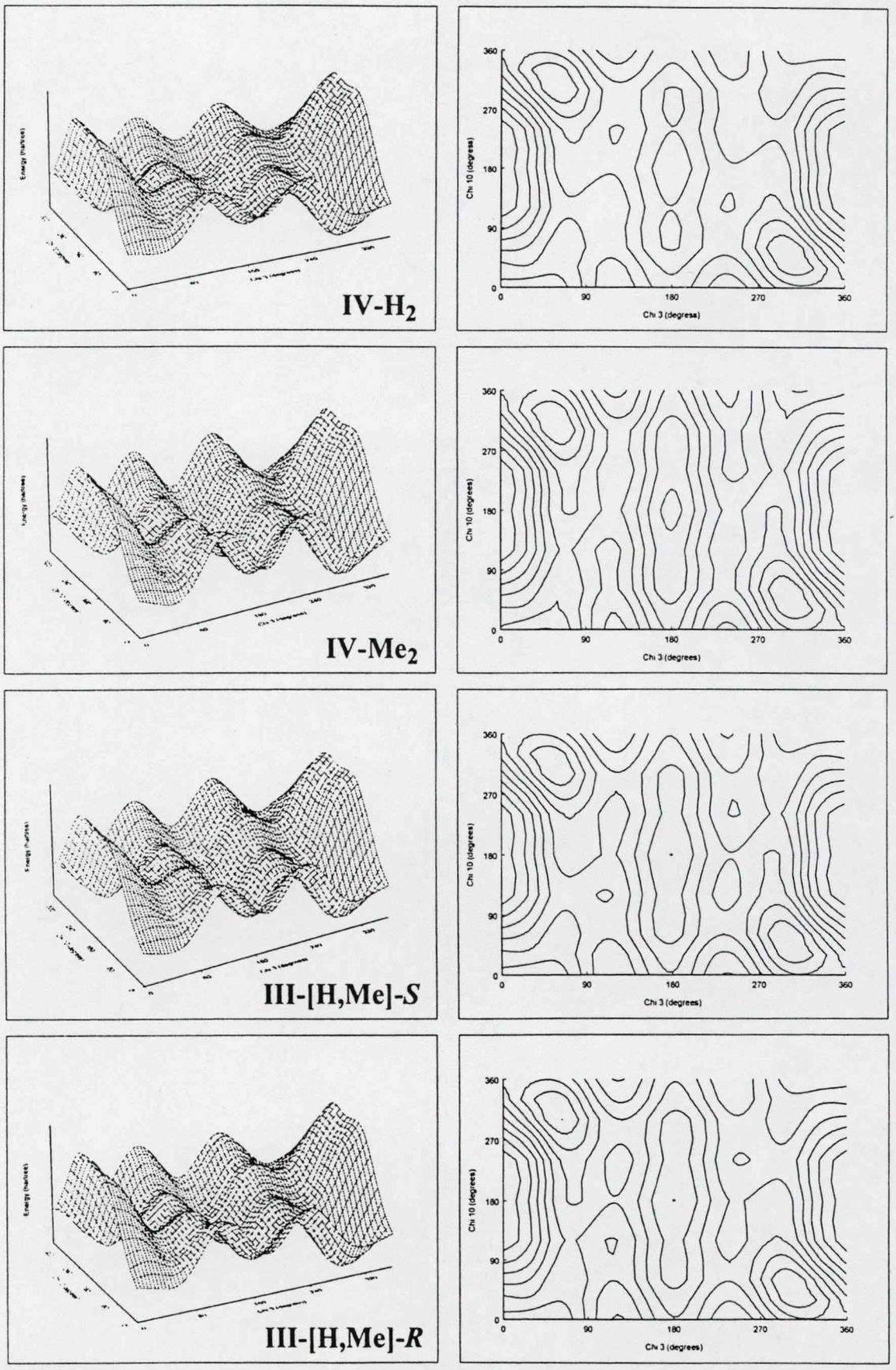

Figure 12. PES $[E = f(\chi_3,\chi_{10})]$ for (from top to bottom) 2-methoxyethan-1-ol (**IV-H$_2$**), 1-methoxy-2-methylpropan-2-ol (**IV-Me$_2$**), (2*S*)-1-methoxypropan-2-ol (**III-[H,Me]-*S***), and (2*R*)-1-methoxypropan-2-ol (**III-[H,Me]-*R***). The torsional angle χ_2 was frozen at 180.00° during the cross-sectional calculations of the PEHS.

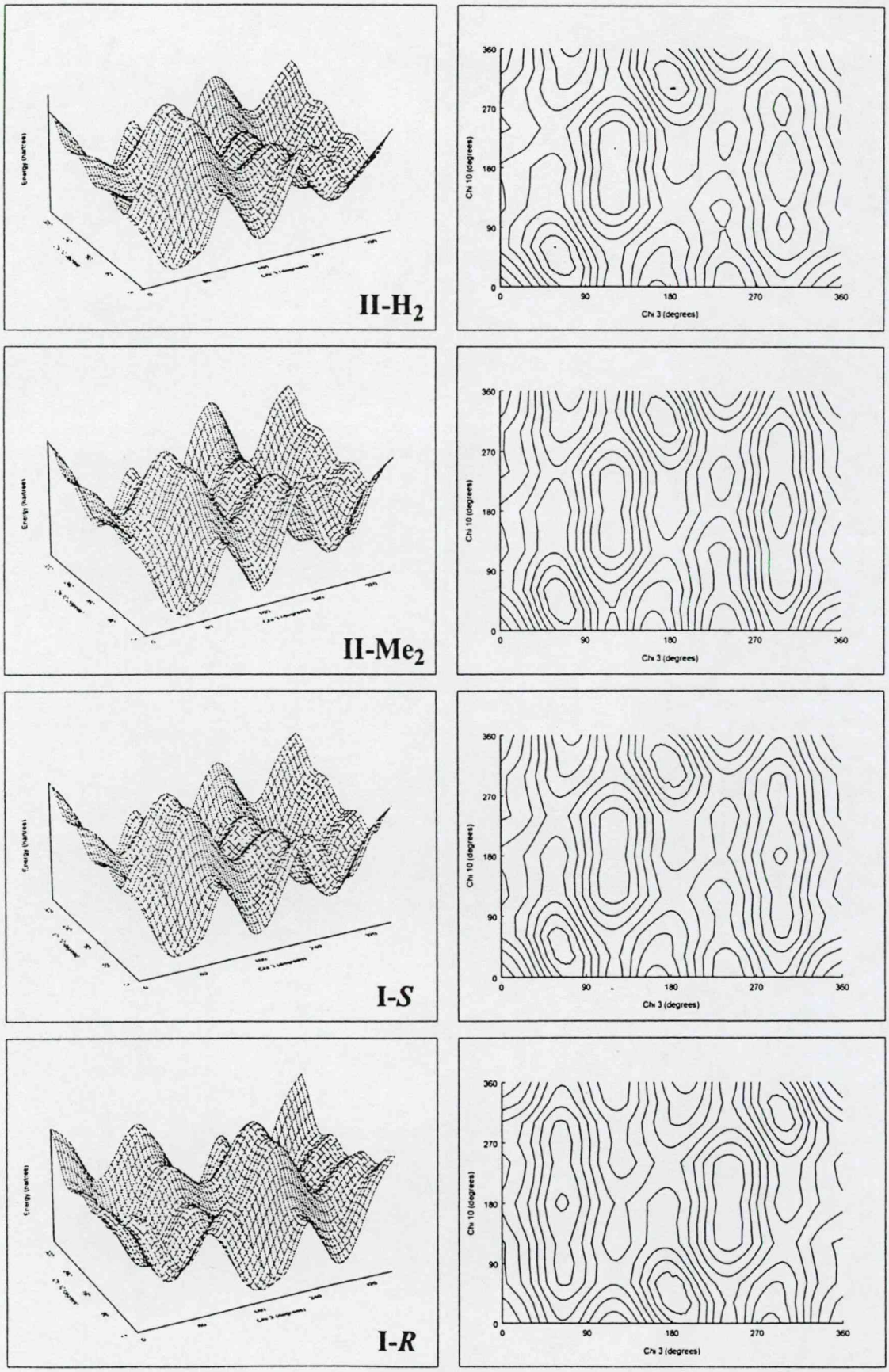

Figure 13. PES $[E = f(\chi_3,\chi_{10})]$ for carbazole-containing analogues (from top to bottom): (2-hydroxyethoxy)carbazol (**II-H$_2$**), (2-hydroxy-2-methylethoxy)carbazol (**II-Me$_2$**), *S*-4-(2-hydroxypropoxy)carbazol (**I-*S***), and *R*-4-(2-hydroxypropoxy)carbazol (**I-*R***). The torsional angles χ_1 and χ_2 were frozen at 180.00° during the cross-sectional calculations of the PEHS.

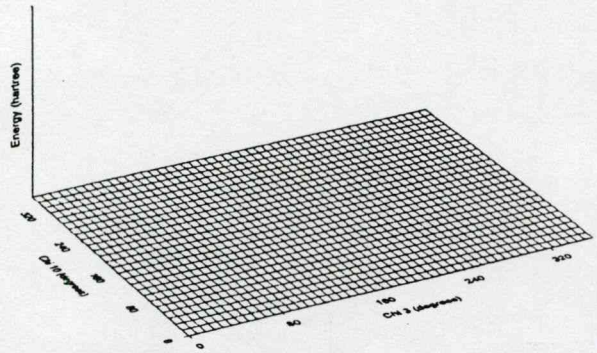

Figure 14. PES addition of carvedilol analogues (as illustrated in Figure 5) **IV-H_2**, **IV-Me_2**, **III-[H,Me]-*S***, and **III-[H,Me]-*R***.

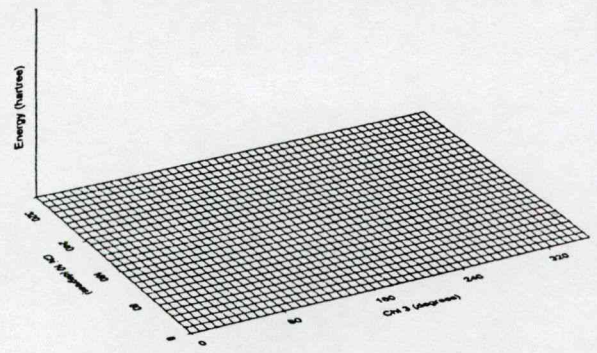

Figure 15. PES addition of carvedilol analogues (as illustrated in Figure 5) **II-H_2**, **II-Me_2**, **I-*S***, and **I-*R***.

example, carvedilol α_1-adrenergic antagonist and antioxidant effects, then would achiral compounds be able to produce qualitatively similar effects? Essentially, would a mixture of achiral carvedilol analogues similar to **II-H_2** and **II-Me_2** (at the stereocenter) be able to still produce α_1-adrenergic antagonist action and antioxidant activity, since it seems that these physiological effects can be produced without the need for chirality? Furthermore, at this stage one may wonder what would be the biological effects of administration of only one of the achiral structures.

Since the present work includes only gas phase results, more work is needed to shed light on these questions. Nonetheless, it would be tempting for drug design to be a fully achiral discipline so that, ideally, problems such as racemization at physiological pH, like that of thalidomide, could be circumvented. At the very least, however, the idea of equivalency between prochiral and chiral structures, as indicated by conformational energies, is a concept that must be clearly elucidated to see if any avenues could be exploited to aid processes like drug synthesis. Further, the data presented also demonstrate that the effects of chiral compounds are interdependent on the respective environment or medium they occupy because solely on the basis of molecular architecture, as quantified with conformational energies, some chiral properties can be both predicted and reproduced with achiral structures.

4. Conclusions

The carbazole-containing fragment of carvedilol, *R*- and *S*-4-(2-hydroxypropoxy)carbazol (fragment A), along with selected prochiral and chiral analogues, was subject to multidimensional conformational analysis (MDCA) of the full conformational space at the ab initio and DFT levels of theory. Conformational analysis revealed the intrinsic energetic profiles associated with point chirality and axis chirality present in these structures. It is shown that axis chirality induced by an asymmetric distribution of electron density (generally as a result of asymmetric conformations) is a feature of all structures and, thus, does not require a point chiral center. Further, the combination of prochiral and chiral structures (R−CH_2−OH, [*R*] and [*S*] R−CHMe−OH, and R−CMe_2−OH) indicates that the conformational energetics of two enantiomers can be negated by the conformational energies of two achiral analogues. This illustrated the concept of energetic equivalency between achiral and chiral structures and may be an avenue that can be exploited in relevant fields such as drug design and synthesis.

Supporting Information Available: Tables of optimized minima for the PEHSs and of the summation values plotted in Figures 12−15. This material is available free of charge via the Internet at http://pubs.acs.org.

References and Notes

(1) Eriksson, T.; Björkman, S.; Roth, B.; Fyge, Å.; Höglund, P. Stereospecific determination, chiral inversion in vitro and pharmacokinetics in humans of the enantiomers of thalidomide. *Chirality* **1995**, *7*, 44−52.

(2) Strong, M. FDA Policy and Regulation of Stereoisomers: Paradigm Shift and the Future of Safer and More Effective Drugs. *Food Drug Law J.* **1999**, *54*, 463−488.

(3) Costante-Crassous, J.; Marrone, T. J.; Briggs, J. M.; McCammon, J. A.; Collet, A. Absolute Configuration of Bromochlorofluoromethane from Molecular Dynamics Simulation of Its Enantioselective Complexation by Cryptophane-C. *J. Am. Chem. Soc.* **1997**, *119* (16), 3818−3823.

(4) Carroll, F. A. *Perspectives on Structure and Mechanism in Organic Chemistry*; Brooks/Cole Publishing Company: Pacific Grove, CA, 1998; pp 78−80.

(5) Hirschmann, H.; Hanson, K. R. On factoring chirality and stereoisomerism. *Top. Stereochem.* **1983**, *14*, 183−229.

(6) Agosta, W. C. The Absolute Configuration of Pentadiendioic Acid. *J. Am. Chem. Soc.* **1964**, *86* (13), 2638−2642.

(7) Carlson, W.; Oberg, K. Clinical Pharmacology of Carvedilol. *J. Cardiovasc. Pharmacol. Ther.* **1999**, *4* (4), 205−218.

(8) Capomolla, S.; Febo, O.; Gnemmi, M.; Riccardi, G.; Opasich, C.; Carporotondi, A.; Mortara, A.; Pinna, G.; Cobelli, F. Beta-blockade therapy in chronic heart failure: diastolic function and mitral regurgitation improvement by carvedilol. *Am. Heart J.* **2000**, *139* (4), 596−608.

(9) Metra, M.; Nodari, S.; D'Aloia, A.; Bontempi, L.; Boldi, E.; Cas, L. D. A rationale for the use of beta-blockers as standard treatment for heart failure. *Am. Heart J.* **2000**, *139* (3), 511−521.

(10) Feuerstein, G.; Ruffolo, R. R., Jr. Beta-blockers in congestive heart failure: the pharmacology of carvedilol, a vasodilating beta-blocker and antioxidant, and its therapeutic utility in congestive heart failure. *Adv. Pharmacol. (San Diego)* **1998**, *42*, 611−615.

(11) Saijonmaa, O.; Metsarinne, K.; Fyhrquist, F. Carvedilol and its metabolites suppress endothelin-1 production in human endothelial cell culture. *Blood Pressure* **1997**, *6* (1), 24−28.

(12) Packer, M.; Bristow, M. R.; Cohn, J. N.; Colucci, W. S.; Fowler, M. B.; Gilbert, E. M.; Shusterman, N. H. The effect of carvedilol on morbidity and mortality in patients with chronic heart failure. U.S. Carvedilol Heart Failure Study Group. *N. Engl. J. Med.* **1996**, *334* (21), 1349−1355.

(13) Berg, M. A.; Chasse, G. A.; Deretey, E.; Fuzery, A. K.; Fung, B. M.; Fung, D. Y. K.; Henry-Riyad, H.; Lin, A. C.; Mak, M. L.; Mantas, A.; Patel, M.; Repyakh, I. V.; Staikova, M.; Salpietro, S. J.; Ting-Hua Tang; Vank, J. C.; Perczel, A.; Csonka, G. I.; Farkas, O.; Torday, L. L.; Szekely, Z.; Csizmadia, I. G. Prospects in computational molecular medicine: a millennial mega-project on peptide folding. *THEOCHEM* **2000**, *500*, 5−58.

(14) Feuerstein, G.; Yue, T. L.; Ma, X.; Ruffolo, R. R. Novel mechanisms in the treatment of heart failure: inhibition of oxygen radicals and apoptosis by carvedilol. *Prog. Cardiovasc. Dis.* **1998**, *41* (1 Suppl 1), 17−24.

(15) Searlee, A. J. F.; Gree, C.; Wilson, R. L. Ellipticines and carbazoles as antioxidants. In *Oxygen Radicals and Biology*; Borns, W., Saran, M., Tait, D., Eds.; Walter de Gruyter & Co.: Berlin, 1984; pp 377−381.

(16) Oldham, H. G.; Clarke, S. E. In vitro identification of the human cytochrome P450 enzymes involved in the metabolism of R(+)- and S(−)-carvedilol. *Drug Metab. Dispos.* **1997**, *25* (8), 970−977.

(17) Feuerstein, R.; Yue, T. L. A potent antioxidant, SB209995, inhibits oxygen-radical-mediated lipid peroxidation and cytotoxicity. *Pharmacology* 1994, *48* (6), 385−391.

(18) Yue, T. L.; Mckenna, P. J.; Lysko, P. G.; Gu, J. L.; Lysko, K. A.; Ruffolo, R. R., Jr.; Feuerstein, G. Z. SB 211475, a metabolite of carvedilol, a novel antihypertensive agent, is a potent antioxidant. *Eur. J. Pharmacol.* 1994, *251* (2−3), 237−243.

(19) Gehr, T. W.; Tenero, D. M.; Boyle, D. A.; Qian, Y.; Sica, D. A.; Shusterman, N. H. The pharmacokinetics of carvedilol and its metabolites after single and multiple dose oral administration in patients with hypertension and renal insufficiency. *Eur. J. Clin. Pharmacol.* 1999, *55* (4), 269−277.

(20) van der Does, R.; Hauf-Zachariou, U.; Pfarr, E.; Holtbrugge, W.; Konig, S.; Griffiths, M.; Lahiri, A. Comparison of safety and efficacy of carvedilol and metoprolol in stable angina pectoris. *Am. J. Cardiol.* 1999, *83* (5), 643−649.

(21) Ruffolo, R. R., Jr.; Gellai, M.; Hieble, J. P.; Willette, R. N.; Nichols, A. J. The pharmacology of carvedilol. *Eur. J. Clin. Pharmacol.* 1990, *38* (Suppl 2), S82−S88.

(22) Oliveira, P. J.; Marques, M. P.; Batista de Carvalho, L. A. E.; Moreno, A. J. M. Effects of Carvedilol on Isolated Heart Mitochondria: Evidence for a Protonophoretic Mechanism. *Biochem. Biophys. Res. Commun.* 2000, *276*, 82−87.

(23) Frisch, M. J.; Trucks, G. W.; Schlegel, H. B.; Scuseria, G. E.; Robb, M. A.; Cheeseman, J. R.; Zakrzewski, V. G.; Montgomery, J. A., Jr.; Stratmann, R. E.; Burant, J. C.; Dapprich, S.; Millam, J. M.; Daniels, A. D.; Kudin, K. N.; Strain, M. C.; Farkas, O.; Tomasi, J.; Barone, V.; Cossi, M.; Cammi, R.; Mennucci, B.; Pomelli, C.; Adamo, C.; Clifford, S.; Ochterski, J.; Petersson, G. A.; Ayala, P. Y.; Cui, Q.; Morokuma, K.; Malick, D. K.; Rabuck, A. D.; Raghavachari, K.; Foresman, J. B.; Cioslowski, J.; Ortiz, J. V.; Baboul, A. G.; Stefanov, B. B.; Liu, G.; Liashenko, A.; Piskorz, P.; Komaromi, I.; Gomperts, R.; Martin, R. L.; Fox, D. J.; Keith, T.; Al-Laham, M. A.; Peng, C. Y.; Nanayakkara, A.; Gonzalez, C.; Challacombe, M.; Gill, P. M. W.; Johnson, B. G.; Chen, W.; Wong, M. W.; Andres, J. L.; Head-Gordon, M.; Replogle, E. S.; Pople, J. A. *Gaussian 98* (Revision A.9); Gaussian, Inc.: Pittsburgh, PA, 1998.

(24) Becke, A. D. Density-functional thermochemistry. III. The role of exact exchange. *J. Chem. Phys.* 1993, *98* (7), 5648−5652.

(25) *Axum 5.0C for Windows*; MathSoft Incorporated: 1996.

(26) Almeida, D. R. P.; Pisterzi, L. F.; Chass, G. A.; Torday, L. L.; Varro, A.; Papp, J. Gy.; Csizmadia, I. G. Density Functional Molecular Study on the Full Conformational Space of the *S*-4-(2-Hydroxypropoxy)-carbazol Fragment of Carvedilol (1-(9H-Carbazol-4-yloxy)-3-[2-(2-methoxyphenoxy)ethylamino]-2-propanol) in a Vacuum and in Different Solvent Media. *J. Phys. Chem. A* 2002, *106* (43), 10423−10436.

ELSEVIER

Journal of Molecular Structure (Theochem) 666–667 (2003) 557–580

THEO CHEM

www.elsevier.com/locate/theochem

Conformational-dependent basicity of carvedilol Fragment C: an ab initio study on the primary amine, aminoethoxy-2-methoxy-benzene

David R.P. Almeida[a,*], Donna M. Gasparro[a], Luca F. Pisterzi[a], Jason R. Juhasz[a], Ferenc Fülöp[b], Imre G. Csizmadia[a,c,d]

[a]*Lash Miller Laboratories, Department of Chemistry, University of Toronto, 80 St George Street, Toronto, Ont., Canada M5S 3H6*
[b]*Institute of Pharmaceutical Chemistry, Albert Szent-Györgyi Medical University, Szeged University, Eötvös u. 6., H-6720 Szeged, Hungary*
[c]*Global Institute of Computational Molecular and Materials Science (GIOCOMMS), 1422 Edenrose Street, Mississauga, Ont., Canada L5V 1H3*
[d]*Department of Medical Chemistry, University of Szeged, Dóm tér 8, 6720 Szeged, Hungary*

Abstract

Carvedilol produces various physiological effects via multiple modes of action. In mitochondria, it is purported that carvedilol is cardioprotective by acting as a mild uncoupler of oxidative phosphorylation; the mechanism is thought to involve the protonable amino group in its side-chain. This uncoupling subsequently leads to a decrease in production of reactive oxygen species and reduced mitochondrial oxidative stress. In the current work, the carvedilol fragment aminoethoxy-2-methoxy-benzene (Fragment C) has been investigated to illustrate the effects of molecular conformation on intrinsic basicity as related to such proton shuttling pathways. It has been previously been shown for carvedilol Fragment B that molecular conformation dictates the energetics of deprotonation. Fragment C is also studied in this context because, as a primary amine which may be deprotonated via three different protons, it provides an ideal structure to elucidate such conformational effects. By calculating the associated energies of deprotonation for each proton, the relative effects of conformation on intrinsic basicity can be determined. The ab initio Hartree–Fock, RHF/3-21G, level of theory was employed for structural analysis and the potential energy hypersurface of Fragment C was computed with geometry optimizations of the conformational minima. Energies of deprotonation were determined with vertical and adiabatic calculations for each proton in each converged minima. Multi-dimensional conformational analysis of the protonated potential energy hypersurface revealed a total of 24 converged minima out of a possible 81 (≈30% convergence). Conformers with the lowest relative energies possessed a motif consisting of bifurcated hydrogen-bonds forming an eight-membered ring. Hydrogen bond networks forming five-membered rings along with intramolecular dipole-type interactions were also evident. In contrast, protonated conformers with large relative energies were devoid of any significant structural features. Geometry optimization of the deprotonated potential energy hypersurface revealed similar structural features; further, optimization of conformational minima belonging to the deprotonated hypersurface revealed a novel amine–aromatic pi electronic interaction currently under study. In analyzing the derived energetics of deprotonation for the primary amine, it was found that conformers lacking significant stabilizing structural motifs were favored and possessed the lowest energies of deprotonation for Fragment C. The route with the lowest energy of deprotonation (optimized) was via the deprotonation of conformer ag^+ag^+ which required 238.34 kcal mol^{-1}. It can thus be concluded that,

* Corresponding author.
E-mail addresses: dalmeida@medscape.com (D.R.P. Almeida), dgasparro@medscape.com (D.M. Gasparro), lpisterzi@medscape.com (L.F. Pisterzi), jasonjuhasz@medscape.com (J.R. Juhasz), fulop@pharma.szote.u-szeged.hu (F. Fülöp), icsizmad@alchemy.chem.utoronto.ca (I.G. Csizmadia).

0166-1280/$ - see front matter
doi:10.1016/j.theochem.2003.08.080

as previously shown for the secondary amine Fragment B, and now for the primary amine Fragment C, proton shuttling mechanisms involving carvedilol, and amines in general, will favor conformations with minimal intramolecular stabilization. As such, molecular conformation and associated structural features will determine, at least with regards to energetics, the intrinsic basicity of compounds and can be used to describe and predict favored substrate conformations for protonophoretic pathways as that postulated for carvedilol in mitochondria.

Keywords: Carvedilol fragment; Aminoethoxy-2-methoxy-benzene; Proton affinity; Basicity; RHF

1. Introduction

1.1. Biological background

Carvedilol, 1-(9*H*-carbazol-4-yloxy)-3-[2-(2-methoxy-phenoxy)ethylamino]-2-propanol ($C_{24}H_{26}N_2O_4$), is a lipophilic multiple-action neurohormonal antagonist [1]. As a β-blocker, carvedilol antagonizes noradrenaline non-selectively at β_1- (heart muscle, kidney) and β_2- (certain blood vessels, smooth muscle of some organs) adrenergic receptors, reducing total cardiac work-load [1–3]. Carvedilol is also a selective α_1-adrenergic receptor (found in most sympathetic target tissues) antagonist causing vasodilation at peripheral resistance vessels, which decreases pre- and after-load, thereby reducing cardiac work and wall tensions [4]. Therapeutically, carvedilol is a cardiovascular drug of proven efficiency in the treatment of mild to moderate congestive heart failure (CHF), essential hypertension, angina, and in improvement of left ventricular function [1,5]. The US Data and Safety Monitoring Board stopped, for ethical reasons, the clinical investigations of carvedilol before its completion due to greatly lowered mortality rates [6,7].

Aside from its neurohormonal modes of actions, carvedilol possesses direct myocardial-protective antioxidant properties. The carbazole ring gives carvedilol the ability to donate electrons to directly 'scavenge' the activities of oxygen-containing free radicals (or reactive oxygen species; ROS) such as: oxygen superoxide ($O_2^{\cdot-}$), hydrogen peroxide (H_2O_2), hydroxyl radical ($^{\cdot}OH$), and peroxynitrite ($ONOO^-$), helping to protect against the deleterious effects of free radical damage [8]. The striking free-radical scavenging ability of carbazole, such as that seen against lipid peroxidation, is enhanced by its relatively high lipid solubility [9].

Further work has indicated that carvedilol may exert indirect cardiac antioxidant effects by protecting mitochondria from oxidative stress by acting as a mild uncoupler of oxidative phosphorylation via a protonophoretic pathway involving the amino group of carvedilol's side-chain [10]. Due to the high demand of ATP from working cardiac muscles, a constant mitochondrial input is required and a compromise of mitochondrial bioenergetics leads to a failure to maintain calcium homeostasis which triggers pathways of cell death and suppresses delivery of ATP to heart muscles [11].

Carvedilol may also play a role in the prevention of Alzheimer's disease. It is generally accepted that the neuronal cell loss in Alzheimer's patients is associated with the formation of fibrils from β-amyloid peptide (Aβ) monomers (39-43 residue peptide) and that preventing this aggregation of Aβ might provide a method of slowing the pathology of Alzheimer's disease [12]. Carvedilol acts as a novel anti-fibrillar agent (by inhibiting fibril formation) due to three factors: (1) possession of one central basic amino pharmacophore, (2) possession of two cyclic hydrophobic ring centroids, and (3) the molecular flexibility to adopt a specific three-dimensional pharmacophore conformation [12]. However, it is currently not known if carvedilol binds to Aβ monomers or to small oligomers to prevent fibril formation [12].

Carvedilol contains one stereocentre and is commercially available as a racemic mixture of both its enantiomers (*R*[+] and *S*[−]) (Fig. 1). However, the enantiomers of carvedilol show marked stereoselective properties; both enantiomers have equal α_1 blocking activity and antioxidant activity but only the *S*[−] enantiomer contains the non-selective β-adrenergic blocking activity [13]. As such, neither enantiomer alone has the same pharmacologic profile as the racemic mixture of

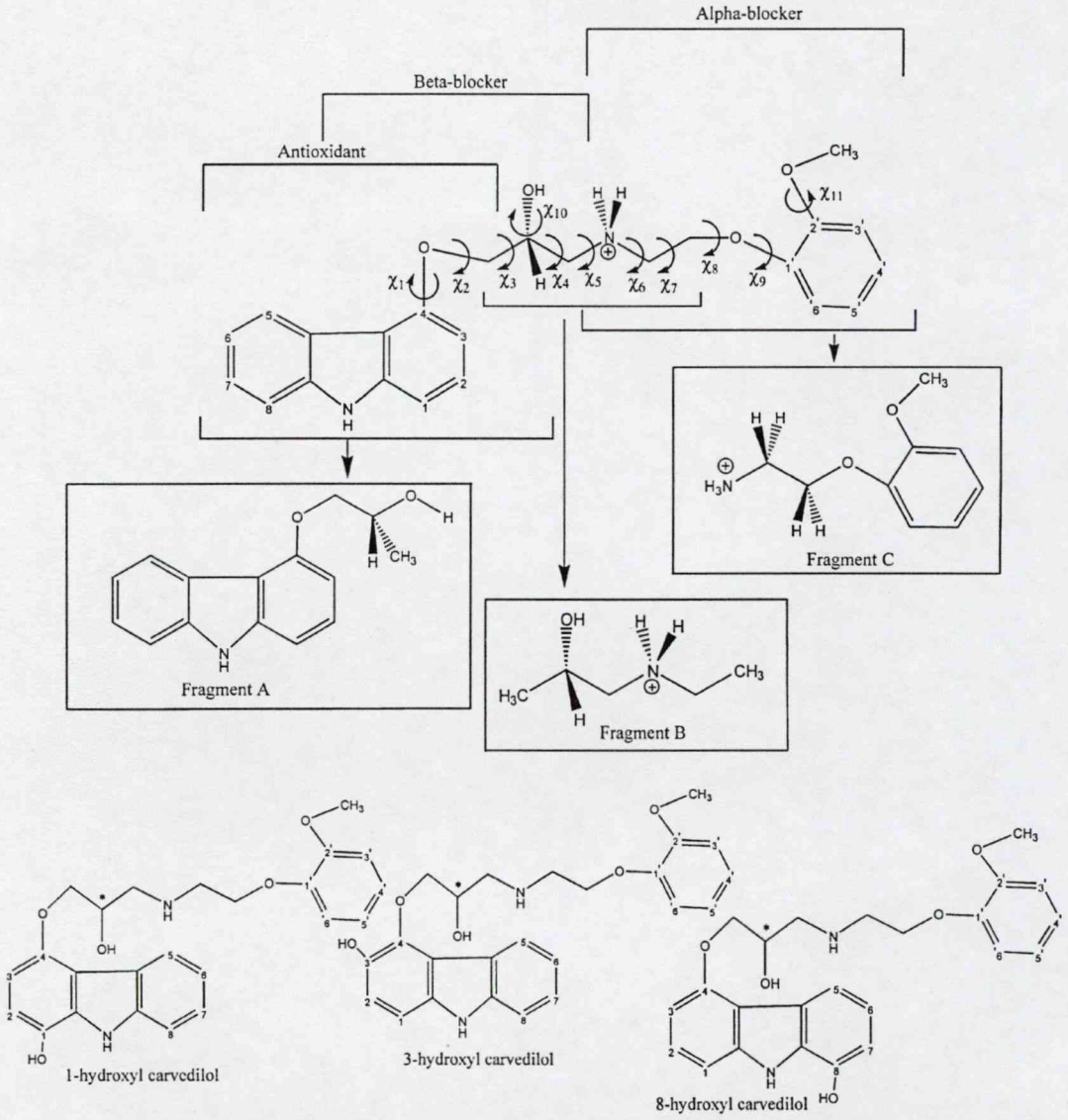

Fig. 1. The complete molecular structure and function of *N*-protonated carvedilol indicating all eleven torsional angles and its three pharmocophoric fragments: *R*- and *S*-4-(2-hydroxypropoxy)carbazol (Fragment A), 2(*R* and *S*)-1-(ethylamonium)propane-2-ol (Fragment B), and aminoethoxy-2-methoxy-benzene (Fragment C) (top). Biotransformation of carvedilol produces three hydroxylated metabolites with varying biological activity: 1-hydroxyl, 3-hydroxyl, and 8-hydroxyl carvedilol (bottom).

carvedilol used clinically [14]. The hydroxylated metabolites of carvedilol: 1-, 3-, and 8-hydroxyl carvedilol (Fig. 1), retain the direct antioxidant properties of carvedilol due to the presence of the carbazole moiety [8], the ability to act as uncouplers of oxidative phosphorylation due to the presence of the protonable amino group [10], and to act as anti-fibrillar agents due to possession of the three characteristics described above [12]. As such, it can be postulated that the analysis of the conformational

space of carvedilol's molecular fragments can be extrapolated to the active hydroxylated metabolites as well.

1.2. Chemical background

Carvedilol is composed of three distinct pharmacophores (Fig. 1) and was therefore divided into three molecular fragments: *R*- and *S*-4-(2-hydroxypropoxy)carbazol (Fragment A) is responsible for the carbazole-related antioxidant effects of carvedilol, 2(*R* and *S*)-1-(ethylamonium)propane-2-ol (Fragment B) contains the protonophoretic amino group responsible for the uncoupling of mitochondrial oxidative phosphorylation, and aminoethoxy-2-methoxy-benzene (Fragment C) provides the α_1-antagonist action of carvedilol. (Beta-blockage is exerted by the composite of both Fragments A and B.) While Fragments A [15] and B [16] have been studied, the current objective is the analysis of Fragment C.

Normally, catecholamine (i.e. noradrenaline) binding to an α_1-adrenergic receptor activates phospholipase C (PLC) and inositol 1,4,5-trisphosphate (IP_3) leading to the opening of calcium (Ca^{2+}) channels in the cell membrane and/or releasing Ca^{2+} from intracellular stores [17]. The resulting intracellular Ca^{2+} signal leads to muscle contraction. Antagonism at this adrenergic receptor subtype by carvedilol inhibits the cardiac and smooth muscle autonomic nervous system (ANS) effectors responsible for muscle contraction leading to the cardiovascular effect of reduced wall tensions via vasodilation [17]. Since α_1-adrenergic receptor antagonism by carvedilol provides a vital function, the full conformational space of Fragment C will be investigated in this study.

With regards to the uncoupling of oxidative phosphorylation, carvedilol's secondary amino group decreases the mitochondrial electric potential via a weak protonophoretic mechanism [10]. An uncoupler exerts its effects by eliminating the essential mitochondrial proton gradient by freely exchanging protons across the mitochondrial membranes [18]. It is proposed that the amino group of carvedilol ($pK_a = 7.9$) binds a proton in the low pH intermembrane space, crosses the membrane in the positively charged protonated form into the relatively higher pH mitochondrial matrix (driven by its high lipid solubility and the electric potential which is negative in the matrix with regards to the intermembrane space), releases the proton in the matrix, and then returns to the cytosolic leaflet in the deprotonated neutral from [10]. The phenomenon known as 'mild uncoupling' occurs when a small decrease in mitochondrial electric potential induces a reduction in the ROS produced by the mitochondrial respiratory chain, thereby producing protective effects [10,19,20].

Classical uncouplers such as salicylanilides [2′,5-dichloro-3-*tert*-butyl-4′-nitrosalicylanilide (S-13) and 3,4′,5-trichlorosalicylanilide (DCC)], carbonyl cyanide phenylhydrazones [carbonylcyanide *p*-triflouromethoxyphenylhydrazone (FCCP) and carbonylcyanide *m*-chlorophenyl hydrazone (CCCP)], along with carvedilol and Fragment B, all possess secondary amino groups with two protons available for deprotonation. However, Fragment C and its primary amino group presents a scenario in which there exists possibilities for deprotonation via three different protons. It has been shown for Fragment B that the conformation adopted will influence the proton abstracted because molecular conformation biases protons differently, thereby resulting in different energies of deprotonation [16]. As such, higher energy structures with lower energies of deprotonation will be better candidates for protonophoretic pathways as that postulated for carvedilol in the mitochondria. Compounding these findings with the high variability in mitochondria uncoupling believed to be due to molecular conformation [10], the intrinsic basicity of Fragment C will also be investigated along with its full conformational space to illustrate if molecular conformation exerts the same influence on the protonophoretics of primary amines. Such a challenge does not appear for tertiary amines because only one proton can be abstracted and neither for quaternary ammonium compounds because of the lack of protons at the nitrogen centre.

2. Computational method

Fragment C possesses four torsional angles of interest and a terminal amino group (Fig. 2). The conformers of its potential energy hypersurface (PEHS) can be described by Eq. (1). It is expected that, as shown for Fragment A [15], the achiral

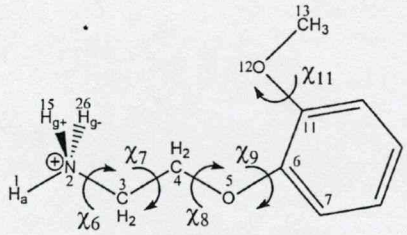

aminoethoxy-2-methoxy-benzene
(Fragment C)

$E = f(\chi_7, \chi_8, \chi_9, \chi_{11})$

χ_7 = O5-C4-C3-N2
χ_8 = C6-O5-C4-C3
χ_9 = C7-C6-O5-C4
χ_{11} = C13-O12-C11-C6

Fig. 2. Numbering and definition of torsional angles for aminoethoxy-2-methoxy-benzene (Fragment C). Numbers placed beside atoms indicates numbering used as z-matrix input for GAUSSIAN 98.

analogues of Fragments A [21], B [16], C will display axis chirality as described by Eq. (2). Eq. (2) states that for an achiral structure with two energetically equivalent minima belonging to the PEHS, plus (P) and minus (M), all torsional angles for those minima are switched from clockwise (CW) to counter-clockwise (CCW) rotation

$$E = f(\chi_7, \chi_8, \chi_9, \chi_{11}) \tag{1}$$

$$E_P = E_M \tag{2}$$

$$f_P(\chi_7, \chi_8, \chi_9, \chi_{11}) = f_M(-\chi_7, -\chi_8, -\chi_9, -\chi_{11})$$

Structural analysis of Fragment C was studied by multi-dimensional conformational analysis (MDCA) and its PEHS was computed with optimizations of the conformational minima. With four torsional angles (χ_7, χ_8, χ_9, χ_{11}) and three possible minima for each torsional angle (*gauche plus*, g^+; *anti*, *a*; *gauche minus*, g^-), there are expected a grand total of $3^4 = 81$ possible minima for Fragment C.

As mentioned, the structure of Fragment C (Fig. 2) can be deprotonated via the removal of three protons. If any of these protons were replaced with deuterium, one would have deuterium in either of three positions: *anti* position (H1, denoted as H_a), the g^+ position (H15, denoted as H_{g+}), or the g^- position (H26, denoted as H_{g-}). Due to these possibilities, a three prong methodology was applied to analyze the conformational-dependent basicity of Fragment C. (The methodology applied here is similar to the methodology applied to the secondary amine molecular fragment of carvedilol, Fragment B [16].)

For each unique converged conformation of the PEHS, protonated Fragment C (CH^+) was deprotonated of protons H_a, H_{g+}, and H_{g-}, independent of each other, and the vertical energies of deprotonation were calculated with single-point energy (SPE) calculations. These energy values are denoted as $\Delta E_{vert}(a)$, $\Delta E_{vert}(g^+)$, and $\Delta E_{vert}(g^-)$ (Eqs. (3)–(5)). The H_a, H_{g+}, and H_{g-} deprotonated Fragment C (C) conformers were then geometrically optimized and adiabatic energies of deprotonation were calculated based on fully optimized values. These values are denoted as $\Delta E_{opt}(a)$, $\Delta E_{opt}(g^+)$, and $\Delta E_{opt}(g^-)$ (Eqs. (6)–(8)). A third set of values, denoted as $\Delta\Delta E(a)$, $\Delta\Delta E(g^+)$, and $\Delta\Delta E(g^-)$, represent the differences between the vertical and the optimized adiabatic energies of deprotonation for each conformer (Eqs. (9)–(11)). These latter values can be interpreted as the stabilization experienced by Fragment C conformers as they adopted an optimized conformation after deprotonation. The above methodology is illustrated in Fig. 3. (A positive value for the energy of deprotonation appears because bond-breaking is always an endothermic process.)

$$\Delta E_{vert}(a) = |E_{opt}[CH^+] - E_{SP}[C]| \tag{3}$$

(H_a deprotonation)

$$\Delta E_{vert}(g^+) = |E_{opt}[CH^+] - E_{SP}[C]| \tag{4}$$

(H_{g+} deprotonation)

$$\Delta E_{vert}(g^-) = |E_{opt}[CH^+] - E_{SP}[C]| \tag{5}$$

(H_{g-} deprotonation)

$$\Delta E_{opt}(a) = |E_{opt}[CH^+] - E_{opt}[C]| \tag{6}$$

(H_a deprotonation)

$$\Delta E_{opt}(g^+) = |E_{opt}[CH^+] - E_{opt}[C]| \tag{7}$$

(H_{g+} deprotonation)

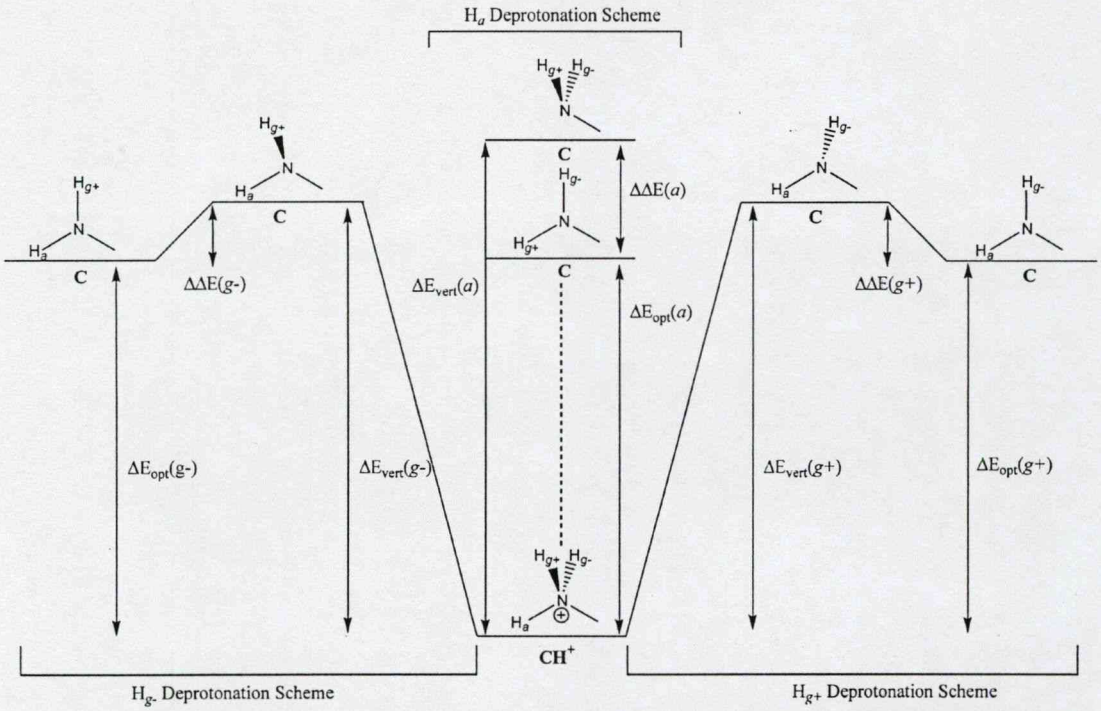

Fig. 3. Methodology employed to analyze the conformational-dependent basicity of the amino group of Fragment C. Each converged minima of the protonated Fragment C PEHS was subject to the deprotonation of H_a (H1), H_{g+} (H15), and H_{g-} (H26) protons.

$$\Delta E_{opt}(g^-) = |E_{opt}[CH^+] - E_{opt}[C]| \quad (8)$$

(H_{g-} deprotonation)

$$\Delta\Delta E(a) = \Delta E_{vert}(a) - \Delta E_{opt}(a) \quad (9)$$

(H_a deprotonation)

$$\Delta\Delta E(g^+) = \Delta E_{vert}(g^+) - \Delta E_{opt}(g^+) \quad (10)$$

(H_{g+} deprotonation)

$$\Delta\Delta E(g^-) = \Delta E_{vert}(g^-) - \Delta E_{opt}(g^-) \quad (11)$$

(H_{g-} deprotonation)

All computations were performed using the GAUSSIAN 98 software program [22]. Fragment C was exclusively defined using the GAUSSIAN 98 z-matrix internal coordinate system, to specify molecular structure, stereochemistry, and geometry. All calculations were performed at the Hartree–Fock, RHF/3-21G, level of theory. Graphical data was plotted using Axum 5.0 [23].

3. Results and discussion

3.1. MDCA of the protonated aminoethoxy-2-methoxy-benzene (Fragment C) PEHS

MDCA of the protonated Fragment C PEHS revealed that, instead of the expected 81 conformers, a total of 24 converged minima were found [24/81 ≈ 30% convergence and (81 − 24)/81 ≈ 70% annihilated] (Table 1). Conformational structural assignments for the conformational minima were made according to Eq. (12). This is based on the general observation that, if one were to rotate

Table 1
Optimized minima for the PEHS of aminoethoxy-2-methoxy-benzene (Fragment C) at the RHF/3-21G level of theory

Conformational assignment				χ_7	χ_8	χ_9	χ_{11}	E (hartree)	Relative energy (kcal mol^{-1})
χ_7	χ_8	χ_9	χ_{11}						
g^+	g^+	g^+	g^+		Not found moved to			$g^+g^-g^-g^+$	
g^+	g^+	g^+	a		Not found moved to			$g^+g^+g^+g^-$	
g^+	g^+	g^+	g^-	44.46	71.68	70.76	-98.81	−549.873068247	*0.00*
g^+	g^+	a	g^+		Not found moved to			g^+aaa	
g^+	g^+	a	A		Not found moved to			g^+aaa	
g^+	g^+	a	g^-		Not found moved to			$g^+g^+g^+g^-$	
g^+	g^+	g^-	g^+		Not found moved to			$g^+ag^-g^A$	
g^+	g^+	g^-	a		Not found moved to			$g^+ag^-g^A$	
g^+	g^+	g^-	g^-		Not found moved to			$g^+g^-g^-g^+$	
g^+	a	g^+	g^+		Not found moved to			$g^+ag^-g^B$	
g^+	a	g^+	a		Not found moved to			g^+aaa	
g^+	a	g^+	g^-		Not found moved to			g^+aaa	
g^+	a	a	g^+		Not found moved to			$g^+ag^-g^A$	
g^+	a	a	a	41.80	122.91	120.56	−179.67	−549.863583899	5.95
g^+	a	a	g^-		Not found moved to			$g^+ag^-g^B$	
g^+	a	g^-	g^+		Not found moved to			$g^+ag^-g^C$	
g^+	a	g^-	a^A	38.30	−137.12	−115.57	−169.54	−549.872527050	0.34
g^+	a	g^-	a^B	59.99	−140.29	−81.29	156.52	−549.870278796	1.75
g^+	a	g^-	a^C	61.03	−135.10	−77.42	144.54	−549.870234030	1.78
g^+	a	g^-	g^-		Not found moved to			$g^+ag^-g^B$	
g^+	g^-	g^+	g^+		Not found moved to			$g^+ag^-g^A$	
g^+	g^-	g^+	a		Not found moved to			$g^+ag^-g^B$	
g^+	g^-	g^+	g^-		Not found moved to			$g^+g^-g^-g^+$	
g^+	g^-	a	g^+		Not found moved to			g^+aaa	
g^+	g^-	a	a		Not found moved to			$g^+ag^-g^A$	
g^+	g^-	a	g^-	95.14	−39.40	135.84	−96.81	−549.861239554	7.42
g^+	g^-	g^-	g^+	62.23	−116.45	−73.64	90.67	−549.871425222	1.03
g^+	g^-	g^-	a		Not found moved to			$g^+g^-g^-g^+$	
g^+	g^-	g^-	g^-		Not found moved to			$g^+g^-g^-g^+$	
a	g^+	g^+	g^+		Not found moved to			$aaaa^A$	
a	g^+	g^+	a		Not found moved to			$aaaa^D$	
a	g^+	g^+	g^-	−175.06	102.35	95.80	−95.49	−549.842004194	19.49
a	g^+	a	g^+	−174.20	77.79	−127.36	93.40	−549.837892957	22.07
a	g^+	a	a	−179.37	85.80	−129.12	152.78	−549.837297717	22.45
a	g^+	a	g^-		Not found moved to			$aaaa^A$	
a	g^+	g^-	g^+		Not found moved to			ag^+ag^+	
a	g^+	g^-	a		Not found moved to			ag^+aa	
a	g^+	g^-	g^-		Not found moved to			$aaaa^D$	
a	a	g^+	g^+		Not found moved to			$ag^-g^-g^+$	
a	a	g^+	a		Not found moved to			$aaaa^D$	
a	a	g^+	g^-		Not found moved to			$aaaa^D$	
a	a	a	g^+		Not found moved to			$aaaa^C$	
a	a	a	a^A	−177.24	−120.95	−125.46	170.49	−549.843128026	18.79
a	a	a	a^B	−173.85	−154.80	136.74	−170.71	−549.839012663	21.37
a	a	a	a^C	173.93	154.89	−136.52	170.67	−549.839012786	21.37
a	a	a	a^D	177.21	120.95	125.47	−170.55	−549.843128037	18.79
a	a	a	g^-		Not found moved to			$aaaa^B$	
a	a	g^-	g^+		Not found moved to			$aaaa^A$	
a	a	g^-	a		Not found moved to			$aaaa^A$	

(*continued on next page*)

Table 1 (*continued*)

Conformational assignment				χ_7	χ_8	χ_9	χ_{11}	E (hartree)	Relative energy (kcal mol^{-1})
χ_7	χ_8	χ_9	χ_{11}						
a	a	g^-	g^-		Not found moved to			$ag^+g^+g^-$	
a	g^-	g^+	g^+		Not found moved to			$aaaa^A$	
a	g^-	g^+	a		Not found moved to			ag^-aa	
a	g^-	g^+	g^-		Not found moved to			ag^-ag^-	
a	g^-	a	g^+		Not found moved to			$aaaa^D$	
a	g^-	a	a	178.28	-85.73	129.14	−152.73	−549.837297782	22.45
a	g^-	a	g^-	174.22	−77.75	127.31	−93.33	−549.837893074	22.07
a	g^-	g^-	g^+	174.87	−102.32	−95.66	94.96	−549.842004180	19.49
a	g^-	g^-	a		Not found moved to			$aaaa^A$	
a	g^-	g^-	g^-		Not found moved to			$aaaa^D$	
g^-	g^+	g^+	g^+		Not found moved to			$g^-g^+g^+g^-$	
g^-	g^+	g^+	a		Not found moved to			$g^-g^+g^+g^-$	
g^-	g^+	g^+	g^-	−62.22	116.49	73.65	−90.73	−549.871425197	1.03
g^-	g^+	a	g^+	−95.37	38.43	−135.16	96.23	−549.861238102	7.42
g^-	g^+	a	a		Not found moved to			$g^-ag^+g^C$	
g^-	g^+	a	g^-		Not found moved to			g^-aaa	
g^-	g^+	g^-	g^+		Not found moved to			$g^-ag^+g^C$	
g^-	g^+	g^-	a		Not found moved to			$g^-ag^+g^C$	
g^-	g^+	g^-	g^-		Not found moved to			$g^-ag^+g^C$	
g^-	a	g^+	g^+		Not found moved to			$g^-ag^+g^B$	
g^-	a	g^+	a^A	−60.90	135.26	77.29	−144.62	−549.870235279	1.78
g^-	a	g^+	a^B	−60.10	139.67	80.64	−155.33	−549.870277713	1.75
g^-	a	g^+	a^C	−38.27	137.07	115.59	169.53	−549.872526998	0.34
g^-	a	g^+	g^-		Not found moved to			$g^-ag^+g^A$	
g^-	a	a	g^+		Not found moved to			$g^-ag^+g^B$	
g^-	a	a	a	−42.04	−122.90	−120.37	179.24	−549.863582322	5.95
g^-	a	a	g^-		Not found moved to			$g^-ag^+g^C$	
g^-	a	g^-	g^+		Not found moved to			g^-aaa	
g^-	a	g^-	a		Not found moved to			g^-aaa	
g^-	a	g^-	g^-		Not found moved to			$g^-ag^+g^B$	
g^-	g^-	g^+	g^+		Not found moved to			$g^-ag^+g^C$	
g^-	g^-	g^+	a		Not found moved to			$g^-ag^+g^C$	
g^-	g^-	g^+	g^-		Not found moved to			$g^-ag^+g^C$	
g^-	g^-	a	g^+		Not found moved to			$g^-ag^+g^C$	
g^-	g^-	a	a		Not found moved to			g^-aaa	
g^-	g^-	a	g^-		Not found moved to			g^-aaa	
g^-	g^-	g^-	g^+	−44.44	−71.70	−70.74	98.83	−549.873068367	*0.00*
g^-	g^-	g^-	a		Not found moved to			$g^-g^-g^-g^+$	
g^-	g^-	g^-	g^-		Not found moved to			$g^-g^+g^+g^-$	

a tetrahedral carbon against another tetrahedral carbon, the minima would generally fall within the above ranges. Out of the 24 converged minima, only 17 were unique conformational assignments, while the remaining seven conformers (or 29% of the converged minima) were variations of a few conformational assignments (g^+ag^-a, *aaaa*, and g^-ag^+a) and are denoted with superscripts A, B, C, etc. for a given conformational assignment subset.

$$\begin{aligned} &\textit{gauche plus}\ (g^+) = 60\ (\text{ideal}) \pm 60^\circ \\ &\textit{anti}\ (a) = 180\ (\text{ideal}) \pm 60^\circ \\ &\textit{gauche minus}\ (g^-) = -60\ (\text{ideal}) \pm 60^\circ \end{aligned} \tag{12}$$

The axis chirality described by Eq. (2) is evident in the protonated Fragment C PEHS. Axis chirality occurs when the structures adopt conformations with asymmetric electron distribution. Therefore, irrespective of the presence of a point chiral stereocentre with four different substituents, the chirality induced by an asymmetric distribution of electron density is always present whenever the structure adopts asymmetric conformations and, like enantiomers of point chirality, axis chiral conformers come in pairs.

In this case, however, there is a lack of a fully symmetric conformation devoid of axis chirality that separates all minima for a given PEHS. This conformation (usually with all torsional angles in the *anti* position) has a symmetric electron density with respect to a plane of symmetry, and therefore, lacks axis chirality. Fragment C was found to contain a subset of four conformations with all torsional angles in the *anti* position: $aaaa^{A}$, $aaaa^{B}$, $aaaa^{C}$, and $aaaa^{D}$, all of which were asymmetric and occurred in pairs. To illustrate the axis chirality of these minima, the deviation ($\Delta\chi_T$) of each optimized torsional angle (χ_T) from an ideal value of 180° was calculated based on Eq. (13) (T = torsional angle of interest) (Table 2). The respective $\Delta\chi_T$ values indicate the deviation from an ideal structure with a fully symmetric conformation (this is graphically illustrated in Fig. 4). With regards to Eq. (13), a positive value indicates an optimized torsional angle beyond 180° and a negative value indicates an optimized torsional angle below 180°. From Table 2 and Fig. 4 it is evident that the axis chiral pairs deviated the same amount but in opposite directions (i.e. CW versus CCW) and have the same energetics as expected from Eq. (2). The subset of *aaaa* conformers, like all converged conformers with torsional angle χ_7 in the *anti* position, did not possess any distinct structural features except the fact that they had fully extended side-chains

$$\Delta\chi_T = \Delta\chi_T - 180° \tag{13}$$

PEHS conformers were stabilized by internal hydrogen bonding between nitrogen protons (H1, H15, H26) and oxygen atoms (O5 and O12). Strong intramolecular ion–dipole interactions were also present between the protonated positive nitrogen centre and the oxygen atoms. The protonated PEHS global minima, conformation $g^{+}g^{+}g^{+}g^{-}$ (and it axis chiral pair $g^{-}g^{-}g^{-}g^{+}$), possesses an eight-membered ring formed by a short hydrogen bond between H1 and O12 and a longer hydrogen bond between H1 and O5 forming a five-membered ring (Fig. 5, left). The bifurcated hydrogen bonding in the global minima allows for the formation of a very stable structure. Further, both oxygen atoms oriented towards the positive nitrogen centre allows dominant intramolecular ion–dipole interactions to be present. The bifurcated hydrogen bond split between both oxygen atoms and forming the eight-membered ring was the most prevalent structural feature of the protonated Fragment C PEHS; conformers with the lowest relative energies, under 2 kcal mol^{-1}, all contained this structural feature in the conformation they adopted (Table 7(I)).

Conformers with moderate relative energies were found in geometries which only possessed one hydrogen bond as opposed to the hydrogen bond split between both oxygen atoms as mentioned above. Conformations $g^{+}aaa$ and $g^{+}g^{-}ag^{-}$ (and their axis chiral pairs) had relative energies of 5.95 and

Table 2
Optimized geometries (χ_T) and degree deviation ($\Delta\chi_T$) for the converged *aaaa* conformers relative to an ideal symmetric *aaaa* conformation lacking axis chirality (χ_T = 180.00, $\Delta\chi_T$ = 0; c.f. Eq. (13)) for aminoethoxy-2-methoxy-benzene (Fragment C) (T = torsional angle of interest)

Converged conformation				$\chi_7(\Delta\chi_7)$	$\chi_8(\Delta\chi_8)$	$\chi_9(\Delta\chi_9)$	$\chi_{11}(\Delta\chi_{11})$	Relative energy (kcal mol^{-1})
χ_7	χ_8	χ_9	χ_{11}					
a	*a*	*a*	a^{A}	−177.24(2.76)	−120.95(59.05)	−125.46(54.54)	170.49(−9.51)	18.79
a	*a*	*a*	a^{B}	−173.85(6.15)	−154.80(25.20)	136.74(−43.26)	−170.71(9.29)	21.37
a	*a*	*a*	a^{C}	173.93(−6.07)	154.89(−25.11)	−136.52(43.48)	170.67(−9.33)	21.37
a	*a*	*a*	a^{D}	177.21(−2.79)	120.95(−59.05)	125.47(−54.53)	−170.55(9.45)	18.79

The geometrical and energetic properties of such axis chiral conformers can be predicted from Eq. (2).

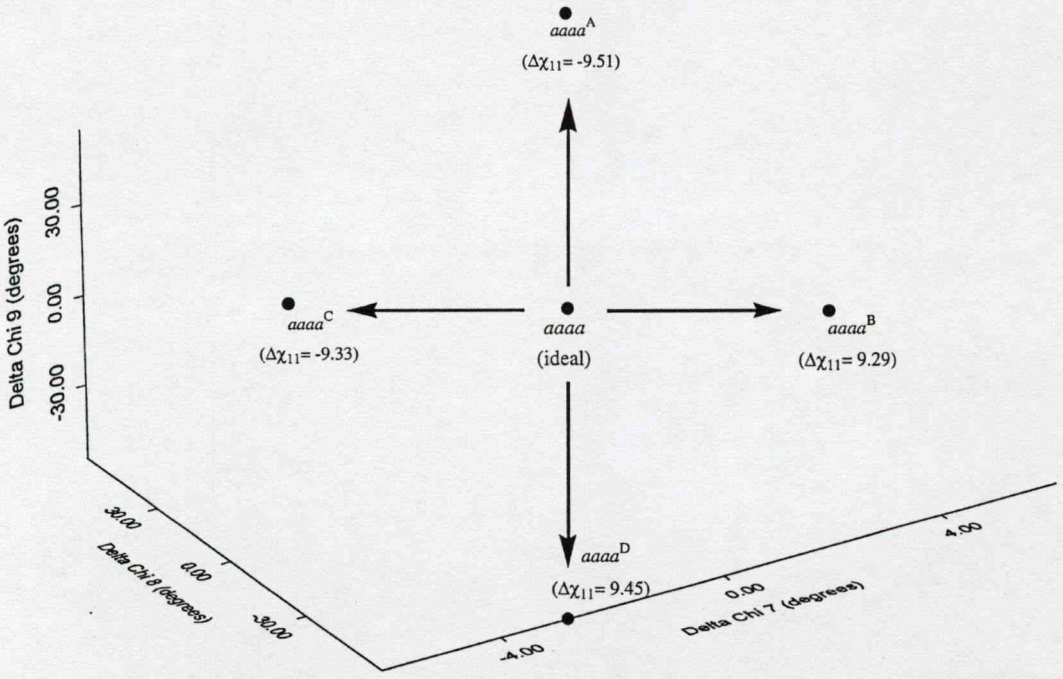

Fig. 4. Graphical illustration of the four converged *aaaa* axis chiral conformers (*aaaa* ^{A}, *aaaa* ^{B}, *aaaa* ^{C}, and *aaaa* ^{D}) and their deviation from an ideal *aaaa* structure ($\chi_T = 180.00$, $\Delta\chi_T = 0$). Conformation *aaaa* (ideal) would possess symmetrical electron density with regards to a plane of symmetry, and therefore, would be devoid of axis chirality. However, such a structure was not found for the PEHS of Fragment C; instead, two pairs of *aaaa* converged conformers were found and the arrows above represent their geometrical deviation from the *aaaa* (ideal) structure.

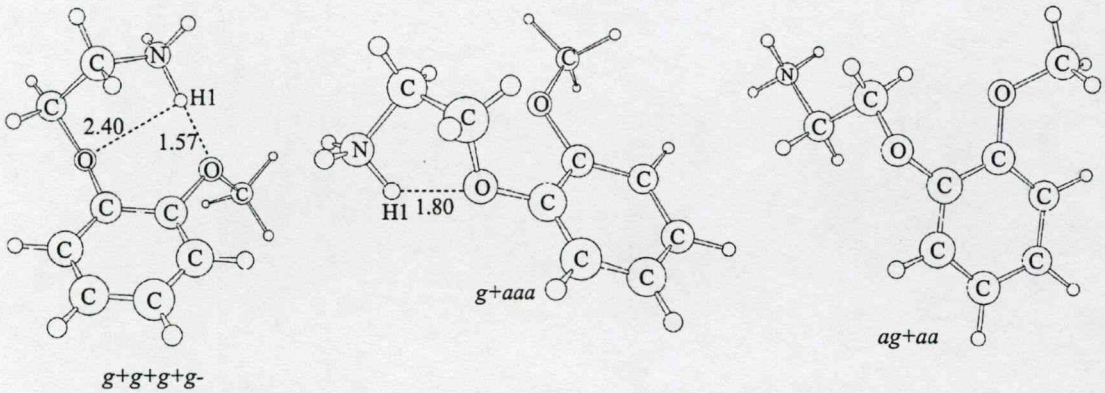

Fig. 5. Optimized global minima of the protonated Fragment C PEHS ($g^+g^+g^+g^-$) exhibits both a five- and eight-membered ring with bifurcated hydrogen bonds (along with the global minima, all protonated conformers with relative energy less than 2 kcal mol^{-1} has this structural feature). Conformer g^+aaa has a moderate relative energy (5.95 kcal mol^{-1}) and exhibits a five-membered ring while conformer ag^+aa had the largest relative energy (22.45 kcal mol^{-1}) of the protonated PEHS and possesses a fully extended conformation.

7.42 kcal mol^{-1}, respectively. Conformation g^+aaa contained a 1.80 Å hydrogen bond forming a five-membered ring with O5 (Fig. 5, middle) while conformation $g^+g^-ag^-$ contained a 1.54 Å hydrogen bond forming an eight-membered ring with O12. The latter eight-membered was similar to that seen in the global minima except that O5 was not involved in any other hydrogen bonding. Finally, structures with torsional angle χ_7 oriented in the *anti* position had the side-chain positioned away from the ring, and therefore, were not able to form any internal hydrogen bonds. The disparity in the relative energies of these conformers, about 20 kcal mol^{-1}, is indicative of their lack of stabilization. Conformation ag^+aa possessed the highest relative energy of the PEHS (Fig. 5, right).

As shown above with the four *aaaa* conformers, the protonated Fragment C PEHS contained a number of different converged structures within a respective conformational assignment (conformations g^+ag^-a, *aaaa*, and g^-ag^+a). Although the majority of subset conformers were very similar to each other, conformer $g^+ag^-a^A$ and $g^+ag^-a^B$ converged to very different geometries. The former conformer was the only structure with two different protons involved in two distinct hydrogen bonds forming separate five- and eight-membered rings (Fig. 6, left). Conformer $g^+ag^-a^B$ and $g^+ag^-a^C$ possessed the more prevalent bifurcated hydrogen bond structural feature (Fig. 6, middle and right).

3.2. Conformational analysis of H_a, H_{g+}, and H_{g-} deprotonated aminoethoxy-2-methoxy-benzene (Fragment C) conformers

All converged protonated conformers were deprotonated of H_a, H_{g+}, and H_{g-} protons. SPE calculations were initially performed on all deprotonated conformers (Table 3) followed by full geometry optimizations (Tables 4–6). With regards to the H_a (H1) deprotonated conformers (Tables 4 and 7(II)), the global minima $g^+g^+g^+g^{-B}$ possesses a H15···O12 hydrogen bond forming an eight-membered ring similar to that exhibited by protonated conformers (Fig. 7, left). Conformers with bifurcated hydrogen bonds were also evident in the deprotonated state such as that for $g^+ag^-a^A$ (Fig. 7, middle), however, these were longer hydrogen bonds than present in the protonated conformers due to a lack of any intramolecular ion–dipole interactions between the nitrogen and oxygen heteroatoms. In the protonated PEHS, all conformers with torsional angle χ_7 in the *anti* position have fully extended conformations and no significant structural features. In the H_a deprotonated PEHS, converged conformers like $g^+ag^-a^B$ (Fig. 7, right), also contained no structural features and possessed larger relative energies.

H_{g+} (H15) deprotonated Fragment C conformers converged to different conformations than did H_a

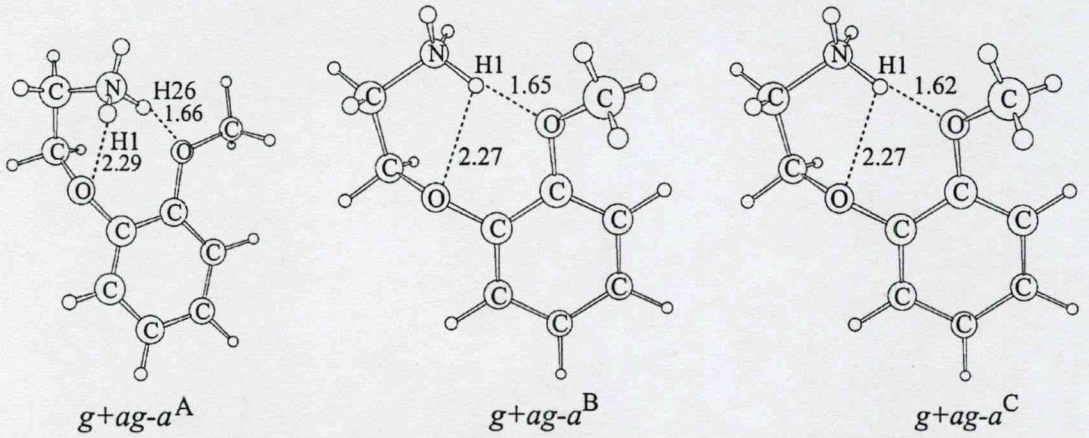

Fig. 6. Converged minima of the protonated Fragment C PEHS g^+ag^-a subset: $g^+ag^-a^A$ (0.34 kcal mol^{-1}), $g^+ag^-a^B$ (1.75 kcal mol^{-1}), and $g^+ag^-a^C$ (1.78 kcal mol^{-1}).

Table 3
Relative energies for the converged minima of the protonated aminoethoxy-2-methoxy-benzene (Fragment C) PEHS computed at the RHF/3-21G level of theory

Conformational assignment				Protonated relative energy (kcal mol^{-1})	H_a deprotonation SPE (hartree)	$\Delta E_{vert}(a)$ (kcal mol^{-1})	H_{g^+} deprotonation SPE (hartree)	$\Delta E_{vert}(g^+)$ (kcal mol^{-1})	H_{g^-} deprotonation SPE (hartree)	$\Delta E_{ven}(g^-)$ (kcal mol^{-1})
χ_7	χ_8	χ_9	χ_{11}							
g^+	g^+	g^+	g^-	*0.00*	−549.426174969	280.43	−549.442280486	270.32	−549.441928160	270.54
g^+	a	a	a	5.95	−549.443611717	263.54	−549.442851892	264.01	−549.434031483	269.55
g^+	a	g^-	a^A	0.34	−549.432586758	276.07	−549.439878833	271.49	−549.430288227	277.51
g^+	a	g^-	a^B	1.75	−549.425684138	278.99	−549.443172996	268.01	−549.441413643	269.12
g^+	a	g^-	a^C	1.78	−549.424896018	279.45	−549.442854134	268.18	−549.440728544	269.52
g^+	g^-	a	g^-	7.42	−549.437153444	266.12	−549.426047877	273.09	−549.435637888	267.07
g^+	g^-	g^-	g^+	1.03	−549.427346075	278.66	−549.444060000	268.18	−549.442394356	269.22
a	g^+	g^+	g^-	19.49	−549.445822784	248.61	−549.447282769	247.69	−549.445584545	248.76
a	g^+	a	g^+	22.07	−549.447502744	244.97	−549.448266733	244.49	−549.449480983	243.73
a	g^+	a	a	22.45	−549.446176571	245.43	−549.446244896	245.39	−549.447671383	244.49
a	a	a	a^A	18.79	−549.446798634	248.70	−549.448213075	247.81	−549.446483903	248.90
a	a	a	a^B	21.37	−549.448057940	245.33	−549.446928686	246.04	−549.447228542	245.85
a	a	a	a^C	21.37	−549.447239890	245.84	−549.446932064	246.03	−549.448066994	245.32
a	a	a	a^D	18.79	−549.446488127	246.31	−549.448216115	245.23	−549.446797719	246.12
a	g^-	a	a	22.45	−549.446163539	245.44	−549.447663524	244.50	−549.446240118	245.39
a	g^-	a	g^-	22.07	−549.447513088	244.97	−549.449490572	243.73	−549.448276170	244.49
a	g^-	g^-	g^+	19.49	−549.445623108	248.73	−549.447324349	247.67	−549.445877477	248.57
g^-	g^+	g^+	g^-	1.03	−549.427328185	278.68	−549.442367243	269.24	−549.444029127	268.20
g^-	g^+	a	g^+	7.42	−549.426000793	273.12	−549.437205701	266.08	−549.435694955	267.03
g^-	a	g^+	a^A	1.78	−549.424870211	279.47	−549.440701940	269.54	−549.442836385	268.20
g^-	a	g^+	a^B	1.75	−549.425583135	279.05	−549.441348512	269.16	−549.443182477	268.01
g^-	a	g^+	a^C	0.34	−549.430300136	277.50	−549.439888909	271.48	−549.432587532	276.07
g^-	a	a	a	5.95	−549.434112751	269.50	−549.442963271	263.94	−549.443703675	263.48
g^-	g^-	g^-	g^+	*0.00*	−549.426168078	280.43	−549.441929596	270.54	−549.442283555	270.32

Full optimizations were followed by SPE calculations for independent deprotonation of H_a (H1), H_{g^+} (H15), and H_{g^-} (H26) protons.

Table 4
Optimized conformational minima for the H_a (H1) deprotonated PEHS of aminoethoxy-2-methoxy-benzene (Fragment C) at the RHF/3-21G level of theory

Optimized protonated conformation				Optimized deprotonated conformation				χ_7 (deg)	χ_8 (deg)	χ_9 (deg)	χ_{11} (deg)	E (hartree)	Relative energy (kcal mol^{-1})	$\Delta E_{opt}(g^+)$ (kcal mol^{-1})	$\Delta\Delta E(g^+)$ (kcal mol^{-1})
χ_7	χ_8	χ_9	χ_{11}	χ_7	χ_8	χ_9	χ_{11}								
g^+	g^+	g^+	g^-	g^+	g^+	g^+	g^{-A}	70.67	88.77	86.24	−56.91	−549.456031486	3.80	261.69	18.74
g^+	a	a	a	g^+	a	a	a	55.44	128.64	122.81	−173.00	−549.457605177	2.82	254.76	8.78
g^+	a	g^-	a^A	g^+	a	g^-	a^A	61.11	−153.94	−109.91	173.12	−549.458403320	2.32	259.87	16.20
g^+	a	g^-	a^B	g^+	a	g^-	a^B	71.22	174.11	−119.92	168.63	−549.449098582	8.15	264.29	14.70
g^+	a	g^-	a^C	g^+	a	g^-	a^B						8.15	264.29	15.16
g^+	g^-	a	g^-	g^+	g^+	g^+	g^{-B}	58.06	59.91	66.85	−69.71	−549.462092585	*0.00*	250.47	15.65
g^+	g^-	g^-	g^+	g^+	g^-	g^-	g^+	67.80	−115.76	−67.17	70.52	−549.461457783	0.40	257.26	21.40
a	g^+	g^+	g^-	a	g^+	g^+	g^-	−177.49	93.20	85.38	−68.05	−549.458328292	2.36	240.76	7.85
a	g^+	a	g^+	a	g^+	g^-	g^+	176.07	77.69	−113.64	70.94	−549.458069229	2.52	238.34	6.63
a	g^+	a	a	a	g^+	g^-	a	176.87	78.85	−118.50	173.00	−549.455143308	4.36	239.81	5.62
a	a	a	a^A	a	a	a	a^A	−176.22	−127.35	−123.29	178.77	−549.456320232	3.62	242.73	5.97
a	a	a	a^B	a	a	g^+	a	179.84	179.61	115.49	−171.18	−549.455665083	4.03	240.55	4.78
a	a	a	a^C	a	a	g^-	a	179.78	179.23	−115.19	173.14	−549.456079419	3.77	240.29	5.55
a	a	a	a^D	a	a	a	a^B	177.03	128.42	122.87	−173.47	−549.456075063	3.78	240.30	6.01
a	g^-	a	a	a	g^-	g^+	a	−176.87	−78.85	118.50	−173.00	−549.455143308	4.36	239.81	5.63
a	g^-	a	g^-	a	g^-	g^+	g^-	−176.07	−77.69	113.64	−70.94	−549.458069229	2.52	238.34	6.63
a	g^-	g^-	g^+	a	g^-	g^-	g^+	178.08	−93.71	−87.49	69.23	−549.458374431	2.33	240.73	8.00
g^-	g^+	g^+	g^-	g^-	g^+	g^+	g^-	−67.82	115.72	67.20	−70.49	−549.461457804	0.40	257.26	21.42
g^-	g^+	a	g^+	g^-	g^+	g^-	g^+	−73.56	118.87	−72.23	64.73	−549.455865572	3.91	254.38	18.74
g^-	a	g^+	a^A	g^-	a	g^+	a^A	−71.19	−174.09	119.88	−168.63	−549.449098573	8.15	264.27	15.20
g^-	a	g^+	a^B	g^-	a	g^+	a^A						8.15	264.27	14.78
g^-	a	g^+	a^C	g^-	a	g^+	a^B	−71.02	154.69	105.64	175.30	−549.458468802	2.27	259.83	17.67
g^-	a	a	a	g^-	a	a	a	−60.91	−131.67	−121.62	174.22	−549.457379459	2.96	254.90	14.60
g^-	g^-	g^-	g^+	g^-	g^-	g^-	g^+	−70.67	−88.77	−86.24	56.91	−549.456031485	3.80	261.69	18.74

Table 5
Optimized conformational minima for the H_{g+} (H15) deprotonated PEHS of aminoethoxy-2-methoxy-benzene (Fragment C) at the RHF/3-21G level of theory

Optimized protonated conformation				Optimized deprotonated conformation				χ_7 (deg)	χ_8 (deg)	χ_9 (deg)	χ_{11} (deg)	E (hartree)	Relative energy (kcal mol^{-1})	$\Delta E_{opt}(g^+)$ (kcal mol^{-1})	$\Delta\Delta E(g^+)$ (kcal mol^{-1})
χ_7	χ_8	χ_9	χ_{11}	χ_7	χ_8	χ_9	χ_{11}								
g^+	g^+	g^+	g^-	g^+	g^+	g^+	g^-	53.60	63.53	67.58	−69.43	−549.461502854	0.37	258.26	12.06
g^+	a	a	a	g^+	a	a	a	60.94	131.73	121.62	−174.12	−549.457379474	2.96	254.90	9.11
g^+	a	g^-	a^A	g^+	a	g^-	a	61.12	−153.95	−109.92	173.17	−549.458403331	2.32	259.87	11.62
g^+	a	g^-	a^B	g^+	a	g^-	a					−549.458403331	2.32	258.46	9.55
g^+	a	g^-	a^C	g^+	a	g^-	a					−549.458403331	2.32	258.43	9.75
g^+	g^-	a	g^-	g^+	g^-	g^+	g^-	73.55	−118.85	72.27	−64.75	−549.455865605	3.91	254.38	18.71
g^+	g^-	g^-	g^+	g^+	g^-	g^-	g^+	63.50	−109.60	−67.91	69.69	−549.461778373	0.20	257.06	11.12
a	g^+	g^+	g^-	a	g^+	g^+	g^-	−178.19	98.38	88.26	−69.43	−549.457609028	2.81	241.21	6.48
a	g^+	a	g^+	a	g^+	g^-	g^+	178.07	78.63	−115.16	71.31	−549.458326171	2.36	238.18	6.31
a	g^+	a	a	a	g^+	g^-	a	178.18	79.54	−119.67	169.09	−549.454953224	4.48	239.92	5.47
a	a	a	a^A	a	a	a	a^A	−176.81	−126.11	−124.42	171.92	−549.456063978	3.78	242.89	4.92
a	a	a	a^B	a	a	g^+	a	178.52	177.67	115.38	−174.31	−549.455937215	3.86	240.38	5.66
a	a	a	a^C	a	a	g^-	a	−178.52	−177.66	−115.39	174.31	−549.455937212	3.86	240.38	5.65
a	a	a	a^D	a	a	a	a^B	176.81	126.11	124.42	−171.92	−549.456063980	3.78	240.30	4.93
a	g^-	a	a	a	g^-	g^+	a	−177.46	−78.65	118.83	−169.29	−549.454914807	4.50	239.95	4.55
a	g^-	a	g^-	a	g^-	g^+	g^-	−177.84	−78.65	114.14	−71.72	−549.458060719	2.53	238.35	5.38
a	g^-	g^-	g^+	a	g^-	g^-	g^+	178.18	−98.38	−88.25	69.42	−549.457609009	2.81	241.21	6.46
g^-	g^+	g^+	g^-	g^-	g^+	g^+	g^-	−67.79	115.72	67.16	−70.49	−549.461457796	0.40	257.26	11.98
g^-	g^+	a	g^+	g^-	g^-	g^-	g^+					−549.462092524	*0.00*	250.47	15.61
g^-	a	g^+	a^A	g^-	a	g^+	a^A	−70.99	154.66	105.61	175.29	−549.458468747	2.27	258.39	11.15
g^-	a	g^+	a^B	g^-	a	g^+	a^A					−549.458468747	2.27	258.41	10.75
g^-	a	g^+	a^C	g^-	a	g^+	a^B	−61.12	153.95	109.92	−173.17	−549.458403331	2.32	259.87	11.61
g^-	a	a	a	g^-	a	a	a	−60.94	−131.73	−121.62	174.13	−549.457379476	2.96	254.90	9.04
g^-	g^-	g^-	g^+	g^-	g^-	g^-	g^+	−58.01	−59.89	−66.89	69.63	−549.462092524	*0.00*	257.89	12.65

Table 6
Optimized conformational minima for the H_{g-} (H26) deprotonated PEHS of aminoethoxy-2-methoxy-benzene (Fragment C) at the RHF/3-21G level of theory

Optimized protonated conformation				Optimized deprotonated conformation				χ_7 (deg)	χ_8 (deg)	χ_9 (deg)	χ_{11} (deg)	E (hartree)	Relative energy (kcal mol^{-1})	$\Delta E_{opt}(g^+)$ (kcal mol^{-1})	$\Delta\Delta E(g^+)$ (kcal mol^{-1})
χ_7	χ_8	χ_9	χ_{11}	χ_7	χ_8	χ_9	χ_{11}								
g^+	g^+	g^+	g^-	g^+	g^+	g^+	g^-	58.06	59.89	66.88	−69.69	−549.462092596	*0.00*	257.89	12.65
g^+	a	a	a	g^+	a	a	a	60.93	131.73	121.64	−174.18	−549.457379464	2.96	254.90	14.65
g^+	a	g^-	a^A	g^+	a	g^-	a	71.03	−154.66	−105.63	−175.26	−549.458468814	2.27	259.83	17.68
g^+	a	g^-	a^B	g^+	a	g^-	a						2.27	258.41	10.71
g^+	a	g^-	a^C	g^+	a	g^-	a						2.27	258.39	11.13
g^+	g^-	a	g^-	g^+	g^-	g^+	g^-	74.09	−79.55	119.88	−72.92	−549.457178397	3.08	253.55	13.52
g^+	g^-	g^-	g^+	g^+	g^-	g^-	g^+	67.80	−115.71	−67.18	70.49	−549.461457808	0.40	257.26	11.96
a	g^+	g^+	g^-	a	g^+	g^+	g^-	−178.11	93.55	87.45	−69.22	−549.458374259	2.33	240.73	8.03
a	g^+	a	g^+	a	g^+	g^-	g^+	177.82	78.70	−114.10	71.72	−549.458060658	2.53	238.35	5.38
a	g^+	a	a	a	g^+	g^-	a	177.46	78.57	−118.84	169.29	−549.454914788	4.50	239.95	4.54
a	a	a	a^A	a	a	a	a^A	−177.01	−128.27	−123.01	173.58	−549.456074882	3.78	242.88	6.02
a	a	a	a^B	a	a	g^+	a	−179.80	−179.32	115.11	−173.21	−549.456079310	3.77	240.29	5.56
a	a	a	a^C	a	a	g^-	a	−179.78	−179.69	−115.48	171.25	−549.455664913	4.03	240.55	4.77
a	a	a	a^D	a	a	a	a^B	176.24	127.31	123.33	−178.98	−549.456320114	3.62	240.14	5.98
a	g^-	a	a	a	g^-	g^+	a	−178.20	−79.41	119.68	−169.01	−549.454953180	4.48	239.92	5.47
a	g^-	a	g^-	a	g^-	g^+	g^-	−178.06	−78.71	115.18	−71.29	−549.458326128	2.36	238.18	6.31
a	g^-	g^-	g^+	a	g^-	g^-	g^+	177.48	−93.23	−85.36	68.04	−549.458328330	2.36	240.76	7.81
g^-	g^+	g^+	g^-	g^-	g^+	g^+	g^-	−63.55	109.58	67.97	−69.63	−549.461778325	0.20	257.06	11.14
g^-	g^+	a	g^+	g^-	g^+	g^-	g^+	−74.23	79.52	−119.76	72.89	−549.457178317	3.08	253.55	13.48
g^-	a	g^+	a^A	g^-	a	g^+	a	−61.16	154.09	109.87	−173.16	−549.458403144	2.32	258.43	9.77
g^-	a	g^+	a^B	g^-	a	g^+	a						2.32	258.46	9.55
g^-	a	g^+	a^C	g^-	a	g^+	a						2.32	259.87	16.20
g^-	a	a	a	g^-	a	a	a	−55.45	−128.60	−122.88	173.01	−549.457605176	2.82	254.75	8.73
g^-	g^-	g^-	g^+	g^-	g^-	g^-	g^+	−53.56	−63.60	−67.55	69.45	−549.461502806	0.37	258.26	12.06

Table 7
Structural features of converged conformers of the aminoethoxy-2-methoxy-benzene (Fragment C) PEHS

Conformational assignment				Structural features	Relative energy (kcal mol^{-1})
χ_7	χ_8	χ_9	χ_{11}		
I. Protonated conformers (CH^+)					
g^+	g^+	g^+	g^-	1.57 Å H1···O12 H-bond, 2.40 Å H1···O5 H-bond forming an 8-membered ring	*0.00*
g^+	a	a	a	1.80 Å H26···O5 H-bond forming a 5-membered ring	5.95
g^+	a	g^-	a^A	1.66 Å H26···O12 H-bond forming an 8-membered ring, 2.29 Å H1···O5 H-bond forming a 5-membered ring	0.34
g^+	a	g^-	a^B	1.65 Å H1···O12 H-bond, 2.22 Å H1···O5 H-bond forming an 8-membered ring	1.75
g^+	a	g^-	a^C	1.62 Å H1···O12 H-bond, 2.27 Å H1···O5 H-bond forming an 8-membered ring	1.78
g^+	g^-	a	g^-	1.54 Å H15···O12 H-bond forming an 8-membered ring	7.42
g^+	g^-	g^-	g^+	1.56 Å H1···O12 H-bond, 2.47 Å H1···O5 H-bond forming an 8-membered ring	1.03
a	g^+	g^+	g^-	–	19.49
a	g^+	a	g^+	–	22.07
a	g^+	a	a	–	22.45
a	a	a	a^A	–	18.79
a	a	a	a^B	–	21.37
a	a	a	a^C	–	21.37
a	a	a	a^D	–	18.79
a	g^-	a	a	–	22.45
a	g^-	a	g^-	–	22.07
a	g^-	g^-	g^+	–	19.49
g^-	g^+	g^+	g^-	1.56 Å H1···O12 H-bond, 2.47 Å H1···O5 H-bond forming an 8-membered ring	1.03
g^-	g^+	a	g^+	1.53 Å H1···O12 H-bond forming an 8-membered ring	7.42
g^-	a	g^+	a^A	1.63 Å H1···O12 H-bond, 2.27 Å H1···O5 H-bond forming an 8-membered ring	1.78
g^-	a	g^+	a^B	1.65 Å H1···O12 H-bond, 2.22 Å H1···O5 H-bond forming an 8-membered ring	1.75
g^-	a	g^+	a^C	1.66 Å H1···O12 H-bond forming an 8-membered ring, 2.29 Å H26···O5 H-bond forming a 5-membered ring	0.34
g^-	a	a	a	1.80 Å H1···O5 H-bond forming a 5-membered ring	5.95
g^-	g^-	g^-	g^+	1.57 Å H1···O12 H-bond, 2.40 Å H1···O5 H-bond forming an 8-membered ring	*0.00*
II. H_a deprotonated conformers (C)					
g^+	g^+	g^+	g^{-A}	–	3.80
g^+	a	a	a	2.45 Å H26···O5 H-bond forming a 5-membered ring	2.82
g^+	a	g^-	a^A	2.80 Å H26···O12 H-bond, 2.44 Å H26···O5 H-bond forming an 8-membered ring	2.32
g^+	a	g^-	a^B	–	8.15
g^+	g^+	g^+	g^{-B}	2.11 Å H15···O12 H-bond forming an 8-membered ring	*0.00*
g^+	g^-	g^-	g^+	2.10 Å H26···O12 H-bond, 2.60 Å H26···O5 H-bond forming an 8-membered ring	0.40
a	g^+	g^+	g^-	–	2.36
a	g^+	g^-	g^+	–	2.52
a	g^+	g^-	a	–	4.36
a	a	a	a^A	–	3.62
a	a	g^+	a	–	4.03

Table 7 (*continued*)

Conformational assignment				Structural features	Relative energy (kcal mol^{-1})
χ_7	χ_8	χ_9	χ_{11}		
a	*a*	g^-	*a*	–	3.77
a	*a*	*a*	a^B	–	3.78
a	g^-	g^+	*a*	–	4.36
a	g^-	g^+	g^-	–	2.52
a	g^-	g^-	g^+	–	2.33
g^-	g^+	g^+	g^-	2.09 Å H15···O12 H-bond, 2.60 Å H15···O5 H-bond forming an 8-membered ring	0.40
g^-	g^+	g^-	g^+	–	3.91
g^-	*a*	g^+	a^A	–	8.15
g^-	*a*	g^+	a^B	2.33 Å H15···O12 H-bond, 2.44 Å H15···O5 H-bond forming an 8-membered ring	2.27
g^-	*a*	*a*	*a*	2.35 Å H15···O5 H-bond forming a 5-membered ring	2.96
g^-	g^-	g^-	g^+	–	3.80
III. H_{g+} deprotonated conformers (C)					
g^+	g^+	g^+	g^-	2.12 Å H1···O12 H-bond, 2.73 Å H1···O5 H-bond forming an 8-membered ring	0.37
g^+	*a*	*a*	*a*	2.35 Å H26···O5 H-bond forming a 5-membered ring	2.96
g^+	*a*	g^-	*a*	2.80 Å H26···O12 H-bond, 2.43 Å H26···O5 H-bond forming an 8-membered ring	2.32
g^+	g^-	g^+	g^-	–	3.91
g^+	g^-	g^-	g^+	2.09 Å H1···O12 H-bond, 2.72 Å H1···O5 H-bond forming an 8-membered ring	0.20
a	g^+	g^+	g^-	–	2.81
a	g^+	g^-	g^+	–	2.36
a	g^+	g^-	*a*	–	4.48
a	*a*	*a*	a^A	–	3.78
a	*a*	g^+	*a*	–	3.86
a	*a*	g^-	*a*	–	3.86
a	*a*	*a*	a^B	–	3.78
a	g^-	g^+	*a*	–	4.50
a	g^-	g^+	g^-	–	2.53
a	g^-	g^-	g^+	–	2.81
g^-	g^+	g^+	g^-	2.09 Å H1···O12 H-bond, 2.60 Å H1···O5 H-bond forming an 8-membered ring	0.40
g^-	*a*	g^+	a^A	2.33 Å H1···O12 H-bond, 2.44 Å H1···O5 H-bond forming an 8-membered ring	2.27
g^-	*a*	g^+	a^B	2.80 Å H26···O12 H-bond, 2.43 Å H26···O5 H-bond forming an 8-membered ring	2.32
g^-	*a*	*a*	*a*	2.35 Å H1···O5 H-bond forming a 5-membered ring	2.96
g^-	g^-	g^-	g^+	2.11 Å H1···O12 H-bond, 2.58 Å H1···O5 H-bond forming an 8-membered ring	*0.00*
IV. H_{g-} deprotonated conformers (C)					
g^+	g^+	g^+	g^-	2.11 Å H1···O12 H-bond, 2.58 Å H1···O5 H-bond forming an 8-membered ring	*0.00*
g^+	*a*	*a*	*a*	2.35 Å H1···O5 H-bond forming a 5-membered ring	2.96
g^+	*a*	g^-	*a*	2.33 Å H1···O12 H-bond, 2.45 Å H1···O5 H-bond forming an 8-membered ring	2.27
g^+	g^-	g^+	g^-	3.11 Å H15···π-electron interaction, 3.96 Å H1···π-electron interaction	3.08

(*continued on next page*)

Table 7 (*continued*)

Conformational assignment				Structural features	Relative energy (kcal mol^{-1})
χ_7	χ_8	χ_9	χ_{11}		
g^+	g^-	g^-	g^+	2.09 Å H1···O12 H-bond, 2.60 Å H1···O5 H-bond forming an 8-membered ring	0.40
a	g^+	g^+	g^-	–	2.33
a	g^+	g^-	g^+	–	2.53
a	g^+	g^-	a	–	4.50
a	a	a	a^A	–	3.78
a	a	g^+	a	–	3.77
a	a	g^-	a	–	4.03
a	a	a	a^B	–	3.62
a	g^-	g^+	a	–	4.48
a	g^-	g^+	g^-	–	2.36
a	g^-	g^-	g^+	–	2.36
g^-	g^+	g^+	g^-	2.08 Å H1···O12 H-bond, 2.72 Å H1···O5 H-bond forming an 8-membered ring	0.20
g^-	g^+	g^-	g^+	3.11 Å H1···π-electron interaction, 3.96 Å H15···π-electron interaction	3.08
g^-	a	g^+	a	2.81 Å H1···O12 H-bond, 2.43 Å H1···O5 H-bond forming an 8-membered ring	2.32
g^-	a	a	a	2.45 Å H1···O5 H-bond forming a 5-membered ring	2.82
g^-	g^-	g^-	g^+	2.12 Å H1···O12 H-bond, 2.73 Å H1···O5 H-bond forming an 8-membered ring	0.37

All structures presented in this table have been geometrically optimized at the RHF/3-21G level of theory.

deprotonated conformers upon optimization (Tables 5 and 7(III)) further emphasizing that the protonated conformation and the choice of proton abstracted have a large influence on the subsequent converged deprotonated minima. In this case, the global minima structure was conformer $g^-g^-g^-g^+$ which was very similar to the protonated PEHS global minima with bifurcated hydrogen bonds from H1 (Fig. 8, left). Due to the prevalence of this structural motif in the protonated PEHS, combined with the fact that in the majority of protonated conformers the split hydrogen bonds come from H1, it is reasonable to expect that H_{g+} deprotonated conformers would maintain this bifurcated hydrogen bond intact upon optimization.

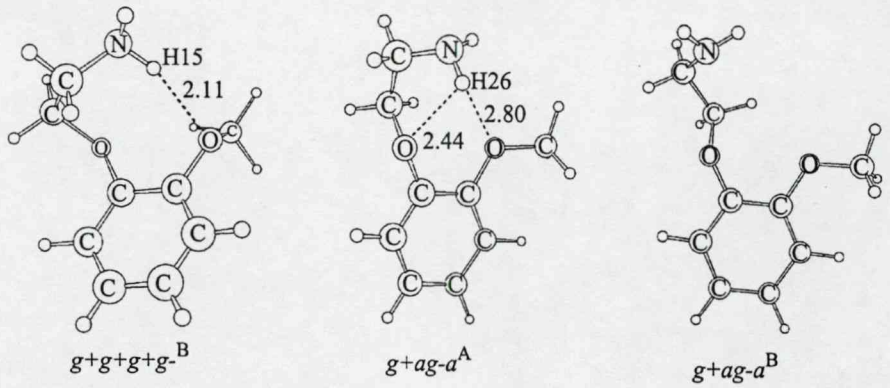

Fig. 7. Converged H_a (H1) deprotonated Fragment C conformers: global minima $g^+g^+g^+g^{-B}$ (0.00 kcal mol^{-1}), $g^+ag^-a^A$ (2.32 kcal mol^{-1}), and $g^+ag^-a^B$ (8.15 kcal mol^{-1}).

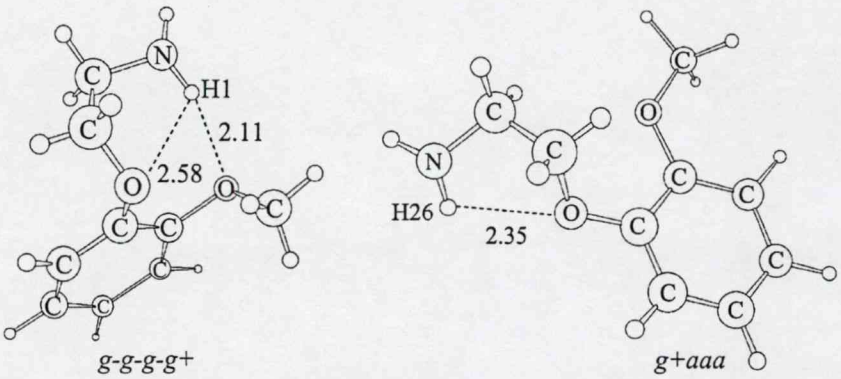

Fig. 8. Converged H_{g+} (H15) deprotonated Fragment C conformers: global minima $g^-g^-g^-g^+$ (0.00 kcal mol^{-1}) and g^+aaa (2.96 kcal mol^{-1}).

H_{g+} deprotonated conformer g^+aaa (Fig. 8, right) is very similar to the protonated g^+aaa conformation. Conformers with torsional angle χ_7 in the *anti* position had the side-chain fully extended and lacked any structural features; conformer ag^-g^+a had the largest relative energy of 4.50 kcal mol^{-1}.

The H_{g-} (H26) deprotonated Fragment C PEHS (Tables 6 and 7(IV)) global minima was conformer $g^+g^+g^+g^-$ (Fig. 9, left) which was similar to the protonated conformation and possessed an intact H1 bifurcated hydrogen bond. Optimization of the H_{g-} deprotonated conformers revealed a novel interaction in the Fragment C PEHS; conformer $g^+g^-g^+g^-$, and its axis chiral pair $g^-g^+g^-g^+$, possess an internal H1$\cdots$ and H15$\cdots$pi(π)-electron interaction (Fig. 9, middle) with a relative energy of 3.08 kcal mol^{-1}. This amine–aromatic π interaction is a novel interactions not previously encountered in the literature and confers moderate stability to the deprotonated Fragment C PEHS conformers.

Upon convergence of the deprotonated $g^+g^-g^+g^-$ and $g^-g^+g^-g^+$ conformers, protonated $g^+g^-g^+g^-$ and $g^-g^+g^-g^+$ conformers were re-computed to see if this amine–aromatic π interaction had been missed because it follows intuitively that a protonated positive nitrogen centre would be a more likely structure to form a cation–aromatic π interaction due to its greater electron deficiency. However, these protonated structures were not missed; instead, protonated conformers

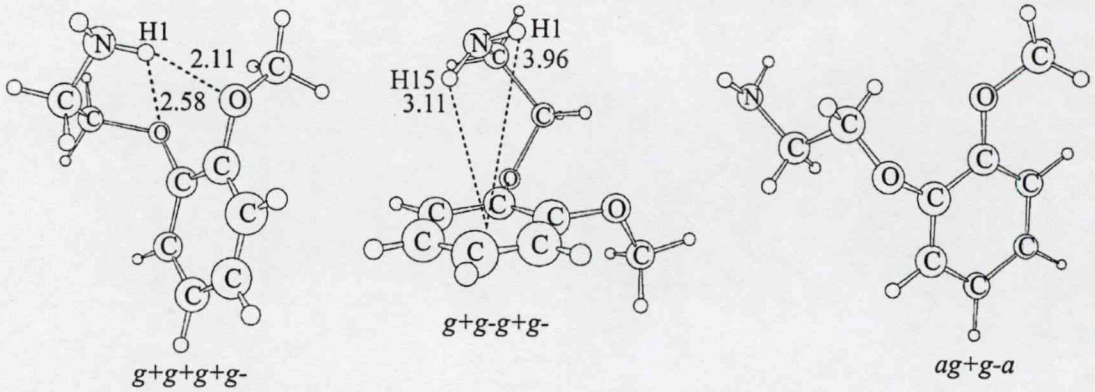

Fig. 9. Converged H_{g-} (H26) deprotonated Fragment C conformers: global minima $g^+g^+g^+g^-$ (0.00 kcal mol^{-1}), $g^+g^-g^+g^-$ (3.08 kcal mol^{-1}), and ag^+g^-a (4.50 kcal mol^{-1}).

$g^+g^-g^+g^-$ and $g^-g^+g^-g^+$ converged to conformers $g^+g^-g^-g^+$ (1.56 Å H1···O12 and 2.47 Å H1···O5 hydrogen bonds forming an eight-membered ring; 1.03 kcal mol^{-1} relative energy) and $g^-ag^+a^C$ (1.66 Å H1···O12 hydrogen bond forming an eight-membered ring and a 2.29 Å H26···O5 hydrogen bond forming a five-membered ring; 0.34 kcal mol^{-1} relative energy), respectively. This illustrates that the presence of nearby inductively electron-donating oxygen atoms (O5 and O12) favors hydrogen bond and intramolecular ion–dipole formation between the positive nitrogen centre and the oxygen atoms over the cation–aromatic π interaction. Currently, the authors of this work are investigating this novel amine–aromatic π interaction and trying to discern possible confounding activation effects by O5 and O12, which are bound to the benzene ring. Finally, like the protonated PEHS, the only conformers with no structural features were those with torsional angle χ_7 in the *anti* position (conformer ag^+g^-a is shown in Fig. 9, right).

3.3. Intrinsic conformational-dependent basicity of aminoethoxy-2-methoxy-benzene (Fragment C)

Once the protonated PEHS of Fragment C was computed, energies of deprotonation were determined with both SPE calculations and full geometry optimizations for H_a, H_{g+}, and H_{g-} deprotonation events (summary of values in Tables 3 and 8). For vertical energies of deprotonation (i.e. SPE calculations), it was found that conformers showed the greatest difference in their respective $\Delta E_{vert}(a)$, $\Delta E_{vert}(g^+)$, and $\Delta E_{vert}(g^-)$ values when protons involved in internal stabilization were abstracted. In these instances, the proton not involved in intramolecular stabilization (such as hydrogen bond formation) was relatively easily deprotonated. Protons involved in hydrogen bonding required, on average, an additional 5–10 kcal mol^{-1} compared to non-hydrogen bonded protons for deprotonation. Contrasting, high relative energy conformers (i.e. conformations with torsional angle χ_7 in the *anti* position) had energies of deprotonation 25–35 kcal mol^{-1} lower than that of low relative energy conformers. Also, although large variation was found in energies of deprotonation for the same conformation (with regards to the three protons) in low relative energy conformers, the high relative energy conformers all possessed comparable energies of deprotonation for all three protons for a given conformational assignment because of the lack of intramolecular stabilization directly involving any proton(s).

After all the non-optimized energies of deprotonation were calculated, all H_a (c.f. $\Delta E_{opt}(a)$ in Table 4), H_{g+} (c.f. $\Delta E_{opt}(g^+)$ in Table 5), and H_{g-} (c.f. $\Delta E_{opt}(g^-)$ in Table 6) deprotonated conformers were subject to full geometry optimizations. By majority, unique protonated conformational assignments converged to unique deprotonated conformational assignments with little redundancy. Geometry optimizations reduced most of the energies of deprotonation, however, conformations with internal stabilization still required significantly more energy (20–30 kcal mol^{-1}) for deprotonation. The inherent stability of these conformers made deprotonation a more energetically demanding task; for example, the H_{g-} deprotonation of $g^+g^+g^+g^-$ ($\Delta E_{opt}(g^-) = 257.89$ kcal mol^{-1}) or the H_a deprotonation of $g^+ag^-a^C$ ($\Delta E_{opt}(a) = 264.29$ kcal mol^{-1}) versus the H_{g+} deprotonation of $aaaa^A$ ($\Delta E_{opt}(g^+) = 242.89$ kcal mol^{-1}) or the H_a deprotonation of ag^-aa ($\Delta E_{opt}(a) = 239.81$ kcal mol^{-1}). These dramatic differences in optimized energies of deprotonation are indicative of the fact that the protonated conformation has significant influence on the energetics of protonophoretic pathways and mechanisms.

When analyzing the differences between vertical and optimized energies of deprotonation, the values of $\Delta\Delta E(a)$, $\Delta\Delta E(g^+)$, and $\Delta\Delta E(g^-)$ (Table 8) were used to compare the stabilization gained by a respective deprotonated conformer upon geometry optimization. These values were typically large and in the range of 8–21 kcal mol^{-1} for conformers with intramolecular stabilization present. This can be interpreted as the initial deprotonation event producing a high energy structure that requires major geometrical alterations to reach local minima. On the other hand, conformers with no intramolecular stabilization usually had $\Delta\Delta E$ values of less than 8 kcal mol^{-1} indicating that the protonated conformations were ideal structures for deprotonation and did not require major geometrical changes to rearrange into a local minima.

Carvedilol, with a pK_a of 7.9, is expected to have its amino group involved in a large number of

Table 8
Summary of different energies of deprotonation for each converged conformation of aminoethoxy-2-methoxy-benzene (Fragment C) at the RHF/3-21G level of theory

Optimized protonated conformation				$\Delta E_{vert}(a)$ (kcal mol^{-1})	$\Delta E_{opt}(a)$ (kcal mol^{-1})	$\Delta\Delta E(a)$ (kcal mol^{-1})	$\Delta E_{vert}(g^+)$ (kcal mol^{-1})	$\Delta E_{opt}(g^+)$ (kcal mol^{-1})	$\Delta\Delta E(g^+)$ (kcal mol^{-1})	$\Delta E_{vert}(g-)$ (kcal mol^{-1})	$\Delta E_{opt}(g^-)$ (kcal mol^{-1})	$\Delta\Delta E(g^-)$ (kcal mol^{-1})
χ_7	χ_8	χ_9	χ_{11}									
g^+	g^+	g^+	g^-	280.43	261.69	18.74	270.32	258.26	12.06	270.54	257.89	12.65
g^+	a	a	a	263.54	254.76	8.78	264.01	254.90	9.11	269.55	254.90	14.65
g^+	a	g^-	a^A	276.07	259.87	16.20	271.49	259.87	11.62	277.51	259.83	17.68
g^+	a	g^-	a^B	278.99	264.29	14.70	268.01	258.46	9.55	269.12	258.41	10.71
g^+	a	g^-	a^C	279.45	264.29	15.16	268.18	258.43	9.75	269.52	258.39	11.13
g^+	g^-	a	g^-	266.12	250.47	15.65	273.09	254.38	18.71	267.07	253.55	13.52
g^+	g^-	g^-	g^+	278.66	257.26	21.40	268.18	257.06	11.12	269.22	257.26	11.96
a	g^+	g^+	g^-	248.61	240.76	7.85	247.69	241.21	6.48	248.76	240.73	8.03
a	g^+	a	g^+	244.97	238.34	6.63	244.49	238.18	6.31	243.73	238.35	5.38
a	g^+	a	a	245.43	239.81	5.62	245.39	239.92	5.47	244.49	239.95	4.54
a	a	a	a^A	248.70	242.73	5.97	247.81	242.89	4.92	248.90	242.88	6.02
a	a	a	a^B	245.33	240.55	4.78	246.04	240.38	5.66	245.85	240.29	5.56
a	a	a	a^C	245.84	240.29	5.55	246.03	240.38	5.65	245.32	240.55	4.77
a	a	a	a^D	246.31	240.30	6.01	245.23	240.30	4.93	246.12	240.14	5.98
a	g^-	a	a	245.44	239.81	5.63	244.50	239.95	4.55	245.39	239.92	5.47
a	g^-	a	g^-	244.97	238.34	6.63	243.73	238.35	5.38	244.49	238.18	6.31
a	g^-	g^-	g^+	248.73	240.73	8.00	247.67	241.21	6.46	248.57	240.76	7.81
g^-	g^+	g^+	g^-	278.68	257.26	21.42	269.24	257.26	11.98	268.20	257.06	11.14
g^-	g^+	a	g^+	273.12	254.38	18.74	266.08	250.47	15.61	267.03	253.55	13.48
g^-	a	g^+	a^A	279.47	264.27	15.20	269.54	258.39	11.15	268.20	258.43	9.77
g^-	a	g^+	a^B	279.05	264.27	14.78	269.16	258.41	10.75	268.01	258.46	9.55
g^-	a	g^+	a^C	277.50	259.83	17.67	271.48	259.87	11.61	276.07	259.87	16.20
g^-	a	a	a	269.50	254.90	14.60	263.94	254.90	9.04	263.48	254.75	8.73
g^-	g^-	g^-	g^+	280.43	261.69	18.74	270.54	257.89	12.65	270.32	258.26	12.06

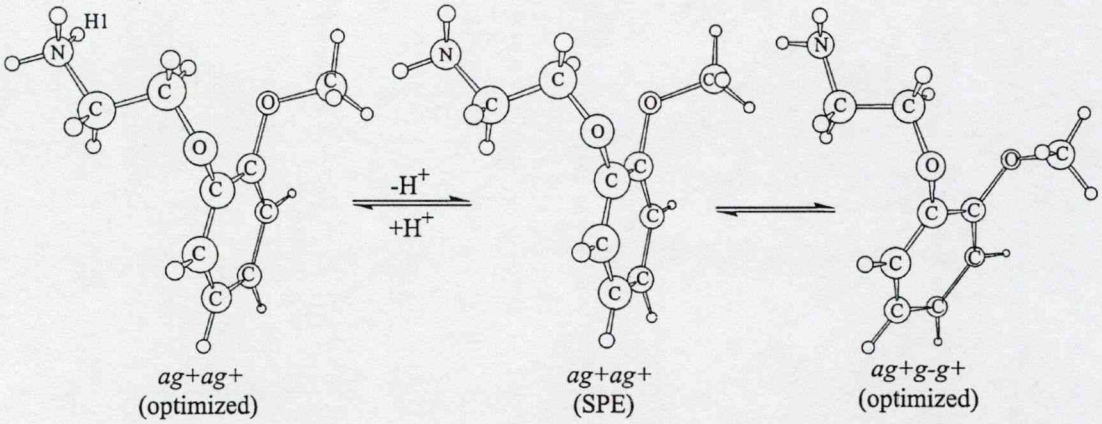

Fig. 10. The route with the lowest energy of deprotonation (optimized) for Fragment C was found to be via the H_a (H1) deprotonation of conformer ag^+ag^+ to the $ag^+g^-g^+$ conformation (238.34 kcal mol^{-1}).

protonophoretic pathways. At a physiological pH of 7.4, about two-thirds of the amino group is in its protonated form. In this light, the pathway with the lowest energy of deprotonation (optimized) for Fragment C was the H_a (H1) deprotonation of conformers ag^+ag^+ (Fig. 10). Conformer ag^+ag^+ has a fully extended conformation with proton H1 oriented away from the core of the structure and as such can be easily deprotonated. The vertical energy for this deprotonation was calculated at 244.97 kcal mol^{-1}. Upon optimization, the converged local minima structure was conformer $ag^+g^-g^+$ with an energy of deprotonation of 238.34 kcal mol^{-1}. Upon deprotonation, only a slight rotation of torsional angle χ_9 from the *anti* to the g^- position was needed for convergence to a nearby local minima on the PEHS. The minor geometry alteration is further emphasized with a low $\Delta\Delta E(a)$ value of 6.63 kcal mol^{-1}.

On the other hand, protonated conformers $g^+ag^-a^B$ and $g^+ag^-a^C$ required 264.29 kcal mol^{-1} for deprotonation of the H1 proton (Fig. 11). The $g^+ag^-a^B$ and $g^+ag^-a^C$ conformations contained a bifurcated H1 hydrogen bond to O5 and O12 forming the preferred eight-membered ring. This deprotonation required that the proton be abstracted from the core of the structure. The SPE for this deprotonation was 278.99 and 279.45 kcal mol^{-1} for $g^+ag^-a^B$ and $g^+ag^-a^C$ conformers, respectively. Upon optimization, both of these conformers converged to the $g^+ag^-a^B$ with $\Delta\Delta E(a)$ values of 14.70 and 15.16 kcal mol^{-1} for $g^+ag^-a^B$ and $g^+ag^-a^C$ conformers, respectively. Although the conformational assignment remained the same for this deprotonation, the large $\Delta\Delta E$ values indicate the large geometrical alterations that were needed for convergence to a local minima; for example, torsional angle χ_8 rotated about 45° and χ_9 about 40°.

Previous work done on carvedilol has revealed energies of deprotonation of 234 and 238 kcal mol^{-1} for only two conformations, irrespective of the protons deprotonated, at the RHF/6-31G(d) level of theory [10]. Work on Fragment B of carvedilol has revealed energies of deprotonation ranging from 245 to 262 kcal mol^{-1} for the entire PEHS of Fragment B with full optimizations at the RHF/3-21G level of theory [16]. The values obtained here for Fragment C through full optimizations of the entire PEHS range from 238 to 264 kcal mol^{-1} and are comparable with greater selectivity and variation in the values. This indicates that the RHF/3-21G level of theory is adequate to quantify the energetics of carvedilol and its fragments and that the methodology to analyze differences at the proton and conformation level are significant and needed.

With regards to deprotonation schemes, pathways of proton abstraction will vary depending on the molecular conformation of the protonated structure. As such, in assessing the conformers of a particular PEHS, it is important to analyze not only dominant

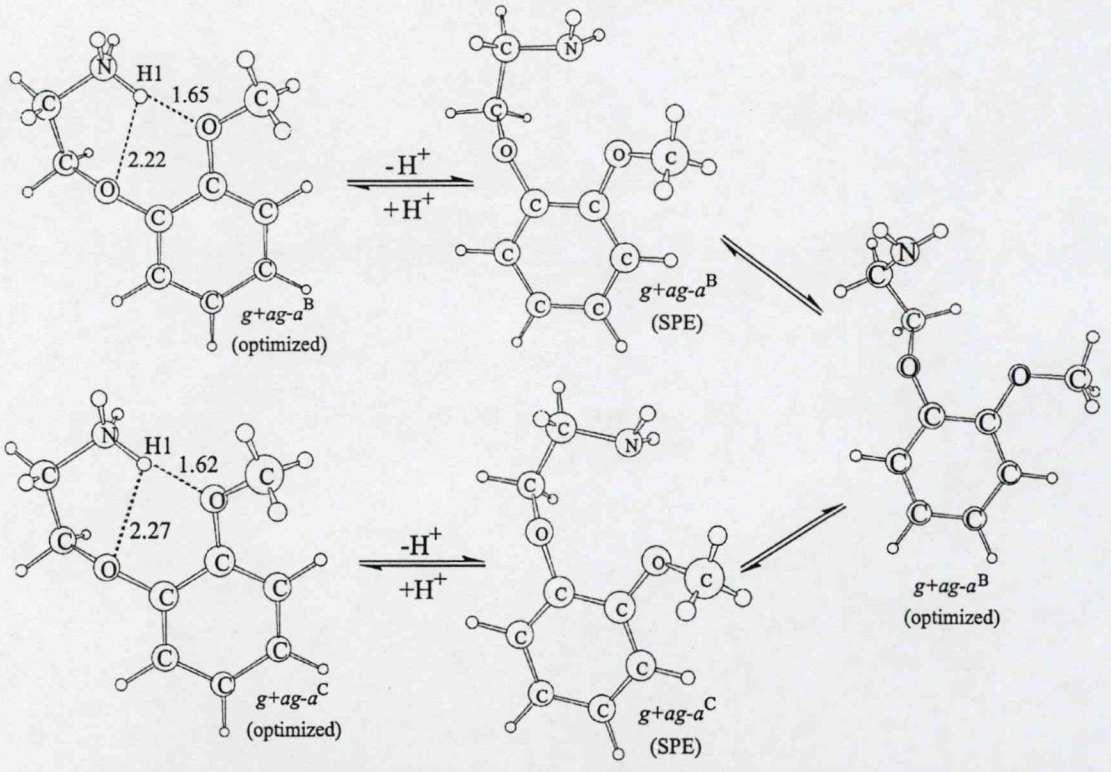

Fig. 11. The route with the largest energy of deprotonation (optimized) for Fragment C was found to be via the H_a (H1) deprotonation of conformers $g^+ag^-a^B$ and $g^+ag^-a^C$ (264.29 kcal mol^{-1}), both of which converged to the $g^+ag^-a^B$ conformation.

structures with low relative energies but also to realize that favored structures will vary widely depending on the mechanism in question. As shown here, and for Fragment B [16], in assessing protonophoretic pathways, the ideal structures for deprotonation will be those of higher relative energies with minimal internal stabilization. Thus, molecular conformation and intrinsic structural motifs will predetermine, at least with regards to energetics, the type of protonophoretic mechanism most utilized or favored by enzymes and substrates in proton shuttling pathways (such as that postulated for carvedilol in the uncoupling of oxidative phosphorylation in the mitochondria). The differences in the energies of deprotonation that are dependent on molecular conformation can help explain why such diverse effects have been seen in mitochondrial uncoupling by carvedilol and attributed to the molecular conformations adopted by carvedilol [10]. To put differently, carvedilol is believed to possess large conformational flexibility and should possess a PEHS with very diverse conformational minima. Thus, it is expected that different structures will be more likely to participate in proton shuttling across the mitochondrial membrane and be better at the uncoupling effects seen in mitochondria.

4. Conclusions

The data presented here for the primary amine Fragment C agrees with the results obtained for the secondary amine Fragment B and indicates that for carvedilol, and any general protonophoretic pathways involving primary and secondary amines, reactions and events of deprotonation will not only favor higher energy conformations but will also favor protons differentially according to their orientation. It may be expected that the abstracted proton will be one

oriented maximally away from the core of the structure devoid of any intermolecular formation for favored energetics.

As is evident from the deprotonation data presented here, it is not the proton per se that determines whether the energy of deprotonation is large or small; rather, it is the molecular conformation adopted by a structure that determines the respective orientation of a given proton, and therefore, predetermines the energetics of the deprotonation event. This is to say that, protons may be indistinguishable one from the other, but depending on the molecular conformations and the protonophoretic mechanisms in question, rarely are two protons the same. Finally, a novel amine–aromatic π interaction was discovered in the deprotonated Fragment C PEHS. Further work is ongoing to further elucidate the characteristics of this interaction.

Acknowledgements

One of the authors (IGC) wishes to thank the Ministry of Education for a Szent-Györgyi Visiting Professorship.

References

[1] W. Carlson, K. Oberg, J. Cardiovasc. Pharmacol. Ther. 4 (1999) 205.
[2] M. Metra, S. Nodari, A. D'Aloia, L. Bontempi, E. Boldi, L. Dei Cas, Am. Heart J. 139 (2000) 511.
[3] G. Feuerstein, R.R. Ruffolo Jr., Adv. Pharmacol. 42 (1998) 611.
[4] O. Saijonmaa, K. Metsarinne, F. Fyhrquist, Blood Press. 6 (1997) 24.
[5] S. Capomolla, O. Febo, M. Gnemmi, G. Riccardi, C. Opasich, A. Carporotondi, A. Mortara, G. Pinna, F. Cobelli, Am. Heart J. 139 (2000) 596.
[6] M. Packer, M.R. Bristow, J.N. Cohn, W.S. Colucci, M.B. Fowler, E.M. Gilbert, N.H. Shusterman, N. Engl. J. Med. 334 (1996) 1349.
[7] M.A. Berg, G.A. Chasse, E. Deretey, A.K. Kuzery, B.M. Fung, D.Y.K. Fung, H. Henry-Riyad, A.C. Lin, M.L. Mak, A. Mantas, M. Patel, I.V. Repyakh, M. Staikova, S.J. Salpietro, T.-H. Tang, J.C. Vank, A. Perczel, G.I. Csonka, O. Farkas, L.L. Torday, Z. Szekely, I.G. Csizmadia, J. Mol. Struct. (THEOCHEM) 500 (2000) 5.
[8] G. Feuerstein, T.L. Yue, X. Ma, R.R. Ruffolo, Prog. Cardiovasc. Dis. 41 (1 suppl 1) (1998) 17.
[9] A.J.F. Searlee, C. Gree, R.L. Wilson, Ellipticines and carbazoles as antioxidants, in: W. Borns, M. Saran, D. Tait (Eds.), Oxygen Radicals and Biology, Walter de Gruyter, Berlin, 1984, pp. 377–381.
[10] P.J. Oliveira, M.P. Marques, L.A.E. Batista de Carvalho, A.J.M. Moreno, Biochem. Biophys. Res. Commun. 276 (2000) 82.
[11] R. Ferrari, J. Cardiovasc. Pharmacol. 28 (1996) S1.
[12] D.R. Howlett, A.R. George, D.E. Owen, R.V. Ward, R.E. Markwell, Biochem. J. 343 (1999) 419.
[13] H.G. Oldham, S.E. Clarke, Drug Metab. Dispos. 25 (1997) 970.
[14] R.R. Ruffolo Jr., M. Gellai, J.P. Hieble, R.N. Willette, A.J. Nichols, Eur. J. Clin. Pharmacol. 38 (1990) S82.
[15] D.R.P. Almeida, L.F. Pisterzi, G.A. Chass, L.L. Torday, A. Varro, J. Gy. Papp, I.G. Csizmadia, J. Phys. Chem. 106 (2002) 10423.
[16] D.R.P. Almeida, D.M. Gasparro, L.F. Pisterzi, L.L. Torday, A. Varro, J. Gy. Papp, B. Penke, J. Mol. Struct. (Theochem), 631 (2003) 251.
[17] D.U. Silverthorn, W.C. Ober, C.W. Garrison, A.C. Silverthorn, Human Physiology: An Integrated Approach, second ed., Prentice Hall, Upper Saddle River, NJ, 1998.
[18] P.G. Heytler, Uncouplers of Oxidative Phosphorylation, in: Methods in Enzymology, LV, Academic Press, New York, 1979, pp. 462–472.
[19] A. Tzagoloff, Mitochondria, Plenum Press, New York, 1982.
[20] [.2.0.].S.S. Korshunov, V.P. Skulachev, A.A. Starkov, FEBS Lett. 416 (1997) 15.
[21] D.R.P. Almeida, D.M. Gasparro, L.F. Pisterzi, L.L Torday, A. Varro, J. Gy. Papp, B. Penke, I.G. Csizmadia, J. Phys. Chem. A, 107 (2003) 5594.
[22] M.J. Frisch, G.W. Trucks, H.B. Schlegel, G.E. Scuseria, M.A. Robb, J.R. Cheeseman, V.G. Zakrzewski, J.A. Montgomery, Jr., R.E. Stratmann, J.C. Burant, S. Dapprich, J.M. Millam, A.D. Daniels, K.N. Kudin, M.C. Strain, O. Farkas, J. Tomasi, V. Barone, M. Cossi, R. Cammi, B. Mennucci, C. Pomelli, C. Adamo, S. Clifford, J. Ochterski, G.A. Petersson, P.Y. Ayala, Q. Cui, K. Morokuma, D.K. Malick, A.D. Rabuck, K. Raghavachari, J.B. Foresman, J. Cioslowski, J.V. Ortiz, A.G. Baboul, B.B. Stefanov, G. Liu, A. Liashenko, P. Piskorz, I. Komaromi, R. Gomperts, R.L. Martin, D.J. Fox, T. Keith, M.A. Al-Laham, C.Y. Peng, A. Nanayakkara, C. Gonzalez, M. Challacombe, P.M.W. Gill, B.G. Johnson, W. Chen, M.W. Wong, J.L. Andres, M. Head-Gordon, E.S. Replogle, J.A. Pople, GAUSSIAN 98 (Revision A.9), Gaussian Inc., Pittsburgh, PA, 1998.
[23] Axum 5.0C for Windows, MathSoft Incorporated, 1996.

ELSEVIER

Journal of Molecular Structure (Theochem) 666–667 (2003) 537–545

THEO CHEM

www.elsevier.com/locate/theochem

Predicting the conformations of carvedilol based on its pharmacophore fragments: a gas phase and solvation ab initio and density functional study

David R.P. Almeida[a,*], Donna M. Gasparro[a], Luca F. Pisterzi[a], Jason R. Juhasz[a], Ferenc Fülöp[b], Imre G. Csizmadia[a,c,d]

[a]*Lash Miller Laboratories, Department of Chemistry, University of Toronto, 80 St George Street, Toronto, Ont., Canada M5S 3H6*
[b]*Institute of Pharmaceutical Chemistry, Albert Szent-Györgyi Medical University, Szeged University, Eötvös u. 6, Szeged H-6720, Hungary*
[c]*Global Institute of Computational Molecular and Materials Science (GIOCOMMS)@1422, Edenrose St, Mississauga, Ont., Canada L5V 1H3*
[d]*Department of Medical Chemistry, University of Szeged, Dóm tér 8, Szeged 6720, Hungary*

Abstract

Carvedilol is a cardiovascular drug of proven efficacy with multiple modes of action. As a novel anti-fibrillar agent, carvedilol is able to inhibit amyloid-beta (Aβ) fibril formation and may have uses in the treatment of Alzheimer's disease. However, it is currently not known what form of Aβ carvedilol binds to or what type of inhibitory interaction occurs. Previously, we developed a scheme to fragment and study the pharmacophores of carvedilol individually so that the results could be used to predict the dominant features and conformations of whole carvedilol. In the present study, these predictions are tested and this methodology evaluated. Further, the conformational character of carvedilol is investigated to elucidate how it might be related to its anti-fibrillar mechanism. Conformational and structural predictions were tested on protonated *S*-carvedilol with molecular orbital computations of its potential energy hypersurface using restricted Hartree–Fock (RHF) and density functional theory (DFT with the Becke 3LYP hybrid exchange-correlation functional). Full gas phase optimizations were carried out at the RHF/3-21G and B3LYP/6-31G(d) level of theory and subsequent single point energy (SPE) calculations were performed on B3LYP/6-31G(d) converged conformers at the B3LYP/6-311 + G(2d,p) level of theory. B3LYP/6-31G(d) solvation SPE calculations were performed according to the polarized continuum model (PCM) of Tomasi and coworkers in DMSO and water. Six carvedilol conformations (C1–C6) were evaluated. The lowest energy conformers, C3, C4, and C6, possessed all predicted intramolecular features and their respective conformational assignments were also largely predicted from the carvedilol fragments. Solvation calculations in both aprotic (DMSO) and protic (water) solvents revealed the same trends seen in the gas phase. Generally, gas phase and solvation ab initio and DFT results were in sound agreement with each other. Given these results, the current study gives credence to the idea that large molecular systems can be studied by rational fragmentation of pharmacophores and other structure–activity moieties. Furthermore, the conformations presently evaluated are ideal starting points towards deciphering the molecular basis of the inhibitory interaction between carvedilol and Aβ.

Keywords: Carvedilol; Molecular fragments; Anti-fibrillar; Restricted Hartree–Fock; DFT-Becke 3LYP hybrid functional

* Corresponding author.
E-mail addresses: dalmeida@medscape.com (D.R.P. Almeida), dgasparro@medscape.com (D.M. Gasparro), lpisterzi@medscape.com (L.F. Pisterzi), jasonjuhasz@medscape.com (J.R. Juhasz), fulop@pharma.szote.u-szeged.hu (F. Fülöp), icsizmad@alchemy.chem.utoronto.ca (I.G. Csizmadia).

0166-1280/$ - see front matter © 2003 Elsevier B.V. All rights reserved.
doi:10.1016/j.theochem.2003.08.078

1. Introduction

Carvedilol, 1-(9H-Carbazol-4-yloxy)-3-[2-(2-methoxy-phenoxy)ethylamino]-2-propanol ($C_{24}H_{26}N_2O_4$), is a cardiovascular drug with multiple modes of action. Its major molecular targets are membrane adrenoceptors (antagonist at α_1, β_1, and β_2), reactive oxygen species (ROS), and ion channels (K^+ and Ca^{2+}) [1]. Carvedilol provides hemodynamic benefits, such as reduction of cardiac work and peripheral vasodilation, from its balanced adrenergic receptor blockage [1,2]. Carvedilol also exerts potent cardiovascular protection (anti-proliferative/anti-atherogenic, anti-hypertrophic, anti-ischemic, and anti-arrhythmic actions) via antioxidant effects, improvement of glucose/lipid metabolism, modulation of neurohormonal factors (e.g. nitric oxides), and beneficial cardiac electrophysiological properties (reviewed in Ref. [1]). Due to its hemodynamic and cardioprotective effects, carvedilol has proven efficacy in the treatment of hypertension, ischemic heart disease (IHD), and congestive heart failure (CHF) [1,3]. A further cardioprotective effect of carvedilol is related to its ability to protect mitochondria from oxidative stress by acting as a mild uncoupler of oxidative phosphorylation by means of a postulated protonophoretic mechanism [4].

Work has indicated that carvedilol, and its active hydroxylated analogues, act as novel anti-fibrillar agents [able to inhibit amyloid-beta (Aβ) fibril formation] [5]. According to the amyloid cascade hypothesis of Alzheimer's disease (AD), accumulation of Aβ in extracellular senile plaques (SPs) in brain tissues is the primary influence driving AD pathogenesis [6]. SPs contain aggregated amyloid fibrils formed from 39–43 amino acid Aβ peptides [7]. Aβ peptides consisting of 42 or 43 amino acids (abbreviated as Aβ1-42) are more prone to aggregate than Aβ1-40, and thus, promote aggregation and deposition of fibrillar Aβ [7]. The amyloid hypothesis states that increased Aβ1-42 production and accumulation leads to Aβ1-42 oligomerization and deposition in diffuse plaques [6]. Aβ oligomers cause progressive synaptic and neuritic injury alongside microglial and astrocytic activation (complement factors, cytokines, neuroinflammation, etc.) [6,8]. Neurotoxicity causes neuronal ionic disturbances and oxidative injury producing neurofibrillary tangles (NFTs), widespread neuronal dysfunction, cell death, and neurotransmitter deficits that all culminate in AD dementia [6]. These observations provide strong rationale that the inhibition and elimination of Aβ fibrils may be viable therapeutic targets for the treatment of AD [7].

It has been shown that Aβ oligomers (dimers, trimers, or higher oligomers), in the absence of monomers and amyloid fibrils, are neurotoxic [8] and there is growing support that Aβ oligomers are the main neurotoxic component of AD [9–11]. Given the above, along with the fact that carvedilol may inhibit oligomer formation [5], it may be postulated that carvedilol may have uses in the prevention or slowing down of AD pathology. The effectiveness of carvedilol's inhibition of Aβ fibril formation is due to three factors: (1) a central basic amino pharmacophore, (2) two cyclic hydrophobic ring centroids, and (3) the molecular flexibility to adopt a specific three-dimensional pharmacophore conformation [5]. Although these three factors are elucidated, it is currently not known if carvedilol binds to Aβ monomers, dimers, or other oligomers [5] or what type of interaction occurs between carvedilol and the Aβ peptide(s).

We have previously [12] developed a scheme to fragment the three pharmacophores of carvedilol vis-à-vis structure–activity (c.f. Fig. 1) as a means to study the conformational profile of each pharmacophore and attempt to predict the conformations and features of the entire drug molecule; such an approach allows for the study of large molecules by rational fragmentation of their pharmacophores. In the current study, these predictions are tested to evaluate such a methodology. Further, since carvedilol's AD effects are due to its pharmacophores and conformational flexibility (factors 1–3 above), which have been studied, the conformational profile of carvedilol is analyzed in the hope of clarifying current and future communications on its anti-fibrillar mechanism of action.

2. Methods

Carvedilol is composed of three distinct pharma-

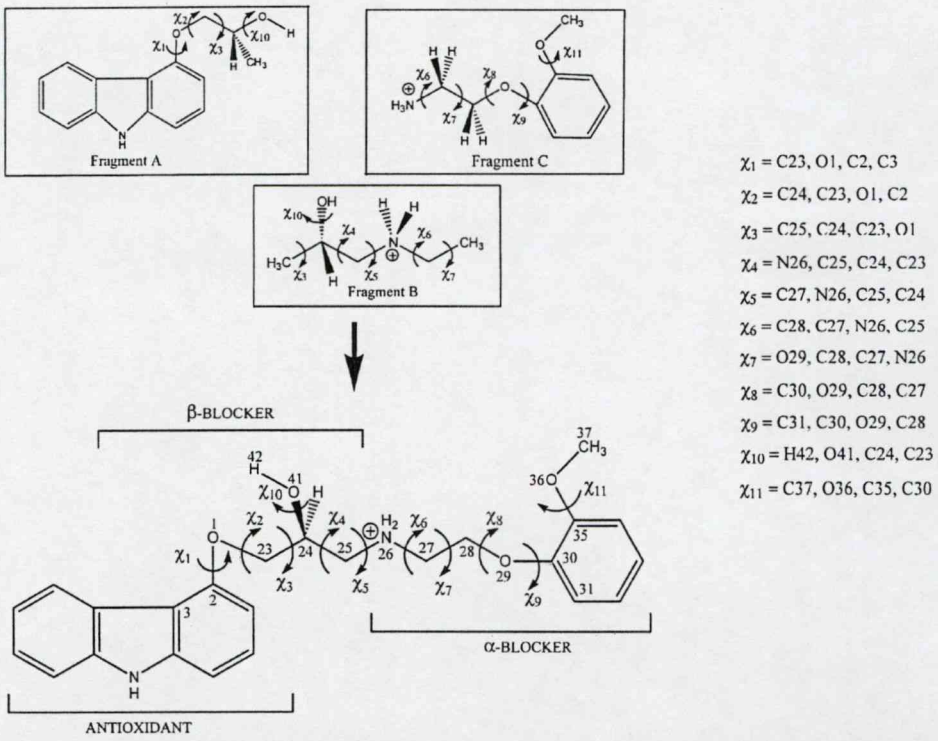

Fig. 1. Carvedilol was divided into three pharmacophoric fragments: *R*- and *S*-4-(2-hydroxypropoxy)carbazol (Fragment A) [12,13], 2(*R* and *S*)-1-(ethylamonium)propane-2-ol (Fragment B) [14], and aminoethoxy-2-methoxy-benzene (Fragment C) [15] (top). These fragments were individually computed and the results were used to predict the conformations and features of *N*-protonated carvedilol (*S*-configuration) (bottom). Numbers placed beside atoms were used to define all torsional angles for carvedilol in the z-matrix input for Gaussian 98 (right).

cophores and was thus divided into three molecular fragments: *R*- and *S*-4-(2-hydroxypropoxy)carbazol (Fragment A) possesses the carbazole-related antioxidant effects of carvedilol [12,13], 2(*R* and *S*)-1-(ethylamonium)propane-2-ol (Fragment B) contains the protonophoretic amino group implicated in the cardioprotective uncoupling of mitochondrial oxidative phosphorylation [14], and aminoethoxy-2-methoxy-benzene (Fragment C) is the α_1-adrenergic antagonist pharmacophore of carvedilol [15] (c.f. Fig. 1). Nonselective β-blockage is exerted by both Fragments A and B.

To allow explicit prediction of conformation, a systematic numbering system was used for all structures such that corresponding torsional angles in fragments and carvedilol were defined in the same manner. Further, conformational structural assignments for the conformational minima of a respective potential energy hypersurface (PEHS) were made according to Eq. (1).

$$\begin{aligned} &\text{gauche plus } (g^+) = 60 \text{ (ideal)} \pm 60^\circ \\ &\text{anti } (a) = 180 \text{ (ideal)} \pm 60^\circ \\ &\text{gauche minus } (g^-) = -60 \text{ (ideal)} \pm 60^\circ \end{aligned} \quad (1)$$

To fully investigate the predictions, it is necessary to briefly review the individual fragments. The PEHS of Fragment A revealed a planar carbazole ring with intramolecular hydrogen bonding between the ether oxygen and the hydroxyl group proton as the dominant interaction [12,13]. The global minima possessed a conformation with torsional angles χ_1, χ_2, χ_3, and χ_{10} in the *a*, *a*, *a*, and g^- position [*S*-configuration; B3LYP/6-31G(d) results], respectively

[12,13]. The global minima of the Fragment B PEHS had a conformation with torsional angles χ_4, χ_5, χ_6, and χ_{10} in the *a*, *a*, *a*, and g^+ position (*S*-configuration; RHF/3-21G results), respectively, and the dominant interaction was an intramolecular hydrogen bond between the stereocentre hydroxyl oxygen and an amine proton [14]. Finally, the Fragment C PEHS revealed a pair of axis chiral global minima (see Ref. [13] for explanation) with torsional angles χ_7, χ_8, χ_9, and χ_{11} in the g^+, g^+, g^+, and g^- position, respectively (other axis chiral conformation was g^-, g^-, g^-, and g^+, respectively; RHF/3-21G results) [15]. The dominant interaction was a bifurcated hydrogen bond between an amine proton and the ether and methoxy oxygen atoms on the substituted benzene [15]. Consequently, it is predicted that the lowest energy conformers of carvedilol will possess the above intramolecular features and have a conformation predicted by Eq. (2) (torsional angle positions in brackets [ ] are representative of the possible axis chiral conformations of Fragment C).

$$\begin{aligned} &\chi_1 = a\ \chi_4 = a\ \chi_7 = g^+[g^-]\ \chi_{10} = g^- \\ &\chi_2 = a\ \chi_5 = a\ \chi_8 = g^+[g^-]\ \chi_{11} = g^-[g^+] \\ &\chi_3 = a\ \chi_6 = a\ \chi_9 = g^+[g^-] \end{aligned} \quad (2)$$

The predictions were tested on protonated *S*-carvedilol (c.f. Fig. 1) with molecular orbital (MO) optimizations of the PEHS conformational minima. All calculations were carried out using the Gaussian 98 software program [16]. Initially, full optimizations in the gas phase ($\varepsilon = 0.0$) on carvedilol structures were performed at the restricted Hartree–Fock, RHF/3-21G, level of theory. Converged conformers were subsequently optimized using density functional theory (DFT) with the Becke 3LYP hybrid exchange-correlation functional [17] at the B3LYP/6-31G(d) level of theory; separate vibrational frequency calculations were performed on all converged conformers for full structural characterization. Single point energy (SPE) calculations were computed on B3LYP/6-31G(d) converged conformers at the B3LYP/6-311 + G(2d,p) level of theory. Full optimizations were performed at both RHF and DFT model chemistries for comparison. B3LYP/6-31G(d) solvation SPE computations of the DFT converged minima were computed according to the polarized continuum (overlapping spheres) model (PCM) of Tomasi and coworkers with reaction-field calculations [18–20] in aprotic (dimethyl sulfoxide, DMSO; $\varepsilon = 46.7$) and protic (water; $\varepsilon = 78.39$) solvents. Graphical data was plotted using Axum 5.0 [21].

3. Results and discussion

Six carvedilol conformations (C1–C6) were computed. Conformational assignments of RHF/3-21G and B3LYP/6-31G(d) optimized minima are displayed in Table 1; total energies and relative energies for conformers evaluated at RHF/3-21G, B3LYP/6-31G(d), and B3LYP/6-311 + G(2d,p) are tabulated in Table 2; explicit values of RHF/3-21G and B3LYP/6-31G(d) converged minima are shown in Table 3;

Table 1
Protonated carvedilol structure codes are defined according to optimized molecular conformation

Structure code	Torsional angle conformation										
	χ_1	χ_2	χ_3	χ_4	χ_5	χ_6	χ_7	χ_8	χ_9	χ_{10}	χ_{11}
C1	[*a*/*a*]	[*a*/*a*]	[*a*/*a*]	[*a*/*a*]	[*a*/*a*]	[*a*/*a*]	[*a*/*a*]	[*a*/*a*]	[*a*/*a*]	[*a*/*a*]	[*a*/*a*]
C2	[*a*/*a*]	[*a*/*a*]	[*a*/*a*]	[*a*/*a*]	[*a*/*a*]	[*a*/*a*]	[*a*/*a*]	[*a*/*a*]	[*a*/*a*]	[g^-/g^-]	[*a*/*a*]
C3	[*a*/*a*]	[*a*/*a*]	[*a*/*a*]	[*a*/*a*]	[*a*/*a*]	[*a*/*a*]	[g^+/g^+]	[g^+/g^+]	[g^+/g^+]	[g^-/g^-]	[g^-/*a*]
C4	[*a*/*a*]	[*a*/*a*]	[*a*/*a*]	[*a*/*a*]	[g^-/g^-]	[*a*/*a*]	[g^+/g^+]	[g^+/g^+]	[g^+/g^+]	[g^-/g^-]	[g^-/g^-]
C5	[*a*/*a*]	[*a*/*a*]	[*a*/*a*]	[*a*/*a*]	[g^-/g^-]	[*a*/*a*]	[*a*/*a*]	[g^+/g^+]	[g^+/g^+]	[g^-/g^-]	[g^-/g^-]
C6	[*a*/*a*]	[*a*/*a*]	[*a*/*a*]	[g^-/g^-]	[*a*/*a*]	[*a*/*a*]	[g^+/g^+]	[g^+/g^+]	[g^+/g^+]	[g^-/g^-]	[g^-/g^-]

Molecular conformation is displayed as [RHF/3-21G optimized torsional angle geometry/B3LYP/6-31G(d) optimized torsional angle geometry] for converged conformers (explicit values of torsional angles are found in Table 3).

Table 2
Total and relative energies for fully optimized protonated carvedilol conformers at the RHF/3-21G and B3LYP/6-31G(d) level of theory

Structure code	RHF/3-21G total energy (hartree)	RHF/3-21G relative energy (kcal mol^{-1})	B3LYP/6-31G(d) total energy (hartree)	B3LYP/6-31G(d) Relative energy (kcal mol^{-1})	B3LYP/6-311 + G(2d,p) total energy (hartree)	B3LYP/6-311 + G(2d,p) relative energy (kcal mol^{-1})
C1	−1325.27429917	42.05	−1340.93763474	30.53	−1341.33778950	26.60
C2	−1325.31609523	15.83	−1340.96910024	10.78	−1341.36611515	8.82
C3	−1325.33656270	2.98	−1340.98558392	0.44	−1341.37858877	1.00
C4	−1325.34028445	0.65	−1340.98628696	0.00	−1341.38017747	0.00
C5	−1325.31708384	15.21	−1340.96478904	13.49	−1341.36057420	12.30
C6	−1325.34131460	0.00	−1340.98619251	0.06	−1341.37848989	1.06

Single point energy (SPE) calculations were performed on all B3LYP/6-31G(d) converged conformers at the B3LYP/6-311 + G(2d,p) level of theory.

solvation results for carvedilol conformers are presented in Table 4. Structures of B3LYP/6-31G(d) optimized conformers are shown in Fig. 2.

Conformer C1 was optimized with all torsional angles frozen in the *a* position as a reference structure with no intramolecular interactions (c.f. Fig. 2). B3LYP/6-31G(d) vibrational analysis revealed two negative frequencies associated with this high energy saddle point (c.f. Table 3). C1 was subsequently optimized in a fully relaxed state to the local minima C2; this structure has an all *a* conformation except torsional angle χ_{10} (g^- position) and possesses the intramolecular hydrogen bond motif, O1···H42–O41···H46, predicted by Fragment A and B (c.f. Fig. 2) with a moderate relative energy of 8.82 kcal mol^{-1} (c.f. Table 2).

The conformational prediction in Eq. (2) was fully tested with C3. Evident in this structure is

Table 3
Optimized values for the converged conformers of the protonated carvedilol surface at the RHF/3-21G and B3LYP/6-31G(d) level of theory

Structure code	Torsional angles											Relative energy (kcal mol^{-1})
	χ_1	χ_2	χ_3	χ_4	χ_5	χ_6	χ_7	χ_8	χ_9	χ_{10}	χ_{11}	
RHF/3-21G optimized torsional angles												
C1	180.00	180.00	180.00	180.00	180.00	180.00	180.00	180.00	180.00	180.00	180.00	42.05
C2	−174.25	178.62	168.48	−159.83	160.15	−154.67	176.54	122.84	124.90	−39.44	−171.25	15.83
C3	−176.23	−178.75	172.96	−160.84	−156.19	156.00	44.94	75.34	74.72	−44.48	−111.64	2.98
C4	−174.64	178.56	169.56	−156.97	−80.76	176.72	47.47	66.69	69.46	−69.03	−87.84	0.65
C5	−175.71	177.39	168.39	−160.43	−80.19	153.22	−155.26	98.05	93.12	−41.56	−87.84	15.21
C6	179.71	−173.33	150.96	−81.36	−161.72	179.58	48.28	62.13	67.18	−40.44	−81.74	0.00
B3LYP/6-31G(d) optimized torsional angles												
C1[a]	180.00	180.00	180.00	180.00	180.00	180.00	180.00	180.00	180.00	180.00	180.00	30.53
C2	168.45	−168.60	171.48	−165.94	165.81	−178.96	175.53	127.97	120.62	−40.90	−174.36	10.78
C3	169.54	−169.80	173.49	−172.78	−174.88	166.24	44.73	85.82	80.56	−43.19	−166.59	0.44
C4	173.93	−172.47	172.56	−162.24	−74.80	−179.73	46.80	69.08	68.74	−40.33	−95.13	0.00
C5	173.77	−172.33	172.56	−163.03	−77.83	177.01	−178.32	93.36	89.37	−42.62	−92.23	13.49
C6	166.15	−164.75	166.91	−79.39	−158.63	178.63	48.12	66.12	67.09	−37.87	−88.28	0.06

[a] Conformer C1 possesses two negative (imaginary) frequencies (−189.0871 cm^{-1} and −78.7329 cm^{-1}).

Table 4
Solvation total and relative energies derived from single point energy (SPE) calculations performed on converged conformers of the protonated carvedilol surface with Tomasi's polarized continuum model (PCM) at the B3LYP/6-31G(d) level of theory

Structure code	DMSO total energy (hartree)	DMSO relative energy (kcal mol^{-1})	Water total energy (hartree)	Water relative energy (kcal mol^{-1})
C1	−1341.03014946	15.61	−1341.06581487	8.71
C2	−1341.04332120	7.34	−1341.07123498	5.31
C3	−1341.05501806	0.00	−1341.07970247	0.00
C4	−1341.05205372	1.86	−1341.07538836	2.71
C5	−1341.03866190	10.26	−1340.96478904	72.11
C6	−1341.05181550	2.01	−1341.07479423	3.08

the Fragment A and B hydrogen bond motif, O1···H42–O41···H46, along with a triple hydrogen bond involving an amine proton (H46) and O41, O29, and O36 (c.f. Fig. 2). Fragment C predicted a bifurcated hydrogen bond, however, it is plausible that this bifurcated hydrogen bond could extend to bond with O41 which was not part of the Fragment C structure. Conformational assignment for C3 was

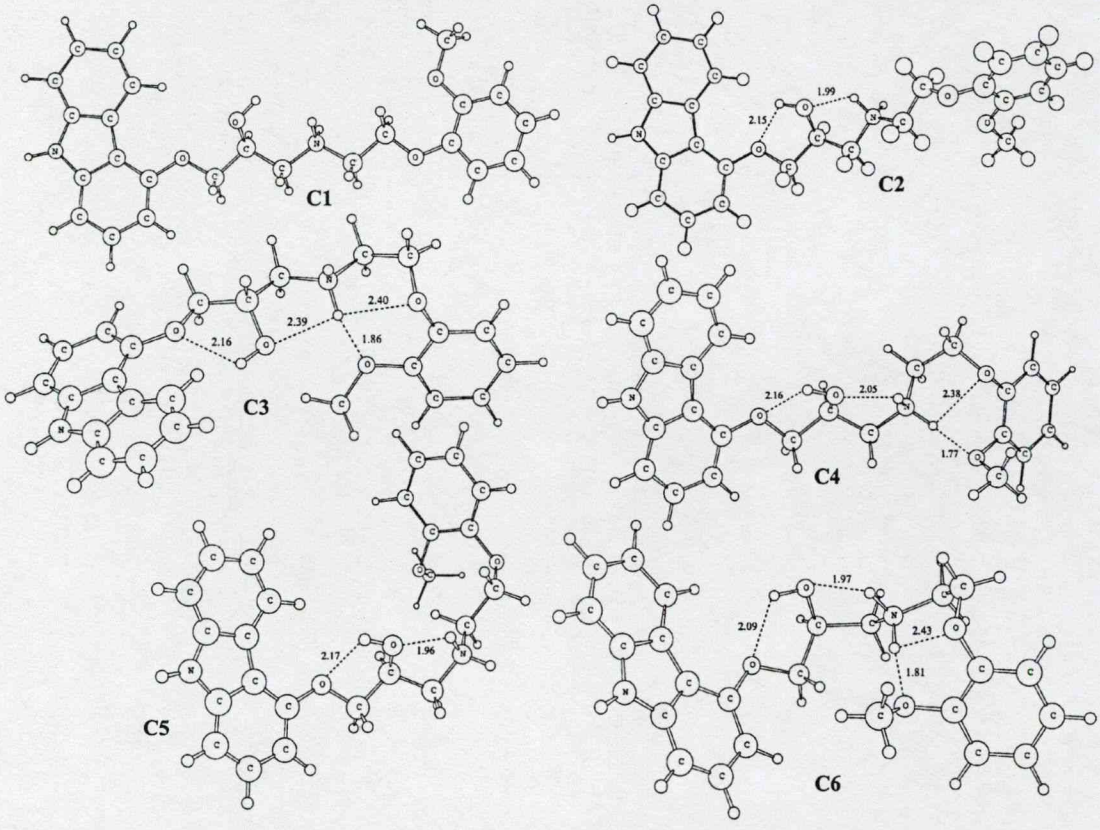

Fig. 2. Molecular structures of fully optimized B3LYP/6-31G(d) converged minima (C1–C6) for the protonated carvedilol potential energy hypersurface (PEHS).

exactly as predicted for the RHF/3-21G results but slightly different for the B3LYP/6-31G(d) results with torsional angle χ_{11} rotating from the g^- to a position (c.f. Tables 1 and 3); this conformer has a relative energy of 1.00 kcal mol^{-1} (c.f. Table 2).

Next, C4 was tested for the sole bifurcated hydrogen bond interaction discovered in Fragment C. C4 revealed all interactions in Fragment A, B, and C; and as predicted, has the lowest DFT relative energy (c.f. Fig. 2 and Table 2). C4 possesses the O1···H42–O41···H57 hydrogen bond motif found in Fragment A and B along the bifurcated intramolecular hydrogen bond, O29···H46···O36, in Fragment C (c.f. Fig. 2). With regards to the conformational assignment, C4 has the conformation predicted by Eq. (2), with the exception of torsional angle χ_5 which optimized in the g^- position to allow both amine protons to be involved in different hydrogen bond networks (c.f. Tables 1 and 3).

The remaining carvedilol conformers, C5 and C6, are miscellaneous converged conformers that display large conformational flexibility (c.f. Fig. 2). C5 is similar to C2 with the same hydrogen bond motif and a relatively high energy (c.f. Tables 2 and 3). C6, like C4, has all the interactions predicted to be in low energy conformers from the carvedilol fragments (c.f. Fig. 2), and consequently, has a low relative energy of 1.06 kcal mol^{-1} (c.f. Tables 2 and 3). Hence, these results indicate that the intramolecular features of the lowest energy conformers of carvedilol: C3, C4, and C6, were all successfully predicted by the individual fragments of carvedilol. Furthermore, the conformational assignments were, by in large, also predicted from the individual fragments. It is thus evident that this methodology is a viable approach to study large molecular systems explicitly via the rational fragmentation of their pharmacophores.

B3LYP/6-31G(d) SPE solvation calculations performed on conformers C1–C6 using the PCM method revealed that, similar to the gas phase, C3, C4, and C6 had the lowest energies in both DMSO and water (c.f. Table 4). The latter is likely due to a high degree of polarized character inherent in the conformations possessing extensive hydrogen bond networks (c.f. Fig. 2). C5 has a very large relative energy in water (72.11 kcal mol^{-1}; c.f. Table 4) due to the folding of the substituted benzene on itself which makes it difficult to solvate the entire structure and disrupts primary and secondary water molecule ordering surrounding the carvedilol cavity. C2,

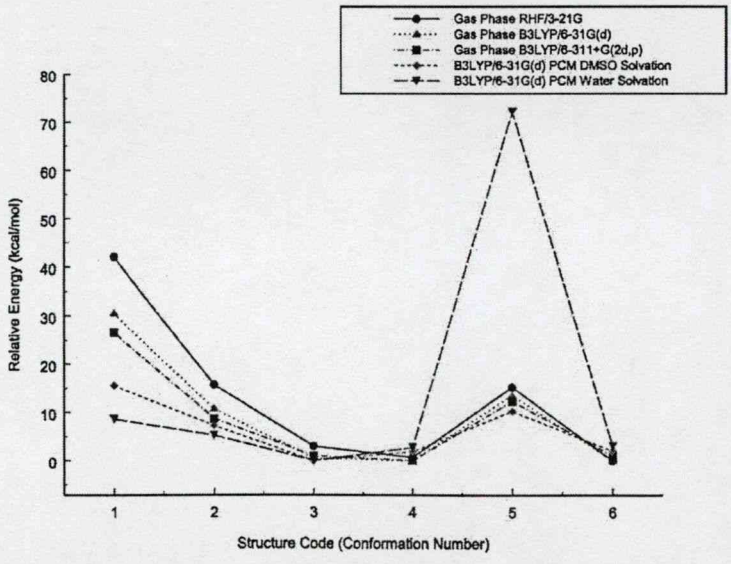

Fig. 3. Graphical plot of the gas phase and solvation ab initio and DFT relative energies of all carvedilol conformers (C1–C6) analyzed in this study.

while possessing the same interactions as C5, has a fully extended conformation, and thus, is more easily solvated by water (c.f. Fig. 2 and Table 4).

In plotting relative energy as a function of conformation number, generally, the trend is similar for all levels of theory in the gas phase and solvation (c.f. Fig. 3). The exception, as described above, is the large DFT water solvation energy of C5. Overall, although DFT energies are regarded as more accurate, ab initio and DFT energies and structural information are in sound agreement with each other. This indicates that the ab initio, RHF/3-21G level of theory, is a good predictor of the conformational character of fragments and molecules at a minimal computational expense.

This study, along with the analysis of the carvedilol fragments, is an ideal starting point for the investigation of the novel carvedilol anti-fibrillar mechanism of action with Aβ because this mechanism is believed to be dependent on the conformational flexibility of the pharmacophores of carvedilol [5]. Thus, it is necessary to decipher bona fide conformations that carvedilol may assume before subsequent testing between carvedilol and Aβ peptide(s) to elucidate the inhibitory interaction between carvedilol and Aβ.

4. Conclusions

Presently, we have predicted all dominant interactions, and to a large extent conformational assignment, of expected low energy carvedilol conformers from the complete analysis of its fragments. The current study validates the idea that large molecular systems with numerous torsional modes and exhaustive conformational possibilities can be studied via the rational fragmentation of structure–activity sections such as pharmacophores. Although only the low energy conformers were evaluated in this study, it is expected that broad analysis of the PEHSs of all fragments will significantly illustrate the trends in carvedilol. This is ideal because one can use the individual fragment PEHSs to identify specific interactions in carvedilol and then solely test these interactions in question without having to fully analyze the entire carvedilol PEHS. Such an approach is useful in deciphering the molecular basis of the anti-fibrillar action of carvedilol which may have possible uses in alleviating the progression of AD pathology.

Acknowledgements

One of the authors (IGC) wishes to thank the Ministry of Education for a Szent-Györgyi Visiting Professorship.

References

[1] J. Cheng, K. Kamiya, I. Kodama, Cardiovasc. Drug Rev. 19 (2001) 152.
[2] S. Capomolla, O. Febo, M. Gnemmi, G. Riccardi, C. Opasich, A. Carporotondi, A. Mortara, G. Pinna, F. Cobelli, Am. Heart J. 139 (2000) 596.
[3] W. Carlson, K. Oberg, J. Cardiovasc. Pharmacol. Ther. 4 (1999) 205.
[4] P.J. Oliveira, M.P. Marques, L.A.E. Batista de Carvalho, A.J.M. Moreno, Biochem. Biophys. Res. Commun. 276 (2000) 82.
[5] D.R. Howlett, A.R. George, D.E. Owen, R.V. Ward, R.E. Markwell, Biochem. J. 343 (1999) 419.
[6] J. Hardy, J. Selkoe, Science 297 (2002) 353.
[7] V.M.-Y. Lee, Neurobiol. Aging 23 (2002) 1039.
[8] D.M. Walsh, I. Klyubin, J.V. Fadeeva, W.K. Cullen, R. Anwyl, M.S. Wolfe, M.J. Rowan, D.J. Selkoe, Nature 416 (2002) 535.
[9] M.P. Lambert, A.K. Barlow, B.A. Chromy, C. Edwards, R. Freed, M. Liosatos, T.E. Morgan, I. Rozovsky, B. Trommer, K. Viola, P. Wals, C. Zhang, C.E. Finch, G.A. Krafft, W.L. Klein, Proc. Natl Acad. Sci. USA 95 (1998) 6448.
[10] D.M. Walsh, D.M. Hartley, Y. Kusumoto, Y. Fezoui, M.M. Condron, A. Lomakin, G.B. Benedek, D.J. Selkoe, D.B. Teplow, J. Biol. Chem. 274 (1999) 25945.
[11] D.-H. Chui, H. Tanahashi, K. Ozawa, S. Ikeda, F. Checler, O. Ueda, H. Suzuki, W. Araki, H. Inoue, K. Shirotani, K. Takahashi, F. Gallyas, T. Tabira, Nature Med. 5 (1999) 560.
[12] D.R.P. Almeida, L.F. Pisterzi, G.A. Chass, L.L. Torday, A. Varro, J.Gy. Papp, I.G. Csizmadia, J. Phys. Chem. A 106 (2002) 10423.
[13] D.R.P. Almeida, D.M. Gasparro, L.F. Pisterzi, L. Torday, A. Varro, J.Gy. Papp, B. Penke, I.G. Csizmadia, J. Phys. Chem. A107 (2003) 5594.
[14] D.R.P. Almeida, D.M. Gasparro, L.F. Pisterzi, L.L. Torday, A. Varro, J.Gy. Papp, B. Penke, J. Mol. Struct. (Theochem) 631 (2003) 251.
[15] D.R.P. Almeida, D.M. Gasparro, L.F. Pisterzi, J.R. Juhasz, F. Fülöp, I.G. Csizmadia, J. Mol. Struct. (Theochem) (2003) in press.
[16] M.J. Frisch, G.W. Trucks, H.B. Schlegel, G.E. Scuseria, M.A. Robb, J.R. Cheeseman, V.G. Zakrzewski, J.A. Montgomery

Jr., R.E. Stratmann, J.C. Burant, S. Dapprich, J.M. Millam, A.D. Daniels, K.N. Kudin, M.C. Strain, O. Farkas, J. Tomasi, V. Barone, M. Cossi, R. Cammi, B. Mennucci, C.Pomelli, C. Adamo, S. Clifford, J. Ochterski, G.A. Petersson, P.Y. Ayala, Q. Cui, K. Morokuma, D.K. Malick, A.D. Rabuck, K. Raghavachari, J.B. Foresman, J. Cioslowski, J.V. Ortiz, A.G. Baboul, B.B. Stefanov, G. Liu, A. Liashenko, P. Piskorz, I. Komaromi, R. Gomperts, R.L. Martin, D.J. Fox, T. Keith, M.A. Al-Laham, C.Y. Peng, A. Nanayakkara, C. Gonzalez, M. Challacombe, P.M.W. Gill, B.G. Johnson, W. Chen, M.W. Wong, J.L. Andres, M. Head-Gordon, E.S. Replogle, J.A. Pople, Gaussian 98 (Revision A.9), Gaussian, Inc., Pittsburgh PA, 1998.

[17] A.D. Becke, J. Chem. Phys. 98 (1993) 5648.

[18] S. Miertus, J. Tomasi, Chem. Phys. 65 (1982) 239.

[19] S. Miertus, E. Scrocco, J. Tomasi, Chem. Phys. 55 (1981) 117.

[20] M. Cossi, V. Barone, R. Cammi, J. Tomasi, Chem. Phys. Lett. 255 (1996) 327.

[21] Axum 5.0C for Windows, MathSoft Incorporated, 1996.

Pharmacophore Fragment-Based Prediction and Gas Phase *Ab Initio* Optimization of Carvedilol Conformations

David R. P. Almeida*[a,b], Donna M. Gasparro[a], Ferenc Fülöp[b], and Imre G. Csizmadia[a,c]

[a]Department of Chemistry, Lash Miller Laboratories, University of Toronto, 80 St. George Street, Toronto, Ontario, Canada M5S 3H6

[b]Institute of Pharmaceutical Chemistry, University of Szeged, 6720 Szeged, Eotvos u. 6, Hungary

[c]Department of Medicinal Chemistry, University of Szeged, Dom ter 8, 6720 Szeged, Hungary

*Corresponding author.
dalmeida@medscape.com (D.R.P. Almeida), dgasparro@medscape.com (D.M. Gasparro), fulop@pharma.szote.u-szeged.hu (F. Fülöp), icsizmad@alchemy.chem.utoronto.ca (I.G. Csizmadia).

Abstract

This current communication gives the results of a novel computational molecular method of selecting, from a vast number of possible conformations, the dominant low energy states of a large molecule by dividing it into separately analyzable structure-activity fragments. Carvedilol is a cardiovascular drug of proven efficacy with multiple molecular targets: it acts as a non-selective β-adrenoceptor (β_1 and β_2) and selective α_1-adrenoceptor antagonist, antioxidant able to reduce reactive oxygen species (ROS)-mediated oxidative stress, beneficial modulator of cardiac electrophysiological properties (K^+ and Ca^{2+} ion channels), multi-faceted cardioprotector, and novel anti-fibrillar agent able to inhibit amyloid-beta (Aβ) fibril formation. Given carvedilol's varied pharmacodynamic profiles, and the fact that a thorough analysis of its potential energy hypersurface (PEHS) has not yet been performed, an original molecular fragmentation method was developed to reveal carvedilol's low energy states in order to divulge their relevance to its biological activity. Multi dimensional conformational analysis (MDCA) leads to a total of 177 147 (3^{11}) conformational possibilities whereas fragmentation studies predict 240 gas phase conformations. Structural predictions were tested on protonated *R*-carvedilol with gas phase molecular orbital (MO) computations of PEHS minima at the restricted Hartree-Fock (RHF), RHF/3-21G, level of theory using the Gaussian 98 software program. Computation of the 240 predicted (input) carvedilol conformations revealed 121 converged (i.e., fully optimized) structures, of which nine possessed a conformer relative energy of less than four Kcal•mol^{-1}. Seven of these nine conformers possess a unique "tetra-centric" (four-centred) spiro-type structure composed of two rings (six- and eight-membered) enclosed by two O···H-N hydrogen bonds (H-bonds) that are connected *via*

the protonated nitrogen atom in the side-chain of carvedilol; this conformation is largely determined by the carbazole-containing pharmacophore (Fragment A) of carvedilol. With regards to the utility of the rational molecular fragmentation method employed to predict and optimize the carvedilol structures, it is determined that eight of the 11 torsional angles were accurately predicted (72.7%) according to torsional angle conformation distribution. The strength of this fragmentation method relies on full MDCA optimization of the individual fragments which are then used to predict the carvedilol conformations. As such, the predicted inputs possess an inherent degree of energy minimization, and thus, are able to provide a better hypothesis of relevant sections of the carvedilol surface versus random sampling of the PEHS. The elucidation of carvedilol's conformational identity greatly aids the full molecular understanding of carvedilol's adrenoceptor binding structure and carvedilol's involvement, at the molecular level, in ameliorating pathological states such as oxidative stress and Alzheimer's disease.

Keywords: Molecular Fragmentation, Carvedilol, Conformation, RHF.

1. Introduction

Carvedilol, 1-(9H-Carbazol-4-yloxy)-3-[2-(2-methoxy-phenoxy)ethylamino]-2-propanol ($C_{24}H_{26}N_2O_4$), is a cardiovascular drug possessing multiple modes of action and is used in the treatment of hypertension, ischemic heart disease (IHD), and congestive heart failure (CHF).[1,2] The major molecular targets of carvedilol include: antagonist action at α_1, β_1, and β_2 membrane adrenoceptors, reduction of reactive oxygen species (ROS), and modulation of K^+ and Ca^{2+} ion channels.[1] Carvedilol provides hemodynamic benefits such as peripheral vasodilation and reduction in cardiac work from balanced non-selective β-receptor blockage (β_1 and β_2) and selective α_1-receptor blockage.[1-3] With regards to cardioprotection, carvedilol exerts anti-proliferative/anti-atherogenic, anti-hypertrophic, anti-ischemic, and anti-arrhythmic actions by means of antioxidant effects, improvement of glucose and lipid metabolism, modulation of neurohormonal factors (e.g., nitric oxides), and beneficial cardiac electrophysiological properties (reviewed in reference **1**).

Another cardioprotective effect of carvedilol resides in its ability to protect mitochondria from oxidative stress by uncoupling oxidative phosphorylation *via* a weak protonophoretic (proton transfer) mechanism involving the amino group ($pK_a = 7.9$) of its side-chain.[4] It has been proposed that carvedilol's amino group decreases the mitochondrial electric potential by the following mechanism: carvedilol binds a proton in the cytosolic leaflet of the inner mitochondrial membrane (low pH mitochondrial intermembrane space), crosses the mitochondrial membrane in the positive protonated form (driven by its high lipid solubility and mitochondria pH gradient), releases the proton in the higher pH mitochondrial matrix, and then returns to the intermembrane

space in the neutral deprotonated form; the process can then begin again (4). This phenomenon known as "mild uncoupling" occurs when a small decrease in mitochondrial electric potential induces a significant reduction in the ROS produced by the mitochondrial respiratory chain.[4-6]

It has been shown that carvedilol and its active hydroxylated analogues act as novel anti-fibrillar agents able to inhibit amyloid-beta (Aβ) fibril formation.[7] According to the amyloid cascade hypothesis of Alzheimer's disease (AD), accumulation of Aβ in extracellular senile plaques (SPs) in brain tissues drives AD pathogenesis.[8] The culprits of these processes are Aβ peptides consisting of 42 or 43 amino acids (abbreviated as Aβ1-42) which are prone to aggregation, oligomerization, and deposition in diffuse plaques and cause progressive synaptic and neuritic injury.[8-10] Recently, it has been shown that Aβ oligomers (dimers, trimers, or higher oligomers), in the absence of monomers and amyloid fibrils, are the main neurotoxic component of AD.[10-13] Given the above, as an anti-fibrillar agent, carvedilol may have uses in the prevention or slowing down of AD pathology. The effectiveness of carvedilol's inhibition of Aβ fibril formation is due to three factors: (1) a central basic amino pharmacophore, (2) two cyclic hydrophobic ring centroids, and (3) the molecular flexibility to adopt a specific three-dimensional pharmacophore conformation.[7] Although these three factors are recognized, it is currently not known if carvedilol binds to Aβ monomers, dimers, or other oligomers[7] or what type of interaction occurs between carvedilol and the Aβ peptide(s).

Given the multi-faceted nature of carvedilol, it is necessary to reveal its complete molecular identity and conformational profile as a means to fully divulge the structural properties of its adrenoceptor binding conformation and further clarify its function in

hemodynamic and cardioprotective mechanisms. Likewise, to expound carvedilol's role in antioxidant pathways, the uncoupling of oxidative phosphorylation in mitochondria, and with Aβ peptide(s) in AD, its conformational identity is requisite as conformation is a fundamental part of all of these processes. However, given carvedilol's 11 associated torsional angles and 177 147 (3^{11}) conformational possibilities (each torsional angle can assume *gauche plus*, *anti*, or *gauche minus* orientations), this task is exceptionally extensive (c.f. **Figure 1**). To remedy this problem, we previously developed a method to fragment the three pharmacophores of carvedilol into three independent structure-activity molecular fragments (c.f. **Figure 2**).[14] This has been done both as a prelude to the evaluation of the entire drug molecule and to assess the success of such a methodological approach, i.e., rational molecular fragmentation of structure-activity regions, such as pharmacophores, as a means to study large complex molecular systems in great detail.

Earlier we investigated all three fragments exhaustively[14-17], analyzed the chiral properties of carvedilol[17], and optimized several hydrogen bond (H-bond) intramolecular attractive forces (IMAFs) present in the carvedilol molecule[18]. In this study, the development of this methodology is continued by using the previous results from the individual fragments to predict and subsequently optimize a comprehensive list of possible carvedilol conformations based on low energy fragment conformations. This is done so as to determine the conformations of carvedilol expected to dominate a gas phase sample. Further, these results highlight a novel computational approach, entitled rational molecular fragmentation that allows selecting, from a vast number of possible conformations, the dominant low energy states of a complex molecular system by independently investigating pharmacophore fragments.

2. Methods

To allow explicit prediction and definition of conformation, a systematic numbering system has been used for all structures such that corresponding torsional angles in fragments (A, B, and C) and carvedilol are all defined in the same manner (c.f. torsional angle definitions in **Figure 1**). Further, conformational structural assignments for the conformational minima of a respective potential energy hypersurface (PEHS) are made according to **equation 1**.

gauche plus (*g*+)	= 60. (ideal) ± 60°	**EQUATION 1**
anti (*a*)	= 180. (ideal) ± 60°	
gauche minus (*g*-)	= -60. (ideal) ± 60°	

Carvedilol is composed of three distinct pharmacophores (c.f. **Figure 1** and **2**) and was thus divided into three molecular fragments which were studied *via* multi dimensional conformational analysis (MDCA): *R*- and *S*-4-(2-hydroxypropoxy)carbazol (Fragment A) possesses the carbazole ring responsible for the direct antioxidant effects of carvedilol[14,17], 2(*R* and *S*)-1-(ethylamonium)propane-2-ol (Fragment B) contains the protonophoretic amino group involved in the cardioprotective uncoupling of mitochondrial oxidative phosphorylation[15], and aminoethoxy-2-methoxy-benzene (Fragment C) is the α_1-adrenergic antagonist pharmacophore of carvedilol[16]. The chiral parameters and interactions of Fragment A and carvedilol have also been described.[17]

The major H-bond IMAF of carvedilol has been shown to be an O1···H42-O41···H57 hydrogen bond motif initially found in Fragment A and B along with a bifurcated intramolecular hydrogen bond, O29···H46···O36 (H46 is an amine hydrogen), originally found in Fragment C (c.f. reference **18** for specific structural information).

Although some IMAF of carvedilol have been evaluated[18], this latter study addressed only on a few conformations of carvedilol while the current study analyzes a novel comprehensive list of possible carvedilol conformers not previously found in the literature. This comprehensive list is based on the MDCA results from the individual fragments as an attempt to arrive at the set of carvedilol's low energy gas phase conformations.

To ensure that all fragments correspond stereochemically with each other (i.e., torsional angle χ_{10} has the same orientation in all structures), only the B3LYP/6-31G(d) results of the *R*-Fragment A PEHS (from reference **17**), RHF/3-21G results of the *S*-Fragment B PEHS (from reference **15**), and RHF/3-21G results of the Fragment C PEHS (from reference **16**) were used (c.f. **Figure 2**). The selection criteria employed utilizes all fragment geometries with a conformer relative energy $\leq$ 2.00 Kcal•mol^{-1} from the individual PEHSs (c.f. **Table 1**) as an attempt to predict only significantly populated, low energy conformers of carvedilol. Continuing, the predictions were made for conformations of *R*-carvedilol only (c.f. **Figure 1**). The PEHS conformers of carvedilol can be described by **equation 2**.

$$E = f(\chi_1, \chi_2, \chi_3, \chi_4, \chi_5, \chi_6, \chi_7, \chi_8, \chi_9, \chi_{10}, \chi_{11}) \qquad \textbf{EQUATION 2}$$

The conformations of the low energy converged fragment structures found in **Table 1** were combined to create a maximum total of 240 distinct, non-redundant *R*-carvedilol conformations (c.f. **Table S1**; note that **Table S1** also displays the output optimized torsional angle conformation if a structure successfully converged and may not be the same as the input conformation). The only incidence of overlapping, non-

symmetrical torsional angles between the three fragments was torsional angle χ_{10} in Fragments A and B (c.f. **Table 1**); however, Fragments A and B only differed in their χ_{10} orientation in one conformation. Consequently, carvedilol predictions all possessed torsional angle χ_{10} in the *g*+ position except for those combinations involving Fragment A conformation *aag-g-* (with regards to torsional angles χ_1, χ_2, χ_3, and χ_{10}, respectively) which has resulting conformational predictions with torsional angle χ_{10} in the both the *g*+ and *g*- positions (c.f. **Table S1**). The total conformational combinations for *R*-carvedilol with torsional angle χ_{10} in the *g*+ and *g*- position are displayed in **equations 3** and **4**, respectively. Thus, the total predicted number of unique carvedilol conformations based on the Fragment A, B, and C low energy conformers in **Table 1** is 240 as summed by: **equation 3** ($\chi_{10} = g+$) + **equation 4** ($\chi_{10} = g-$) = 192 ($\chi_{10} = g+$) + 48 ($\chi_{10} = g-$) = 240 (c.f. **Table S1**). Finally, it should be noted that the six Fragment C conformations are not unique but rather are axis chiral pairs (see reference **17** for explanation) but were all included in this study for completeness.

(4 Fragment A conformations) x (8 Fragment B conformations) x (6 Fragment C conformations) = 192 *R*-carvedilol unique conformations **EQUATION 3**
(All possess torsional angle χ_{10} in the *g*+ position.)

(1 Fragment A conformation) x (8 Fragment B conformations) x (6 Fragment C conformations) = 48 *R*-carvedilol unique conformations **EQUATION 4**
(All possess torsional angle χ_{10} in the *g*- position.)

The conformational predictions for *R*-carvedilol in **Table S1** were tested with molecular orbital (MO) optimization of the PEHS conformational minima. Full geometry optimizations were performed in the gas phase ($\varepsilon = 0.0$) on *R*-carvedilol at the restricted Hartree-Fock, RHF/3-21G, level of theory. All calculations were carried out using the

Gaussian 98 (G98) software program and *R*-carvedilol was fully structurally defined using the G98 Cartesian and z-matrix internal coordinate system to specify molecular structure, stereochemistry, and geometry.[19] Graphical data was plotted using Axum 5.0.[20]

3. Results and Discussion

3.1 Review of Converged Carvedilol Conformations

All 240 carvedilol input (i.e., predicted) structures (conformations C-*R*-1 to C-*R*-240 found in **Table S1**) were optimized at the RHF/3-21G level of theory. Consequently, this optimization process revealed a total of 121 unique carvedilol conformations with a range in relative conformer energy of ~23 Kcal•mol^{-1} (c.f. **Table S2**). However, not all of the 121 converged conformations were predicted from the fragment analysis; 35 novel conformations were revealed by optimization (indicated as conformations C-*R*-241 to C-*R*-275 in **Table S1** and **S2**). Thus, there was a convergence of 44% (121/275) for all carvedilol conformers evaluated. The input and optimized conformation of all carvedilol structures is found in **Table S1** while all explicit optimized values and energies, as well as tabulations of conformers that moved to different parts of the PEHS and annihilated conformers, are displayed in **Table S2**.

As previously discussed in the literature[4,7,14-18], and now shown for the first time in **Table S2**, the carvedilol PEHS possesses large and dramatic conformational flexibility. Carvedilol conformations converged at various points on the PEHS and numerous structures were able to move to both nearby and distant conformations from starting input orientations that did not converge. Although it was common for groups of structures with similar conformations to converge (c.f. conformers C-*R*-55 to C-*R*-59, C-*R*-117[a] to C-*R*-119, C-*R*-193 to C-*R*-204 in **Table S2**) it was also frequently found that single conformations converged among parts of the PEHS that were scarcely populated and filled with large numbers of annihilated structures (c.f. C-*R*-106, C-*R*-156, C-*R*-171, C-*R*-184 in **Table S2**).

3.2 Structural Analysis of Carvedilol Low Energy Conformers

In order to arrive at a set of low energy conformers for the carvedilol PEHS, all converged conformations were plotted according to their respective relative energy (c.f. **Figure 3**). The plot illustrates the inherent flexibility of the carvedilol molecule as converged conformations are dispersed over a large range of relative energies. However, there is a definitive set of nine low energy conformations in the bottom right-hand corner of **Figure 3**; these conformations are bounded by a conformer relative energy of less than four Kcal•mol^{-1} and are clearly divided from the rest of the converged structures. These nine conformations are: C-*R*-246 to C-*R*-251, C-*R*-258, C-*R*-272, and C-*R*-273 (c.f. molecular structures in **Figure 4** and optimized parameters in **Table 2**).

Close scrutiny of the low energy conformations reveals a surprising finding that seven (C-*R*-246 to C-*R*-250, C-*R*-258, and C-*R*-272) of the nine conformations possess a distinctive common structural motif. These seven carvedilol structure are dominated by a "tetra-centric" (i.e., four-centred) conformation (c.f. **Figure 5**). The tetra-centric conformation is flanked on one side ("left side" of carvedilol) by the 13-membered aromatic carbazole ring (centre 1) which is connected to a six-membered ring closed *via* an intramolecular O···H-N H-bond between the carbazole ether oxygen and a proton of the positive nitrogen atom of carvedilol (ring **a**; centre 2). The same protonated secondary nitrogen atom forms an eight-membered ring (ring **b**; centre 3) through another intramolecular O···H-N H-bond to the methoxy oxygen of carvedilol. The "right side" of the carvedilol conformation is flanked by the di-substituted benzene ring (centre 4) which also forms part of ring **b**. Rings **a** and **b** are formed *via* short, strong H-bonds that are in

all cases less than two Angstroms. Conformations C-*R*-251 and C-*R*-273 do not form any IMAF with the methoxy oxygen, O36, and thus, do not form ring **b**.

The most striking feature of this tetra-centric conformation is the necessary protonated secondary nitrogen in the side-chain of carvedilol. This positive nitrogen centre is required for the concomitant formation of the two essential O···H-N H-bonds because it would not be possible to form these two H-bonds, and subsequently rings **a** and **b**, with a bifurcated H-bond involving only one amine proton. Moreover, the argument can be extended in that an electron-deficient nitrogen atom will be optimally stabilized by the formation of rings **a** and **b** because this will allow better electron induction to the nitrogen centre.

As far as we know, such a carvedilol conformation as shown in **Figure 5** has not previously been presented or discussed in the literature. It has in the past been postulated that internal H-bonding between the ether carbazole oxygen, amine centre, and catechol oxygen atoms are dominant, but non-specific, IMAF of carvedilol.[4,7] We have earlier shown such conformations do exist and the most significant intramolecular H-bond network is an O1···H42-O41···H57 double H-bond (left side) along with a bifurcated O29···H46···O36 H-bond (right side).[18] Therefore, this communication is the first instance of a specific carvedilol conformation that contains no such H-bond network present because H42 does not H-bond with any other atoms in the tetra-centric structure (c.f. **Figure 4** and **5**).

The torsional angle orientations basic for carvedilol to assume this tetra-centric conformation are shown in **equation 5** (forward slash "/" indicates "or"). Although the carvedilol PEHS is one of large conformational flexibility, this tetra-centric conformation

possess uncanny rigidity in that five (χ_1, χ_2, χ_3, χ_4, and χ_{10}) of the 11 torsional angles only assume one orientation. Since all five of these rigid torsional angles belong to Fragment A, it can thus be stated that it is the carbazole-containing pharmacophore that characterizes this prevalent and extremely stable conformation.

$$\chi_1 = g+ \quad \chi_6 = g+/a/g- \qquad \textbf{EQUATION 5}$$

$$\chi_2 = a \quad \chi_7 = g+/g-$$

$$\chi_3 = g- \quad \chi_8 = g+/a/g-$$

$$\chi_4 = g+ \quad \chi_9 = g+/g-$$

$$\chi_5 = g+/a \quad \chi_{10} = g+$$

$$\chi_{11} = g+/a/g-$$

Upon closer investigation of the molecular structures in **Figure 4**, aside from the tetra-centric motif, converged conformations possessing further intramolecular H-bond networks are found, albeit these are composed of much longer H-bonds compared to those of enclosed rings **a** and **b**. Aside from differences related to the tetra-centric conformational motif, the nine low energy carvedilol structures can be divided into two groups: those with three internal H-bonds (C-*R*-246, C-*R*-247, C-*R*-249, C-*R*-251, C-*R*-258, C-*R*-272, and C-*R*-274) and those with four internal H-bonds (C-*R*-248 and C-*R*-250) (c.f. **Figure 4**).

In the case of structures with three H-bonds, C-*R*-246 forms a five-membered ring *via* a 2.44 Å O29···H-N H-bond while C-*R*-247 forms a similar five-membered ring with a 2.35 Å O29···H-N H-bond. The global minima C-*R*-249 forms a different five-membered ring with the hydroxyl oxygen (at the carvedilol stereocentre) through a 2.51 Å O41···H-N H-bond while oxygen O29 does not partake in any specific IMAF. Conformer C-*R*-251

does not possess the tetra-centric motif (lacks ring **b**) and forms a five-membered ring with a 2.15 Å O41···H-N H-bond and an additional five-membered ring *via* a 2.06 Å O29···H-N H-bond. Carvedilol structure C-*R*-258 forms a five-membered ring through a 2.49 Å O29···H-N H-bond and besides being described by the tetra-centric motif, its conformation resembles that of a "clam shell" where the two flanking aromatic centroids are separated by about 5.2 Å. C-*R*-272 forms a five-membered ring with a 2.54 Å O29···H-N H-bond. Finally, conformer C-*R*-273 does not display the tetra-centric motif; instead, it is characterized by the same two five-membered rings displayed by the only other low energy conformation to not have the tetra-centric design (C-*R*-251): a five-membered ring with a 2.01 Å O41···H-N H-bond and a five-membered ring connected by a 2.17 Å O29···H-N H-bond.

With regards to the two conformers with four internal H-bonds, C-*R*-248 and C-*R*-250, both possess the tetra-centric structure. Further, C-*R*-248 possesses a five-membered ring with a 2.50 Å O41···H-N H-bond and another five-membered ring by means of a 2.50 Å O29···H-N H-bond. Conformer C-*R*-250 is similar to the latter structure with a five-membered ring *via* a 2.32 Å O41···H-N H-bond and a five-membered ring connected by a 2.40 Å O29···H-N H-bond. All low energy conformations have double bifurcated H-bonds, although not all are the same, while conformers C-*R*-248 and C-*R*-250 assume an orientation with a triple H-bond bifurcation (the former and latter are with respect to one amine proton).

3.3 Evaluation of Pharmacophore Fragmentation as a Method to Predict and Optimize Low Energy Conformations of Carvedilol

As discussed previously in the **Introduction**, given carvedilol's varied and versatile pharmacological actions and multi-faceted pharmacodynamic and therapeutic nature, it is exceptionally relevant to bring to light carvedilol's complete molecular identity at the fundamental level of conformation. Elucidation of carvedilol's conformational identity should greatly aid further molecular understanding of carvedilol's adrenoceptor binding conformation and its amelioration in pathological states such as oxidative stress (through inhibition of ROS) and AD (as an anti-fibrillar agent). Nonetheless, given the current cost of computer processing power and the fact that carvedilol's PEHS possesses an exorbitant number of conformational possibilities (3^{11} = 177 147 conformational possibilities), traditional MDCA approaches to solving its PEHS are daunting and unfeasible. In reality, the problem of solving carvedilol's PEHS is analogous to the difficulties encountered in deciphering complete conformational profiles for any medium- to large-sized molecular system such as drug molecules and proteins with large degrees of freedom.

The current authors have sought to circumvent the problem of solving carvedilol's conformations by creating a method in which carvedilol was divided into three molecular fragments, according to pharmacophore structure-activity, and each fragment optimized with MDCA (c.f. **Figure 1** and **2**). The results from previous studies were used here to predict possible conformations of carvedilol based on the idea that, since only low energy fragment conformations would be used, these would ultimately lead to the discovery and optimization of low energy conformations for the whole carvedilol molecule. After having performed the aforementioned tasks, it is vital to evaluate the success of this novel

approach; this evaluation addresses both the accuracy and overall usefulness (i.e., utility and expediency) of this method.

Superficially, given that all nine low energy conformations (c.f. **Table 2**) are described by conformational assignments not predicted by the individual fragment analysis, it would seem that such a method was not able to accurately predict the low energy conformations of carvedilol. All low energy conformations for carvedilol comprise a *g*+ orientation for torsional angle χ_1 while no Fragment A low energy structure ($\leq$ two Kcal•mol^{-1}) had this orientation. Instead, Fragment A conformers with χ_1 = g+ possessed conformer relative energies of 2.26, 5.11, and 6.34 Kcal•mol^{-1} (c.f. reference **17**). Since the lowest energy of these conformers was greater than the two Kilocalorie threshold applied, it was not included as a low energy fragment structure, and thus, not utilized to predict carvedilol conformations. However, this in itself does not invalidate the accuracy of this methodology as a distinct set of low energy conformers were ultimately discovered and optimized. Due to this issue, it is necessary to look closer at the predicted conformations generated and the low energy structures discovered.

In order to compare the predictions and eventual optimized results in depth, the conformation distribution for each torsional angle for the optimized results (taken from **Table 2**) and the initial predicted conformation (taken from **Table 1**) must be noted (c.f. **Table 3**). Upon inspection and comparison, we see that the conformation distribution of eight (χ_2, χ_5, χ_6, χ_7, χ_8, χ_9, χ_{10}, and χ_{11}) of the 11 torsional angles were accurately predicted (72.7%). Given this assessment, one can deem the accuracy of this method as satisfactory. The reason that all nine of the low energy conformations were not present in our predictions had to do with our inability to predict the conformation of torsional angles

χ_1, χ_3, and χ_4 which were essentially localized in one torsional angle orientation for all low energy conformations; the latter allows the formation of the tetra-centric structural motif. It is postulated that the inability to predict these torsional angles arises from the fact that Fragment A only had a terminal methyl group for χ_4, and therefore, the complexity of this section of the carvedilol structure could not be fully described. Even so, the accuracy of this method is satisfactory as the inability to predict some conformation distributions was compensated by a high degree of prediction in other torsional angles such as χ_2, χ_5, χ_7, χ_9, and χ_{10} (c.f. **Table 3**). The final result is that this method of evaluation allowed us to not only find a defined set of low energy carvedilol conformers upon optimization of predicted inputs, but also to reveal a novel structural motif.

With regards to utility and expediency, it is clear that the current fragmentation method has greatly aided the problem of deciphering the low energy conformations of carvedilol. This is to say, the robustness of this methodological approach allowed us to take an exhaustive PEHS and convert it into a series of smaller, well-defined, and more manageable conformational surfaces, while retaining some major properties of the whole system in each fragment. Although such a method has obvious shortcomings, it is able to achieve its overall objectives and goals.

As theoretical and computational methods move progressively into the realm of larger molecular systems, certain workers have emphasized the need for studies to find ever-evolving methods, rather than relying on brute computing force, to effectively evaluate every possible conformation of such complicated systems.[21] These methods will likely rely on the ability to sample parts of a PEHS as a means to arrive at the

significantly populated conformations; in other words, the challenge of sampling conformations is to ensure that one is able to ultimately consider the most populated and significant states because, according to basic thermodynamics, only low energy states will be significantly occupied.[21] It has been previously postulated that, the success of such novel methodological approaches to finding the dominant conformations of large PEHSs *via* sampling, will depend on the ability of these methods to generate starting points (on parts of a PEHS) with some amount of energy minimization.[21] This will allow investigators to efficiently realize which parts of a PEHS they should focus on.

The fragmentation methodology used in this study achieves the goal described above because the carvedilol map is not sampled randomly in an attempt to discover highly populated, low energy states. Rather, the carvedilol fragments are optimized to generate inputs (i.e., from low energy optimized fragment conformations) with an inherent amount of energy minimization/optimization. This methodological standpoint greatly simplifies sampling a large PEHS like that of carvedilol's because it is oriented to hypothesized low energy conformers.

4. Conclusions

In the current study, a set of gas phase low energy carvedilol conformations have been evaluated and presented; 240 carvedilol conformers were initially optimized revealing 121 converged structures. Employing a rational molecular fragmentation method, nine converged low energy conformations were discovered, of which seven possessed a unique "tetra-centric" (four-centred) conformational motif not previously encountered in the literature. Further evaluation of these conformations, by means of optimizations and structural analysis at high level, electron-correlated model chemistries, is currently being carried out. Furthermore, optimization of these nine low energy conformers in the solvent phase, and not merely single point energy (SPE) calculations, will greatly benefit the characterization of the magnitude of a solvent effect on these carvedilol conformations. With respect to further evaluation of the molecular fragmentation method used here, experimental analysis of carvedilol conformations, such as with nuclear magnetic resonance (NMR) spectroscopy, would allow full comparison between the theoretically- and experimentally-determined carvedilol structures. Together, this will lead to the solution of the dominant conformations of carvedilol expected to dominate gas and solvent phase samples, which in turn, will further expound carvedilol's molecular profile and pharmacodynamic attributes.

Acknowledgements

One of the authors (IGC) wishes to thank the Hungarian Ministry of Education for a Szent-Györgyi Visiting Professorship.

References

1. Cheng, J.; Kamiya, K.; Kodama, I. *Cardiovasc. Drug Rev.* **2001**, *19*, 152.

2. Carlson, W.; Oberg, K. *J. Cardiovasc. Pharmacol. Ther.* **1999**, *4*, 205.

3. Capomolla, S.; Febo, O.; Gnemmi, M.; Riccardi, G.; Opasich, C.; Carporotondi, A.; Mortara, A.; Pinna, G.; Cobelli, F. *Am. Heart J.* **2000**, *139*, 596.

4. Oliveira, P.J; Marques, M.P.; Batista de Carvalho, L.A.E.; Moreno, A.J.M. *Biochem. Biophys. Res. Commun.* **2000**, *276*, 82.

5. Tzagoloff, A. **1982**. *Mitochondria*, Plenum Press, New York.

6. Korshunov, S.S.; Skulachev, V.P.; Starkov, A.A. *FEBS Lett.* **1997**, *416*, 15.

7. Howlett, D.R.; George, A.R.; Owen, D.E.; Ward, R.V.; Markwell, R.E. *Biochem. J.* **1999**, *343*, 419.

8. Hardy, J.; Selkoe, J. *Science* **2002**, *297*, 353.

9. Lee, V.M.-Y. *Neurobiol. Aging* **2002**, *23*, 1039.

10. Walsh, D.M.; Klyubin, I.; Fadeeva, J.V.; Cullen, W.K.; Anwyl, R.; Wolfe, M.S.; Rowan, M.J.; Selkoe, D.J. *Nature* **2002**, *416*, 535.

11. Lambert, M.P.; Barlow, A.K.; Chromy, B.A.; Edwards, C.; Freed, R.; Liosatos, M.; Morgan, T.E.; Rozovsky, I.; Trommer, B.; Viola, K.L; Wals, P.; Zhang, C.; Finch, C.E.; Krafft, G.A.; Klein, W.L. *Proc. Natl. Acad. Sci. USA* **1998**, *95*, 6448.

12. Walsh, D.M.; Hartley, D.M.; Kusumoto, Y.; Fezoui, Y.; Condron, M.M.; Lomakin, A.; Benedek, G.B.; Selkoe, D.J.; Teplow, D.B. *J. Biol. Chem.* **1999**, *274*, 25945.

13. Chui, D.-H.; Tanahashi, H.; Ozawa, K.; Ikeda, S.; Checler, F.; Ueda, O.; Suzuki, H.; Araki, W.; Inoue, H.; Shirotani, K.; Takahashi, K.; Gallyas, F.; Tabira, T. *Nature Med.* **1999**, *5*, 560.

14. Almeida, D.R.P.; Pisterzi, L.F.; Chass, G.A.; Torday, L.L.; Varro, A.; Papp, J.Gy.; Csizmadia, I.G. *J. Physical Chem. A* **2002**, *106*, 10423.

15. Almeida, D.R.P.; Gasparro, D.M.; Pisterzi, L.F.; Torday, L.L.; Varro, A.; Papp, J.Gy.; Penke, B. *J. Mol. Str.* (THEOCHEM) **2003**, *631*, 251.

16. Almeida, D.R.P.; Gasparro, D.M.; Pisterzi, L.F.; Juhasz, J.R.; Fülöp, F.; Csizmadia, I.G. *J. Mol. Str.* (THEOCHEM) **2003**, *666-667*, 557.

17. Almeida, D.R.P.; Gasparro, D.M.; Pisterzi, L.F.; Torday, L.L.; Varro, A.; Papp, J.Gy.; Penke, B.; Csizmadia, I.G. *J. Physical Chem. A* **2003**, *107*, 5594.

18. Almeida, D.R.P.; Gasparro, D.M.; Pisterzi, L.F.; Juhasz, J.R.; Fülöp, F.; Csizmadia, I.G. *J. Mol. Str.* (THEOCHEM) **2003**, *666-667*, 537.

19. Gaussian 98 (Revision A.9), M. J. Frisch, G. W. Trucks, H. B. Schlegel, G. E. Scuseria, M. A. Robb, J. R. Cheeseman, V. G. Zakrzewski, J. A. Montgomery, Jr., R. E. Stratmann, J. C. Burant, S. Dapprich, J. M. Millam, A. D. Daniels, K. N. Kudin, M. C. Strain, O. Farkas, J. Tomasi, V. Barone, M. Cossi, R. Cammi, B. Mennucci, C.Pomelli, C. Adamo, S. Clifford, J. Ochterski, G. A. Petersson, P. Y. Ayala, Q. Cui, K. Morokuma, D. K. Malick, A. D. Rabuck, K. Raghavachari, J. B. Foresman, J. Cioslowski, J. V. Ortiz, A. G. Baboul, B. B. Stefanov, G. Liu, A. Liashenko, P. Piskorz, I. Komaromi, R. Gomperts, R. L. Martin, D. J. Fox, T. Keith, M. A. Al-Laham, C. Y. Peng, A. Nanayakkara, C. Gonzalez, M. Challacombe, P. M. W. Gill, B. G. Johnson, W. Chen, M. W. Wong, J. L. Andres, M. Head-Gordon, E. S. Replogle and J. A. Pople, Gaussian, Inc., Pittsburgh PA, 1998.

20. Axum 5.0C for Windows, MathSoft Incorporated, 1996.

21. Billings, E. Molecular Modeling and Drug Design. In *Foye's Principles of Medicinal Chemistry*, 5th ed.; Williams, D.A., Lemke, T.L., Eds.; Lippincott Williams & Wilkins: New York, 2002; pp 68-85.

Figure Captions

Figure 1: Molecular structure and pharmacophore structure-activity of N-protonated *R*-carvedilol and all torsional angle definitions used in the current study (numbers placed beside atoms were used to define all torsional angles for *R*-carvedilol in the z-matrix input for Gaussian 98).

Figure 2: Carvedilol was divided into three molecular fragments based on pharmacophore structure-activity: *R*- and *S*-4-(2-hydroxypropoxy)carbazol (Fragment A)[14,17], 2(*R* and *S*)-1-(ethylamonium)propane-2-ol (Fragment B)[15], and aminoethoxy-2-methoxy-benzene (Fragment C)[16]. The results of *R*-Fragment A, *S*-Fragment B, and Fragment C (c.f. **Table 1**) were used in this study to predict a comprehensive list of possible low energy conformations for N-protonated carvedilol (*R*-configuration) (c.f. **Table S1**). Predicted conformations were then subject to geometry optimization at the RHF/3-21G level of theory (c.f. **Table S2**).

Figure 3: Conformer relative energies for all carvedilol structures optimized in the current study. The plot identifies a group of nine low energy conformations in the bottom right-hand corner bounded by a relative conformer energy of less than four Kcal•mol^{-1} (c.f. **Table 2** and **Figure 4** for the respective optimized parameters and structures of these low energy conformers).

Figure 4: Molecular structures of the nine low energy protonated carvedilol conformers revealed in the current study. Structures were fully optimized at the RHF/3-21G level of theory (relative energy for each structure is denoted in brackets; c.f. **Table 2** for optimized parameters).

Figure 5: Schematic representation of the "tetra-centric" conformational motif exhibited by seven (C-*R*-246 to C-*R*-250, C-*R*-258, and C-*R*-272) of the nine carvedilol low energy conformations (c.f. **Figure 4**). This structural motif consists of a six-membered ring (ring **a**) bonded to the terminal carbazole centroid (left side of carvedilol) and an eight-membered ring (ring **b**) bonded to the terminal substituted benzene (right side of carvedilol); the rings are connected to each other *via* the protonated secondary nitrogen of carvedilol. The two intramolecular rings are formed by means of two (one in each ring) O···H-N hydrogen bonds (H-bonds) which in all cases are short H-bonds less than two Angstroms (Å) in distance. For carvedilol to form this structural motif, the following conformation is required: $\chi_1 = g+$, $\chi_2 = a$, $\chi_3 = g-$, $\chi_4 = g+$, $\chi_5 = g+/a$, $\chi_6 = g+/a/g-$, $\chi_7 = g+/g-$, $\chi_8 = g+/a/g-$, $\chi_9 = g+/g-$, $\chi_{10} = g+$, and $\chi_{11} = g+/a/g-$.

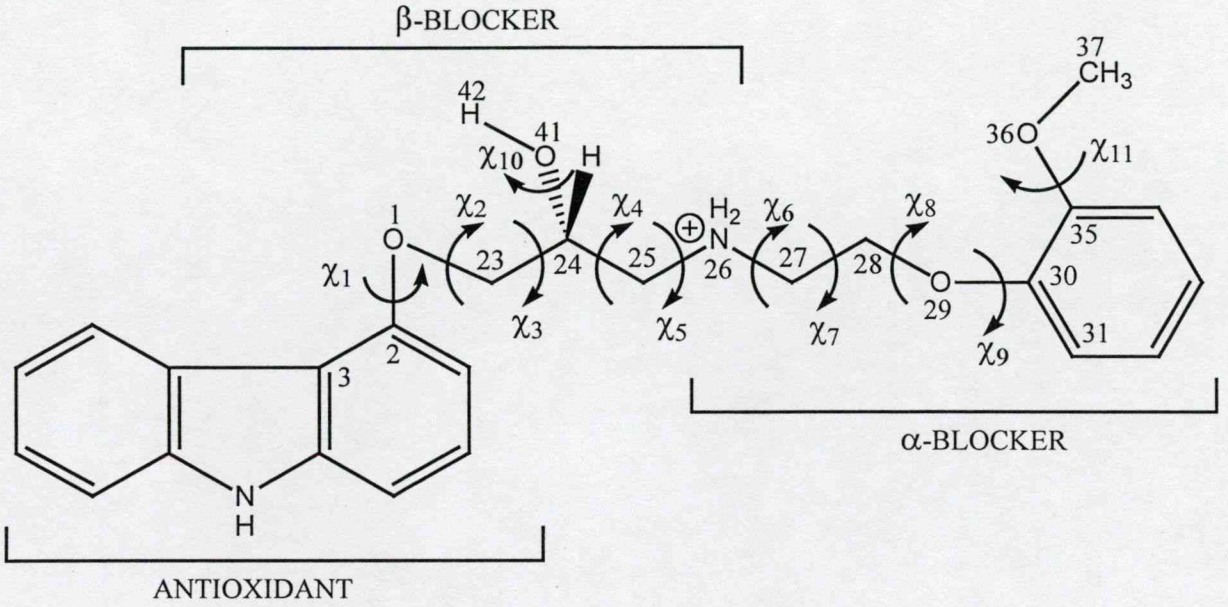

χ_1 = C23, O1, C2, C3

χ_2 = C24, C23, O1, C2

χ_3 = C25, C24, C23, O1

χ_4 = N26, C25, C24, C23

χ_5 = C27, N26, C25, C24

χ_6 = C28, C27, N26, C25

χ_7 = O29, C28, C27, N26

χ_8 = C30, O29, C28, C27

χ_9 = C31, C30, O29, C28

χ_{10} = H42, O41, C24, C23

χ_{11} = C37, O36, C35, C30

Figure 1

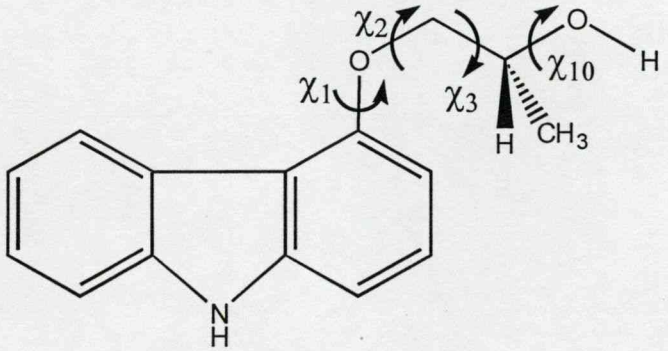

Fragment A

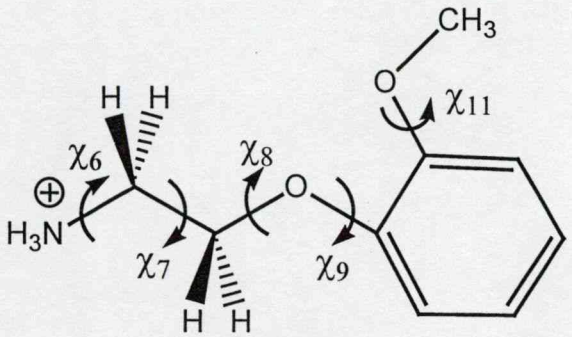

Fragment C

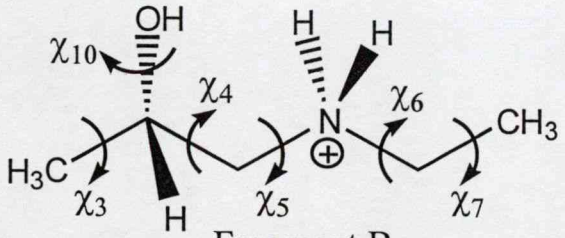

Fragment B

Figure 2

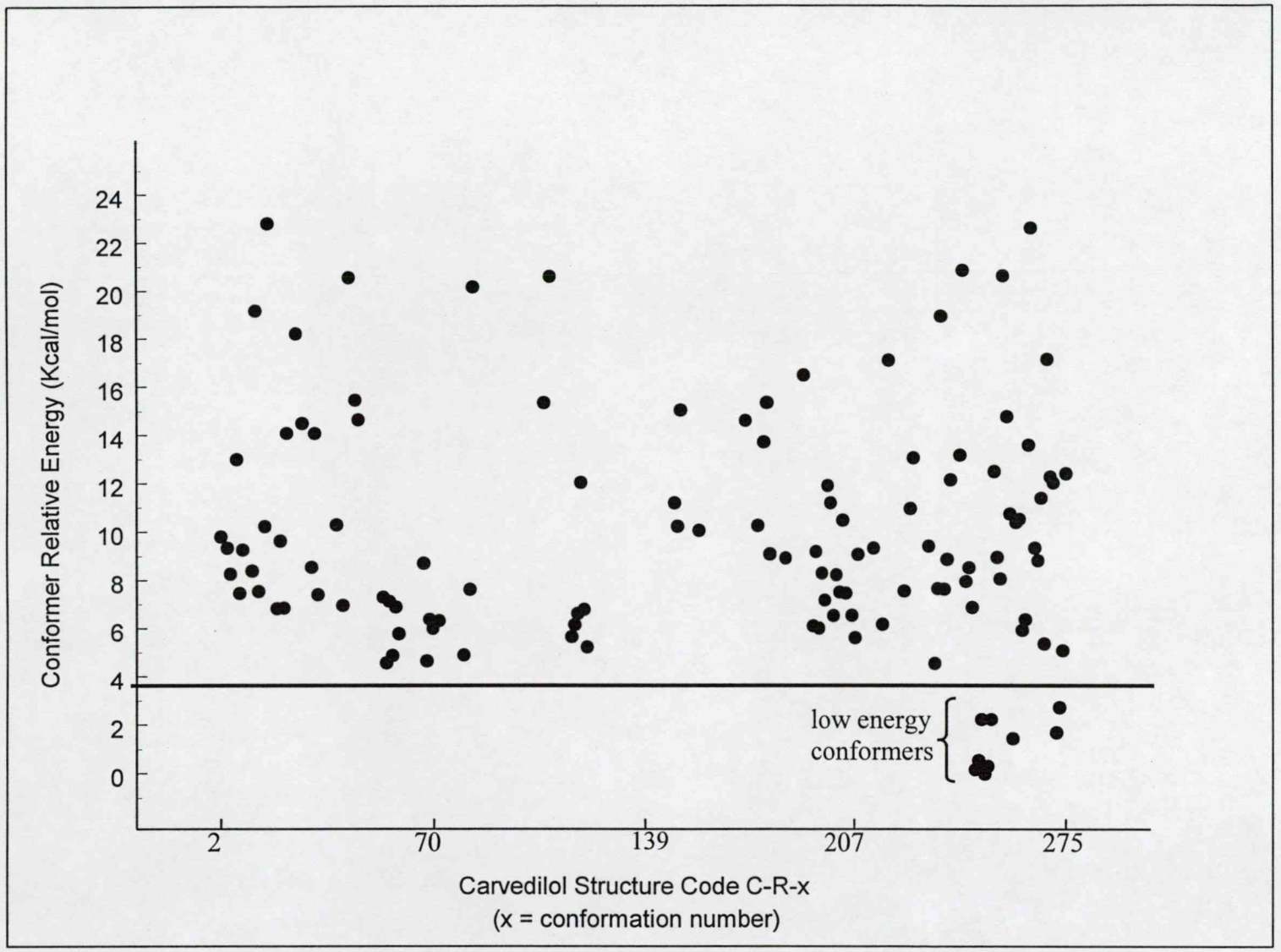
Conformer Relative Energy (Kcal/mol)
24
22
20
18
16
14
12
10
8
6
4
2
0
low energy
conformers
2
70
139
207
275
Carvedilol Structure Code C-R-x
(x = conformation number)

Figure 3

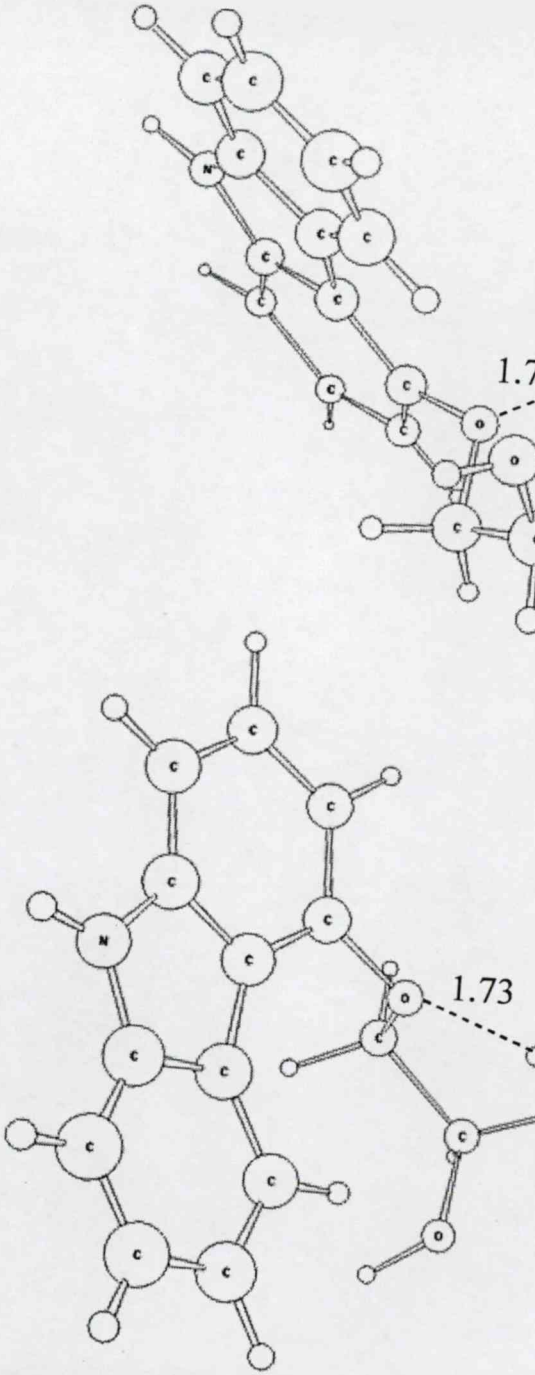
1.7
1.73

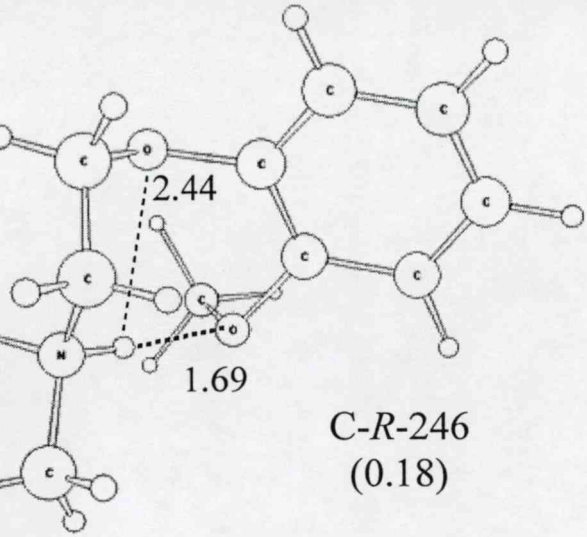

C-*R*-246
(0.18)

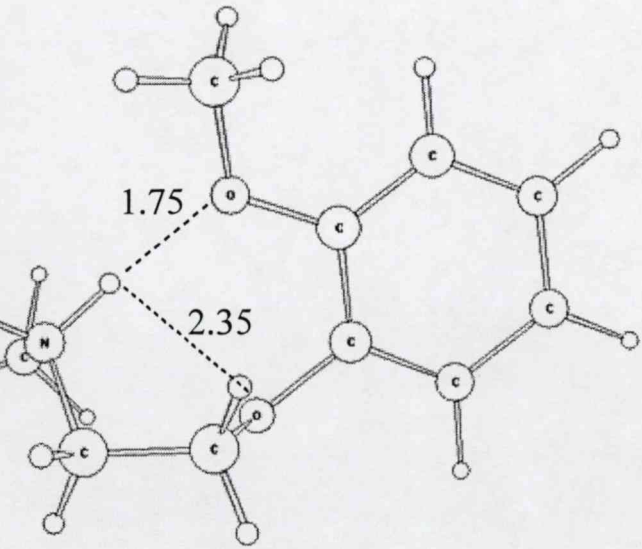

C-*R*-247
(0.54)

Figure 4

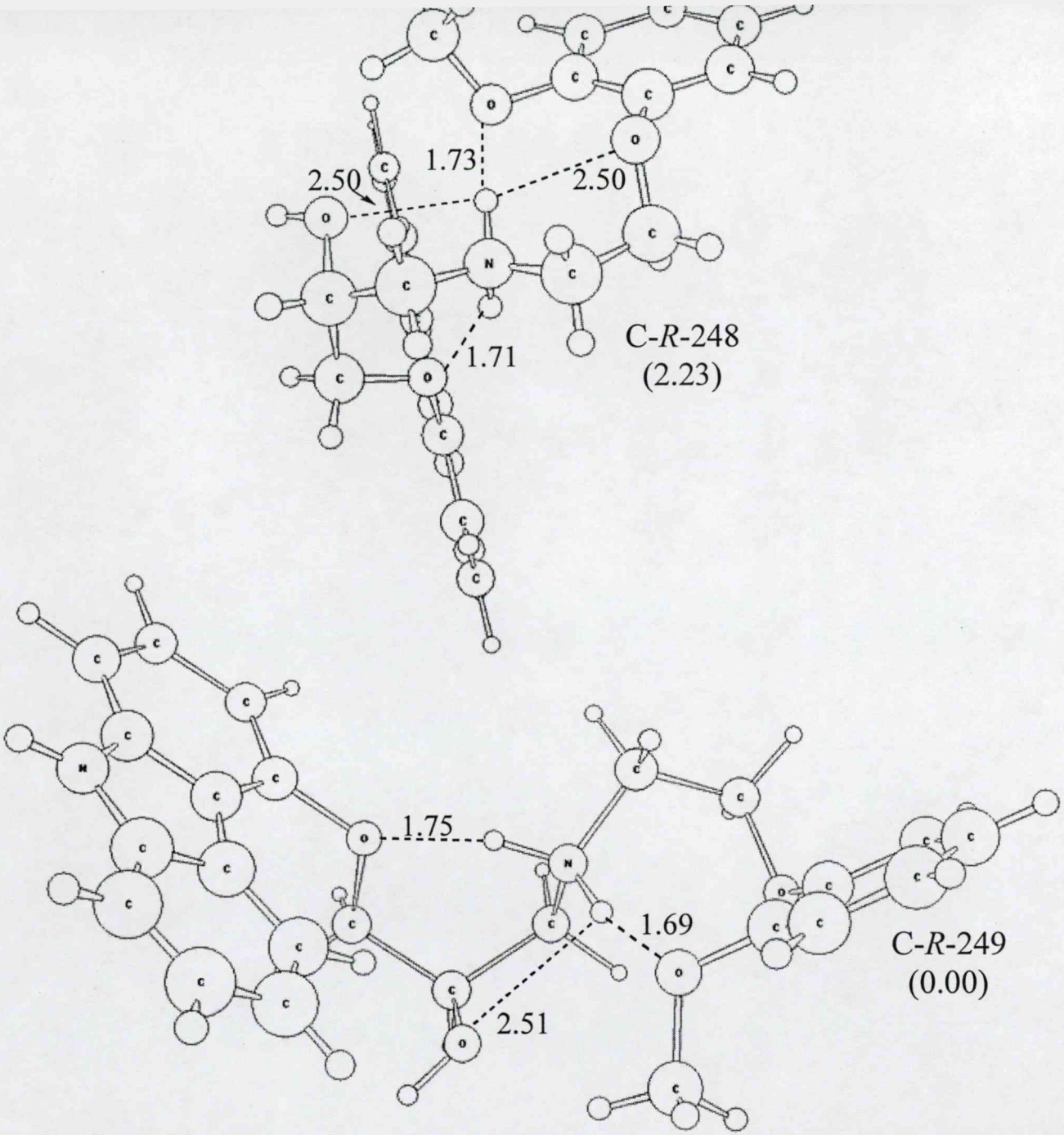

Figure 4
continued

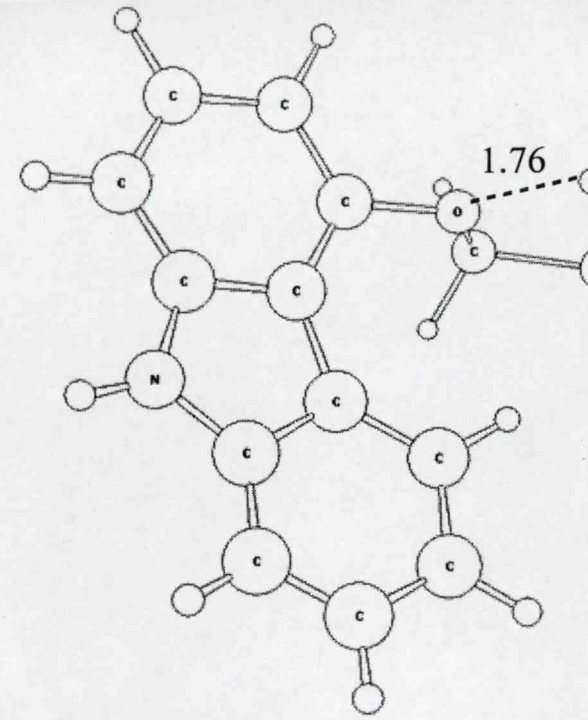
1.76
C
O
N

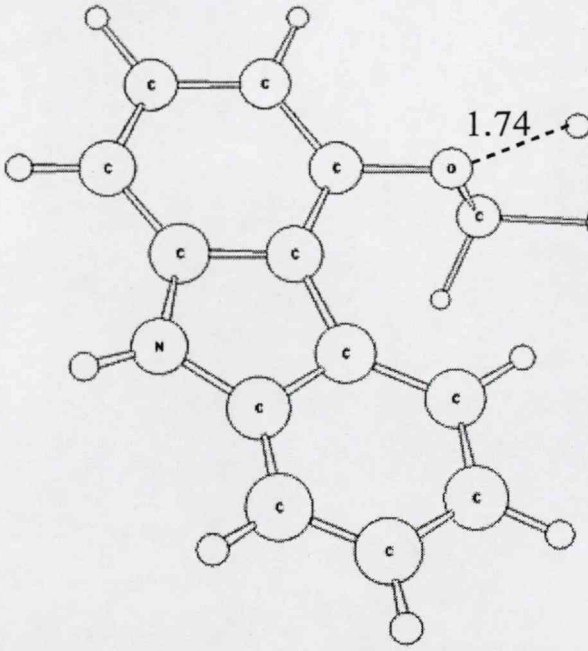
1.74
C
O
N

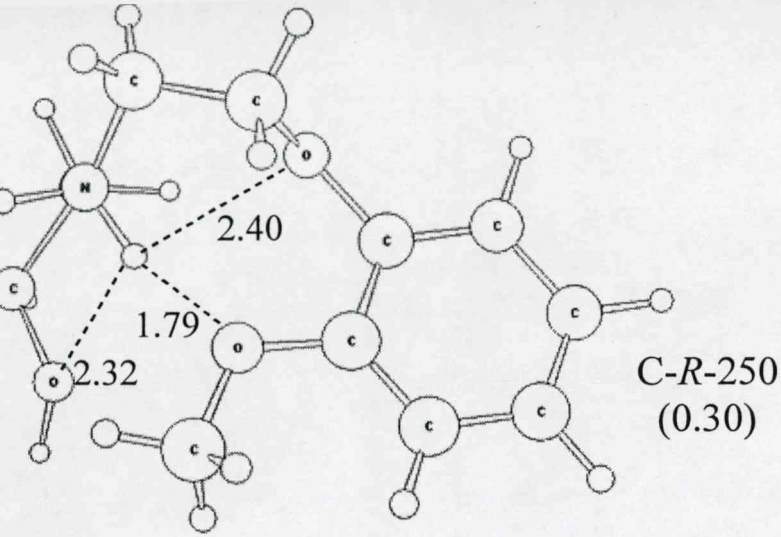

C-*R*-250
(0.30)

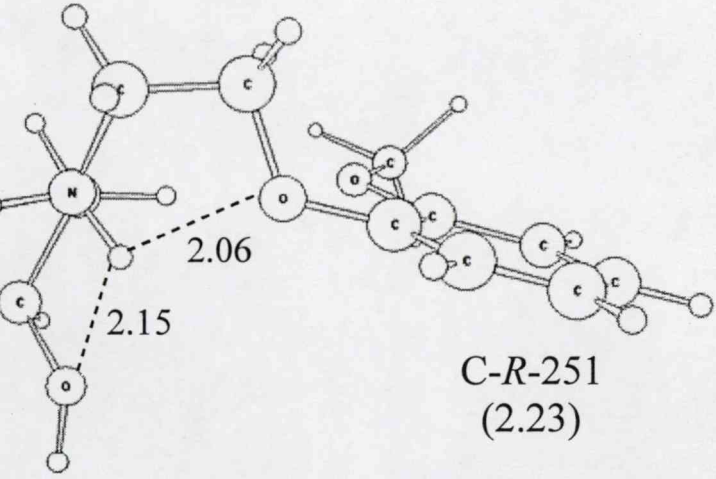

C-*R*-251
(2.23)

Figure 4
continued

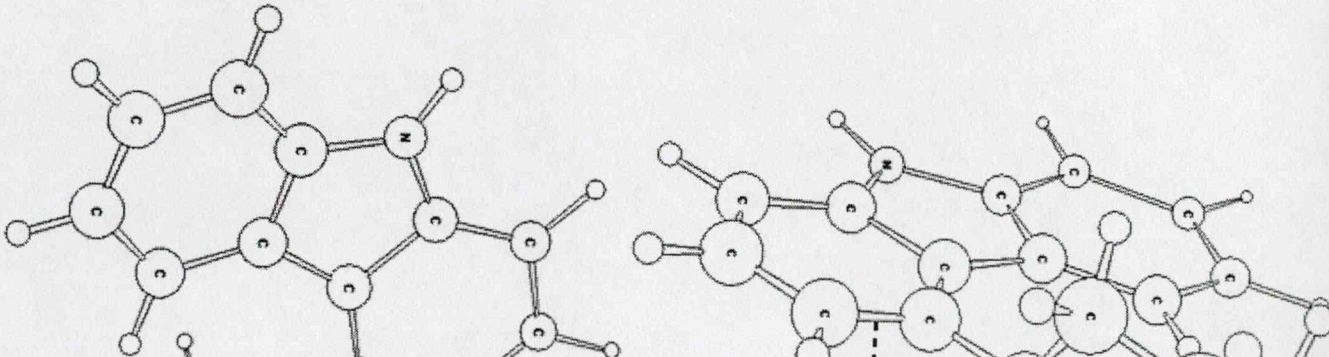

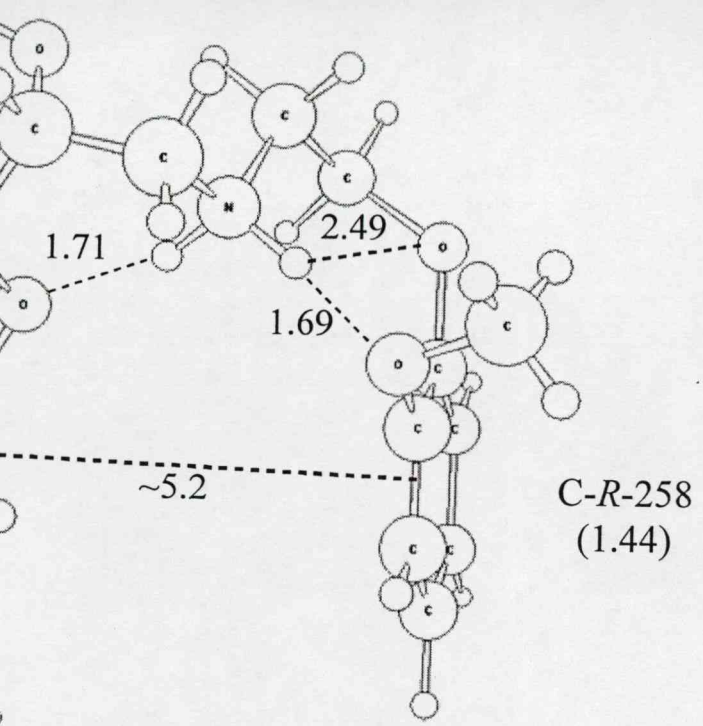

C-*R*-258
(1.44)

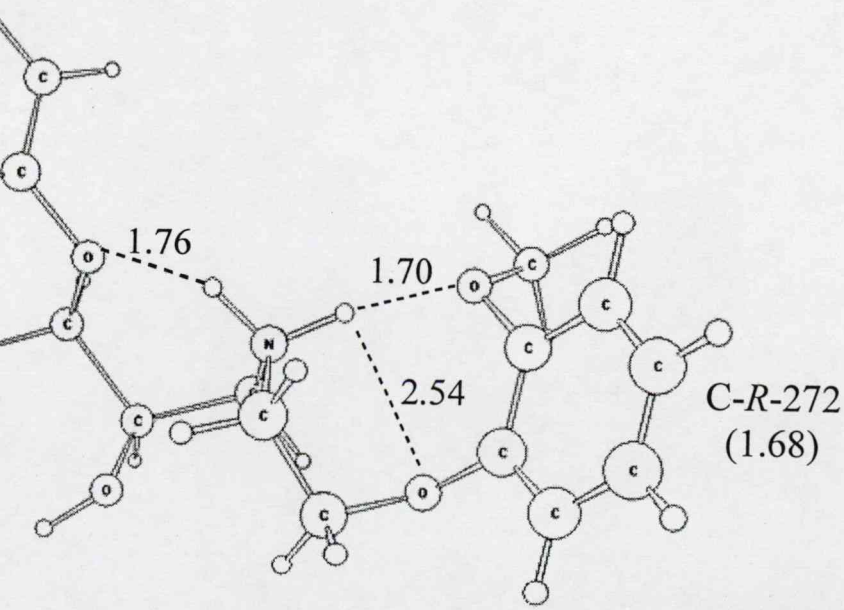

C-*R*-272
(1.68)

Figure 4
continued

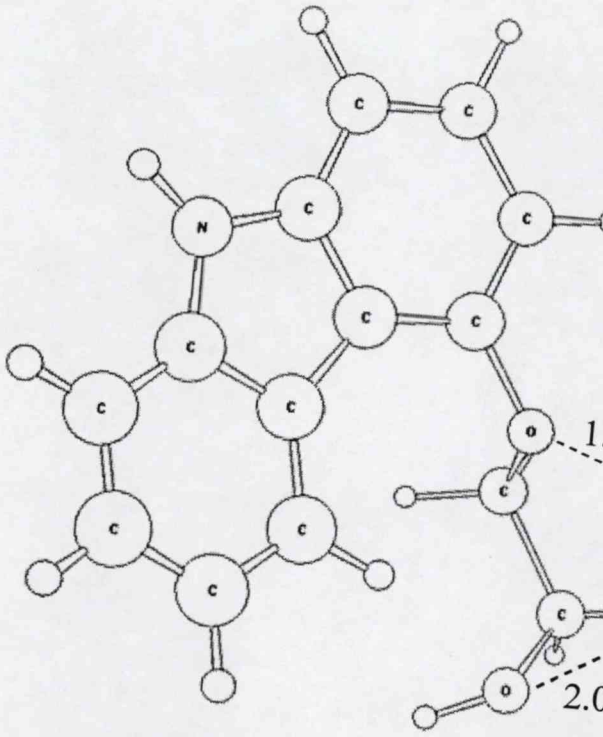
C
N
O
1.
2.0

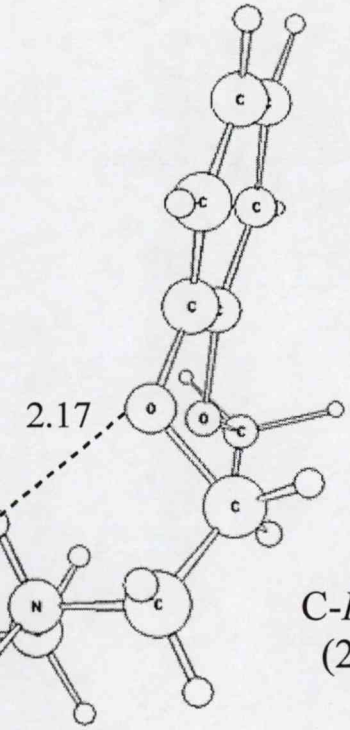

C-*R*-273
(2.72)

Figure 4
continued

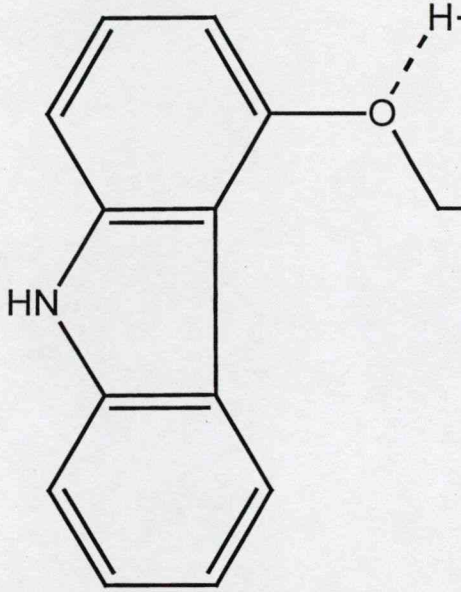
H
O
HN

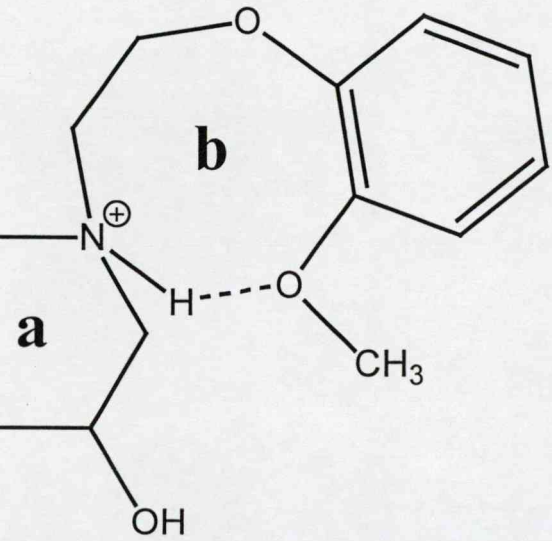

Figure 5

Table 1: Selected optimized Fragment A, B, and C conformers used to predict low energy carvedilol conformations in this study. All individual fragment structures with a conformer relative energy of ≤ 2.00 Kcal•mol^{-1} were deemed low energy conformers and incorporated to generate the carvedilol conformations found in **Table S1** (c.f. **Methods**).

Converged Torsional Angle Conformation					**Relative Energy (Kcal•mol^{-1})**
Fragment A (reference **17**) (*R*-configuration) (B3LYP/6-31G(d) results)	χ_1	χ_2	χ_3	χ_{10}	
	a	*a*	*a*	*g*+	0.00
	a	*a*	*g*-	*g*-	0.87
	a	*g*-	*a*	*g*+	1.47
	g-	*a*	*a*	*g*+	1.58
Fragment B (reference **15**) (*S*-configuration) (RHF/3-21G results)	χ_4	χ_5	χ_6	χ_{10}	
	a	*a*	*a*	*g*+	0.00
	a	*g*+	*a*	*g*+	0.36
	a	*a*	*g*-	*g*+	0.63
	g+	*a*	*a*	*g*+	0.66
	a	*a*	*g*+	*g*+	1.17
	a	*g*+	*g*+	*g*+	1.26
	g+	*a*	*g*+	*g*+	1.28
	g+	*a*	*g*-	*g*+	1.83
Fragment C (reference **16**) (no point chirality) (RHF/3-21G results)	χ_7	χ_8	χ_9	χ_{11}	
	g+	*g*+	*g*+	*g*-	0.00
	g-	*g*-	*g*-	*g*+	0.00
	g+	*a*	*g*-	*a*	0.34
	g-	*a*	*g*+	*a*	0.34
	g+	*g*-	*g*-	*g*+	1.03
	g-	*g*+	*g*+	*g*-	1.03

Table 2: RHF/3-21G-optimized carvedilol structures identified as gas phase low energy conformers based on a conformer relative energy of < 4.00 Kcal•mol^{-1} (c.f. **Figure 3** and **4**).

Structure Code	Torsional Angle (degrees)											Energy (Hartree)	Relative Energy (Kcal•mol^{-1})
	χ_1	χ_2	χ_3	χ_4	χ_5	χ_6	χ_7	χ_8	χ_9	χ_{10}	χ_{11}		
C-*R*-246	107.18	-170.32	-52.20	67.57	88.63	-173.38	-49.09	-66.13	-69.97	70.21	83.62	-1325.35188899	0.18
C-*R*-247	101.70	-170.50	-51.00	69.07	86.67	98.50	-46.98	142.71	110.99	70.87	172.91	-1325.35131606	0.54
C-*R*-248	96.77	-166.66	-48.97	67.20	-165.27	-168.20	67.84	-131.67	-81.27	59.94	106.32	-1325.34862475	2.23
C-*R*-249	98.61	-171.08	-49.55	72.36	-158.80	-51.98	-43.52	-76.09	-73.32	64.92	104.49	-1325.35217719	0.00
C-*R*-250	93.44	-173.16	-48.64	74.73	-169.46	-99.72	47.43	-141.85	-115.34	81.41	178.02	-1325.35170537	0.30
C-*R*-251	94.83	-172.31	-46.48	75.22	-176.68	-64.80	-40.31	173.62	114.99	78.04	176.41	-1325.34861944	2.23
C-*R*-258	100.47	-171.04	-53.00	65.92	86.99	-179.52	-63.40	113.39	72.09	71.84	-82.95	-1325.34987568	1.44
C-*R*-272	91.15	-172.13	-49.35	66.29	73.28	45.57	42.71	76.44	73.33	74.12	-102.79	-1325.34950697	1.68
C-*R*-273	92.65	-173.48	-49.65	73.96	171.88	60.28	41.82	-175.41	-113.63	71.78	-173.95	-1325.34784915	2.72

Table 3: Summary of the conformation distribution for optimized low energy carvedilol conformations (c.f. **Table 2**) and optimized low energy fragment conformations used to make carvedilol conformation predictions (c.f. **Table 1**). Dominant torsional angle conformation for carvedilol and corresponding fragment conformation is bolded for ease of comparison. (F.A. = Fragment A; F.B. = Fragment B; F.C. = Fragment C; NA = Not Applicable.)

	Conformation Distribution of Optimized Carvedilol Low Energy Conformers (c.f. Table 2)[§]			**Conformation Distribution of Initial Optimized Low Energy Carvedilol Fragments (c.f. Table 1)[¥]**			
Torsional Angle	***g+***	***a***	***g-***		***g+***	***a***	***g-***
χ_1	**9/9 (100%)**	(0%)	(0%)		**(0%)**	3/4 (75%)	1/4 (25%)
χ_2	(0%)	**9/9 (100%)**	(0%)	**A**	(0%)	**3/4 (75%)**	1/4 (25%)
χ_3	(0%)	(0%)	**9/9 (100%)**		(0%)	3/4 (75%)	**1/4 (25%)**
χ_4	**9/9 (100%)**	(0%)	(0%)		**3/8 (37.5%)**	5/8 (62.5%)	(0%)
χ_5	4/9 (44.4%)	**5/9 (55.6%)**	(0%)	**B**	2/8 (25%)	**6/8 (75%)**	(0%)
χ_6	3/9 (33.3%)	3/9 (33.3%)	3/9 (33.3%)		3/8 (37.5%)	3/8 (37.5%)	2/8 (25%)
χ_7	4/9 (44.4%)	(0%)	**5/9 (55.6%)**		3/6 (50%)	(0%)	**3/6 (50%)**
χ_8	2/9 (22.2%)	**5/9 (55.6%)**	2/9 (22.2%)	**C**	2/6 (33.3%)	**2/6 (33.3%)**	2/6 (33.3%)
χ_9	4/9 (44.4%)	(0%)	**5/9 (55.6%)**		3/6 (50%)	(0%)	**3/6 (50%)**
χ_{10}	**9/9 (100%)**	(0%)	(0%)	**A**	**3/4 (75%)**	(0%)	1/4 (25%) F.A.
				B	**8/8 (100%)**	(0%)	(0%)
				C	NA	NA	NA
χ_{11}	3/9 (33.3%)	**4/9 (44.4%)**	2/9 (22.2%)	**C**	2/6 (33.3%)	**2/6 (33.3%)**	2/6 (33.3%)

[§]With regards to the nine carvedilol low energy converged structures, conformation distribution is displayed as: number of conformations with respective torsional angle orientation/total number (i.e., nine) of conformations (corresponding percentage is indicated in parentheses).

[¥]With regards to the low energy carvedilol fragment structures, conformation distribution is displayed as: number of conformations with respective torsional angle orientation/total number of conformations (corresponding percentage is indicated in parentheses). Note that the total number of conformations is dependent on how many fragment structures were found to possess a conformer relative energy $\leq$ 2.00 Kcal•mol^{-1}, and thus, are different for each fragment (Fragment A = four conformations, Fragment B = eight conformations, Fragment C = six conformations).

SUPPLEMENTARY TABLES

Table S1: List of all unique carvedilol conformations generated from the combination of low energy conformers in **Table 1** and conformation of subsequently optimized structures. Molecular conformation is displayed as [predicted torsional angle geometry/RHF/3-21G optimized torsional angle geometry] (explicit values of torsional angles are found in **Table S2**). (AS = annihilated structure, ‡ = additional conformations converged during carvedilol optimizations.)

Structure Code	Torsional Angle Conformation										
	χ_1	χ_2	χ_3	χ_4	χ_5	χ_6	χ_7	χ_8	χ_9	χ_{10}	χ_{11}
C-*R*-1	[*a*/AS]	[*a*/AS]	[*a*/AS]	[*a*/AS]	[*a*/AS]	[*a*/AS]	[*g*+/AS]	[*g*+/AS]	[*g*+/AS]	[*g*+/AS]	[*g*-/AS]
C-*R*-2	[*a*/*a*]	[*a*/*a*]	[*a*/*a*]	[*a*/*a*]	[*a*/*a*]	[*a*/*a*]	[*g*-/*g*-]	[*g*-/*g*-]	[*g*-/*g*-]	[*g*+/*g*+]	[*g*+/*g*+]
C-*R*-3	[*a*/AS]	[*a*/AS]	[*a*/AS]	[*a*/AS]	[*a*/AS]	[*a*/AS]	[*g*+/AS]	[*a*/AS]	[*g*-/AS]	[*g*+/AS]	[*a*/AS]
C-*R*-4	[*a*/*a*]	[*a*/*a*]	[*a*/*a*]	[*a*/*a*]	[*a*/*a*]	[*a*/*a*]	[*g*-/*g*-]	[*a*/*a*]	[*g*+/*g*+]	[*g*+/*g*+]	[*a*/*a*]
C-*R*-5	[*a*/*a*]	[*a*/*a*]	[*a*/*a*]	[*a*/*a*]	[*a*/*a*]	[*a*/*a*]	[*g*+/*g*+]	[*g*-/*g*-]	[*g*-/*g*-]	[*g*+/*g*+]	[*g*+/*g*+]
C-*R*-6‡	[*a*/*a*]	[*a*/*a*]	[*a*/*a*]	[*a*/*a*]	[*a*/*a*]	[*a*/*a*]	[*g*-/*g*-]	[*g*+/*a*]	[*g*+/*g*+]	[*g*+/*g*+]	[*g*-/*g*-]
C-*R*-7	[*a*/*a*]	[*a*/*a*]	[*a*/*a*]	[*a*/*a*]	[*g*+/*g*+]	[*a*/*a*]	[*g*+/*g*+]	[*g*+/*g*+]	[*g*+/*g*+]	[*g*+/*g*+]	[*g*-/*g*-]
C-*R*-8	[*a*/*a*]	[*a*/*a*]	[*a*/*a*]	[*a*/*a*]	[*g*+/*g*+]	[*a*/*a*]	[*g*-/*g*-]	[*g*-/*g*-]	[*g*-/*g*-]	[*g*+/*g*+]	[*g*+/*g*+]
C-*R*-9	[*a*/*a*]	[*a*/*a*]	[*a*/*a*]	[*a*/*a*]	[*g*+/*g*+]	[*a*/*a*]	[*g*+/*g*+]	[*a*/*a*]	[*g*-/*g*-]	[*g*+/*g*+]	[*a*/*a*]
C-*R*-10	[*a*/*a*]	[*a*/*a*]	[*a*/*a*]	[*a*/*a*]	[*g*+/*g*+]	[*a*/*g*+]	[*g*-/*g*-]	[*a*/*a*]	[*g*+/*g*+]	[*g*+/*g*+]	[*a*/*a*]
C-*R*-11‡	[*a*/*g*+]	[*a*/*a*]	[*a*/*a*]	[*a*/*a*]	[*g*+/*g*+]	[*a*/*a*]	[*g*+/*g*+]	[*g*-/*g*-]	[*g*-/*g*-]	[*g*+/*g*+]	[*g*+/*g*+]
C-*R*-12	[*a*/*a*]	[*a*/*a*]	[*a*/*a*]	[*a*/*a*]	[*g*+/*g*+]	[*a*/*a*]	[*g*-/*g*-]	[*g*+/*g*+]	[*g*+/*g*+]	[*g*+/*g*+]	[*g*-/*g*-]
C-*R*-13	[*a*/*a*]	[*a*/*a*]	[*a*/*a*]	[*a*/*a*]	[*a*/*a*]	[*g*-/*g*-]	[*g*+/*g*+]	[*g*+/*g*+]	[*g*+/*g*+]	[*g*+/*g*+]	[*g*-/*g*-]
C-*R*-14	[*a*/*a*]	[*a*/*a*]	[*a*/*a*]	[*a*/*a*]	[*a*/*a*]	[*g*-/*g*-]	[*g*-/*g*-]	[*g*-/*g*-]	[*g*-/*g*-]	[*g*+/*g*+]	[*g*+/*g*+]
C-*R*-15	[*a*/AS]	[*a*/AS]	[*a*/AS]	[*a*/AS]	[*a*/AS]	[*g*-/AS]	[*g*+/AS]	[*a*/AS]	[*g*-/AS]	[*g*+/AS]	[*a*/AS]
C-*R*-16	[*a*/*a*]	[*a*/*a*]	[*a*/*a*]	[*a*/*a*]	[*a*/*a*]	[*g*-/*g*-]	[*g*-/*g*-]	[*a*/*a*]	[*g*+/*g*+]	[*g*+/*g*+]	[*a*/*a*]
C-*R*-17	[*a*/*a*]	[*a*/*a*]	[*a*/*a*]	[*a*/*a*]	[*a*/*a*]	[*g*-/*g*-]	[*g*+/*g*+]	[*g*-/*g*-]	[*g*-/*g*-]	[*g*+/*g*+]	[*g*+/*g*+]
C-*R*-18‡	[*a*/*a*]	[*a*/*a*]	[*a*/*a*]	[*a*/*a*]	[*a*/*a*]	[*g*-/*g*-]	[*g*-/*g*-]	[*g*+/*a*]	[*g*+/*g*+]	[*g*+/*g*+]	[*g*-/*g*-]
C-*R*-19	[*a*/AS]	[*a*/AS]	[*a*/AS]	[*g*+/AS]	[*a*/AS]	[*a*/AS]	[*g*+/AS]	[*g*+/AS]	[*g*+/AS]	[*g*+/AS]	[*g*-/AS]
C-*R*-20	[*a*/*a*]	[*a*/*a*]	[*a*/*a*]	[*g*+/*g*+]	[*a*/*a*]	[*a*/*a*]	[*g*-/*g*-]	[*g*-/*g*-]	[*g*-/*g*-]	[*g*+/*g*+]	[*g*+/*g*+]
C-*R*-21	[*a*/*a*]	[*a*/*a*]	[*a*/*a*]	[*g*+/*g*+]	[*a*/*a*]	[*a*/*a*]	[*g*+/*g*+]	[*a*/*a*]	[*g*-/*g*-]	[*g*+/*g*+]	[*a*/*a*]
C-*R*-22	[*a*/*a*]	[*a*/*a*]	[*a*/*a*]	[*g*+/*g*+]	[*a*/*a*]	[*a*/*a*]	[*g*-/*g*-]	[*a*/*a*]	[*g*+/*g*+]	[*g*+/*g*+]	[*a*/*a*]
C-*R*-23	[*a*/*a*]	[*a*/*a*]	[*a*/*a*]	[*g*+/*g*+]	[*a*/*a*]	[*a*/*a*]	[*g*+/*g*+]	[*g*-/*g*-]	[*g*-/*g*-]	[*g*+/*g*+]	[*g*+/*g*+]
C-*R*-24	[*a*/AS]	[*a*/AS]	[*a*/AS]	[*g*+/AS]	[*a*/AS]	[*a*/AS]	[*g*-/AS]	[*g*+/AS]	[*g*+/AS]	[*g*+/AS]	[*g*-/AS]
C-*R*-25	[*a*/AS]	[*a*/AS]	[*a*/AS]	[*a*/AS]	[*a*/AS]	[*g*+/AS]	[*g*+/AS]	[*g*+/AS]	[*g*+/AS]	[*g*+/AS]	[*g*-/AS]

Table S1 (continued): List of all unique carvedilol conformations generated from the combination of low energy conformers in **Table 1** and conformation of subsequently optimized structures. Molecular conformation is displayed as [predicted torsional angle geometry/RHF/3-21G optimized torsional angle geometry] (explicit values of torsional angles are found in **Table S2**). (AS = annihilated structure, ‡ = additional conformations converged during carvedilol optimizations.)

Structure Code	Torsional Angle Conformation										
	χ_1	χ_2	χ_3	χ_4	χ_5	χ_6	χ_7	χ_8	χ_9	χ_{10}	χ_{11}
C-*R*-26	[*a*/*a*]	[*a*/*a*]	[*a*/*a*]	[*a*/*a*]	[*a*/*a*]	[*g*+/*g*+]	[*g*-/*g*-]	[*g*-/*g*-]	[*g*-/*g*-]	[*g*+/*g*+]	[*g*+/*g*+]
C-*R*-27	[*a*/AS]	[*a*/AS]	[*a*/AS]	[*a*/AS]	[*a*/AS]	[*g*+/AS]	[*g*+/AS]	[*a*/AS]	[*g*-/AS]	[*g*+/AS]	[*a*/AS]
C-*R*-28	[*a*/*a*]	[*a*/*a*]	[*a*/*a*]	[*a*/*a*]	[*a*/*a*]	[*g*+/*g*+]	[*g*-/*g*-]	[*a*/*a*]	[*g*+/*g*+]	[*g*+/*g*+]	[*a*/*a*]
C-*R*-29	[*a*/AS]	[*a*/AS]	[*a*/AS]	[*a*/AS]	[*a*/AS]	[*g*+/AS]	[*g*+/AS]	[*g*-/AS]	[*g*-/AS]	[*g*+/AS]	[*g*+/AS]
C-*R*-30	[*a*/AS]	[*a*/AS]	[*a*/AS]	[*a*/AS]	[*a*/AS]	[*g*+/AS]	[*g*-/AS]	[*g*+/AS]	[*g*+/AS]	[*g*+/AS]	[*g*-/AS]
C-*R*-31	[*a*/*a*]	[*a*/*a*]	[*a*/*a*]	[*a*/*a*]	[*g*+/*g*+]	[*g*+/*g*+]	[*g*+/*g*+]	[*g*+/*g*+]	[*g*+/*g*+]	[*g*+/*g*+]	[*g*-/*g*-]
C-*R*-32	[*a*/AS]	[*a*/AS]	[*a*/AS]	[*a*/AS]	[*g*+/AS]	[*g*+/AS]	[*g*-/AS]	[*g*-/AS]	[*g*-/AS]	[*g*+/AS]	[*g*+/AS]
C-*R*-33	[*a*/AS]	[*a*/AS]	[*a*/AS]	[*a*/AS]	[*g*+/AS]	[*g*+/AS]	[*g*+/AS]	[*a*/AS]	[*g*-/AS]	[*g*+/AS]	[*a*/AS]
C-*R*-34[a,b]	[*a*/*a*]	[*a*/*a*]	[*a*/*a*]	[*a*/*a*]	[*g*+/*g*+]	[*g*+/*g*+]	[*g*-/*g*-]	[*a*/*a*]	[*g*+/*g*+]	[*g*+/*g*+]	[*a*/*a*]
C-*R*-35	[*a*/*a*]	[*a*/*a*]	[*a*/*a*]	[*a*/*a*]	[*g*+/*g*+]	[*g*+/*g*+]	[*g*+/*g*+]	[*g*-/*a*]	[*g*-/*g*-]	[*g*+/*g*+]	[*g*+/*g*+]
C-*R*-36	[*a*/AS]	[*a*/AS]	[*a*/AS]	[*a*/AS]	[*g*+/AS]	[*g*+/AS]	[*g*-/AS]	[*g*+/AS]	[*g*+/AS]	[*g*+/AS]	[*g*-/AS]
C-*R*-37	[*a*/AS]	[*a*/AS]	[*a*/AS]	[*g*+/AS]	[*a*/AS]	[*g*+/AS]	[*g*+/AS]	[*g*+/AS]	[*g*+/AS]	[*g*+/AS]	[*g*-/AS]
C-*R*-38‡	[*a*/*a*]	[*a*/*a*]	[*a*/*a*]	[*g*+/*g*+]	[*a*/*a*]	[*g*+/*g*+]	[*g*-/*g*-]	[*g*-/*g*-]	[*g*-/*g*-]	[*g*+/*g*+]	[*g*+/*a*]
C-*R*-39	[*a*/*a*]	[*a*/*a*]	[*a*/*a*]	[*g*+/*g*+]	[*a*/*a*]	[*g*+/*g*+]	[*g*+/*g*+]	[*a*/*a*]	[*g*-/*g*-]	[*g*+/*g*+]	[*a*/*a*]
C-*R*-40	[*a*/AS]	[*a*/AS]	[*a*/AS]	[*g*+/AS]	[*a*/AS]	[*g*+/AS]	[*g*-/AS]	[*a*/AS]	[*g*+/AS]	[*g*+/AS]	[*a*/AS]
C-*R*-41	[*a*/*a*]	[*a*/*a*]	[*a*/*a*]	[*g*+/*g*+]	[*a*/*a*]	[*g*+/*g*+]	[*g*+/*g*+]	[*g*-/*g*-]	[*g*-/*g*-]	[*g*+/*g*+]	[*g*+/*g*+]
C-*R*-42	[*a*/AS]	[*a*/AS]	[*a*/AS]	[*g*+/AS]	[*a*/AS]	[*g*+/AS]	[*g*-/AS]	[*g*+/AS]	[*g*+/AS]	[*g*+/AS]	[*g*-/AS]
C-*R*-43	[*a*/*a*]	[*a*/*a*]	[*a*/*a*]	[*g*+/*g*+]	[*a*/*a*]	[*g*-/*g*-]	[*g*+/*g*+]	[*g*+/*g*+]	[*g*+/*g*+]	[*g*+/*g*+]	[*g*-/*g*-]
C-*R*-44	[*a*/AS]	[*a*/AS]	[*a*/AS]	[*g*+/AS]	[*a*/AS]	[*g*-/AS]	[*g*-/AS]	[*g*-/AS]	[*g*-/AS]	[*g*+/AS]	[*g*+/AS]
C-*R*-45	[*a*/*a*]	[*a*/*a*]	[*a*/*a*]	[*g*+/*g*+]	[*a*/*a*]	[*g*-/*g*-]	[*g*+/*g*+]	[*a*/*a*]	[*g*-/*g*-]	[*g*+/*g*+]	[*a*/*a*]
C-*R*-46	[*a*/*a*]	[*a*/*a*]	[*a*/*a*]	[*g*+/*g*+]	[*a*/*a*]	[*g*-/*g*-]	[*g*-/*g*-]	[*a*/*a*]	[*g*+/*g*+]	[*g*+/*g*+]	[*a*/*a*]
C-*R*-47	[*a*/AS]	[*a*/AS]	[*a*/AS]	[*g*+/AS]	[*a*/AS]	[*g*-/AS]	[*g*+/AS]	[*g*-/AS]	[*g*-/AS]	[*g*+/AS]	[*g*+/AS]
C-*R*-48‡	[*a*/*a*]	[*a*/*a*]	[*a*/*a*]	[*g*+/*g*+]	[*a*/*g*-]	[*g*-/*g*-]	[*g*-/*g*-]	[*g*+/*a*]	[*g*+/*g*+]	[*g*+/*g*+]	[*g*-/*g*-]
C-*R*-49	[*a*/*a*]	[*a*/*a*]	[*g*-/*g*-]	[*a*/*a*]	[*a*/*a*]	[*a*/*a*]	[*g*+/*g*+]	[*g*+/*g*+]	[*g*+/*g*+]	[*g*+/*g*-]	[*g*-/*g*-]
C-*R*-50	[*a*/*a*]	[*a*/*a*]	[*g*-/*g*-]	[*a*/*a*]	[*a*/*a*]	[*a*/*a*]	[*g*-/*g*-]	[*g*-/*g*-]	[*g*-/*g*-]	[*g*+/*g*-]	[*g*+/*g*+]

Table S1 (continued): List of all unique carvedilol conformations generated from the combination of low energy conformers in **Table 1** and conformation of subsequently optimized structures. Molecular conformation is displayed as [predicted torsional angle geometry/RHF/3-21G optimized torsional angle geometry] (explicit values of torsional angles are found in **Table S2**). (AS = annihilated structure, ‡ = additional conformations converged during carvedilol optimizations.)

Structure Code	Torsional Angle Conformation										
	χ_1	χ_2	χ_3	χ_4	χ_5	χ_6	χ_7	χ_8	χ_9	χ_{10}	χ_{11}
C-*R*-51	[*a*/AS]	[*a*/AS]	[*g*-/AS]	[*a*/AS]	[*a*/AS]	[*a*/AS]	[*g*+/AS]	[*a*/AS]	[*g*-/AS]	[*g*+/AS]	[*a*/AS]
C-*R*-52	[*a*/*a*]	[*a*/*a*]	[*g*-/*g*-]	[*a*/*a*]	[*a*/*a*]	[*a*/*a*]	[*g*-/*g*-]	[*a*/*a*]	[*g*+/*g*+]	[*g*+/*g*-]	[*a*/*a*]
C-*R*-53	[*a*/*a*]	[*a*/*a*]	[*g*-/*g*-]	[*a*/*a*]	[*a*/*a*]	[*a*/*a*]	[*g*+/*g*+]	[*g*-/*g*-]	[*g*-/*g*-]	[*g*+/*g*-]	[*g*+/*g*+]
C-*R*-54	[*a*/AS]	[*a*/AS]	[*g*-/AS]	[*a*/AS]	[*a*/AS]	[*a*/AS]	[*g*-/AS]	[*g*+/AS]	[*g*+/AS]	[*g*+/AS]	[*g*-/AS]
C-*R*-55	[*a*/*a*]	[*a*/*a*]	[*g*-/*g*-]	[*a*/*a*]	[*a*/*a*]	[*a*/*a*]	[*g*+/*g*+]	[*g*+/*g*+]	[*g*+/*g*+]	[*g*-/*g*-]	[*g*-/*g*-]
C-*R*-56[a,b]	[*a*/*a*]	[*a*/*a*]	[*g*-/*g*-]	[*a*/*a*]	[*a*/*a*]	[*a*/*a*]	[*g*-/*g*-]	[*g*-/*g*-]	[*g*-/*g*-]	[*g*-/*g*-]	[*g*+/*g*+]
C-*R*-57	[*a*/*a*]	[*a*/*a*]	[*g*-/*g*-]	[*a*/*a*]	[*a*/*a*]	[*a*/*a*]	[*g*+/*g*+]	[*a*/*a*]	[*g*-/*g*-]	[*g*-/*g*-]	[*a*/*a*]
C-*R*-58	[*a*/*a*]	[*a*/*a*]	[*g*-/*g*-]	[*a*/*a*]	[*a*/*a*]	[*a*/*a*]	[*g*-/*g*-]	[*a*/*a*]	[*g*+/*g*+]	[*g*-/*g*-]	[*a*/*a*]
C-*R*-59	[*a*/*a*]	[*a*/*a*]	[*g*-/*g*-]	[*a*/*a*]	[*a*/*a*]	[*a*/*a*]	[*g*+/*g*+]	[*g*-/*g*-]	[*g*-/*g*-]	[*g*-/*g*-]	[*g*+/*g*+]
C-*R*-60	[*a*/AS]	[*a*/AS]	[*g*-/AS]	[*a*/AS]	[*a*/AS]	[*a*/AS]	[*g*-/AS]	[*g*+/AS]	[*g*+/AS]	[*g*-/AS]	[*g*-/AS]
C-*R*-61	[*a*/*a*]	[*a*/*a*]	[*g*-/*g*-]	[*a*/*a*]	[*g*+/*g*+]	[*a*/*a*]	[*g*+/*g*+]	[*g*+/*g*+]	[*g*+/*g*+]	[*g*+/*g*-]	[*g*-/*g*-]
C-*R*-62	[*a*/*a*]	[*a*/*a*]	[*g*-/*g*-]	[*a*/*a*]	[*g*+/*g*+]	[*a*/*a*]	[*g*-/*g*-]	[*g*-/*g*-]	[*g*-/*g*-]	[*g*+/*g*-]	[*g*+/*g*+]
C-*R*-63	[*a*/*a*]	[*a*/*a*]	[*g*-/*g*-]	[*a*/*a*]	[*g*+/*g*+]	[*a*/*a*]	[*g*+/*g*+]	[*a*/*a*]	[*g*-/*g*-]	[*g*+/*g*-]	[*a*/*a*]
C-*R*-64	[*a*/*a*]	[*a*/*a*]	[*g*-/*g*-]	[*a*/*a*]	[*g*+/*g*+]	[*a*/*a*]	[*g*-/*g*-]	[*a*/*a*]	[*g*+/*g*+]	[*g*+/*g*-]	[*a*/*a*]
C-*R*-65	[*a*/AS]	[*a*/AS]	[*g*-/AS]	[*a*/AS]	[*g*+/AS]	[*a*/AS]	[*g*+/AS]	[*g*-/AS]	[*g*-/AS]	[*g*+/AS]	[*g*+/AS]
C-*R*-66‡	[*a*/*a*]	[*a*/*a*]	[*g*-/*g*-]	[*a*/*a*]	[*g*+/*g*+]	[*a*/*a*]	[*g*-/*g*-]	[*g*+/*a*]	[*g*+/*g*+]	[*g*+/*g*-]	[*g*-/*g*-]
C-*R*-67	[*a*/*a*]	[*a*/*a*]	[*g*-/*g*-]	[*a*/*a*]	[*g*+/*g*+]	[*a*/*a*]	[*g*+/*g*+]	[*g*+/*g*+]	[*g*+/*g*+]	[*g*-/*g*-]	[*g*-/*g*-]
C-*R*-68	[*a*/*a*]	[*a*/*a*]	[*g*-/*g*-]	[*a*/*a*]	[*g*+/*g*+]	[*a*/*a*]	[*g*-/*g*-]	[*g*-/*g*-]	[*g*-/*g*-]	[*g*-/*g*-]	[*g*+/*g*+]
C-*R*-69	[*a*/*a*]	[*a*/*a*]	[*g*-/*g*-]	[*a*/*a*]	[*g*+/*g*+]	[*a*/*a*]	[*g*+/*g*+]	[*a*/*a*]	[*g*-/*g*-]	[*g*-/*g*-]	[*a*/*a*]
C-*R*-70	[*a*/*a*]	[*a*/*a*]	[*g*-/*g*-]	[*a*/*a*]	[*g*+/*g*+]	[*a*/*a*]	[*g*-/*g*-]	[*a*/*a*]	[*g*+/*g*+]	[*g*-/*g*-]	[*a*/*a*]
C-*R*-71	[*a*/AS]	[*a*/AS]	[*g*-/AS]	[*a*/AS]	[*g*+/AS]	[*a*/AS]	[*g*+/AS]	[*g*-/AS]	[*g*-/AS]	[*g*-/AS]	[*g*+/AS]
C-*R*-72	[*a*/*a*]	[*a*/*a*]	[*g*-/*g*-]	[*a*/*a*]	[*g*+/*g*+]	[*a*/*a*]	[*g*-/*g*-]	[*g*+/*g*+]	[*g*+/*g*+]	[*g*-/*g*-]	[*g*-/*g*-]
C-*R*-73	[*a*/AS]	[*a*/AS]	[*g*-/AS]	[*a*/AS]	[*a*/AS]	[*g*-/AS]	[*g*+/AS]	[*g*+/AS]	[*g*+/AS]	[*g*+/AS]	[*g*-/AS]
C-*R*-74	[*a*/*a*]	[*a*/*a*]	[*g*-/*g*-]	[*a*/*a*]	[*a*/*a*]	[*g*-/*g*-]	[*g*-/*g*-]	[*g*-/*g*-]	[*g*-/*g*-]	[*g*+/*g*-]	[*g*+/*g*+]
C-*R*-75	[*a*/*a*]	[*a*/*a*]	[*g*-/*g*-]	[*a*/*a*]	[*a*/*a*]	[*g*-/*a*]	[*g*+/*g*+]	[*a*/*a*]	[*g*-/*g*-]	[*g*+/*g*-]	[*a*/*a*]

Table S1 (continued): List of all unique carvedilol conformations generated from the combination of low energy conformers in **Table 1** and conformation of subsequently optimized structures. Molecular conformation is displayed as [predicted torsional angle geometry/RHF/3-21G optimized torsional angle geometry] (explicit values of torsional angles are found in **Table S2**). (AS = annihilated structure, ‡ = additional conformations converged during carvedilol optimizations.)

Structure Code	Torsional Angle Conformation										
	χ_1	χ_2	χ_3	χ_4	χ_5	χ_6	χ_7	χ_8	χ_9	χ_{10}	χ_{11}
C-*R*-76	[*a*/*a*]	[*a*/*a*]	[*g*-/*g*-]	[*a*/*a*]	[*a*/*a*]	[*g*-/*g*-]	[*g*-/*g*-]	[*a*/*a*]	[*g*+/*g*+]	[*g*+/*g*-]	[*a*/*a*]
C-*R*-77	[*a*/*a*]	[*a*/*a*]	[*g*-/*g*-]	[*a*/*a*]	[*a*/*a*]	[*g*-/*g*-]	[*g*+/*g*+]	[*g*-/*g*-]	[*g*-/*g*-]	[*g*+/*g*-]	[*g*+/*g*+]
C-*R*-78	[*a*/AS]	[*a*/AS]	[*g*-/AS]	[*a*/AS]	[*a*/AS]	[*g*-/AS]	[*g*-/AS]	[*g*+/AS]	[*g*+/AS]	[*g*+/AS]	[*g*-/AS]
C-*R*-79‡	[*a*/*a*]	[*a*/*a*]	[*g*-/*g*-]	[*a*/*a*]	[*a*/*a*]	[*g*-/*g*-]	[*g*+/*g*+]	[*g*+/*g*+]	[*g*+/*g*+]	[*g*-/*g*-]	[*g*-/*a*]
C-*R*-80	[*a*/*a*]	[*a*/*a*]	[*g*-/*g*-]	[*a*/*a*]	[*a*/*a*]	[*g*-/*g*-]	[*g*-/*g*-]	[*g*-/*g*-]	[*g*-/*g*-]	[*g*-/*g*-]	[*g*+/*g*+]
C-*R*-81	[*a*/*a*]	[*a*/*a*]	[*g*-/*g*-]	[*a*/*a*]	[*a*/*a*]	[*g*-/*a*]	[*g*+/*g*+]	[*a*/*a*]	[*g*-/*g*-]	[*g*-/*g*-]	[*a*/*a*]
C-*R*-82	[*a*/*a*]	[*a*/*a*]	[*g*-/*g*-]	[*a*/*a*]	[*a*/*a*]	[*g*-/*g*-]	[*g*-/*g*-]	[*a*/*a*]	[*g*+/*g*+]	[*g*-/*g*-]	[*a*/*a*]
C-*R*-83	[*a*/*a*]	[*a*/*a*]	[*g*-/*g*-]	[*a*/*a*]	[*a*/*a*]	[*g*-/*g*-]	[*g*+/*g*+]	[*g*-/*g*-]	[*g*-/*g*-]	[*g*-/*g*-]	[*g*+/*g*+]
C-*R*-84	[*a*/AS]	[*a*/AS]	[*g*-/AS]	[*a*/AS]	[*a*/AS]	[*g*-/AS]	[*g*-/AS]	[*g*+/AS]	[*g*+/AS]	[*g*-/AS]	[*g*-/AS]
C-*R*-85	[*a*/AS]	[*a*/AS]	[*g*-/AS]	[*g*+/AS]	[*a*/AS]	[*a*/AS]	[*g*+/AS]	[*g*+/AS]	[*g*+/AS]	[*g*+/AS]	[*g*-/AS]
C-*R*-86‡	[*a*/*g*+]	[*a*/*a*]	[*g*-/*g*-]	[*g*+/*g*+]	[*a*/*g*+]	[*a*/*a*]	[*g*-/*g*-]	[*g*-/*g*-]	[*g*-/*g*-]	[*g*+/*g*+]	[*g*+/*g*+]
C-*R*-87	[*a*/AS]	[*a*/AS]	[*g*-/AS]	[*g*+/AS]	[*a*/AS]	[*a*/AS]	[*g*+/AS]	[*a*/AS]	[*g*-/AS]	[*g*+/AS]	[*a*/AS]
C-*R*-88‡	[*a*/*g*+]	[*a*/*a*]	[*g*-/*g*-]	[*g*+/*g*+]	[*a*/*g*+]	[*a*/*g*+]	[*g*-/*g*-]	[*a*/*a*]	[*g*+/*g*+]	[*g*+/*g*+]	[*a*/*a*]
C-*R*-89‡	[*a*/*g*+]	[*a*/*a*]	[*g*-/*g*-]	[*g*+/*g*+]	[*a*/*a*]	[*a*/*a*]	[*g*+/*g*+]	[*g*-/*a*]	[*g*-/*g*-]	[*g*+/*g*+]	[*g*+/*g*+]
C-*R*-90	[*a*/AS]	[*a*/AS]	[*g*-/AS]	[*g*+/AS]	[*a*/AS]	[*a*/AS]	[*g*-/AS]	[*g*+/AS]	[*g*+/AS]	[*g*+/AS]	[*g*-/AS]
C-*R*-91	[*a*/AS]	[*a*/AS]	[*g*-/AS]	[*g*+/AS]	[*a*/AS]	[*a*/AS]	[*g*+/AS]	[*g*+/AS]	[*g*+/AS]	[*g*-/AS]	[*g*-/AS]
C-*R*-92‡	[*a*/*g*+]	[*a*/*a*]	[*g*-/*g*-]	[*g*+/*g*+]	[*a*/*g*+]	[*a*/*a*]	[*g*-/*g*-]	[*g*-/*g*-]	[*g*-/*g*-]	[*g*-/*g*+]	[*g*+/*g*+]
C-*R*-93	[*a*/AS]	[*a*/AS]	[*g*-/AS]	[*g*+/AS]	[*a*/AS]	[*a*/AS]	[*g*+/AS]	[*a*/AS]	[*g*-/AS]	[*g*-/AS]	[*a*/AS]
C-*R*-94	[*a*/AS]	[*a*/AS]	[*g*-/AS]	[*g*+/AS]	[*a*/AS]	[*a*/AS]	[*g*-/AS]	[*a*/AS]	[*g*+/AS]	[*g*-/AS]	[*a*/AS]
C-*R*-95	[*a*/AS]	[*a*/AS]	[*g*-/AS]	[*g*+/AS]	[*a*/AS]	[*a*/AS]	[*g*+/AS]	[*g*-/AS]	[*g*-/AS]	[*g*-/AS]	[*g*+/AS]
C-*R*-96‡	[*a*/*g*+]	[*a*/*a*]	[*g*-/*g*-]	[*g*+/*g*+]	[*a*/*g*+]	[*a*/*a*]	[*g*-/*g*-]	[*g*+/*g*+]	[*g*+/*g*+]	[*g*-/*g*+]	[*g*-/*g*-]
C-*R*-97‡	[*a*/*g*+]	[*a*/*a*]	[*g*-/*g*-]	[*a*/*a*]	[*a*/*a*]	[*g*+/*g*+]	[*g*+/*g*+]	[*g*+/*g*+]	[*g*+/*g*+]	[*g*+/*g*+]	[*g*-/*g*-]
C-*R*-98	[*a*/AS]	[*a*/AS]	[*g*-/AS]	[*a*/AS]	[*a*/AS]	[*g*+/AS]	[*g*-/AS]	[*g*-/AS]	[*g*-/AS]	[*g*+/AS]	[*g*+/AS]
C-*R*-99‡	[*a*/*a*]	[*a*/*a*]	[*g*-/*g*-]	[*a*/*a*]	[*a*/*a*]	[*g*+/*g*+]	[*g*+/*g*+]	[*a*/*a*]	[*g*-/*g*-]	[*g*+/*g*-]	[*a*/*g*+]
C-*R*-100	[*a*/*a*]	[*a*/*a*]	[*g*-/*g*-]	[*a*/*a*]	[*a*/*a*]	[*g*+/*g*+]	[*g*-/*g*-]	[*a*/*a*]	[*g*+/*g*+]	[*g*+/*g*-]	[*a*/*a*]

Table S1 (continued): List of all unique carvedilol conformations generated from the combination of low energy conformers in **Table 1** and conformation of subsequently optimized structures. Molecular conformation is displayed as [predicted torsional angle geometry/RHF/3-21G optimized torsional angle geometry] (explicit values of torsional angles are found in **Table S2**). (AS = annihilated structure, ‡ = additional conformations converged during carvedilol optimizations.)

Structure Code	Torsional Angle Conformation										
	χ_1	χ_2	χ_3	χ_4	χ_5	χ_6	χ_7	χ_8	χ_9	χ_{10}	χ_{11}
C-*R*-101	[*a*/*a*]	[*a*/*a*]	[*g*-/*g*-]	[*a*/*a*]	[*a*/*a*]	[*g*+/*a*]	[*g*+/*g*+]	[*g*-/*g*-]	[*g*-/*g*-]	[*g*+/*g*-]	[*g*+/*g*+]
C-*R*-102	[*a*/*a*]	[*a*/*a*]	[*g*-/*g*-]	[*a*/*a*]	[*a*/*a*]	[*g*+/*g*+]	[*g*-/*g*-]	[*g*+/*g*+]	[*g*+/*g*+]	[*g*+/*g*-]	[*g*-/*g*-]
C-*R*-103‡	[*a*/*a*]	[*a*/*a*]	[*g*-/*g*-]	[*a*/*a*]	[*a*/*a*]	[*g*+/*g*+]	[*g*+/*g*+]	[*g*+/*g*+]	[*g*+/*g*+]	[*g*-/*g*-]	[*g*-/*a*]
C-*R*-104	[*a*/AS]	[*a*/AS]	[*g*-/AS]	[*a*/AS]	[*a*/AS]	[*g*+/AS]	[*g*-/AS]	[*g*-/AS]	[*g*-/AS]	[*g*-/AS]	[*g*+/AS]
C-*R*-105	[*a*/AS]	[*a*/AS]	[*g*-/AS]	[*a*/AS]	[*a*/AS]	[*g*+/AS]	[*g*+/AS]	[*a*/AS]	[*g*-/AS]	[*g*-/AS]	[*a*/AS]
C-*R*-106	[*a*/*a*]	[*a*/*a*]	[*g*-/*g*-]	[*a*/*a*]	[*a*/*a*]	[*g*+/*g*+]	[*g*-/*g*-]	[*a*/*a*]	[*g*+/*g*+]	[*g*-/*g*-]	[*a*/*a*]
C-*R*-107	[*a*/*a*]	[*a*/*a*]	[*g*-/*g*-]	[*a*/*a*]	[*a*/*a*]	[*g*+/*a*]	[*g*+/*g*+]	[*g*-/*g*-]	[*g*-/*g*-]	[*g*-/*g*-]	[*g*+/*g*+]
C-*R*-108	[*a*/*a*]	[*a*/*a*]	[*g*-/*g*-]	[*a*/*a*]	[*a*/*a*]	[*g*+/*g*+]	[*g*-/*g*-]	[*g*+/*g*+]	[*g*+/*g*+]	[*g*-/*g*-]	[*g*-/*g*-]
C-*R*-109	[*a*/*a*]	[*a*/*a*]	[*g*-/*g*-]	[*a*/*a*]	[*g*+/*g*+]	[*g*+/*g*+]	[*g*+/*g*+]	[*g*+/*g*+]	[*g*+/*g*+]	[*g*+/*g*-]	[*g*-/*g*-]
C-*R*-110	[*a*/AS]	[*a*/AS]	[*g*-/AS]	[*a*/AS]	[*g*+/AS]	[*g*+/AS]	[*g*-/AS]	[*g*-/AS]	[*g*-/AS]	[*g*+/AS]	[*g*+/AS]
C-*R*-111	[*a*/*a*]	[*a*/*a*]	[*g*-/*g*-]	[*a*/*a*]	[*g*+/*g*+]	[*g*+/*g*+]	[*g*+/*g*+]	[*a*/*a*]	[*g*-/*g*-]	[*g*+/*g*-]	[*a*/*a*]
C-*R*-112	[*a*/*a*]	[*a*/*a*]	[*g*-/*g*-]	[*a*/*a*]	[*g*+/*g*+]	[*g*+/*g*+]	[*g*-/*g*-]	[*a*/*a*]	[*g*+/*g*+]	[*g*+/*g*-]	[*a*/*a*]
C-*R*-113	[*a*/*a*]	[*a*/*a*]	[*g*-/*g*-]	[*a*/*a*]	[*g*+/*g*+]	[*g*+/*g*+]	[*g*+/*g*+]	[*g*-/*a*]	[*g*-/*g*-]	[*g*+/*g*-]	[*g*+/*a*]
C-*R*-114‡	[*a*/*a*]	[*a*/*a*]	[*g*-/*g*-]	[*a*/*a*]	[*g*+/*g*+]	[*g*+/*g*+]	[*g*-/*g*-]	[*g*+/*a*]	[*g*+/*g*+]	[*g*+/*g*-]	[*g*-/*g*-]
C-*R*-115	[*a*/*a*]	[*a*/*a*]	[*g*-/*g*-]	[*a*/*a*]	[*g*+/*g*+]	[*g*+/*g*+]	[*g*+/*g*+]	[*g*+/*g*+]	[*g*+/*g*+]	[*g*-/*g*-]	[*g*-/*g*-]
C-*R*-116‡	[*a*/*a*]	[*a*/*a*]	[*g*-/*g*-]	[*a*/*a*]	[*g*+/*g*+]	[*g*+/*g*+]	[*g*-/*g*-]	[*g*-/*g*-]	[*g*-/*g*-]	[*g*-/*g*-]	[*g*+/*a*]
C-*R*-117[a,b]	[*a*/*a*]	[*a*/*a*]	[*g*-/*g*-]	[*a*/*a*]	[*g*+/*g*+]	[*g*+/*g*+]	[*g*+/*g*+]	[*a*/*a*]	[*g*-/*g*-]	[*g*-/*g*-]	[*a*/*a*]
C-*R*-118[a,b]	[*a*/*a*]	[*a*/*a*]	[*g*-/*g*-]	[*a*/*a*]	[*g*+/*g*+]	[*g*+/*g*+]	[*g*-/*g*-]	[*a*/*a*]	[*g*+/*g*+]	[*g*-/*g*-]	[*a*/*a*]
C-*R*-119	[*a*/*a*]	[*a*/*a*]	[*g*-/*g*-]	[*a*/*a*]	[*g*+/*g*+]	[*g*+/*g*+]	[*g*+/*g*+]	[*g*-/*g*-]	[*g*-/*g*-]	[*g*-/*g*-]	[*g*+/*g*+]
C-*R*-120‡	[*a*/*a*]	[*a*/*a*]	[*g*-/*g*-]	[*a*/*a*]	[*g*+/*g*+]	[*g*+/*g*+]	[*g*-/*g*-]	[*g*+/*a*]	[*g*+/*g*+]	[*g*-/*g*-]	[*g*-/*g*-]
C-*R*-121‡	[*a*/*g*+]	[*a*/*a*]	[*g*-/*g*-]	[*g*+/*g*+]	[*a*/*g*+]	[*g*+/*g*+]	[*g*+/*g*+]	[*g*+/*g*+]	[*g*+/*g*+]	[*g*+/*g*+]	[*g*-/*g*-]
C-*R*-122	[*a*/AS]	[*a*/AS]	[*g*-/AS]	[*g*+/AS]	[*a*/AS]	[*g*+/AS]	[*g*-/AS]	[*g*-/AS]	[*g*-/AS]	[*g*+/AS]	[*g*+/AS]
C-*R*-123‡	[*a*/*g*+]	[*a*/*a*]	[*g*-/*g*-]	[*g*+/*g*+]	[*a*/*a*]	[*g*+/*g*+]	[*g*+/*g*+]	[*a*/*a*]	[*g*-/*g*-]	[*g*+/*g*+]	[*a*/*a*]
C-*R*-124‡	[*a*/*g*+]	[*a*/*a*]	[*g*-/*g*-]	[*g*+/*g*+]	[*a*/*a*]	[*g*+/*g*+]	[*g*-/*g*-]	[*a*/*a*]	[*g*+/*g*+]	[*g*+/*g*+]	[*a*/*a*]
C-*R*-125	[*a*/AS]	[*a*/AS]	[*g*-/AS]	[*g*+/AS]	[*a*/AS]	[*g*+/AS]	[*g*+/AS]	[*g*-/AS]	[*g*-/AS]	[*g*+/AS]	[*g*+/AS]

Table S1 (continued): List of all unique carvedilol conformations generated from the combination of low energy conformers in **Table 1** and conformation of subsequently optimized structures. Molecular conformation is displayed as [predicted torsional angle geometry/RHF/3-21G optimized torsional angle geometry] (explicit values of torsional angles are found in **Table S2**). (AS = annihilated structure, ‡ = additional conformations converged during carvedilol optimizations.)

Structure Code	Torsional Angle Conformation										
	χ_1	χ_2	χ_3	χ_4	χ_5	χ_6	χ_7	χ_8	χ_9	χ_{10}	χ_{11}
C-*R*-126‡	[*a*/*g*+]	[*a*/*a*]	[*g*-/*g*-]	[*g*+/*g*+]	[*a*/*a*]	[*g*+/*g*+]	[*g*-/*g*-]	[*g*+/*g*+]	[*g*+/*g*+]	[*g*+/*g*+]	[*g*-/*g*-]
C-*R*-127	[*a*/AS]	[*a*/AS]	[*g*-/AS]	[*g*+/AS]	[*a*/AS]	[*g*+/AS]	[*g*+/AS]	[*g*+/AS]	[*g*+/AS]	[*g*-/AS]	[*g*-/AS]
C-*R*-128	[*a*/AS]	[*a*/AS]	[*g*-/AS]	[*g*+/AS]	[*a*/AS]	[*g*+/AS]	[*g*-/AS]	[*g*-/AS]	[*g*-/AS]	[*g*-/AS]	[*g*+/AS]
C-*R*-129‡	[*a*/*g*+]	[*a*/*a*]	[*g*-/*g*-]	[*g*+/*g*+]	[*a*/*a*]	[*g*+/*g*+]	[*g*+/*g*+]	[*a*/*a*]	[*g*-/*g*-]	[*g*-/*g*+]	[*a*/*a*]
C-*R*-130‡	[*a*/*g*+]	[*a*/*a*]	[*g*-/*g*-]	[*g*+/*g*+]	[*a*/*a*]	[*g*+/*g*+]	[*g*-/*g*-]	[*a*/*a*]	[*g*+/*g*+]	[*g*-/*g*+]	[*a*/*a*]
C-*R*-131	[*a*/AS]	[*a*/AS]	[*g*-/AS]	[*g*+/AS]	[*a*/AS]	[*g*+/AS]	[*g*+/AS]	[*g*-/AS]	[*g*-/AS]	[*g*-/AS]	[*g*+/AS]
C-*R*-132	[*a*/*g*+]	[*a*/*a*]	[*g*-/*g*-]	[*g*+/*g*+]	[*a*/*a*]	[*g*+/*g*+]	[*g*-/*g*-]	[*g*+/*g*+]	[*g*+/*g*+]	[*g*+/*g*+]	[*g*-/*g*-]
C-*R*-133	[*a*/AS]	[*a*/AS]	[*g*-/AS]	[*g*+/AS]	[*a*/AS]	[*g*-/AS]	[*g*+/AS]	[*g*+/AS]	[*g*+/AS]	[*g*+/AS]	[*g*-/AS]
C-*R*-134‡	[*a*/*g*+]	[*a*/*a*]	[*g*-/*g*-]	[*g*+/*g*+]	[*a*/*a*]	[*g*-/*g*-]	[*g*-/*g*-]	[*g*-/*g*-]	[*g*-/*g*-]	[*g*+/*g*+]	[*g*+/*g*+]
C-*R*-135‡	[*a*/*g*+]	[*a*/*a*]	[*g*-/*g*-]	[*g*+/*g*+]	[*a*/*a*]	[*g*-/*g*-]	[*g*+/*g*+]	[*a*/*a*]	[*g*-/*g*-]	[*g*+/*g*+]	[*a*/*a*]
C-*R*-136‡	[*a*/*g*+]	[*a*/*a*]	[*g*-/*g*-]	[*g*+/*g*+]	[*a*/*a*]	[*g*-/*g*-]	[*g*-/*g*-]	[*a*/*a*]	[*g*+/*g*+]	[*g*+/*g*+]	[*a*/*a*]
C-*R*-137‡	[*a*/*g*+]	[*a*/*a*]	[*g*-/*g*-]	[*g*+/*g*+]	[*a*/*a*]	[*g*-/*g*-]	[*g*+/*g*+]	[*g*-/*g*-]	[*g*-/*g*-]	[*g*+/*g*+]	[*g*+/*g*+]
C-*R*-138	[*a*/AS]	[*a*/AS]	[*g*-/AS]	[*g*+/AS]	[*a*/AS]	[*g*-/AS]	[*g*-/AS]	[*g*+/AS]	[*g*+/AS]	[*g*+/AS]	[*g*-/AS]
C-*R*-139	[*a*/AS]	[*a*/AS]	[*g*-/AS]	[*g*+/AS]	[*a*/AS]	[*g*-/AS]	[*g*+/AS]	[*g*+/AS]	[*g*+/AS]	[*g*-/AS]	[*g*-/AS]
C-*R*-140‡	[*a*/*g*+]	[*a*/*a*]	[*g*-/*g*-]	[*g*+/*g*+]	[*a*/*a*]	[*g*-/*g*-]	[*g*-/*g*-]	[*g*-/*g*-]	[*g*-/*g*-]	[*g*-/*g*+]	[*g*+/*g*+]
C-*R*-141	[*a*/AS]	[*a*/AS]	[*g*-/AS]	[*g*+/AS]	[*a*/AS]	[*g*-/AS]	[*g*+/AS]	[*a*/AS]	[*g*-/AS]	[*g*-/AS]	[*a*/AS]
C-*R*-142‡	[*a*/*g*+]	[*a*/*a*]	[*g*-/*g*-]	[*g*+/*g*+]	[*a*/*a*]	[*g*-/*g*-]	[*g*-/*g*-]	[*a*/*a*]	[*g*+/*g*+]	[*g*-/*g*+]	[*a*/*a*]
C-*R*-143‡	[*a*/*g*+]	[*a*/*a*]	[*g*-/*g*-]	[*g*+/*g*+]	[*a*/*a*]	[*g*-/*g*-]	[*g*+/*g*+]	[*g*-/*g*-]	[*g*-/*g*-]	[*g*-/*g*+]	[*g*+/*g*+]
C-*R*-144	[*a*/AS]	[*a*/AS]	[*g*-/AS]	[*g*+/AS]	[*a*/AS]	[*g*-/AS]	[*g*-/AS]	[*g*+/AS]	[*g*+/AS]	[*g*-/AS]	[*g*-/AS]
C-*R*-145	[*a*/AS]	[*g*-/AS]	[*a*/AS]	[*a*/AS]	[*a*/AS]	[*a*/AS]	[*g*+/AS]	[*g*+/AS]	[*g*+/AS]	[*g*+/AS]	[*g*-/AS]
C-*R*-146	[*a*/AS]	[*g*-/AS]	[*a*/AS]	[*a*/AS]	[*a*/AS]	[*a*/AS]	[*g*-/AS]	[*g*-/AS]	[*g*-/AS]	[*g*+/AS]	[*g*+/AS]
C-*R*-147	[*a*/*g*-]	[*g*-/*a*]	[*a*/*a*]	[*a*/*a*]	[*a*/*a*]	[*a*/*a*]	[*g*+/*g*+]	[*a*/*a*]	[*g*-/*g*-]	[*g*+/*g*+]	[*a*/*a*]
C-*R*-148	[*a*/*a*]	[*g*-/*g*-]	[*a*/*a*]	[*a*/*a*]	[*a*/*a*]	[*a*/*a*]	[*g*-/*g*-]	[*a*/*a*]	[*g*+/*g*+]	[*g*+/*g*+]	[*a*/*a*]
C-*R*-149	[*a*/*a*]	[*g*-/*g*-]	[*a*/*a*]	[*a*/*a*]	[*a*/*a*]	[*a*/*a*]	[*g*+/*g*+]	[*g*-/*g*-]	[*g*-/*g*-]	[*g*+/*g*+]	[*g*+/*g*+]
C-*R*-150	[*a*/*a*]	[*g*-/*g*-]	[*a*/*a*]	[*a*/*a*]	[*a*/*a*]	[*a*/*a*]	[*g*-/*g*-]	[*g*+/*g*+]	[*g*+/*g*+]	[*g*+/*g*+]	[*g*-/*g*-]

Table S1 (continued): List of all unique carvedilol conformations generated from the combination of low energy conformers in **Table 1** and conformation of subsequently optimized structures. Molecular conformation is displayed as [predicted torsional angle geometry/RHF/3-21G optimized torsional angle geometry] (explicit values of torsional angles are found in **Table S2**). (AS = annihilated structure, ‡ = additional conformations converged during carvedilol optimizations.)

Structure Code	Torsional Angle Conformation										
	χ_1	χ_2	χ_3	χ_4	χ_5	χ_6	χ_7	χ_8	χ_9	χ_{10}	χ_{11}
C-*R*-151	[*a*/AS]	[*g*-/AS]	[*a*/AS]	[*a*/AS]	[*g*+/AS]	[*a*/AS]	[*g*+/AS]	[*g*+/AS]	[*g*+/AS]	[*g*+/AS]	[*g*-/AS]
C-*R*-152	[*a*/AS]	[*g*-/AS]	[*a*/AS]	[*a*/AS]	[*g*+/AS]	[*a*/AS]	[*g*-/AS]	[*g*-/AS]	[*g*-/AS]	[*g*+/AS]	[*g*+/AS]
C-*R*-153	[*a*/AS]	[*g*-/AS]	[*a*/AS]	[*a*/AS]	[*g*+/AS]	[*a*/AS]	[*g*+/AS]	[*a*/AS]	[*g*-/AS]	[*g*+/AS]	[*a*/AS]
C-*R*-154	[*a*/*a*]	[*g*-/*g*-]	[*a*/*a*]	[*a*/*a*]	[*g*+/*g*+]	[*a*/*g*+]	[*g*-/*g*-]	[*a*/*a*]	[*g*+/*g*+]	[*g*+/*g*+]	[*a*/*a*]
C-*R*-155	[*a*/AS]	[*g*-/AS]	[*a*/AS]	[*a*/AS]	[*g*+/AS]	[*a*/AS]	[*g*+/AS]	[*g*-/AS]	[*g*-/AS]	[*g*+/AS]	[*g*+/AS]
C-*R*-156	[*a*/*a*]	[*g*-/*g*-]	[*a*/*a*]	[*a*/*a*]	[*g*+/*g*+]	[*a*/*a*]	[*g*-/*g*-]	[*g*+/*g*+]	[*g*+/*g*+]	[*g*+/*g*+]	[*g*-/*g*-]
C-*R*-157	[*a*/AS]	[*g*-/AS]	[*a*/AS]	[*a*/AS]	[*a*/AS]	[*g*-/AS]	[*g*+/AS]	[*g*+/AS]	[*g*+/AS]	[*g*+/AS]	[*g*-/AS]
C-*R*-158‡	[*a*/*a*]	[*g*-/*g*-]	[*a*/*a*]	[*a*/*a*]	[*a*/*a*]	[*g*-/*g*-]	[*g*-/*g*-]	[*g*-/*g*-]	[*g*-/*g*-]	[*g*+/*g*+]	[*g*+/*a*]
C-*R*-159	[*a*/AS]	[*g*-/AS]	[*a*/AS]	[*a*/AS]	[*a*/AS]	[*g*-/AS]	[*g*+/AS]	[*a*/AS]	[*g*-/AS]	[*g*+/AS]	[*a*/AS]
C-*R*-160	[*a*/AS]	[*g*-/AS]	[*a*/AS]	[*a*/AS]	[*a*/AS]	[*g*-/AS]	[*g*-/AS]	[*a*/AS]	[*g*+/AS]	[*g*+/AS]	[*a*/AS]
C-*R*-161	[*a*/AS]	[*g*-/AS]	[*a*/AS]	[*a*/AS]	[*a*/AS]	[*g*-/AS]	[*g*+/AS]	[*g*-/AS]	[*g*-/AS]	[*g*+/AS]	[*g*+/AS]
C-*R*-162	[*a*/AS]	[*g*-/AS]	[*a*/AS]	[*a*/AS]	[*a*/AS]	[*g*-/AS]	[*g*-/AS]	[*g*+/AS]	[*g*+/AS]	[*g*+/AS]	[*g*-/AS]
C-*R*-163	[*a*/AS]	[*g*-/AS]	[*a*/AS]	[*g*+/AS]	[*a*/AS]	[*a*/AS]	[*g*+/AS]	[*g*+/AS]	[*g*+/AS]	[*g*+/AS]	[*g*-/AS]
C-*R*-164	[*a*/AS]	[*g*-/AS]	[*a*/AS]	[*g*+/AS]	[*a*/AS]	[*a*/AS]	[*g*-/AS]	[*g*-/AS]	[*g*-/AS]	[*g*+/AS]	[*g*+/AS]
C-*R*-165	[*a*/AS]	[*g*-/AS]	[*a*/AS]	[*g*+/AS]	[*a*/AS]	[*a*/AS]	[*g*+/AS]	[*a*/AS]	[*g*-/AS]	[*g*+/AS]	[*a*/AS]
C-*R*-166	[*a*/*a*]	[*g*-/*g*-]	[*a*/*a*]	[*g*+/*g*+]	[*a*/*a*]	[*a*/*g*+]	[*g*-/*g*-]	[*a*/*a*]	[*g*+/*g*+]	[*g*+/*g*+]	[*a*/*a*]
C-*R*-167	[*a*/AS]	[*g*-/AS]	[*a*/AS]	[*g*+/AS]	[*a*/AS]	[*a*/AS]	[*g*+/AS]	[*g*-/AS]	[*g*-/AS]	[*g*+/AS]	[*g*+/AS]
C-*R*-168	[*a*/AS]	[*g*-/AS]	[*a*/AS]	[*g*+/AS]	[*a*/AS]	[*a*/AS]	[*g*-/AS]	[*g*+/AS]	[*g*+/AS]	[*g*+/AS]	[*g*-/AS]
C-*R*-169‡	[*a*/*g*-]	[*g*-/*a*]	[*a*/*a*]	[*a*/*a*]	[*a*/*a*]	[*g*+/*g*+]	[*g*+/*g*+]	[*g*+/*g*+]	[*g*+/*g*+]	[*g*+/*g*+]	[*g*-/*a*]
C-*R*-170	[*a*/*g*-]	[*g*-/*a*]	[*a*/*a*]	[*a*/*a*]	[*a*/*a*]	[*g*+/*g*+]	[*g*-/*g*-]	[*g*-/*g*-]	[*g*-/*g*-]	[*g*+/*g*+]	[*g*+/*g*+]
C-*R*-171	[*a*/*a*]	[*g*-/*g*-]	[*a*/*a*]	[*a*/*a*]	[*a*/*a*]	[*g*+/*g*+]	[*g*+/*g*+]	[*a*/*a*]	[*g*-/*g*-]	[*g*+/*g*+]	[*a*/*a*]
C-*R*-172	[*a*/AS]	[*g*-/AS]	[*a*/AS]	[*a*/AS]	[*a*/AS]	[*g*+/AS]	[*g*-*AS*/]	[*a*/AS]	[*g*+/AS]	[*g*+/AS]	[*a*/AS]
C-*R*-173	[*a*/AS]	[*g*-/AS]	[*a*/AS]	[*a*/AS]	[*a*/AS]	[*g*+/AS]	[*g*+/AS]	[*g*-/AS]	[*g*-/AS]	[*g*+/AS]	[*g*+/AS]
C-*R*-174	[*a*/AS]	[*g*-/AS]	[*a*/AS]	[*a*/AS]	[*a*/AS]	[*g*+/AS]	[*g*-/AS]	[*g*+/AS]	[*g*+/AS]	[*g*+/AS]	[*g*-/AS]
C-*R*-175	[*a*/*a*]	[*g*-/*g*-]	[*a*/*a*]	[*a*/*a*]	[*g*+/*g*+]	[*g*+/*g*+]	[*g*+/*g*+]	[*g*+/*g*+]	[*g*+/*g*+]	[*g*+/*g*+]	[*g*-/*g*-]

Table S1 (continued): List of all unique carvedilol conformations generated from the combination of low energy conformers in **Table 1** and conformation of subsequently optimized structures. Molecular conformation is displayed as [predicted torsional angle geometry/RHF/3-21G optimized torsional angle geometry] (explicit values of torsional angles are found in **Table S2**). (AS = annihilated structure, ‡ = additional conformations converged during carvedilol optimizations.)

Structure Code	Torsional Angle Conformation										
	χ_1	χ_2	χ_3	χ_4	χ_5	χ_6	χ_7	χ_8	χ_9	χ_{10}	χ_{11}
C-*R*-176	[*a*/AS]	[*g*-/AS]	[*a*/AS]	[*a*/AS]	[*g*+/AS]	[*g*+/AS]	[*g*-/AS]	[*g*-/AS]	[*g*-/AS]	[*g*+/AS]	[*g*+/AS]
C-*R*-177	[*a*/*a*]	[*g*-/*g*-]	[*a*/*a*]	[*a*/*a*]	[*g*+/*g*+]	[*g*+/*g*+]	[*g*+/*g*+]	[*a*/*a*]	[*g*-/*g*-]	[*g*+/*g*+]	[*a*/*a*]
C-*R*-178[a,b]	[*a*/*a*]	[*g*-/*g*-]	[*a*/*a*]	[*a*/*a*]	[*g*+/*g*+]	[*g*+/*g*+]	[*g*-/*g*-]	[*a*/*a*]	[*g*+/*g*+]	[*g*+/*g*+]	[*a*/*a*]
C-*R*-179	[*a*/AS]	[*g*-/AS]	[*a*/AS]	[*a*/AS]	[*g*+/AS]	[*g*+/AS]	[*g*+/AS]	[*g*-/AS]	[*g*-/AS]	[*g*+/AS]	[*g*+/AS]
C-*R*-180	[*a*/*g*-]	[*g*-/*a*]	[*a*/*a*]	[*a*/*a*]	[*g*+/*g*+]	[*g*+/*a*]	[*g*-/*g*-]	[*g*+/*a*]	[*g*+/*g*+]	[*g*+/*g*+]	[*g*-/*a*]
C-*R*-181	[*a*/AS]	[*g*-/AS]	[*a*/AS]	[*g*+/AS]	[*a*/AS]	[*g*+/AS]	[*g*+/AS]	[*g*+/AS]	[*g*+/AS]	[*g*+/AS]	[*g*-/AS]
C-*R*-182‡	[*a*/*g*-]	[*g*-/*a*]	[*a*/*a*]	[*g*+/*g*+]	[*a*/*a*]	[*g*+/*g*+]	[*g*-/*g*-]	[*g*-/*g*-]	[*g*-/*g*-]	[*g*+/*g*+]	[*g*+/*a*]
C-*R*-183	[*a*/*g*-]	[*g*-/*a*]	[*a*/*a*]	[*g*+/*g*+]	[*a*/*a*]	[*g*+/*g*+]	[*g*+/*g*+]	[*a*/*a*]	[*g*-/*g*-]	[*g*+/*g*+]	[*a*/*a*]
C-*R*-184	[*a*/*a*]	[*g*-/*g*-]	[*a*/*a*]	[*g*+/*g*+]	[*a*/*a*]	[*g*+/*g*+]	[*g*-/*g*-]	[*a*/*a*]	[*g*+/*g*+]	[*g*+/*g*+]	[*a*/*a*]
C-*R*-185	[*a*/AS]	[*g*-/AS]	[*a*/AS]	[*g*+/AS]	[*a*/AS]	[*g*+/AS]	[*g*+/AS]	[*g*-/AS]	[*g*-/AS]	[*g*+/AS]	[*g*+/AS]
C-*R*-186	[*a*/AS]	[*g*-/AS]	[*a*/AS]	[*g*+/AS]	[*a*/AS]	[*g*+/AS]	[*g*-/AS]	[*g*+/AS]	[*g*+/AS]	[*g*+/AS]	[*g*-/AS]
C-*R*-187	[*a*/*g*-]	[*g*-/*a*]	[*a*/*a*]	[*g*+/*g*+]	[*a*/*a*]	[*g*-/*g*-]	[*g*+/*g*+]	[*g*+/*g*+]	[*g*+/*g*+]	[*g*+/*g*+]	[*g*-/*g*-]
C-*R*-188	[*a*/*g*-]	[*g*-/*a*]	[*a*/*a*]	[*g*+/*g*+]	[*a*/*a*]	[*g*-/*g*-]	[*g*-/*g*-]	[*g*-/*g*-]	[*g*-/*g*-]	[*g*+/*g*+]	[*g*+/*g*+]
C-*R*-189	[*a*/AS]	[*g*-/AS]	[*a*/AS]	[*g*+/AS]	[*a*/AS]	[*g*-/AS]	[*g*+/AS]	[*a*/AS]	[*g*-/AS]	[*g*+/AS]	[*a*/AS]
C-*R*-190	[*a*/*a*]	[*g*-/*g*-]	[*a*/*a*]	[*g*+/*g*+]	[*a*/*a*]	[*g*-/*g*-]	[*g*-/*g*-]	[*a*/*a*]	[*g*+/*g*+]	[*g*+/*g*+]	[*a*/*a*]
C-*R*-191‡	[*a*/*g*-]	[*g*-/*a*]	[*a*/*a*]	[*g*+/*g*+]	[*a*/*a*]	[*g*-/*g*-]	[*g*+/*a*]	[*g*-/*g*-]	[*g*-/*g*-]	[*g*+/*g*+]	[*g*+/*g*+]
C-*R*-192‡	[*a*/*g*-]	[*g*-/*a*]	[*a*/*a*]	[*g*+/*a*]	[*a*/*a*]	[*g*-/*g*-]	[*g*-/*g*-]	[*g*+/*a*]	[*g*+/*g*+]	[*g*+/*g*+]	[*g*-/*g*-]
C-*R*-193	[*g*-/*g*-]	[*a*/*a*]	[*a*/*a*]	[*a*/*a*]	[*a*/*a*]	[*a*/*a*]	[*g*+/*g*+]	[*g*+/*g*+]	[*g*+/*g*+]	[*g*+/*g*+]	[*g*-/*g*-]
C-*R*-194	[*g*-/*g*-]	[*a*/*a*]	[*a*/*a*]	[*a*/*a*]	[*a*/*a*]	[*a*/*a*]	[*g*-/*g*-]	[*g*-/*g*-]	[*g*-/*g*-]	[*g*+/*g*+]	[*g*+/*g*+]
C-*R*-195	[*g*-/*g*-]	[*a*/*a*]	[*a*/*a*]	[*a*/*a*]	[*a*/*a*]	[*a*/*a*]	[*g*+/*g*+]	[*a*/*a*]	[*g*-/*g*-]	[*g*+/*g*+]	[*a*/*a*]
C-*R*-196	[*g*-/*g*-]	[*a*/*a*]	[*a*/*a*]	[*a*/*a*]	[*a*/*a*]	[*a*/*a*]	[*g*-/*g*-]	[*a*/*a*]	[*g*+/*g*+]	[*g*+/*g*+]	[*a*/*a*]
C-*R*-197	[*g*-/*g*-]	[*a*/*a*]	[*a*/*a*]	[*a*/*a*]	[*a*/*a*]	[*a*/*a*]	[*g*+/*g*+]	[*g*-/*g*-]	[*g*-/*g*-]	[*g*+/*g*+]	[*g*+/*g*+]
C-*R*-198	[*g*-/*g*-]	[*a*/*a*]	[*a*/*a*]	[*a*/*a*]	[*a*/*a*]	[*a*/*a*]	[*g*-/*g*-]	[*g*+/*g*+]	[*g*+/*g*+]	[*g*+/*g*+]	[*g*-/*g*-]
C-*R*-199	[*g*-/*g*-]	[*a*/*a*]	[*a*/*a*]	[*a*/*a*]	[*g*+/*g*+]	[*a*/*a*]	[*g*+/*g*+]	[*g*+/*g*+]	[*g*+/*g*+]	[*g*+/*g*+]	[*g*-/*g*-]
C-*R*-200	[*g*-/*g*-]	[*a*/*a*]	[*a*/*a*]	[*a*/*a*]	[*g*+/*g*+]	[*a*/*a*]	[*g*-/*g*-]	[*g*-/*g*-]	[*g*-/*g*-]	[*g*+/*g*+]	[*g*+/*g*+]

Table S1 (continued): List of all unique carvedilol conformations generated from the combination of low energy conformers in **Table 1** and conformation of subsequently optimized structures. Molecular conformation is displayed as [predicted torsional angle geometry/RHF/3-21G optimized torsional angle geometry] (explicit values of torsional angles are found in **Table S2**). (AS = annihilated structure, ‡ = additional conformations converged during carvedilol optimizations.)

Structure Code	Torsional Angle Conformation										
	χ_1	χ_2	χ_3	χ_4	χ_5	χ_6	χ_7	χ_8	χ_9	χ_{10}	χ_{11}
C-*R*-201	[*g*-/*g*-]	[*a*/*a*]	[*a*/*a*]	[*a*/*a*]	[*g*+/*g*+]	[*a*/*a*]	[*g*+/*g*+]	[*a*/*a*]	[*g*-/*g*-]	[*g*+/*g*+]	[*a*/*a*]
C-*R*-202	[*g*-/*g*-]	[*a*/*a*]	[*a*/*a*]	[*a*/*a*]	[*g*+/*g*+]	[*a*/*a*]	[*g*-/*g*-]	[*a*/*a*]	[*g*+/*g*+]	[*g*+/*g*+]	[*a*/*a*]
C-*R*-203	[*g*-/*g*-]	[*a*/*a*]	[*a*/*a*]	[*a*/*a*]	[*g*+/*g*+]	[*a*/*a*]	[*g*+/*g*+]	[*g*-/*g*-]	[*g*-/*g*-]	[*g*+/*g*+]	[*g*+/*g*+]
C-*R*-204	[*g*-/*g*-]	[*a*/*a*]	[*a*/*a*]	[*a*/*a*]	[*g*+/*g*+]	[*a*/*a*]	[*g*-/*g*-]	[*g*+/*g*+]	[*g*+/*g*+]	[*g*+/*g*+]	[*g*-/*g*-]
C-*R*-205	[*g*-/*g*-]	[*a*/*a*]	[*a*/*a*]	[*a*/*a*]	[*a*/*a*]	[*g*-/*a*]	[*g*+/*g*+]	[*g*+/*g*+]	[*g*+/*g*+]	[*g*+/*g*+]	[*g*-/*g*-]
C-*R*-206	[*g*-/*g*-]	[*a*/*a*]	[*a*/*a*]	[*a*/*a*]	[*a*/*a*]	[*g*-/*g*-]	[*g*-/*g*-]	[*g*-/*g*-]	[*g*-/*g*-]	[*g*+/*g*+]	[*g*+/*g*+]
C-*R*-207	[*g*-/*g*-]	[*a*/*a*]	[*a*/*a*]	[*a*/*a*]	[*a*/*a*]	[*g*-/*g*-]	[*g*+/*g*+]	[*a*/*a*]	[*g*-/*g*-]	[*g*+/*g*+]	[*a*/*a*]
C-*R*-208	[*g*-/*g*-]	[*a*/*a*]	[*a*/*a*]	[*a*/*a*]	[*a*/*a*]	[*g*-/*g*-]	[*g*-/*g*-]	[*a*/*a*]	[*g*+/*g*+]	[*g*+/*g*+]	[*a*/*a*]
C-*R*-209	[*g*-/AS]	[*a*/AS]	[*a*/AS]	[*a*/AS]	[*a*/AS]	[*g*-/AS]	[*g*+/AS]	[*g*-/AS]	[*g*-/AS]	[*g*+/AS]	[*g*+/AS]
C-*R*-210‡	[*g*-/*g*-]	[*a*/*a*]	[*a*/*a*]	[*a*/*a*]	[*a*/*a*]	[*g*-/*g*-]	[*g*-/*g*-]	[*g*+/*a*]	[*g*+/*g*+]	[*g*+/*g*+]	[*g*-/*g*-]
C-*R*-211	[*g*-/AS]	[*a*/AS]	[*a*/AS]	[*g*+/AS]	[*a*/AS]	[*a*/AS]	[*g*+/AS]	[*g*+/AS]	[*g*+/AS]	[*g*+/AS]	[*g*-/AS]
C-*R*-212	[*g*-/AS]	[*a*/AS]	[*a*/AS]	[*g*+/AS]	[*a*/AS]	[*a*/AS]	[*g*-/AS]	[*g*-/AS]	[*g*-/AS]	[*g*+/AS]	[*g*+/AS]
C-*R*-213	[*g*-/*g*-]	[*a*/*a*]	[*a*/*a*]	[*g*+/*g*+]	[*a*/*a*]	[*a*/*a*]	[*g*+/*g*+]	[*a*/*a*]	[*g*-/*g*-]	[*g*+/*g*+]	[*a*/*a*]
C-*R*-214	[*g*-/AS]	[*a*/AS]	[*a*/AS]	[*g*+/AS]	[*a*/AS]	[*a*/AS]	[*g*-/AS]	[*a*/AS]	[*g*+/AS]	[*g*+/AS]	[*a*/AS]
C-*R*-215	[*g*-/*g*-]	[*a*/*a*]	[*a*/*a*]	[*g*+/*g*+]	[*a*/*a*]	[*a*/*a*]	[*g*+/*g*+]	[*g*-/*a*]	[*g*-/*g*-]	[*g*+/*g*+]	[*g*+/*a*]
C-*R*-216	[*g*-/*g*-]	[*a*/*a*]	[*a*/*a*]	[*g*+/*g*+]	[*a*/*a*]	[*a*/*a*]	[*g*-/*g*-]	[*g*+/*g*+]	[*g*+/*g*+]	[*g*+/*g*+]	[*g*-/*g*-]
C-*R*-217	[*g*-/AS]	[*a*/AS]	[*a*/AS]	[*a*/AS]	[*a*/AS]	[*g*+/AS]	[*g*+/AS]	[*g*+/AS]	[*g*+/AS]	[*g*+/AS]	[*g*-/AS]
C-*R*-218	[*g*-/*g*-]	[*a*/*a*]	[*a*/*a*]	[*a*/*a*]	[*a*/*a*]	[*g*+/*g*+]	[*g*-/*g*-]	[*g*-/*g*-]	[*g*-/*g*-]	[*g*+/*g*+]	[*g*+/*g*+]
C-*R*-219	[*g*-/AS]	[*a*/AS]	[*a*/AS]	[*a*/AS]	[*a*/AS]	[*g*+/AS]	[*g*+/AS]	[*a*/AS]	[*g*-/AS]	[*g*+/AS]	[*a*/AS]
C-*R*-220	[*g*-/AS]	[*a*/AS]	[*a*/AS]	[*a*/AS]	[*a*/AS]	[*g*+/AS]	[*g*-/AS]	[*a*/AS]	[*g*+/AS]	[*g*+/AS]	[*a*/AS]
C-*R*-221	[*g*-/AS]	[*a*/AS]	[*a*/AS]	[*a*/AS]	[*a*/AS]	[*g*+/AS]	[*g*+/AS]	[*g*-/AS]	[*g*-/AS]	[*g*+/AS]	[*g*+/AS]
C-*R*-222	[*g*-/AS]	[*a*/AS]	[*a*/AS]	[*a*/AS]	[*a*/AS]	[*g*+/AS]	[*g*-/AS]	[*g*+/AS]	[*g*+/AS]	[*g*+/AS]	[*g*-/AS]
C-*R*-223	[*g*-/*g*-]	[*a*/*a*]	[*a*/*a*]	[*a*/*a*]	[*g*+/*g*+]	[*g*+/*g*+]	[*g*+/*g*+]	[*g*+/*g*+]	[*g*+/*g*+]	[*g*+/*g*+]	[*g*-/*g*-]
C-*R*-224	[*g*-/AS]	[*a*/AS]	[*a*/AS]	[*a*/AS]	[*g*+/AS]	[*g*+/AS]	[*g*-/AS]	[*g*-/AS]	[*g*-/AS]	[*g*+/AS]	[*g*+/AS]
C-*R*-225	[*g*-/*g*-]	[*a*/*a*]	[*a*/*a*]	[*a*/*a*]	[*g*+/*g*+]	[*g*+/*g*+]	[*g*+/*g*+]	[*a*/*a*]	[*g*-/*g*-]	[*g*+/*g*+]	[*a*/*a*]

Table S1 (continued): List of all unique carvedilol conformations generated from the combination of low energy conformers in **Table 1** and conformation of subsequently optimized structures. Molecular conformation is displayed as [predicted torsional angle geometry/RHF/3-21G optimized torsional angle geometry] (explicit values of torsional angles are found in **Table S2**). (AS = annihilated structure, ‡ = additional conformations converged during carvedilol optimizations.)

Structure Code	Torsional Angle Conformation										
	χ_1	χ_2	χ_3	χ_4	χ_5	χ_6	χ_7	χ_8	χ_9	χ_{10}	χ_{11}
C-*R*-226	[*g*-/*g*-]	[*a*/*a*]	[*a*/*a*]	[*a*/*a*]	[*g*+/*g*+]	[*g*+/*g*+]	[*g*-/*g*-]	[*a*/*a*]	[*g*+/*g*+]	[*g*+/*g*+]	[*a*/*a*]
C-*R*-227‡	[*g*-/*g*-]	[*a*/*a*]	[*a*/*a*]	[*a*/*a*]	[*g*+/*g*+]	[*g*+/*g*+]	[*g*+/*g*+]	[*g*-/*a*]	[*g*-/*g*-]	[*g*+/*g*+]	[*g*+/*g*+]
C-*R*-228‡	[*g*-/*g*-]	[*a*/*a*]	[*a*/*a*]	[*a*/*a*]	[*g*+/*g*+]	[*g*+/*g*+]	[*g*-/*a*]	[*g*+/*g*+]	[*g*+/*g*+]	[*g*+/*g*+]	[*g*-/*g*-]
C-*R*-229	[*g*-/AS]	[*a*/AS]	[*a*/AS]	[*g*+/AS]	[*a*/AS]	[*g*+/AS]	[*g*+/AS]	[*g*+/AS]	[*g*+/AS]	[*g*+/AS]	[*g*-/AS]
C-*R*-230	[*g*-/AS]	[*a*/AS]	[*a*/AS]	[*g*+/AS]	[*a*/AS]	[*g*+/AS]	[*g*-/AS]	[*g*-/AS]	[*g*-/AS]	[*g*+/AS]	[*g*+/AS]
C-*R*-231	[*g*-/*g*-]	[*a*/*a*]	[*a*/*a*]	[*g*+/*g*+]	[*a*/*a*]	[*g*+/*g*+]	[*g*+/*g*+]	[*a*/*a*]	[*g*-/*g*-]	[*g*+/*g*+]	[*a*/*a*]
C-*R*-232	[*g*-/AS]	[*a*/AS]	[*a*/AS]	[*g*+/AS]	[*a*/AS]	[*g*+/AS]	[*g*-/AS]	[*a*/AS]	[*g*+/AS]	[*g*+/AS]	[*a*/AS]
C-*R*-233	[*g*-/*g*-]	[*a*/*a*]	[*a*/*a*]	[*g*+/*g*+]	[*a*/*a*]	[*g*+/*g*+]	[*g*+/*g*+]	[*g*-/*g*-]	[*g*-/*g*-]	[*g*+/*g*+]	[*g*+/*g*+]
C-*R*-234	[*g*-/AS]	[*a*/AS]	[*a*/AS]	[*g*+/AS]	[*a*/AS]	[*g*+/AS]	[*g*-/AS]	[*g*+/AS]	[*g*+/AS]	[*g*+/AS]	[*g*-/AS]
C-*R*-235	[*g*-/*g*-]	[*a*/*a*]	[*a*/*a*]	[*g*+/*g*+]	[*a*/*a*]	[*g*-/*g*-]	[*g*+/*g*+]	[*g*+/*g*+]	[*g*+/*g*+]	[*g*+/*g*+]	[*g*-/*g*-]
C-*R*-236[a,b]	[*g*-/*g*-]	[*a*/*a*]	[*a*/*a*]	[*g*+/*g*+]	[*a*/*a*]	[*g*-/*g*-]	[*g*-/*g*-]	[*g*-/*g*-]	[*g*-/*g*-]	[*g*+/*g*+]	[*g*+/*g*+]
C-*R*-237	[*g*-/*g*-]	[*a*/*a*]	[*a*/*a*]	[*g*+/*g*+]	[*a*/*a*]	[*g*-/*g*-]	[*g*+/*g*+]	[*a*/*a*]	[*g*-/*g*-]	[*g*+/*g*+]	[*a*/*a*]
C-*R*-238	[*g*-/*g*-]	[*a*/*a*]	[*a*/*a*]	[*g*+/*g*+]	[*a*/*a*]	[*g*-/*g*-]	[*g*-/*g*-]	[*a*/*a*]	[*g*+/*g*+]	[*g*+/*g*+]	[*a*/*a*]
C-*R*-239‡	[*g*-/*g*-]	[*a*/*a*]	[*a*/*a*]	[*g*+/*g*+]	[*a*/*a*]	[*g*-/*g*-]	[*g*+/*a*]	[*g*-/*g*-]	[*g*-/*g*-]	[*g*+/*g*+]	[*g*+/*g*+]
C-*R*-240‡	[*g*-/*g*-]	[*a*/*a*]	[*a*/*a*]	[*g*+/*g*+]	[*a*/*g*-]	[*g*-/*g*-]	[*g*-/*g*-]	[*g*+/*a*]	[*g*+/*g*+]	[*g*+/*g*+]	[*g*-/*a*]
Additional Conformations Converged During Carvedilol Optimizations (indicated with ‡ on conformers C-*R*-1 to C-*R*-240)											
C-*R*-241	*a*	*a*	*a*	*a*	*a*	*a*	*g*-	*a*	*g*+	*g*+	*g*-
C-*R*-242	*g*+	*a*	*a*	*a*	*g*+	*a*	*g*+	*g*-	*g*-	*g*+	*g*+
C-*R*-243	*a*	*a*	*a*	*a*	*a*	*g*-	*g*-	*a*	*g*+	*g*+	*g*-
C-*R*-244	*g*-	*a*	*a*	*a*	*a*	*g*+	*g*+	*g*+	*g*+	*g*+	*a*
C-*R*-245	*g*-	*a*	*a*	*a*	*a*	*g*-	*g*-	*a*	*g*+	*g*+	*g*-
C-*R*-246	*g*+	*a*	*g*-	*g*+	*g*+	*a*	*g*-	*g*-	*g*-	*g*+	*g*+
C-*R*-247	*g*+	*a*	*g*-	*g*+	*g*+	*g*+	*g*-	*a*	*g*+	*g*+	*a*
C-*R*-248	*g*+	*a*	*g*-	*g*+	*a*	*a*	*g*+	*a*	*g*-	*g*+	*g*+
C-*R*-249	*g*+	*a*	*g*-	*g*+	*a*	*g*-	*g*-	*g*-	*g*-	*g*+	*g*+
C-*R*-250	*g*+	*a*	*g*-	*g*+	*a*	*g*-	*g*+	*a*	*g*-	*g*+	*a*

Table S1 (continued): List of all unique carvedilol conformations generated from the combination of low energy conformers in **Table 1** and conformation of subsequently optimized structures. Molecular conformation is displayed as [predicted torsional angle geometry/RHF/3-21G optimized torsional angle geometry] (explicit values of torsional angles are found in **Table S2**). (AS = annihilated structure, ‡ = additional conformations converged during carvedilol optimizations.)

Structure Code	Torsional Angle Conformation										
	χ_1	χ_2	χ_3	χ_4	χ_5	χ_6	χ_7	χ_8	χ_9	χ_{10}	χ_{11}
C-*R*-251	*g*+	*a*	*g*-	*g*+	*a*	*g*-	*g*-	*a*	*g*+	*g*+	*a*
C-*R*-252	*g*+	*a*	*g*-	*g*+	*a*	*g*-	*g*+	*g*-	*g*-	*g*+	*g*+
C-*R*-253	*a*	*a*	*a*	*a*	*g*+	*g*+	*g*+	*a*	*g*-	*g*+	*g*+
C-*R*-254	*g*-	*a*	*a*	*a*	*g*+	*g*+	*g*+	*a*	*g*-	*g*+	*g*+
C-*R*-255	*g*-	*a*	*a*	*a*	*g*+	*g*+	*a*	*g*+	*g*+	*g*+	*g*-
C-*R*-256	*a*	*a*	*a*	*g*+	*a*	*g*+	*g*-	*g*-	*g*-	*g*+	*a*
C-*R*-257	*a*	*a*	*a*	*g*+	*g*-	*g*-	*g*-	*a*	*g*+	*g*+	*g*-
C-*R*-258	*g*+	*a*	*g*-	*g*+	*g*+	*a*	*g*-	*g*+	*g*+	*g*+	*g*-
C-*R*-259	*g*+	*a*	*g*-	*a*	*a*	*g*+	*g*+	*g*+	*g*+	*g*+	*g*-
C-*R*-260	*a*	*a*	*g*-	*a*	*a*	*g*+	*g*+	*a*	*g*-	*g*-	*g*+
C-*R*-261	*a*	*a*	*g*-	*a*	*a*	*g*+	*g*+	*g*+	*g*+	*g*-	*a*
C-*R*-262	*a*	*a*	*g*-	*a*	*g*+	*a*	*g*-	*a*	*g*+	*g*-	*g*-
C-*R*-263	*g*-	*a*	*a*	*g*+	*a*	*g*+	*g*-	*g*-	*g*-	*g*+	*a*
C-*R*-264	*g*-	*a*	*a*	*g*+	*a*	*g*-	*a*	*g*-	*g*-	*g*+	*g*+
C-*R*-265	*g*-	*a*	*a*	*g*+	*g*-	*g*-	*g*-	*a*	*g*+	*g*+	*a*
C-*R*-266	*a*	*g*-	*a*	*a*	*a*	*g*-	*g*-	*g*-	*g*-	*g*+	*a*
C-*R*-267	*a*	*a*	*g*-	*a*	*a*	*g*-	*g*+	*g*+	*g*+	*g*-	*a*
C-*R*-268	*a*	*a*	*g*-	*a*	*a*	*g*-	*g*-	*a*	*g*+	*g*-	*g*-
C-*R*-269	*a*	*a*	*g*-	*a*	*g*+	*g*+	*g*-	*a*	*g*+	*g*-	*g*-
C-*R*-270	*a*	*a*	*g*-	*a*	*g*+	*g*+	*g*-	*g*-	*g*-	*g*-	*a*
C-*R*-271	*a*	*a*	*g*+	*a*	*a*	*g*+	*g*-	*a*	*g*+	*g*+	*a*
C-*R*-272	*g*+	*a*	*g*-	*g*+	*g*+	*g*+	*g*+	*g*+	*g*+	*g*+	*g*-
C-*R*-273	*g*+	*a*	*g*-	*g*+	*a*	*g*+	*g*+	*a*	*g*-	*g*+	*a*
C-*R*-274	*g*+	*a*	*g*-	*g*+	*a*	*g*+	*g*-	*a*	*g*+	*g*+	*a*
C-*R*-275	*g*+	*a*	*g*-	*g*+	*a*	*g*+	*g*-	*g*+	*g*+	*g*+	*g*-

Table S2: Optimized values for the converged conformers of the protonated carvedilol surface at the RHF/3-21G level of theory. (AS = annihilated structure, ‡ = additional conformations converged during carvedilol optimizations.)

Structure Code	Torsional Angle (degrees)											Energy (Hartree)	Relative Energy (Kcal•mol^{-1})
	χ_1	χ_2	χ_3	χ_4	χ_5	χ_6	χ_7	χ_8	χ_9	χ_{10}	χ_{11}		
C-*R*-1	AS												
C-*R*-2	176.11	178.93	-172.94	160.93	156.14	179.28	-44.92	-75.38	-74.69	44.41	111.75	-1325.33656263	9.80
C-*R*-3	AS												
C-*R*-4	175.02	-179.33	-170.75	163.91	-159.00	-165.32	-39.84	137.95	117.26	42.31	169.95	-1325.33730161	9.33
C-*R*-5	175.06	-179.47	-169.80	165.56	-162.47	-176.31	61.70	-115.64	-71.70	42.12	85.92	-1325.33899563	8.27
C-*R*-6	**NOT FOUND → MOVED TO C-*R*-241**												
C-*R*-7	175.07	-178.46	-171.27	156.76	52.40	166.74	45.33	68.80	69.75	37.90	-86.14	-1325.33149280	12.98
C-*R*-8	174.63	-178.57	-169.57	156.96	80.76	-176.72	-47.50	-66.67	-69.48	38.92	87.81	-1325.34028444	7.46
C-*R*-9	174.69	-178.72	-170.41	157.17	72.10	162.81	41.18	-139.27	-115.86	40.01	-171.14	-1325.33741540	9.26
C-*R*-10	**NOT FOUND → MOVED TO C-*R*-34[b]**												
C-*R*-11	**NOT FOUND → MOVED TO C-*R*-242**												
C-*R*-12	174.48	-178.45	-169.57	155.48	78.15	177.66	-61.87	116.20	71.83	38.43	-86.28	-1325.33880923	8.39
C-*R*-13	170.42	-177.20	-165.93	148.57	-140.80	-54.04	75.89	71.25	49.29	37.44	-81.77	-1325.32165616	19.15
C-*R*-14	174.94	-178.81	-170.43	163.22	-159.84	-55.30	-40.61	-78.12	-71.12	40.92	109.02	-1325.34017511	7.53
C-*R*-15	AS												
C-*R*-16	174.88	179.82	-170.52	161.69	-163.82	-69.50	-40.63	172.71	113.56	42.15	175.31	-1325.33589238	10.22
C-*R*-17	174.19	-178.71	-168.65	157.32	-155.44	-74.34	118.16	-93.38	-85.34	39.44	86.30	-1325.31585119	22.79
C-*R*-18	**NOT FOUND → MOVED TO C-*R*-243**												
C-*R*-19	AS												
C-*R*-20	-179.64	173.31	-162.76	81.40	161.69	-179.51	-48.22	-62.21	-67.19	40.40	81.77	-1325.34131424	6.82
C-*R*-21	176.14	-179.01	-169.30	74.76	155.65	166.79	39.57	-137.09	-117.48	43.80	-160.06	-1325.33684422	9.62
C-*R*-22	-179.52	172.74	-167.27	82.18	172.30	139.33	-57.21	147.22	99.74	50.46	167.65	-1325.34127652	6.84
C-*R*-23	-176.42	171.85	-175.19	57.79	147.04	170.97	62.29	-109.81	-74.75	46.51	85.14	-1325.32975460	14.07
C-*R*-24	AS												
C-*R*-25	AS												

Table S2 (continued): Optimized values for the converged conformers of the protonated carvedilol surface at the RHF/3-21G level of theory. (AS = annihilated structure, ‡ = additional conformations converged during carvedilol optimizations.)

Structure Code	Torsional Angle (degrees)											Energy (Hartree)	Relative Energy (Kcal•mol^{-1})
	χ_1	χ_2	χ_3	χ_4	χ_5	χ_6	χ_7	χ_8	χ_9	χ_{10}	χ_{11}		
C-*R*-26	173.84	178.85	-161.47	160.30	-165.53	84.36	-60.16	-76.30	-28.09	34.53	77.64	-1325.32316078	18.21
C-*R*-27	AS												
C-*R*-28	179.10	174.05	-167.36	157.52	-164.35	61.24	-77.30	169.60	108.29	44.85	164.80	-1325.32907821	14.49
C-*R*-29	AS												
C-*R*-30	AS												
C-*R*-31	174.82	-178.51	-169.94	157.25	68.43	55.06	39.58	78.37	71.40	38.99	-104.57	-1325.33855993	8.54
C-*R*-32	AS												
C-*R*-33	AS												
C-*R*-34[a]	174.70	-178.76	-168.62	156.17	69.17	51.29	-75.74	174.93	108.81	38.90	179.81	-1325.32975320	14.07
C-*R*-34[b]	175.12	-179.35	-169.90	159.90	83.14	99.10	-46.78	141.84	111.27	40.46	174.28	-1325.34038180	7.40
C-*R*-35	**NOT FOUND → MOVED TO C-*R*-253**												
C-*R*-36	AS												
C-*R*-37	AS												
C-*R*-38	**NOT FOUND → MOVED TO C-*R*-256**												
C-*R*-39	175.36	179.87	-169.69	78.53	160.42	70.10	40.87	-172.39	-113.01	44.32	-173.50	-1325.33579273	10.28
C-*R*-40	AS												
C-*R*-41	174.25	-179.87	-166.49	80.39	153.01	74.38	59.44	-120.0[α]	-69.72	41.40	87.96	-1325.34110387	6.95
C-*R*-42	AS												
C-*R*-43	176.01	-179.66	-168.43	82.82	154.73	-75.60	68.96	71.93	37.19	43.34	-81.04	-1325.31942856	20.55
C-*R*-44	AS												
C-*R*-45	175.29	-178.59	-167.49	78.96	166.36	-62.02	77.04	139.57	-109.55	39.59	-179.06	-1325.32755241	15.45
C-*R*-46	176.76	179.50	-171.15	81.93	176.16	-65.81	-38.46	172.26	115.96	47.08	178.74	-1325.32884950	14.64
C-*R*-47	AS												
C-*R*-48	**NOT FOUND → MOVED TO C-*R*-257**												
C-*R*-49	**NOT FOUND → MOVED TO C-*R*-55**												
C-*R*-50	**NOT FOUND → MOVED TO C-*R*-56[a]**												

[α] Dihedral value is actually -120.03° which according to the systematic nomenclature used is in the *anti* position, however, in this case it can be rationalized that this should be a *g-* position based on the optimized conformation of the full structure.

Table S2 (continued): Optimized values for the converged conformers of the protonated carvedilol surface at the RHF/3-21G level of theory. (AS = annihilated structure, ‡ = additional conformations converged during carvedilol optimizations.)

Structure Code	Torsional Angle (degrees)											Energy (Hartree)	Relative Energy (Kcal•mol^{-1})
	χ_1	χ_2	χ_3	χ_4	χ_5	χ_6	χ_7	χ_8	χ_9	χ_{10}	χ_{11}		
C-*R*-51	AS												
C-*R*-52	**NOT FOUND → MOVED TO C-*R*-58**												
C-*R*-53	**NOT FOUND → MOVED TO C-*R*-59**												
C-*R*-54	AS												
C-*R*-55	-148.00	147.55	-70.46	159.18	-156.64	179.12	47.68	65.88	69.42	-16.81	-86.02	-1325.34489295	4.57
C-*R*-56[a]	161.36	-176.49	-68.63	164.62	166.81	-176.98	-49.11	-66.75	-72.35	-25.90	81.62	-1325.34053933	7.30
C-*R*-56[b]	-163.21	170.91	-65.60	164.36	-176.94	-165.70	-46.23	-74.82	-74.01	-32.26	96.09	-1325.34082052	7.13
C-*R*-57	-172.41	170.47	-69.40	160.61	-173.01	-148.67	58.69	-146.17	-97.45	-18.15	-174.33	-1325.34440003	4.88
C-*R*-58	-153.03	151.46	-70.10	158.43	-153.27	-169.06	-39.07	137.03	118.60	-17.07	168.71	-1325.34119637	6.89
C-*R*-59	-149.35	148.44	-70.11	160.21	-155.10	-177.93	62.23	-114.60	-72.07	-16.92	84.29	-1325.34297259	5.78
C-*R*-60	AS												
C-*R*-61	**NOT FOUND → MOVED TO C-*R*-67**												
C-*R*-62	**NOT FOUND → MOVED TO C-*R*-68**												
C-*R*-63	**NOT FOUND → MOVED TO C-*R*-69**												
C-*R*-64	**NOT FOUND → MOVED TO C-*R*-70**												
C-*R*-65	AS												
C-*R*-66	**NOT FOUND → MOVED TO C-*R*-262**												
C-*R*-67	168.74	-177.86	-68.51	157.82	49.50	169.82	44.98	69.13	68.99	-27.27	-79.10	-1325.33831397	8.70
C-*R*-68	-170.69	167.17	-69.16	156.31	86.26	-176.65	-46.48	-69.10	-70.20	-17.57	96.05	-1325.34476902	4.65
C-*R*-69	-163.34	163.46	-68.09	153.85	89.13	162.36	41.88	-139.09	-114.97	-19.50	-177.99	-1325.34202754	6.37
C-*R*-70	-174.16	168.43	-69.47	159.08	76.05	147.40	-60.67	146.16	91.04	-15.04	-170.56	-1325.34263072	5.99
C-*R*-71	AS												
C-*R*-72	-178.27	175.94	-68.45	156.31	85.29	179.42	-62.00	114.75	72.16	-19.75	-87.33	-1325.34212245	6.31
C-*R*-73	AS												
C-*R*-74	**NOT FOUND → MOVED TO C-*R*-80**												
C-*R*-75	**NOT FOUND → MOVED TO C-*R*-57**												

Table S2 (continued): Optimized values for the converged conformers of the protonated carvedilol surface at the RHF/3-21G level of theory. (AS = annihilated structure, ‡ = additional conformations converged during carvedilol optimizations.)

Structure Code	Torsional Angle (degrees)											Energy (Hartree)	Relative Energy (Kcal•mol^{-1})
	χ_1	χ_2	χ_3	χ_4	χ_5	χ_6	χ_7	χ_8	χ_9	χ_{10}	χ_{11}		
C-*R*-76	**NOT FOUND → MOVED TO C-*R*-82**												
C-*R*-77	**NOT FOUND → MOVED TO C-*R*-83**												
C-*R*-78	AS												
C-*R*-79	**NOT FOUND → MOVED TO C-*R*-267**												
C-*R*-80	-149.85	149.25	-70.22	158.90	-154.80	-56.43	-41.09	-77.53	-70.90	-17.27	107.65	-1325.34437162	4.90
C-*R*-81	**NOT FOUND → MOVED TO C-*R*-57**												
C-*R*-82	-148.43	149.03	-69.70	159.00	-157.78	-69.39	-42.01	173.15	113.57	-17.31	173.57	-1325.34005125	7.61
C-*R*-83	-178.65	174.07	-69.94	158.93	-154.82	-75.51	120.[β]	-92.12	-88.70	-17.57	97.04	-1325.32008027	20.14
C-*R*-84	AS												
C-*R*-85	AS												
C-*R*-86	**NOT FOUND → MOVED TO C-*R*-246**												
C-*R*-87	AS												
C-*R*-88	**NOT FOUND → MOVED TO C-*R*-247**												
C-*R*-89	**NOT FOUND → MOVED TO C-*R*-248**												
C-*R*-90	AS												
C-*R*-91	AS												
C-*R*-92	**NOT FOUND → MOVED TO C-*R*-246**												
C-*R*-93	AS												
C-*R*-94	AS												
C-*R*-95	AS												
C-*R*-96	**NOT FOUND → MOVED TO C-*R*-258**												
C-*R*-97	**NOT FOUND → MOVED TO C-*R*-259**												
C-*R*-98	AS												
C-*R*-99	**NOT FOUND → MOVED TO C-*R*-260**												
C-*R*-100	**NOT FOUND → MOVED TO C-*R*-106**												

[β]Dihedral value is actually 120.98° which according to the systematic nomenclature used is in the *anti* position, however, in this case it can be rationalized that this should be a *g*+ position based on the optimized conformation of the full structure.

Table S2 (continued): Optimized values for the converged conformers of the protonated carvedilol surface at the RHF/3-21G level of theory. (AS = annihilated structure, ‡ = additional conformations converged during carvedilol optimizations.)

Structure Code	Torsional Angle (degrees)											Energy (Hartree)	Relative Energy (Kcal•mol^{-1})
	χ_1	χ_2	χ_3	χ_4	χ_5	χ_6	χ_7	χ_8	χ_9	χ_{10}	χ_{11}		
C-*R*-101	**NOT FOUND → MOVED TO C-*R*-59**												
C-*R*-102	**NOT FOUND → MOVED TO C-*R*-108**												
C-*R*-103	**NOT FOUND → MOVED TO C-*R*-261**												
C-*R*-104	AS												
C-*R*-105	AS												
C-*R*-106	163.30	-170.16	-76.82	161.22	-175.31	34.20	-71.83	179.81	113.86	-10.41	179.40	-1325.32774747	15.33
C-*R*-107	**NOT FOUND → MOVED TO C-*R*-59**												
C-*R*-108	-177.54	170.63	-70.95	160.49	-164.55	67.22	-120[γ]	71.59	81.72	-13.21	-76.76	-1325.31939644	20.57
C-*R*-109	**NOT FOUND → MOVED TO C-*R*-115**												
C-*R*-110	AS												
C-*R*-111	**NOT FOUND → MOVED TO C-*R*-117[a]**												
C-*R*-112	**NOT FOUND → MOVED TO C-*R*-118[a]**												
C-*R*-113	**NOT FOUND → MOVED TO C-*R*-117[b]**												
C-*R*-114	**NOT FOUND → MOVED TO C-*R*-269**												
C-*R*-115	-166.35	166.08	-68.30	158.08	84.95	60.77	38.22	78.95	70.38	-19.02	-103.61	-1325.34317130	5.65
C-*R*-116	**NOT FOUND → MOVED TO C-*R*-270**												
C-*R*-117[a]	-176.95	171.02	-69.53	157.54	84.58	89.02	58.35	-143.02	-82.15	-15.72	159.26	-1325.34239334	6.14
C-*R*-117[b]	-178.38	170.98	-70.24	155.72	85.98	84.34	57.32	-134.94	-76.32	-15.25	120.74	-1325.34166172	6.60
C-*R*-118[a]	-174.80	172.48	-69.00	159.12	72.25	47.86	-76.47	176.20	109.18	-16.23	-179.56	-1325.33302263	12.02
C-*R*-118[b]	-170.18	164.72	-70.48	156.23	84.55	100.23	-48.93	143.52	103.40	-14.55	-170.80	-1325.34386266	5.22
C-*R*-119	-170.62	-178.86	-64.72	155.44	99.56	75.04	57.75	-115.10	-69.97	-27.72	82.26	-1325.34138347	6.77
C-*R*-120	**NOT FOUND → MOVED TO C-*R*-269**												
C-*R*-121	**NOT FOUND → MOVED TO C-*R*-272**												
C-*R*-122	AS												
C-*R*-123	**NOT FOUND → MOVED TO C-*R*-273**												
C-*R*-124	**NOT FOUND → MOVED TO C-*R*-274**												
C-*R*-125	AS												

[γ]Dihedral value is actually -120.18° which according to the systematic nomenclature used is in the *anti* position, however, in this case it can be rationalized that this should be a *g-* position based on the optimized conformation of the full structure.

Table S2 (continued): Optimized values for the converged conformers of the protonated carvedilol surface at the RHF/3-21G level of theory. (AS = annihilated structure, ‡ = additional conformations converged during carvedilol optimizations.)

Structure Code	Torsional Angle (degrees)											Energy (Hartree)	Relative Energy (Kcal•mol^{-1})
	χ_1	χ_2	χ_3	χ_4	χ_5	χ_6	χ_7	χ_8	χ_9	χ_{10}	χ_{11}		
C-*R*-126	**NOT FOUND → MOVED TO C-*R*-275**												
C-*R*-127	AS												
C-*R*-128	AS												
C-*R*-129	**NOT FOUND → MOVED TO C-*R*-273**												
C-*R*-130	**NOT FOUND → MOVED TO C-*R*-274**												
C-*R*-131	AS												
C-*R*-132	**NOT FOUND → MOVED TO C-*R*-275**												
C-*R*-133	AS												
C-*R*-134	**NOT FOUND → MOVED TO C-*R*-249**												
C-*R*-135	**NOT FOUND → MOVED TO C-*R*-250**												
C-*R*-136	**NOT FOUND → MOVED TO C-*R*-251**												
C-*R*-137	**NOT FOUND → MOVED TO C-*R*-252**												
C-*R*-138	AS												
C-*R*-139	AS												
C-*R*-140	**NOT FOUND → MOVED TO C-*R*-249**												
C-*R*-141	AS												
C-*R*-142	**NOT FOUND → MOVED TO C-*R*-251**												
C-*R*-143	**NOT FOUND → MOVED TO C-*R*-252**												
C-*R*-144	AS												
C-*R*-145	AS												
C-*R*-146	AS												
C-*R*-147	**NOT FOUND → MOVED TO C-*R*-195**												
C-*R*-148	-166.73	-97.78	-166.81	162.23	-158.42	-165.90	-39.94	137.94	117.56	43.42	169.68	-1325.33436565	11.18
C-*R*-149	133.56	-70.46	-172.48	166.09	-161.45	-176.91	61.64	-115.31	-71.62	58.35	85.64	-1325.33590200	10.21
C-*R*-150	130.12	-68.74	-174.56	178.95	177.35	175.70	-71.19	120[δ]	82.84	63.97	-105.50	-1325.32826087	15.01

[δ]Dihedral value is actually 121.24° which according to the systematic nomenclature used is in the *anti* position, however, in this case it can be rationalized that this should be a *g*+ position based on the optimized conformation of the full structure.

Table S2 (continued): Optimized values for the converged conformers of the protonated carvedilol surface at the RHF/3-21G level of theory. (AS = annihilated structure, ‡ = additional conformations converged during carvedilol optimizations.)

Structure Code	Torsional Angle (degrees)											Energy (Hartree)	Relative Energy (Kcal•mol^{-1})
	χ_1	χ_2	χ_3	χ_4	χ_5	χ_6	χ_7	χ_8	χ_9	χ_{10}	χ_{11}		
C-*R*-151	AS												
C-*R*-152	AS												
C-*R*-153	AS												
C-*R*-154	**NOT FOUND → MOVED TO C-*R*-178[b]**												
C-*R*-155	AS												
C-*R*-156	-165.42	-98.18	-165.54	154.19	77.55	177.55	-61.93	116.35	72.03	39.18	-86.24	-1325.33619706	10.03
C-*R*-157	AS												
C-*R*-158	**NOT FOUND → MOVED TO C-*R*-266**												
C-*R*-159	AS												
C-*R*-160	AS												
C-*R*-161	AS												
C-*R*-162	AS												
C-*R*-163	AS												
C-*R*-164	AS												
C-*R*-165	AS												
C-*R*-166	**NOT FOUND → MOVED TO C-*R*-184**												
C-*R*-167	AS												
C-*R*-168	AS												
C-*R*-169	**NOT FOUND → MOVED TO C-*R*-244**												
C-*R*-170	**NOT FOUND → MOVED TO C-*R*-218**												
C-*R*-171	-162.76	-99.02	-164.39	150.96	-168.36	63.19	37.54	-172.72	-114.19	37.97	-167.30	-1325.32892248	14.59
C-*R*-172	AS												
C-*R*-173	AS												
C-*R*-174	AS												
C-*R*-175	-171.17	-94.78	-166.66	155.51	67.79	55.04	39.52	78.32	71.42	40.19	-104.56	-1325.33585267	10.24

Table S2 (continued): Optimized values for the converged conformers of the protonated carvedilol surface at the RHF/3-21G level of theory. (AS = annihilated structure, ‡ = additional conformations converged during carvedilol optimizations.)

Structure Code	Torsional Angle (degrees)											Energy (Hartree)	Relative Energy (Kcal•mol^{-1})
	χ_1	χ_2	χ_3	χ_4	χ_5	χ_6	χ_7	χ_8	χ_9	χ_{10}	χ_{11}		
C-*R*-176	AS												
C-*R*-177	-163.29	-99.05	-165.68	155.56	71.82	64.89	37.47	-173.45	-114.85	40.05	-178.78	-1325.33035988	13.69
C-*R*-178[a]	-158.56	-100.55	-165.26	155.85	69.07	50.64	-76.00	175.21	108.58	39.91	179.75	-1325.32774081	15.33
C-*R*-178[b]	-169.44	-95.66	-166.31	158.70	83.08	98.97	-46.83	141.74	111.46	41.40	174.12	-1325.33771307	9.08
C-*R*-179	AS												
C-*R*-180	**NOT FOUND → MOVED TO C-*R*-202**												
C-*R*-181	AS												
C-*R*-182	**NOT FOUND → MOVED TO C-*R*-263**												
C-*R*-183	**NOT FOUND → MOVED TO C-*R*-231**												
C-*R*-184	125.44	-69.29	-172.62	90.45	174.79	114.08	-49.51	144.84	102.45	73.00	176.02	-1325.33798249	8.91
C-*R*-185	AS												
C-*R*-186	AS												
C-*R*-187	**NOT FOUND → MOVED TO C-*R*-235**												
C-*R*-188	**NOT FOUND → MOVED TO C-*R*-236**												
C-*R*-189	AS												
C-*R*-190	125.31	-67.99	-174.57	82.76	175.86	-65.42	-38.81	172.58	115.84	72.80	178.51	-1325.32594257	16.46
C-*R*-191	**NOT FOUND → MOVED TO C-*R*-264**												
C-*R*-192	**NOT FOUND → MOVED TO C-*R*-245**												
C-*R*-193	-82.32	176.52	-162.12	164.47	-164.03	179.62	47.68	66.07	69.47	45.71	-86.98	-1325.34246477	6.09
C-*R*-194	-82.26	177.49	-165.34	168.75	158.09	-175.33	-46.01	-73.73	-74.50	46.60	104.55	-1325.33755830	9.17
C-*R*-195	-82.42	176.03	-160.03	160.67	-175.46	-141.11	58.65	-145.75	-98.90	39.04	-175.13	-1325.34260973	6.00
C-*R*-196	-81.99	176.49	-162.99	164.44	-158.80	-165.97	-39.65	137.71	117.62	47.86	169.19	-1325.33897668	8.28
C-*R*-197	-82.32	176.60	-162.13	166.19	-162.83	-176.81	61.45	-115.08	-71.47	47.34	85.60	-1325.34077087	7.16
C-*R*-198	-81.88	176.12	-163.95	-176.15	-174.45	-179.88	-69.00	117.97	80.68	48.80	-99.82	-1325.33323818	11.88
C-*R*-199	-79.67	170.15	-159.10	148.77	54.72	170.35	44.71	68.06	68.04	40.58	-80.48	-1325.33436532	11.18
C-*R*-200	-82.57	176.93	-162.42	157.99	80.75	-176.79	-47.44	-66.96	-69.60	44.78	88.58	-1325.34179925	6.51

Table S2 (continued): Optimized values for the converged conformers of the protonated carvedilol surface at the RHF/3-21G level of theory. (AS = annihilated structure, ‡ = additional conformations converged during carvedilol optimizations.)

Structure Code	Torsional Angle (degrees)											Energy (Hartree)	Relative Energy (Kcal•mol^{-1})
	χ_1	χ_2	χ_3	χ_4	χ_5	χ_6	χ_7	χ_8	χ_9	χ_{10}	χ_{11}		
C-*R*-201	-82.06	176.63	-162.71	158.25	72.47	162.48	41.23	-139.37	-115.65	45.66	-171.70	-1325.33909482	8.21
C-*R*-202	-81.56	175.98	-161.93	164.32	75.10	-177.75	-41.68	141.03	115.49	43.95	175.57	-1325.34024838	7.49
C-*R*-203	-81.56	176.86	-164.13	163.15	51.70	172.00	62.39	-108.94	-74.41	45.06	84.81	-1325.33550294	10.46
C-*R*-204	-82.34	177.09	-162.28	157.01	78.01	177.07	-62.14	116.64	72.19	44.19	-86.79	-1325.34031884	7.44
C-*R*-205	**NOT FOUND → MOVED TO C-*R*-193**												
C-*R*-206	-82.14	176.51	-162.87	163.53	-159.52	-55.48	-40.63	-78.25	-71.18	46.59	104.97	-1325.34178842	6.52
C-*R*-207	-82.30	175.86	-161.29	159.00	176.87	-106.53	48.26	-142.84	-100.95	40.09	176.18	-1325.34323892	5.61
C-*R*-208	-81.89	176.60	-162.50	163.11	-163.81	-69.18	-40.45	172.73	113.71	46.99	174.82	-1325.33775809	9.05
C-*R*-209	AS												
C-*R*-210	**NOT FOUND → MOVED TO C-*R*-245**												
C-*R*-211	AS												
C-*R*-212	AS												
C-*R*-213	-78.78	167.10	-153.23	71.31	-142.68	-154.67	64.15	-145.00	-90.75	44.23	160.90	-1325.33734984	9.30
C-*R*-214	AS												
C-*R*-215	**NOT FOUND → MOVED TO C-*R*-213**												
C-*R*-216	-96.96	-175.16	-168.53	77.00	156.69	174.41	-61.88	118.27	72.12	53.47	-86.52	-1325.34237096	6.15
C-*R*-217	AS												
C-*R*-218	-90.33	178.81	-160.87	160.19	-167.68	77.40	-63.55	-69.59	-30.71	45.43	81.41	-1325.32499472	17.06
C-*R*-219	AS												
C-*R*-220	AS												
C-*R*-221	AS												
C-*R*-222	AS												
C-*R*-223	-82.03	176.40	-162.21	157.81	68.60	55.07	39.52	78.30	71.34	44.43	-104.14	-1325.34016255	7.54
C-*R*-224													
C-*R*-225	-81.76	176.66	-162.52	157.82	72.15	64.98	37.49	-173.23	-115.12	44.87	-178.55	-1325.33473594	10.94

Table S2 (continued): Optimized values for the converged conformers of the protonated carvedilol surface at the RHF/3-21G level of theory. (AS = annihilated structure, ‡ = additional conformations converged during carvedilol optimizations.)

Structure Code	Torsional Angle (degrees)											Energy (Hartree)	Relative Energy (Kcal•mol^{-1})
	χ_1	χ_2	χ_3	χ_4	χ_5	χ_6	χ_7	χ_8	χ_9	χ_{10}	χ_{11}		
C-*R*-226	-82.84	176.85	-161.08	156.99	69.23	51.24	-75.94	174.87	108.62	44.28	-179.65	-1325.33144884	13.01
C-*R*-227	**NOT FOUND → MOVED TO C-*R*-254**												
C-*R*-228	**NOT FOUND → MOVED TO C-*R*-255**												
C-*R*-229	AS												
C-*R*-230	AS												
C-*R*-231	-84.35	179.11	-164.56	78.27	162.42	69.13	40.42	-172.79	-113.35	50.35	-174.24	-1325.33722200	9.38
C-*R*-232	AS												
C-*R*-233	-89.62	-179.83	-164.10	78.91	153.41	73.00	60.20	-119.40	-71.14	50.43	91.62	-1325.34494952	4.54
C-*R*-234	AS												
C-*R*-235	-79.33	174.85	-158.79	81.39	166.41	-82.79	64.52	75.84	35.52	47.68	-80.07	-1325.32208063	18.89
C-*R*-236[a]	-78.76	171.21	-157.77	78.75	-159.46	-51.60	-40.65	-78.88	-74.02	45.02	116.86	-1325.34000063	7.64
C-*R*-236[b]	-78.24	166.00	-152.26	72.33	-160.77	-56.76	-42.77	-76.99	-73.22	41.88	106.67	-1325.34005475	7.61
C-*R*-237	-81.44	174.92	-161.32	81.87	-142.80	-99.61	49.23	-143.04	-98.90	48.57	162.67	-1325.33806916	8.85
C-*R*-238	-77.73	171.83	-158.31	79.89	-179.61	-66.87	-38.90	172.41	115.52	49.65	178.91	-1325.33288212	12.11
C-*R*-239	**NOT FOUND → MOVED TO C-*R*-264**												
C-*R*-240	**NOT FOUND → MOVED TO C-*R*-265**												
C-*R*-241‡	175.98	178.37	-172.29	177.26	172.82	172.91	-70.92	123.30	83.03	44.80	-109.91	-1325.33124789	13.13
C-*R*-242‡	104.22	-175.53	-170.88	164.89	87.61	-161.96	108.07	-72.98	-82.59	53.40	78.28	-1325.31904046	20.79
C-*R*-243‡	174.84	-179.03	-169.48	165.65	-166.23	-76.62	-56.77	125.41	70.86	40.43	-99.30	-1325.33952359	7.94
C-*R*-244‡	-81.01	174.66	-161.66	164.95	166.03	53.01	38.10	86.36	78.87	42.01	-150.57	-1325.33863489	8.50
C-*R*-245‡	-81.88	176.11	-161.85	166.08	-165.78	-77.14	-56.96	125.60	70.92	46.17	-98.30	-1325.34126300	6.85
C-*R*-246‡	107.18	-170.32	-52.20	67.57	88.63	-173.38	-49.09	-66.13	-69.97	70.21	83.62	-1325.35188899	0.18
C-*R*-247‡	101.70	-170.50	-51.00	69.07	86.67	98.50	-46.98	142.71	110.99	70.87	172.91	-1325.35131606	0.54
C-*R*-248‡	96.77	-166.66	-48.97	67.20	-165.27	-168.20	67.84	-131.67	-81.27	59.94	106.32	-1325.34862475	2.23
C-*R*-249‡	98.61	-171.08	-49.55	72.36	-158.80	-51.98	-43.52	-76.09	-73.32	64.92	104.49	-1325.35217719	**0.00**
C-*R*-250‡	93.44	-173.16	-48.64	74.73	-169.46	-99.72	47.43	-141.85	-115.34	81.41	178.02	-1325.35170537	0.30

Table S2 (continued): Optimized values for the converged conformers of the protonated carvedilol surface at the RHF/3-21G level of theory. (AS = annihilated structure, ‡ = additional conformations converged during carvedilol optimizations.)

Structure Code	Torsional Angle (degrees)											Energy (Hartree)	Relative Energy (Kcal•mol^{-1})
	χ_1	χ_2	χ_3	χ_4	χ_5	χ_6	χ_7	χ_8	χ_9	χ_{10}	χ_{11}		
C-*R*-251‡	94.83	-172.31	-46.48	75.22	-176.68	-64.80	-40.31	173.62	114.99	78.04	176.41	-1325.34861944	2.23
C-*R*-252‡	94.83	-172.77	-46.52	74.54	-174.85	-70.96	177.70	-91.28	-85.78	74.46	83.70	-1325.33233526	12.45
C-*R*-253‡	174.59	-178.87	-169.97	157.41	84.08	80.03	58.63	-125.26	-72.37	39.87	97.31	-1325.33794442	8.93
C-*R*-254‡	-82.38	177.10	-162.83	158.93	83.98	79.50	58.60	-124.52	-72.18	45.71	96.78	-1325.33937219	8.04
C-*R*-255‡	-82.15	177.09	-161.30	158.95	82.03	74.85	-127.56	83.89	84.56	46.59	-81.25	-1325.31939201	20.57
C-*R*-256‡	175.60	-179.48	-168.57	83.24	145.50	72.07	-56.54	-109.06	-99.62	42.53	177.70	-1325.32868252	14.74
C-*R*-257‡	176.03	-179.86	-170.65	89.13	-103.95	-82.28	-58.26	132.80	75.37	43.14	-112.19	-1325.33510778	10.71
C-*R*-258‡	100.47	-171.04	-53.00	65.92	86.99	-179.52	-63.40	113.39	72.09	71.84	-82.95	-1325.34987568	1.44
C-*R*-259‡	93.51	-174.04	-46.86	167.88	155.27	53.66	42.63	76.71	73.51	62.74	-105.35	-1325.33564955	10.37
C-*R*-260‡	-157.10	166.50	-62.91	165.15	169.69	97.79	67.52	-141.27	-88.28	-38.62	113.37	-1325.33545122	10.50
C-*R*-261‡	-172.43	178.38	-63.73	168.07	-173.52	66.50	44.36	78.89	75.16	-33.45	-141.72	-1325.34276287	5.91
C-*R*-262‡	-166.98	172.11	-66.53	156.85	89.25	168.36	-61.06	130.66	74.18	-23.20	-108.03	-1325.34206269	6.35
C-*R*-263‡	-82.63	178.30	-162.29	82.14	150.61	69.48	-59.14	-106.49	-97.73	47.67	176.64	-1325.33059355	13.54
C-*R*-264‡	-85.13	-179.09	-163.96	81.69	137.68	-72.95	131.21	-79.09	-84.29	49.90	77.71	-1325.31623124	22.56
C-*R*-265‡	-81.74	178.07	-163.80	88.31	-102.67	-84.63	-57.77	138.16	77.70	47.79	-140.65	-1325.33735855	9.30
C-*R*-266‡	-169.00	-95.78	-166.44	161.77	-163.80	-56.38	-35.39	-89.30	-75.94	40.48	163.23	-1325.33815500	8.80
C-*R*-267‡	177.66	177.39	-70.60	155.17	-148.55	-77.81	50.83	113.85	106.91	-16.63	179.99	-1325.33405379	11.37
C-*R*-268‡	-147.70	148.64	-69.71	161.22	-157.42	-74.62	-57.83	123.49	70.66	-18.44	-94.97	-1325.34364188	5.36
C-*R*-269‡	-176.86	172.53	-68.12	159.70	74.58	51.83	-76.41	156.20	25.36	-16.21	-93.46	-1325.32494308	17.09
C-*R*-270‡	-175.29	173.03	-69.03	159.07	75.12	56.05	-70.46	-109.17	-98.98	-18.82	179.02	-1325.33270055	12.22
C-*R*-271‡	-177.39	-172.31	57.84	163.68	168.60	102.59	-49.00	143.67	110.66	62.59	-171.30	-1325.33304933	12.00
C-*R*-272‡	91.15	-172.13	-49.35	66.29	73.28	45.57	42.71	76.44	73.33	74.12	-102.79	-1325.34950697	1.68
C-*R*-273‡	92.65	-173.48	-49.65	73.96	171.88	60.28	41.82	-175.41	-113.63	71.78	-173.95	-1325.34784915	2.72
C-*R*-274‡	93.10	-171.45	-47.08	75.23	171.71	49.83	-73.92	177.03	109.44	76.22	177.48	-1325.34407376	5.08
C-*R*-275‡	93.31	-173.59	-44.00	77.00	175.36	74.14	-118.54	89.20	86.23	77.35	-84.14	-1325.33247861	12.36

Resolution of Carvedilol's Conformational Surface via Gas and Solvent Phase Density Functional Theory Optimizations and NMR Spectroscopy

David R.P. Almeida*[a,b], Donna M. Gasparro[a], Tamas A. Martinek[b], Ferenc Fülöp[b], and Imre G. Csizmadia[a,c]

[a]Department of Chemistry, Lash Miller Chemical Laboratories, University of Toronto, 80 St. George Street, Toronto, Ontario, Canada M5S 3H6

[b]Institute of Pharmaceutical Chemistry, University of Szeged, Eötvös u. 6., H-6720 Szeged, Hungary

[c]Department of Medicinal Chemistry, University of Szeged, Dom ter 8, 6720 Szeged, Hungary

* Corresponding author.
dalmeida@medscape.com (D.R.P. Almeida), dgasparro@medscape.com (D.M. Gasparro), martinek@phanal.szote.u-szeged.hu (T. Martinek), fulop@pharma.szote.u-szeged.hu (F. Fülöp), icsizmad@alchemy.chem.utoronto.ca (I.G. Csizmadia).

Abstract

The pharmaceutical carvedilol acts as a non-selective beta (β_1/β_2) and selective alpha (α_1) adrenoceptor antagonist, cardioprotector, antioxidant, oxidative phosphorylation uncoupler, and amyloid-beta (Aβ) anti-fibrillar agent. Given these diverse pharmacodynamic profiles, the resolution of carvedilol's highly populated conformations are necessary to divulge the basis of its interactions with these molecular targets. However, given carvedilol's sizeable conformational hypersurface (11 torsional angles and 3^{11} conformational possibilities), this task is preferentially achieved by means of a novel rational molecular fragmentation method to minimize computational and experimental resources. Presently we have isolated and optimized nine low energy carvedilol conformers with high level B3LYP/6-31G(d) density functional theory (DFT with the Becke 3LYP hybrid exchange-correlation functional) molecular orbital computations in the gas phase and solvent phase (DMSO and water) with Onsager solvent reaction field calculations as a means to arrive at the uncharacterized low energy structures and solvent effect of carvedilol. Additionally, carvedilol has been analyzed with NMR spectroscopy (in DMSO) to correlate theoretical- and experimental-derived electronic structure. Gas phase results show that seven of the nine conformers possess a novel tetra-centric spiro-type conformation composed of intramolecular six- and eight-membered rings. This structural motif is dictated by the necessary stabilization of the positive nitrogen centre and by the inflexibility of the carbazole aromatic ring. DMSO and water DFT optimizations and NMR spectroscopy closely mirror each other indicating that carvedilol has a subtle energetic and structural solvent effect, and as such, a significant barrier to re-arrangement from gas phase to solvent exists. ROESY and scalar

coupling show further evidence of the rigid rotation about the large carbazole pharmacophore. Given the harmony achieved between theoretical and experimental results, this study suggests the most populated states of carvedilol expected to dominate physical and biological samples and gives credence to the ability of methodically analyzing complex molecular systems by means of theoretical structure-activity fragmentation. Together, this will critically aid the molecular understating of carvedilol's pharmacodynamic mechanisms and structural underpinnings.

Keywords: Carvedilol, DFT-Becke 3LYP hybrid functional, Onsager Solvation Reaction Field, NMR, conformation.

1. Introduction

The cardiovascular pharmaceutical carvedilol, 1-(9H-Carbazol-4-yloxy)-3-[2-(2-methoxy-phenoxy)ethylamino]-2-propanol ($C_{24}H_{26}N_2O_4$), is used in the treatment of hypertension, ischemic heart disease (IHD), and congestive heart failure (CHF).[1,2] Carvedilol's major pharmacodynamic molecular targets include: antagonist action at alpha (α_1) and beta (β_1 and β_2) membrane adrenoceptors, reduction of reactive oxygen species (ROS)-mediated oxidative stress, and modulator of cardiac electrophysiological properties *via* interaction with K^+ and Ca^{2+} ion channels.[1]

Carvedilol's hemodynamic benefits are a result of peripheral vasodilation and reduction in cardiac work from balanced non-selective β-receptor blockage (β_1 and β_2) and selective α_1-receptor blockage.[1-3] As a cardioprotector, carvedilol exerts anti-proliferative/anti-atherogenic, anti-hypertrophic, anti-ischemic, and anti-arrhythmic actions by means of antioxidant effects, improvement of glucose and lipid metabolism, modulation of neurohormonal factors (e.g., nitric oxides), and fine-tuning of cardiac electrophysiological properties.[1] In addition, carvedilol provides further cardioprotection by protecting mitochondria from oxidative stress by uncoupling oxidative phosphorylation *via* a weak protonophoretic (proton transfer) mechanism involving the amino group ($pK_a = 7.9$) of its side-chain.[4]

As a novel anti-fibrillar agent, carvedilol may have uses in the prevention or slowing down of Alzheimer's disease (AD).[5] Work has indicated that carvedilol, and its active hydroxylated analogues, are able to inhibit amyloid-beta (Aβ) fibril formation.[5] The amyloid cascade hypothesis states that increased production and accumulation of Aβ oligomers (dimers, trimers, or higher oligomers) consisting of 42 or 43 amino acids

(abbreviated as Aβ1-42) is the primary influence driving AD pathogenesis.[6-11] It is currently not known if carvedilol binds to Aβ monomers, dimers, or other oligomers or what type of interaction occurs between carvedilol and the Aβ peptide(s).

Given the intricate pharmacodynamic nature of carvedilol, it is evident that revealing carvedilol's conformational profile and its highly populated conformations are indispensable to expounding the molecular basis of its mechanisms of action. However, given carvedilol's 11 associated torsional angles and 177 147 (3^{11}) conformational possibilities (total is arrived at by means of multi dimensional conformation analysis [MDCA] where each torsional angle can assume *gauche plus*, *anti*, or *gauche minus* orientations), it is clear that this is a extensive and laborious task by conventional MDCA or random potential energy hypersurface (PEHS) sampling.

To remedy the above quandary, we previously developed a scheme based on the rational molecular fragmentation of structure-activity regions to fragment the three pharmacophores of carvedilol into three independent fragments[12] (c.f. **Figure 1**). All three fragments were then exhaustively optimized by MDCA[12-14], along with thorough analysis of the chiral properties of carvedilol[15] and several hydrogen bond (H-bond) intramolecular attractive forces (IMAF)[16]. The latter results were cumulatively used to predict 240 conformations hypothesized to be low energy structures.[17] Restricted Hartree-Fock (RHF/3-21G) optimizations revealed 121 unique, converged structures, of which nine possessed a conformer relative energy of less than four Kcal•mol^{-1}.[17] The rational molecular fragmentation method employed was able to predict eight of the 11 torsional angles accurately (72.7%) according to torsional angle conformation distribution.[17]

In the current study, the authors subject these nine novel low energy conformations to high level Density Functional Theory (DFT) optimizations in gas, dimethyl sulfoxide (DMSO), and water phases and analyze carvedilol with nuclear magnetic resonance (NMR) spectroscopy to achieve a twofold aim: (1) discover and describe the most populated (lowest energy) states of carvedilol expected to dominate physical and biological samples and (2) analyze the success of this novel "structure-activity fragmentation" approach to the detailed theoretical study of complex molecular systems.

2. Methods

2.1 Rational Molecular Fragmentation of Carvedilol

Carvedilol is composed of three distinct pharmacophores and was divided into three molecular fragments (c.f. **Figure 1** and **2**). Each fragment has been previously studied by the use of MDCA: *R*- and *S*-4-(2-hydroxypropoxy)carbazol (Fragment A) possesses the carbazole ring responsible for the direct antioxidant effects of carvedilol[12], 2(*R* and *S*)-1-(ethylamonium)propane-2-ol (Fragment B) contains the protonophoretic amino group involved in the cardioprotective uncoupling of mitochondrial oxidative phosphorylation[13], and aminoethoxy-2-methoxy-benzene (Fragment C) is the α_1-adrenergic antagonist pharmacophore of carvedilol[14].

By optimizing a comprehensive list of 240 conformations hypothesized to be low energy carvedilol structures, an authentic set of nine distinct conformers were discovered with a conformer relative energy of less than four Kcal•mol^{-1} at the RHF/3-21G level of theory.[17] The dominant interaction inherent in seven of these nine conformers is a unique "tetra-centric" (four-centred) spiro-type structure composed of two intramolecular rings (six- and eight-membered) enclosed by two O···H-N H-bonds (c.f. **Figure 3**).[17]

Although the RHF/3-21G level of theory performed exceptionally well at optimizing a large number of carvedilol structures and ultimately allowing us to arrive at a set of nine structures[17], the RHF/3-21G gas phase calculations are not enough for full structural and energetic account of focal carvedilol conformers. Furthermore, exclusive gas phase optimizations or solvent phase single point energy (SPE) calculations are not sufficient in of themselves because they do not allow in depth analysis of the as-of-yet uncharacterized solvent effect of carvedilol. As such, in the current communication, we

perform high level gas and solvent phase DFT optimizations on these nine structures and evaluate carvedilol with NMR spectroscopy as to present the conformations of carvedilol expected to preponderate gas and solvent samples. In turn, such a comparison between theoretically- and experimentally-determined carvedilol structures will lead to carvedilol's conformational solution.

2.2 Carvedilol Torsional Angle Definitions

To allow explicit prediction and definition of conformation, a systematic numbering system has been used for all structures such that corresponding torsional angles in fragments and carvedilol are all defined in the same manner (c.f. **Figure 2**). All PEHS conformers of carvedilol can be described by **equation 1**. Further, conformational structural assignments for converged minima are made according to **equation 2** based on the general observation that, if one were to rotate a tetrahedral carbon against another tetrahedral carbon, the minima would generally fall within the above ranges.

$$E = f(\chi_1, \chi_2, \chi_3, \chi_4, \chi_5, \chi_6, \chi_7, \chi_8, \chi_9, \chi_{10}, \chi_{11}) \qquad \textbf{EQUATION 1}$$

gauche plus (*g*+)	= 60. (ideal) ± 60°	**EQUATION 2**
anti (*a*)	= 180. (ideal) ± 60°	
gauche minus (*g*-)	= -60. (ideal) ± 60°	

2.3 Theoretical and Computational Methods

All structures were optimized with molecular orbital (MO) calculations of the PEHS conformational minima using the Gaussian 98 (G98) software program.[18] Initially, full optimizations in the gas phase ($\varepsilon = 0.0$) were performed using density functional

theory (DFT) with the Becke 3LYP hybrid exchange-correlation functional[19] at the B3LYP/6-31G(d) level of theory (the inputs for these gas phase DFT calculations were RHF/3-21G optimized results taken from reference 17).

Proceeding, DFT gas phase optimized carvedilol structures were then used as input for DFT self-consistent reaction field (SCRF) optimizations to characterize the solvent effect (solvent-induced change in energy difference) of carvedilol. Independent molecular volume calculations were first computed on all gas phase DFT converged structures to estimate a solute radius (a_0) for use with the Onsager solvent reaction field method.[20-25] Once the solute radii had been calculated, the Onsager method was utilized at the B3LYP/6-31G(d) level of theory to optimize all structures in aprotic DMSO (ε = 46.70) and protic water (ε = 78.39) solvents. The Onsager method places the solute in a fixed spherical cavity, defined by the solute radius, within the solvent field.[26] Net stabilization is achieved corresponding to the interactions between the molecular dipole (which induces a dipole in the solvent medium) and the electric field applied by the solvent dipole.[26] To satisfy the need of quantitatively-significant results, the self-consistent field (SCF) "tight" option was utilized for volume and Onsager calculations for a more accurate integration by means of an increase in the density of points used. Graphical data was plotted using Axum 5.0[27] and Excel[28].

2.4 Experimental NMR Spectroscopy Methods

A total of 47.7 mg of carvedilol (purchased from ChemPacific Corporation, Baltimore, Maryland, United States) was dissolved in 550 µl of deuterated DMSO (DMSO-d_6) solvent. All of the spectra were obtained on a Bruker DRX 400 MHz NMR spectrometer at 298 Kelvin using tetramethylsilane (TMS) as a reference at zero parts per million (ppm). Proton chemical shifts were assigned and structural information was obtained with decoupled, COSY (correlated spectroscopy), NOESY (nuclear Overhauser enhancement spectroscopy), and ROESY (rotational Overhauser enhancement spectroscopy) spectra. Mixing time was modulated in NOESY experiments for best signal-to-noise ratio in NOE build up curves. All 2D spectra were zero filled once in both dimensions.

Reasons for choosing DMSO (DMSO-d_6) as the solvent for all NMR spectra are threefold: (1) DMSO is polar solvent which generally destroys weak intramolecular H-bonds, therefore, it is a good solvent to test the rigidity of the structure and thereby the strength of any assumed H-bond networks; (2) DMSO is an aprotic solvent preventing the ^1H-^2D exchange with polar protons of the solute (contrary to $CDCl_3$ or D_2O) which allows to obtain information on the chemical shifts of the OH and NH protons; (3) carvedilol NMR spectroscopy in DMSO can be promptly compared with DFT optimizations in DMSO available with the G98 software program.

3. Results and Discussion

3.1 Structural Analysis of Gas Phase Optimized Carvedilol Conformations

According to **equation 2**, a summary of optimized torsional angle conformation for all converged structures of carvedilol is presented in **Table 1**. Upon gas phase DFT optimization, all nine conformations possessed a gas phase relative energy of less than two Kcal•mol^{-1} (c.f. **Table 2**) compared with a conformer relative energy of less than four Kcal•mol^{-1} for the previously computed RHF/3-21G structures[17].

In concordance with the prior RHF/3-21G optimized structures, close scrutiny of these DFT low energy conformations reveals that seven (C-*R*-246 to C-*R*-250, C-*R*-258, and C-*R*-272) of the nine conformations possess the novel tetra-centric spiro-type structural motif (c.f. **Figure 3** and **4**). The tetra-centric conformation is flanked on one side by the 13-membered aromatic carbazole ring (centre 1) which is connected to a six-membered ring closed *via* an intramolecular O···H-N H-bond between the carbazole ether oxygen and a proton of the positive nitrogen centre (ring **a**; centre 2). The same protonated secondary nitrogen atom – via the other proton – forms an eight-membered ring (ring **b**; centre 3) through another intramolecular O···H-N H-bond to the methoxy oxygen of carvedilol. The "right side" of the carvedilol conformation if flanked by the di-substituted benzene ring (centre 4) which also forms part of ring **b**. Rings **a** and **b** are formed *via* short H-bonds that are in all cases less than two Angstroms in length and always involves both protons of the nitrogen centre (c.f. **Figure 4**). Conformations C-*R*-251 and C-*R*-273 do not form any IMAF with the methoxy oxygen (O36), and thus, do not form ring **b**. In order that this tetra-centric structural motif form, it is necessary that the positive protonated nitrogen centre of the carvedilol side-chain is present for the

concomitant formation of the two essential O···H-N H-bonds. If only one proton (in the neutral amine form) is present, instead of the positive protonated centre, it is likely that it would not be possible to form rings **a** and **b**.

Aside from this tetra-centric conformation, the highly populated states of carvedilol presented in **Figure 4** possess various further intramolecular H-bond networks, albeit these are composed of much longer H-bonds compared to those of enclosed rings **a** and **b**. Aside from differences related to the tetra-centric conformational motif, the nine low energy carvedilol structures can be divided into two groups: those with three internal H-bonds (C-*R*-246, C-*R*-247, C-*R*-251, C-*R*-258, C-*R*-272, and C-*R*-273) and those with four internal H-bonds (C-*R*-248, C-*R*-249, and C-*R*-250) (c.f. **Figure 4**). These additional H-bonds form various intramolecular five-membered rings.

As previously evaluated[12,17], the rational molecular fragmentation of protonated carvedilol is based on the deconstruction of carvedilol into three dominant pharmacophore fragments: a positive secondary amine side-chain (Fragment B) flanked by an electron-withdrawing group (EWG) carbazole ring system (Fragment A) and an EWG benzene centroid (Fragment C). Given these three structure-activity considerations, it can be rationalized that the prevalence of the tetra-centric conformation in seven of the nine DFT optimized conformers is a result of stabilizing the positive nitrogen centre. The electronic structure of this motif allows the electron-donating groups (EDG) found on the carbazole (ether oxygen bridge, O1) and benzene (methoxy oxygen, O36) rings to act as EDG to these respective centroids, and also to the positive nitrogen centre. The formation of intramolecular rings **a** and **b** facilitates an electron density redistribution process

whereby the ether (O1) and methoxy (O36) EDG induct electron density into the positive nitrogen centre *via* O···H-N H-bonds.

Although conformations C-*R*-251 and C-*R*-273 do not possess ring **b** of the tetra-centric motif (c.f. **Figure 4**), the net effect inherent in these structures is still the stabilization of the positive nitrogen centre by the use of H-bonds. However, in the case of these two conformers, the O···H-N H-bonds are between amine protons and the hydroxyl oxygen (O41) and second ether oxygen (O29) leading to the formation of independent five-membered rings. In C-*R*-251 and C-*R*-273, these two intramolecular H-bonds operate to produce the similar electron induction into the nitrogen centre.

Given the above, it can be concluded that although the tetra-centric structural motif represents the preferred and likely most populated gas phase conformation of carvedilol, the nitrogen side-chain can be stabilized by various H-bonds that all serve the function of inducting (or redistributing) electron density into the positive centre. In total, the carvedilol intramolecular H-bond networks are composed of various H-bonds that can originate from two amine proton H-bond donors (H46 and H57) to four oxygen H-bond acceptors (O1, O29, O36, and O41).

The chemical literature available is limited with regards to the detailed description of carvedilol's gas phase structure[12-17,29]; thus, it is difficult to compare the above DFT results with previous experimental works. The X-ray diffraction crystal structure of carvedilol, developed by Chen and coworkers[29], utilizes the deprotonated neutral form (with respect to the side-chain nitrogen centre) of carvedilol and displays a pair of carvedilol enantiomers interacting *via* short intermolecular O41-H42···N26 H-bonds (two H-bonds per enantiomer pair).[29] However, since the crystal displays neutral

intermolecular enantiomer structure, it does not elucidate any intramolecular structural parameters of single-molecule protonated carvedilol. The bona fide structural analysis of single-molecule carvedilol performed here is relevant to carvedilol's mechanisms of action because these are a result of one *R*- or *S*-configuration molecule interacting with adrenoceptors, ROS, or Aβ peptides. As such, these single-molecule conformations of carvedilol describe the dominant structures it assumes before any solvent effect occurs and prior to complexing with such molecular targets.

3.2 Structural Analysis of DMSO and Water Phase Optimized Carvedilol Conformations

DFT optimization of carvedilol conformations in aprotic DMSO (c.f. **Figure 5** and **Table 3**) and protic water (c.f. **Figure 6** and **Table 4**) solvents were performed independently, using DFT optimized gas phase results as input files, to bring to light carvedilol's solvent effect. A graphical representation of this solvent effect is displayed in **Figure 7**.

Superficially from **Figure 7**, it is evident that DMSO and water solvation of carvedilol produces the same effects on structural parameters and conformer relative energy; i.e., the same solvent effect is present for both a protic and aprotic solvent as DMSO and water results produced near-identical torsional angle and energy values. Energetically, the overall effect of the two solvents on carvedilol was the augmentation in both the relative and absolute values in all conformers except C-*R*-250 and C-*R*-273 which possessed similar relative energies in all phases (c.f. **Figure 7**). However, the relative orientation of the conformers, with respect to one another, did not change.

Pertaining to electronic structure, torsional angle conformation distribution in **Table 1** indicates that, for a respective carvedilol conformer, torsional angle orientation was essentially consistent between RHF and DFT optimizations as well as between gas, DMSO, and water phase calculations. The latter is suggestive that carvedilol's low energy states are rigid and have significant conformational transition state energy barriers that prevent major re-arrangements and interconversions between states in the solvent phase. In comparing parameters between gas (c.f. **Figure 4**), DMSO (c.f. **Figure 5**), and water (c.f. **Figure 6**) converged conformers, the majority did not undergo any noteworthy changes. Conformers C-*R*-247 (tetra-centric with three H-bonds), C-*R*-248 (tetra-centric with four H-bonds), C-*R*-249 (tetra-centric with four H-bonds), C-*R*-251 (no tetra-centric motif with three H-bonds), C-*R*-258 (tetra-centric with three H-bonds), C-*R*-272 (tetra-centric with three H-bonds), C-*R*-273 (no tetra-centric motif with three H-bonds) all displayed the same conformations in gas, DMSO, and water.

The only conformers that underwent any noticeable structural changes were C-*R*-246 and C-*R*-250. Conformer C-*R*-246 rotated torsional angle χ_1 from the *g*+ position (RHF results from reference **17**) to the *anti* position in all DFT calculations (c.f. **Table 1**). However, this χ_1 rotation only produced a slight change in orientation of the carbazole ring and did not produce any other significant structural alterations as all DFT structures still assumed the tetra-centric motif. Contrasting, C-*R*-250 did undergo a significant conformational change in rotating torsional angle χ_6 from the *g*- position in RHF (reference **17**) and DFT gas phase results (c.f. Table **1** and **2**) to the *anti* position in DFT DMSO and water calculations (c.f. **Table 3** and **4**). In the gas phase, C-*R*-250 possesses the tetra-centric motif with four internal H-bonds (c.f. **Figure 4**). Nevertheless, upon the

χ_6 rotation in DMSO (c.f. **Figure 5**) and water (c.f. **Figure 6**), this conformer re-arranged such that the methoxy oxygen (O36) no longer interacted with any amine protons, and therefore, could not form ring **b** pertaining to the tetra-centric structure. In the solvent phases, C-*R*-250 still possesses a short O1···H46-N H-bond but formed a much stronger O41···H57···O29 bifurcated H-bond with a distance of 2.27 Å and 2.15 Å, respectively, in both DMSO and water (c.f. **Figure 5** and **6**).

This structural change conferred conformer C-*R*-250 with a global minima relative energy in both DMSO and water (c.f. **Figure 7**). This is likely due to the lack of any IMAF involving the methoxy oxygen (O36) which would allow the positive nitrogen and amine protons to be solvated by DMSO and would allow extensive solvation of the positive nitrogen centre, amine protons, and O36 by water. Consequently, C-*R*-250 was the only carvedilol structure to display a solvent (both DMSO and water) relative energy of less than one Kcal•mol^{-1} (c.f. **Figure 7** and **Table 3** and **4**).

Given the current DFT Onsager solvent reaction field calculations, carvedilol can be said to have a subtle solvent effect with regards to energetics and electronic structure. On the whole, most structures did not undergo any major structural alterations upon solvent optimization and preferred the tetra-centric conformation and other IMAF related to stabilizing the carvedilol structure seen in the gas phase. It can thus be stated that the carvedilol gas phase conformations are excellent starting points for any structural or mechanistic analysis of carvedilol. Intuitively, it follows that the carvedilol structure would be better solvated if it lacked any IMAF, however, it is likely that the structures presented here are densely populated and possess significant conformational transition state energy barriers that affect the interconversion rates between the different

conformational states. The latter is simply evidenced by the fact that most conformers converged to solvent structures very similar to their gas phase counterparts.

3.3. Theoretical Resolution of Carvedilol's Conformational Surface

All torsional angle orientations necessary for carvedilol to assume both the tetra-centric conformational motif as well as all other IMAF presented in this communication are jointly expressed in **equation 3** (forward slash "/" indicates "or"). Although the carvedilol PEHS is one of large conformational flexibility, the low energy structures presented here display unanticipated rigidity in several torsional angles. The current DFT results demonstrate that four (χ_2, χ_3, χ_4, and χ_{10}) of the 11 torsional angles assume only one orientation. Compounding the latter with the fact that all four torsional angles belong to Fragment A, and torsional angle χ_1 assumes an *anti* conformation in only one conformer (C-*R*-246) while *g*+ in all other converged carvedilol structures, it can be hypothesized that the large carbazole-containing pharmacophore dictates the prevalent and stable conformations of the carvedilol molecule. Likewise, there is also a dominant *gauche effect* in the stereocentre of carvedilol (torsional angle χ_{10}) indicating further inflexibility in the favoured carvedilol conformations.

EQUATION 3

$$\chi_1 = g+/a \qquad \chi_6 = g+/a/g-$$

$$\chi_2 = a \qquad \chi_7 = g+/g-$$

$$\chi_3 = g- \qquad \chi_8 = g+/a/g-$$

$$\chi_4 = g+ \qquad \chi_9 = g+/g-$$

$$\chi_5 = g+/a \qquad \chi_{10} = g+$$

$$\chi_{11} = g+/a/g-$$

As shown in previous work on the enantiomeric relationships of carvedilol and Fragment A[15], the present results determined for the *R*-configuration of carvedilol can be extrapolated to predict corresponding energetic terms, conformational assignments, structural orientations, and IMAF of *S*-carvedilol. Since all carvedilol minima occur in analogous pairs[15], the PEHSs for both stereoisomers will illustrate that the *R*- and *S*-configurations of carvedilol comprise a molecular system which possesses both point chirality and axis chirality and are exactly enantiomeric as described by **equation 4**. As a result, a true enantiomeric pair requires not only the switching of point chirality from the *R*- to *S*-stereoisomer but also the switching of all torsional angles from clockwise to counter-clockwise rotation as demanded by **equation 4**. Thus, all minima must have an energetically equal enantiomer while all other carvedilol pairs have diastereomeric relationships.

$$E_R = E_S \qquad \textbf{EQUATION 4}$$

$$f_R(\chi_1, \chi_2, \chi_3, \chi_4, \chi_5, \chi_6, \chi_7, \chi_8, \chi_9, \chi_{10}, \chi_{11}) = f_S(-\chi_1, -\chi_2, -\chi_3, -\chi_4, -\chi_5, -\chi_6, -\chi_7, -\chi_8, -\chi_9, -\chi_{10}, -\chi_{11})$$

3.4 NMR Spectroscopy of Carvedilol in DMSO Solvent

Carvedilol NMR chemical shifts and assignments are presented in **Table 5**. Initially, a ROESY spectrum was utilized to analyze the relatively rigid Fragment A structure of carvedilol (i.e., about torsional angles χ_1, χ_2, χ_3, χ_4, and χ_5) (c.f. **equation 3**). The ROESY spectrum shows that the carbazole proton H22 gives good intensity cross peaks to non-equivalent H39 and H40 protons indicating H22 is close to these two protons and there is rigid motion about torsional angles χ_1, χ_2, and χ_3. Moreover, ROESY spectra also indicate that the H44 and H45 protons of centre C25 are also not equivalent,

and as a result, rotation about torsional angles χ_4 and χ_5 is likely hindered. Given these results, along with the fact that DMSO solvent generally destroys weak intramolecular H-bonding, the ROESY spectrum suggests that: (1) the Fragment A associated torsional angles of carvedilol are indeed inflexible, and (2) the intramolecular H-bond networks present in the carvedilol structure are strong and persistent.

With reference to the theoretical DMSO optimized structures, all conformers possess at least one intramolecular H-bond involving an amine proton and the carbazole ether oxygen (O1) while conformers C-*R*-248, C-*R*-249, C-*R*-250, C-*R*-251, and C-*R*-273 contain a further H-bond between an amine proton and the hydroxyl oxygen (O41) (c.f. **Figure 5**). These intramolecular H-bonds severely hinder any rotation involving torsional angles χ_1, χ_2, χ_3, χ_4, and χ_5. In addition, because the nitrogen centre is protonated and further interacts (*via* H-bond formation) with oxygen atoms O29 and O36 bonded to the substituted benzene, further hindrance is placed on the rotation of these five torsional angles. As such, the ROESY spectra substantiates the DFT converged structures in that, given the various intramolecular H-bonds that carvedilol forms, it would be expected that protons H39 and H40 as well as H44 and H45 constitute non-equivalent centres.

Scalar coupling of protons H44 and H45 (C25 centre) to proton H43 (stereocentre C24) was analyzed to closely inspect the behaviour of torsional angle χ_4. Scalar coupling data with integration of NOE intensity curves reveals a large J-coupling value and corresponding large NOE intensity for proton H45 to proton H43 suggesting a dihedral value of ± 60 degrees (c.f. **Figure 8**, left). Meanwhile, low J-coupling and low NOE values were observed for proton H44 to proton H43 implying a dihedral shift of 120 degrees (c.f. **Figure 8**, right).

DMSO optimized carvedilol conformers (c.f. **Figure 5**) and their respective optimized parameters (c.f. **Table 3**) reveal that all low energy carvedilol structures have torsional angle χ_A in the $g+$ orientation; the Newman projection in **Figure 9** displays the $g+$ orientation of torsional angle χ_A. In this *gauche* conformation, proton H45 imparts a large NOE and J-coupling influence to stereocentre proton H43 while proton H44 is shifted relative to torsional angle χ_A. Together, this conformation corroborates the NMR spectroscopy data.

The overlap signal and lack of NMR spectroscopic resolution concerning the aromatic benzene protons (H51, H52, H53, and H54) did not allow for any clear conclusions concerning the Fragment C portion of the carvedilol structure. Overall, the NMR spectroscopy results closely mirror the optimized DFT structures and give full credibility to such high level gas and solvent phase calculations. Furthermore, as a whole, the theoretically- and experimentally-determined carvedilol structures are in extensive agreement and portray carvedilol as a relatively inflexible molecule with various robust IMAF. Hence, carvedilol does not seem to be susceptible to a large solvent effect (versus the gas phase) as its conformers are largely unchanged from gas to solvent phases. Future directions include testing carvedilol's insensitivity to a solvent effect because both the DFT calculations and NMR spectra illustrate rigid intramolecular H-bonds able to withstand the DMSO medium.

4. Conclusions

The DFT optimizations and NMR spectroscopy described here consist of the most detailed account of the electronic structure and significant conformational intricacies of carvedilol (e.g., tetra-centric motif, IMAF, and H-bond networks) available in the literature. Carvedilol, although possessing significant conformational flexibility, also displays uncanny rigidity in several torsional angles (χ_1, χ_2, χ_3, χ_4, and χ_{10}). Given that these torsion dihedrals are respective to the aromatic carbazole centroid, it is likely that this region dictates the most prevalent and stable conformations of carvedilol. With regards to solvent effect, DFT gas phase and Onsager solvent reaction field calculations (in DMSO and water) and NMR spectroscopy (in DMSO) closely parallel each other indicating carvedilol does not have an appreciable solvent effect and its conformations are likely to remain unchanged from gas phase to solvent. The elucidation and resolution of carvedilol's conformational character should greatly aid the molecular understanding of its cardiovascular active conformations and involvement with pathological molecular targets such as in oxidative stress and AD.

As stated earlier, carvedilol's PEHS possesses an exorbitant 177 147 conformational possibilities, making traditional MDCA approaches to solving its populated conformations unfeasible. However, by utilizing an approach based on the basic thermodynamics precept that only low energy states are significantly occupied[17,31], we have been able to advance the carvedilol PEHS and resolve its highly populated conformations in both gas phase and solvent.

The rational molecular fragmentation method applied to carvedilol is as follows: if carvedilol, a molecule with many degrees of freedom (i.e., a large conformational

hypersurface), is divided into simpler structural fragments (e.g., Fragments A, B, and C) with manageable PEHSs but still relevant to the electronic structure of the whole molecule, then these smaller structures can be thoroughly analyzed via MDCA whereas carvedilol cannot. Then, the latter dominant fragment conformations, once optimized and evaluated, can be used to hypothesize low energy conformations of carvedilol itself. Since only highly populated fragment states are utilized, they should ultimately lead to corresponding low energy states of carvedilol.

Rather than relying on profligate computing force, this approach is in harmony with novel methodologies that localize dominant conformations of large PEHSs, not by means of sampling alone, but by designing routes that have the ability to generate starting points with some amount of energy minimization.[31] For example, the current fragmentation methodology does not sample the carvedilol map randomly, but rather, the fragments are optimized to generate inputs with an inherent amount of energy minimization.[17] The approach simplifies PEHS sampling because it is "focused" on conformers hypothesized to be highly populated states.[17] In this manner, the existing authors were successfully able to theoretically arrive at the low energy conformations of carvedilol that are presumed to dominate physical and biological samples *via* a novel methodological approach (i.e., rational molecular fragmentation method); the independent NMR spectroscopy results fully support these findings.

Acknowledgements

One of the authors (IGC) wishes to thank the Hungarian Ministry of Education for a Szent-Györgyi Visiting Professorship.

References

1. Cheng, J.; Kamiya, K.; Kodama, I. *Cardiovasc. Drug Rev.* **2001**, *19*, 152.

2. Carlson, W.; Oberg, K. *J. Cardiovasc. Pharmacol. Ther.* **1999**, *4*, 205.

3. Capomolla, S.; Febo, O.; Gnemmi, M.; Riccardi, G.; Opasich, C.; Carporotondi, A.; Mortara, A.; Pinna, G.; Cobelli, F. *Am. Heart J.* **2000**, *139*, 596.

4. Oliveira, P.J; Marques, M.P.; Batista de Carvalho, L.A.E.; Moreno, A.J.M. *Biochem. Biophys. Res. Commun.* **2000**, *276*, 82.

5. Howlett, D.R.; George, A.R.; Owen, D.E.; Ward, R.V.; Markwell, R.E. *Biochem. J.* **1999**, *343*, 419.

6. Hardy, J.; Selkoe, J. *Science* **2002**, *297*, 353.

7. Lee, V.M.-Y. *Neurobiol. Aging* **2002**, *23*, 1039.

8. Walsh, D.M.; Klyubin, I.; Fadeeva, J.V.; Cullen, W.K.; Anwyl, R.; Wolfe, M.S.; Rowan, M.J.; Selkoe, D.J. *Nature* **2002**, *416*, 535.

9. Lambert, M.P.; Barlow, A.K.; Chromy, B.A.; Edwards, C.; Freed, R.; Liosatos, M.; Morgan, T.E.; Rozovsky, I.; Trommer, B.; Viola, K.L; Wals, P.; Zhang, C.; Finch, C.E.; Krafft, G.A.; Klein, W.L. *Proc. Natl. Acad. Sci. USA* **1998**, *95*, 6448.

10. Walsh, D.M.; Hartley, D.M.; Kusumoto, Y.; Fezoui, Y.; Condron, M.M.; Lomakin, A.; Benedek, G.B.; Selkoe, D.J.; Teplow, D.B. *J. Biol. Chem.* **1999**, *274*, 25945.

11. Chui, D.-H.; Tanahashi, H.; Ozawa, K.; Ikeda, S.; Checler, F.; Ueda, O.; Suzuki, H.; Araki, W.; Inoue, H.; Shirotani, K.; Takahashi, K.; Gallyas, F.; Tabira, T. *Nature Med.* **1999**, *5*, 560.

12. Almeida, D.R.P.; Pisterzi, L.F.; Chass, G.A.; Torday, L.L.; Varro, A.; Papp, J.Gy.; Csizmadia, I.G. *J. Physical Chem. A* **2002**, *106*, 10423.

13. Almeida, D.R.P.; Gasparro, D.M.; Pisterzi, L.F.; Torday, L.L.; Varro, A.; Papp, J.Gy.; Penke, B. *J. Mol. Str.* (THEOCHEM) **2003**, *631*, 251.

14. Almeida, D.R.P.; Gasparro, D.M.; Pisterzi, L.F.; Juhasz, J.R.; Fülöp, F.; Csizmadia, I.G. *J. Mol. Str.* (THEOCHEM) **2003**, *666-667*, 557.

15. Almeida, D.R.P.; Gasparro, D.M.; Pisterzi, L.F.; Torday, L.L.; Varro, A.; Papp, J.Gy.; Penke, B.; Csizmadia, I.G. *J. Physical Chem. A* **2003**, *107*, 5594.

16. Almeida, D.R.P.; Gasparro, D.M.; Pisterzi, L.F.; Juhasz, J.R.; Fülöp, F.; Csizmadia, I.G. *J. Mol. Str.* (THEOCHEM) **2003**, *666-667*, 537.

17. Almeida, D.R.P.; Gasparro, D.M.; Fülöp, F.; Csizmadia, I.G. *J. Physical Chem. A* **2004**, submitted for publication.

18. Gaussian 98 (Revision A.9), M. J. Frisch, G. W. Trucks, H. B. Schlegel, G. E. Scuseria, M. A. Robb, J. R. Cheeseman, V. G. Zakrzewski, J. A. Montgomery, Jr., R. E. Stratmann, J. C. Burant, S. Dapprich, J. M. Millam, A. D. Daniels, K. N. Kudin, M. C. Strain, O. Farkas, J. Tomasi, V. Barone, M. Cossi, R. Cammi, B. Mennucci, C.Pomelli, C. Adamo, S. Clifford, J. Ochterski, G. A. Petersson, P. Y. Ayala, Q. Cui, K. Morokuma, D. K. Malick, A. D. Rabuck, K. Raghavachari, J. B. Foresman, J. Cioslowski, J. V. Ortiz, A. G. Baboul, B. B. Stefanov, G. Liu, A. Liashenko, P. Piskorz, I. Komaromi, R. Gomperts, R. L. Martin, D. J. Fox, T. Keith, M. A. Al-Laham, C. Y. Peng, A. Nanayakkara, C. Gonzalez, M. Challacombe, P. M. W. Gill, B. G. Johnson, W. Chen, M. W. Wong, J. L. Andres, M. Head-Gordon, E. S. Replogle and J. A. Pople, Gaussian, Inc., Pittsburgh PA, 1998.

19. Becke, A.D. *J. Chem. Phys.* **1993**, *98*, 5648.

20. Wong, M.W.; Frisch, M.J.; Wiberg, K.B. *J. Am. Chem. Soc.* **1991**, *113*, 4776.

21. Wong, M.W.; Wiberg, K.B.; Frisch, M.J. *J. Am. Chem. Soc.* **1992**, *114*, 523.

22. Wong, M.W.; Wiberg, K.B.; Frisch, M.J. *J. Chem. Phys.* **1991**, *95*, 8991.

23. Wong, M.W.; Wiberg, K.B.; Frisch, M.J. *J. Am. Chem. Soc.* **1992**, *114*, 1645.

24. Kirkwood, J.G. *J. Chem. Phys.* **1934**, *2*, 351.

25. Onsager, L. *J. Am. Chem. Soc.* **1936**, *58*, 1486.

26. Foresman, J.B.; Frish, A. **1996**, Reaction field models of solvation. In *Exploring Chemistry with Electronic Structure Methods*, 2nd edition, Gaussian Inc., Pittsburgh, pp. 237-249.

27. Axum 5.0C for Windows, MathSoft Incorporated, 1996.

28. Excel for Windows, Microsoft, 2002.

29. Chen, W.-M.; Zeng, L.-M.; Yu, K.-B.; Xu, J.-H. *Chinese J. Struct. Chem.* **1998**, *17*, 325.

30. Schaeffer, W.H.; Politowski, J.; Hwang, B.; Dixon Jr., F.; Goalwin, A.; Gutzait, L.; Anderson, K.; Debrosse, C.; Bean, M.; Rhodes, G.R. *Drug Metab. Dispos.* **1998**, *26*, 958.

31. Billings, E. Molecular Modeling and Drug Design. In *Foye's Principles of Medicinal Chemistry*, 5th ed.; Williams, D.A., Lemke, T.L., Eds.; Lippincott Williams & Wilkins: New York, 2002; pp 68-85.

Figure Captions

Figure 1: Carvedilol was divided into three molecular fragments based on pharmacophore structure-activity: *R*- and *S*-4-(2-hydroxypropoxy)carbazol (Fragment A)[12,15], 2(*R* and *S*)-1-(ethylamonium)propane-2-ol (Fragment B)[13], and aminoethoxy-2-methoxy-benzene (Fragment C)[14].

Figure 2: Molecular structure and pharmacophore structure-function of N-protonated *R*-carvedilol and all torsional angle definitions used in the current study. Numbers placed beside atoms were used to define torsional angles for *R*-carvedilol in the z-matrix input for Gaussian 98 and for NMR spectroscopic analysis.

Figure 3: Schematic representation of the "tetra-centric" spiro-type conformational motif exhibited by most carvedilol low energy conformations (figure adapted from reference **17**). This structural motif consists of a six-membered ring (ring **a**) bonded to the terminal carbazole centroid and an eight-membered ring (ring **b**) bonded to the terminal substituted benzene. The intramolecular rings are formed by means of two short O···H-N H-bonds.

Figure 4: Molecular structures (and relative energies) of gas phase B3LYP/6-31G(d) optimized carvedilol conformations (c.f. **Table 2** for optimized parameters). Note that seven (C-*R*-246 to C-*R*-250, C-*R*-258, and C-*R*-272) of the nine conformers possess the tetra-centric motif (c.f. **3.1 Results and Discussion**).

Figure 5: Molecular structures (and relative energies) of DMSO solvent phase B3LYP/6-31G(d) optimized carvedilol conformations (c.f. **Table 3** for optimized parameters).

Figure 6: Molecular structures (and relative energies) of water solvent phase B3LYP/6-31G(d) optimized carvedilol conformations (c.f. **Table 4** for optimized parameters).

Figure 7: Graphical representation of the solvent effect of carvedilol. Gas, DMSO, and water phase relative energies are presented for all carvedilol structures optimized. Note that the DMSO and water relative energies extensively overlap each other due to near identical values (c.f. **3.2 Results and Discussion** and **Table 3** and **4**).

Figure 8: Graphical representation of the relationship between J-coupling and NOE intensity for protons H45 (left) and H44 (right) to stereocentre proton H43.

Figure 9: Newman projection of the *g*+ orientation of carvedilol torsional angle χ_4.

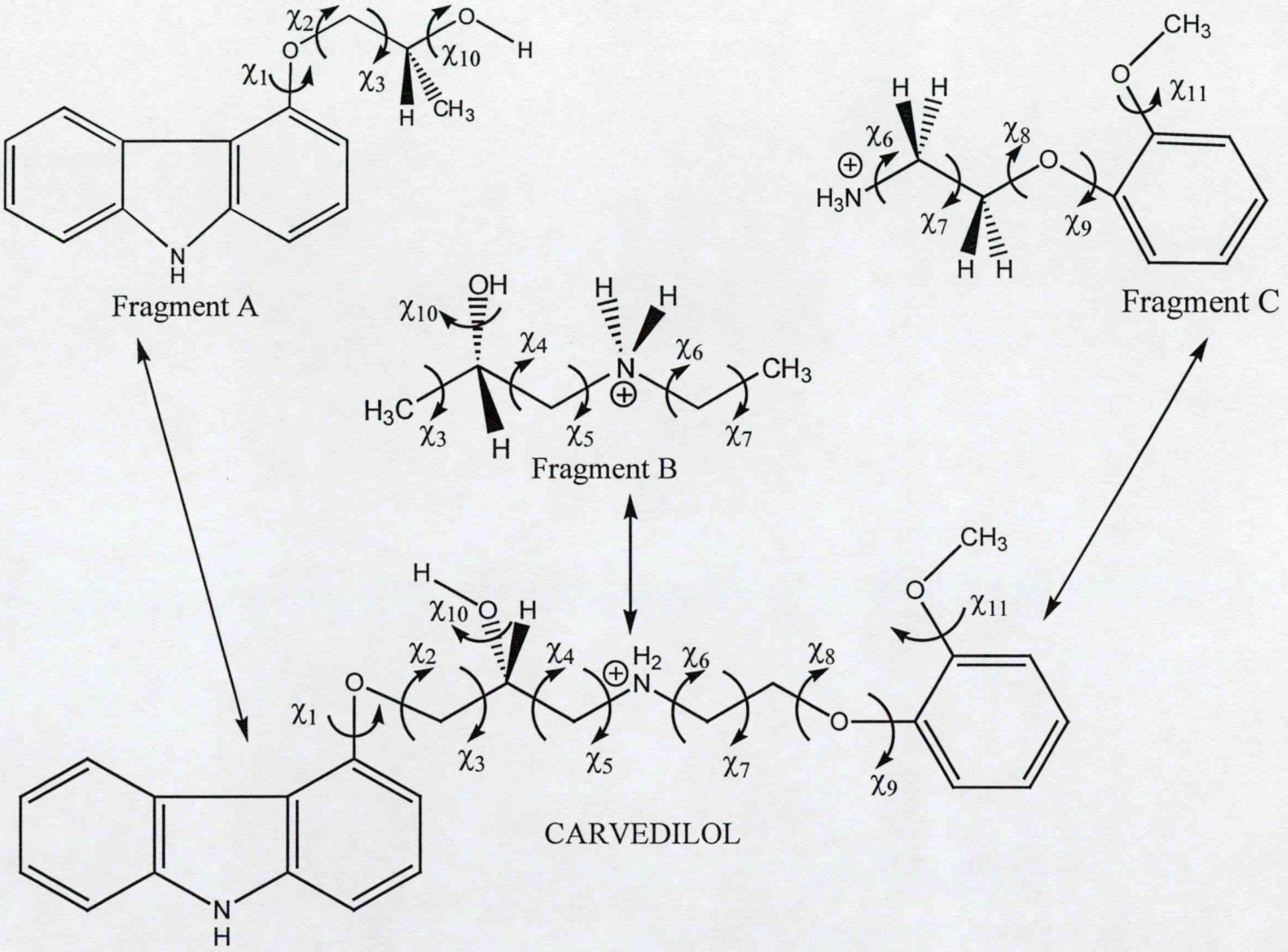

Figure 1

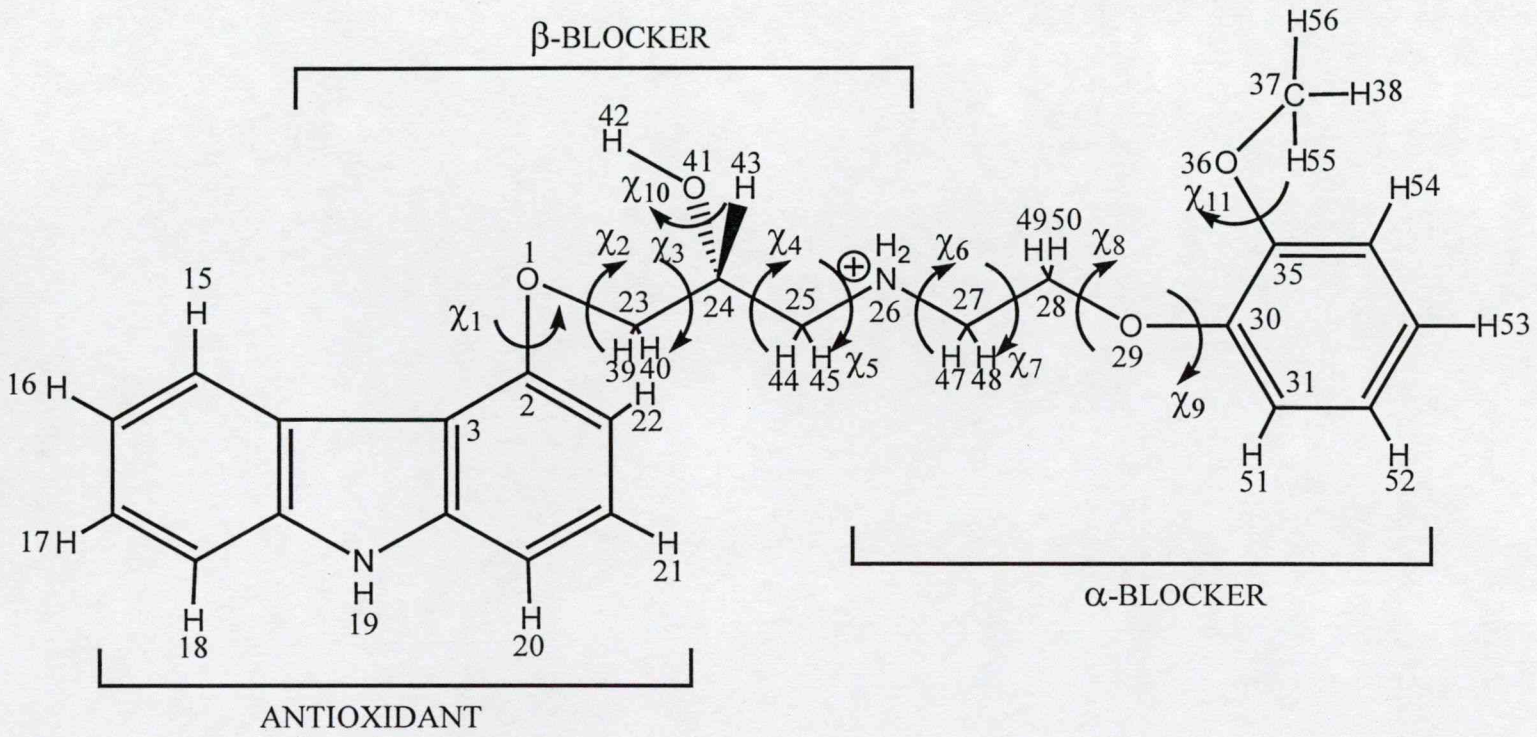

χ_1 = C23, O1, C2, C3 χ_2 = C24, C23, O1, C2 χ_3 = C25, C24, C23, O1

χ_4 = N26, C25, C24, C23 χ_5 = C27, N26, C25, C24 χ_6 = C28, C27, N26, C25

χ_7 = O29, C28, C27, N26 χ_8 = C30, O29, C28, C27 χ_9 = C31, C30, O29, C28

χ_{10} = H42, O41, C24, C23 χ_{11} = C37, O36, C35, C30

Figure 2

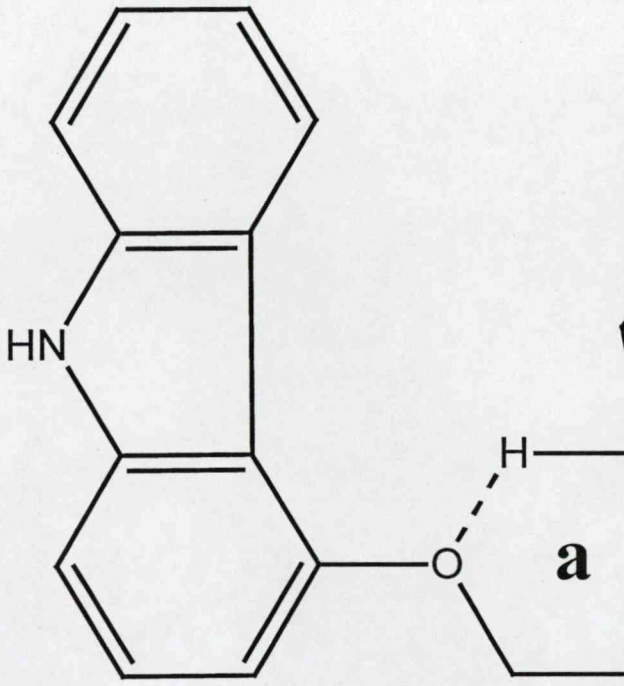
HN
H
O
a

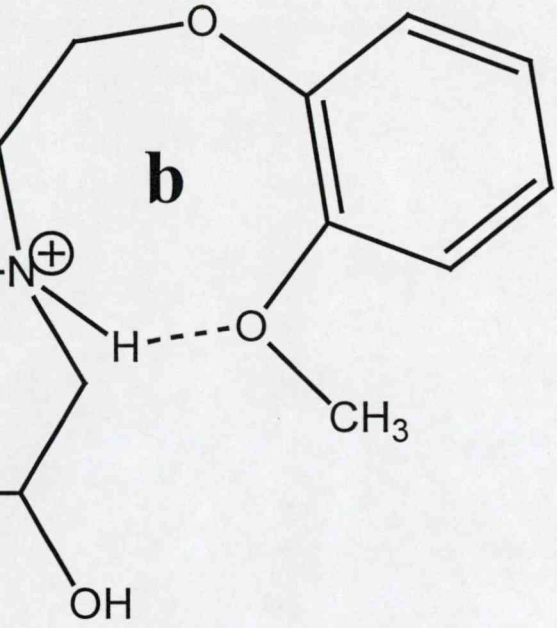

Figure 3

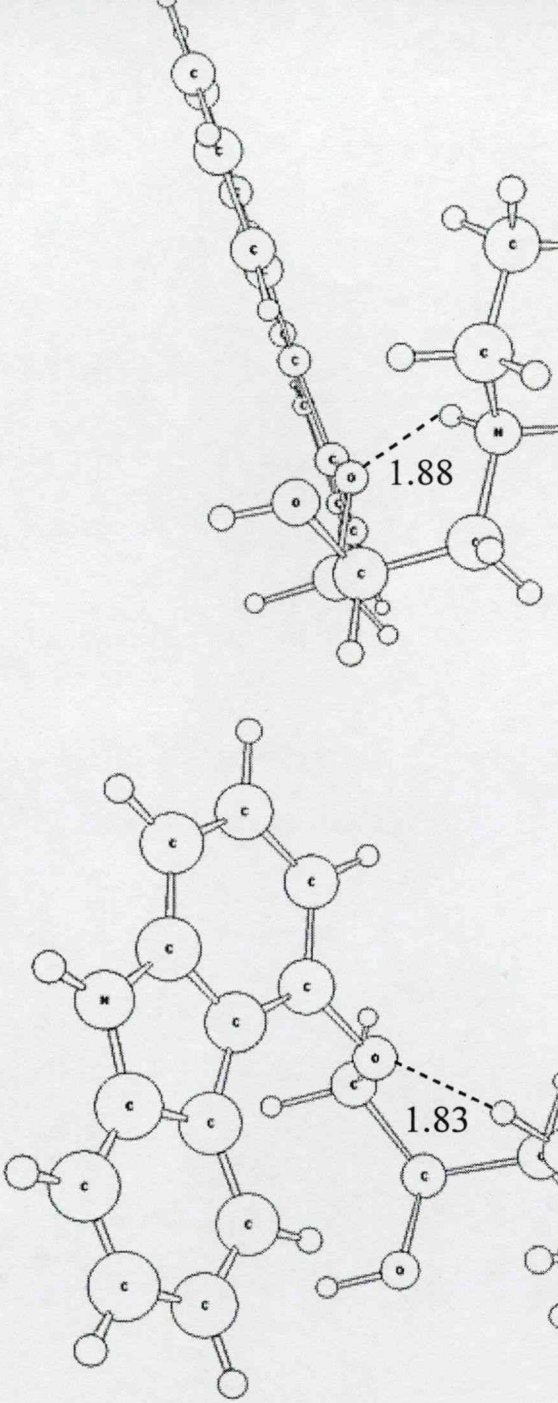
1.88
1.83

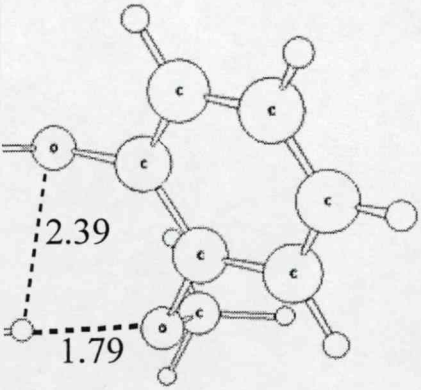

C-*R*-246
(0.11)

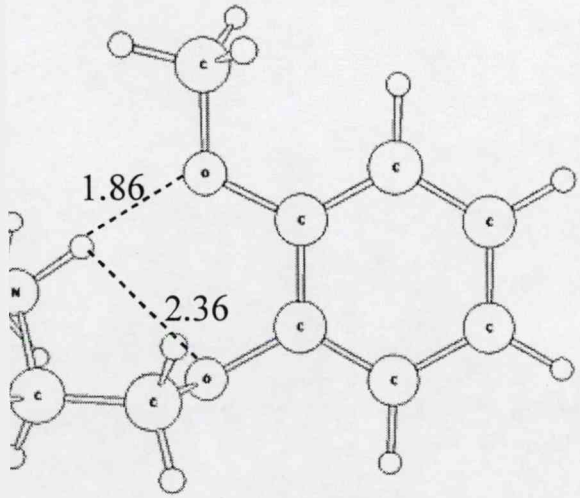

C-*R*-247
(1.01)

Figure 4

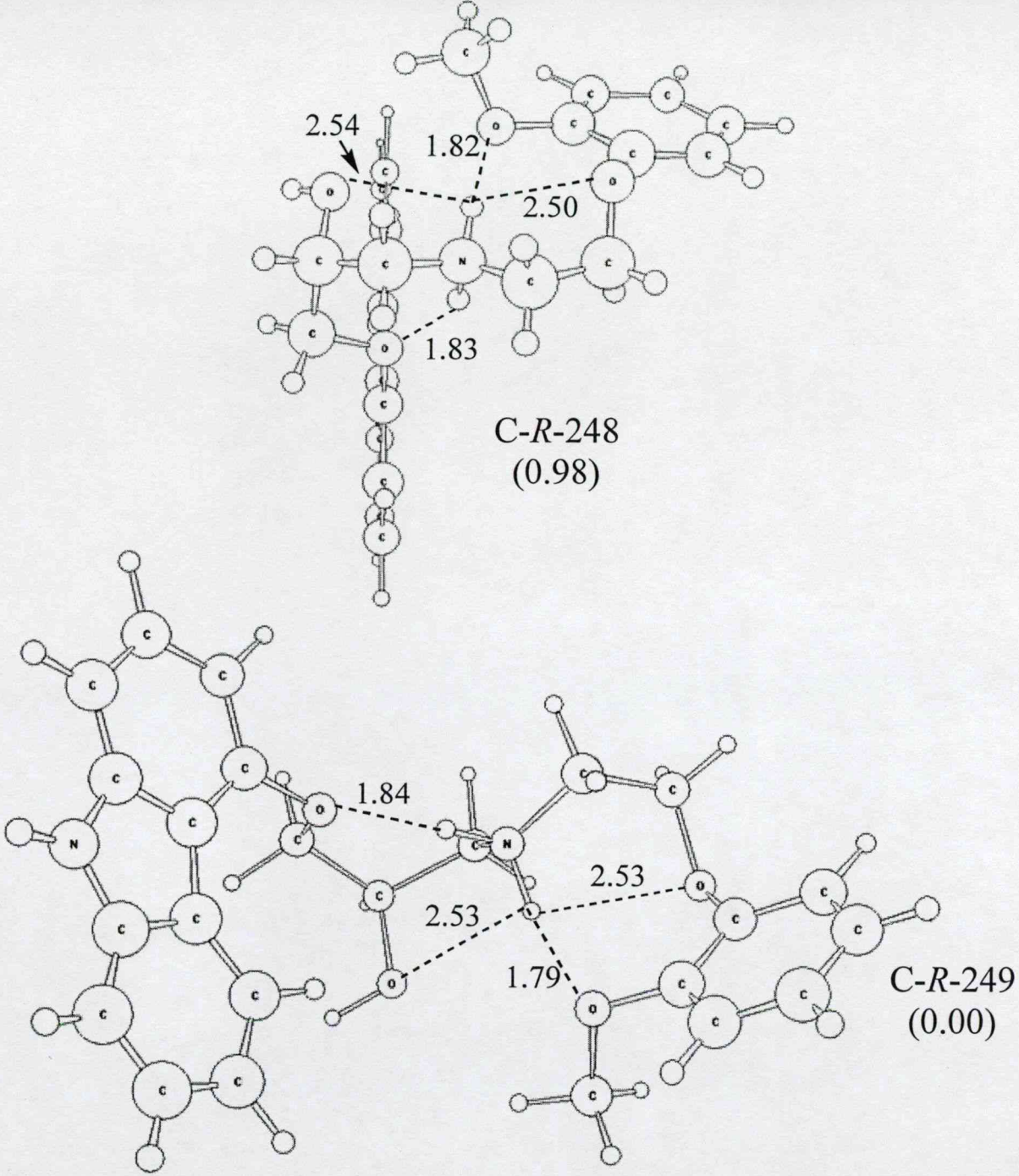

Figure 4 cont'd

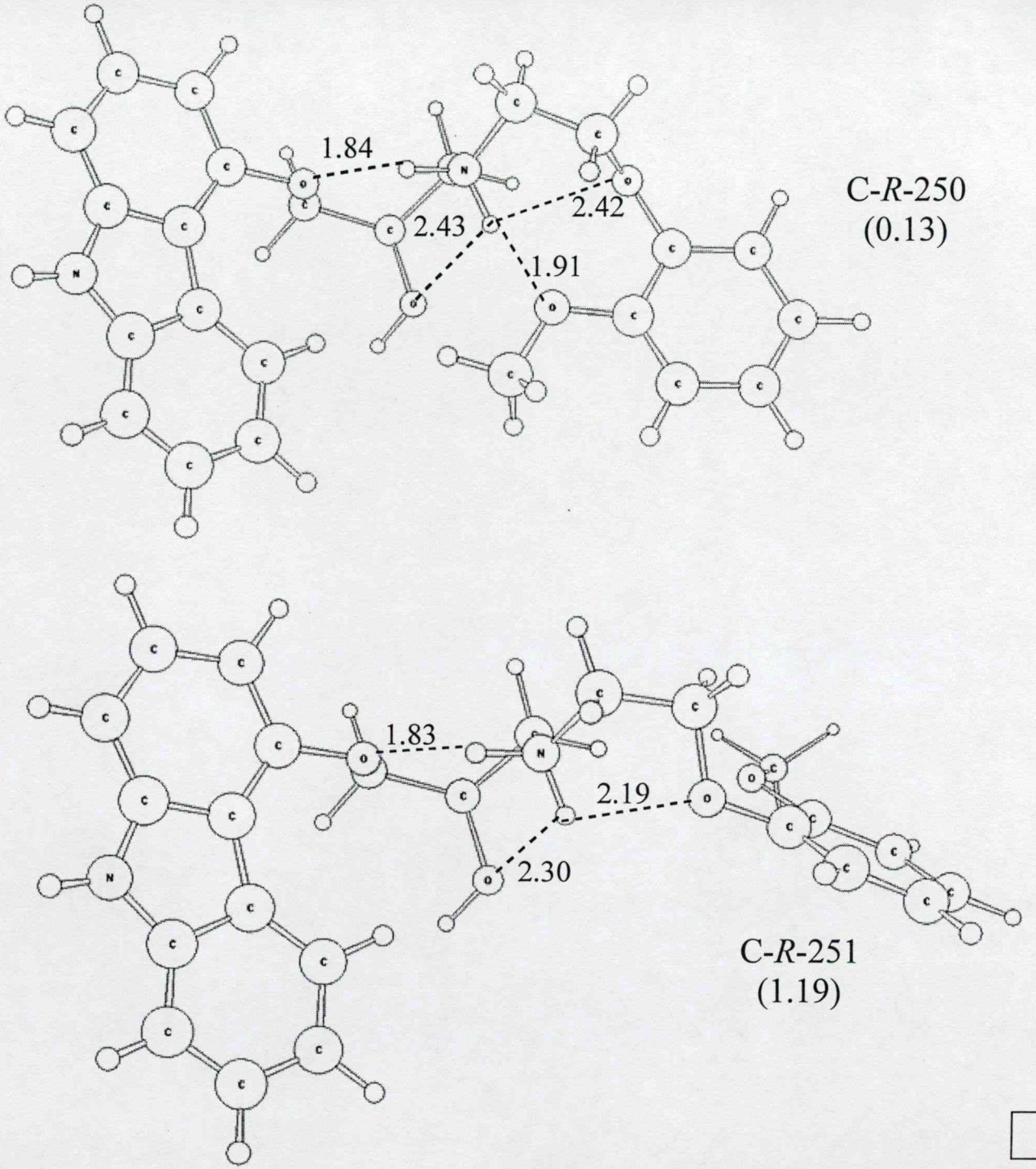

Figure 4 cont'd

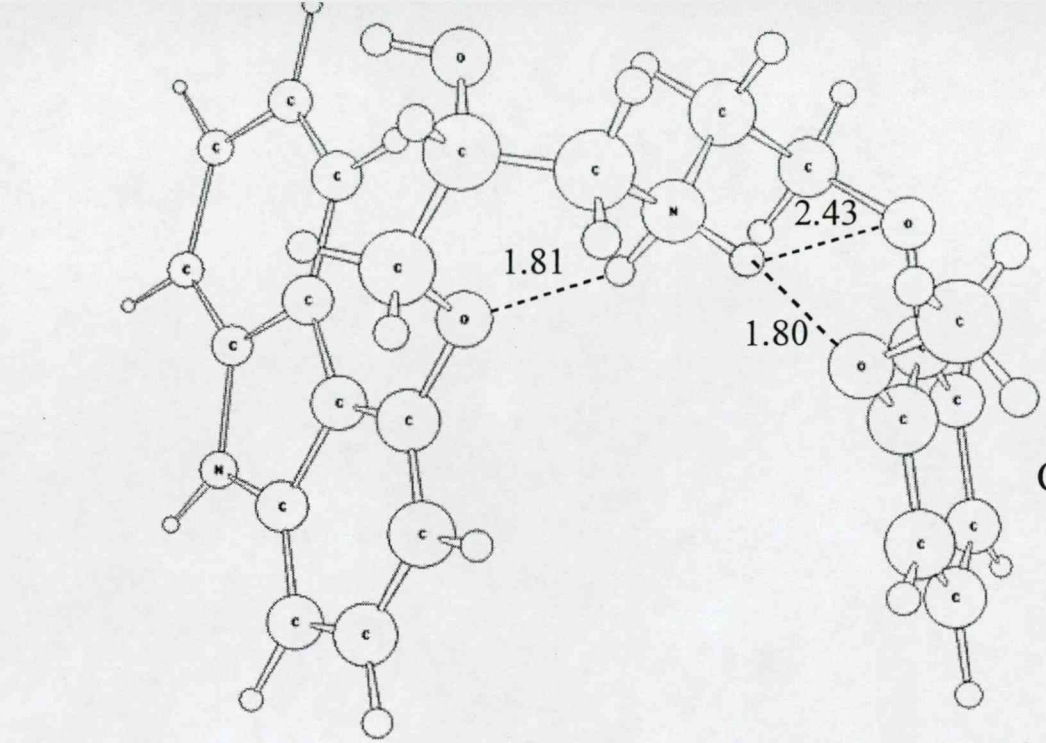

C-*R*-258
(1.36)

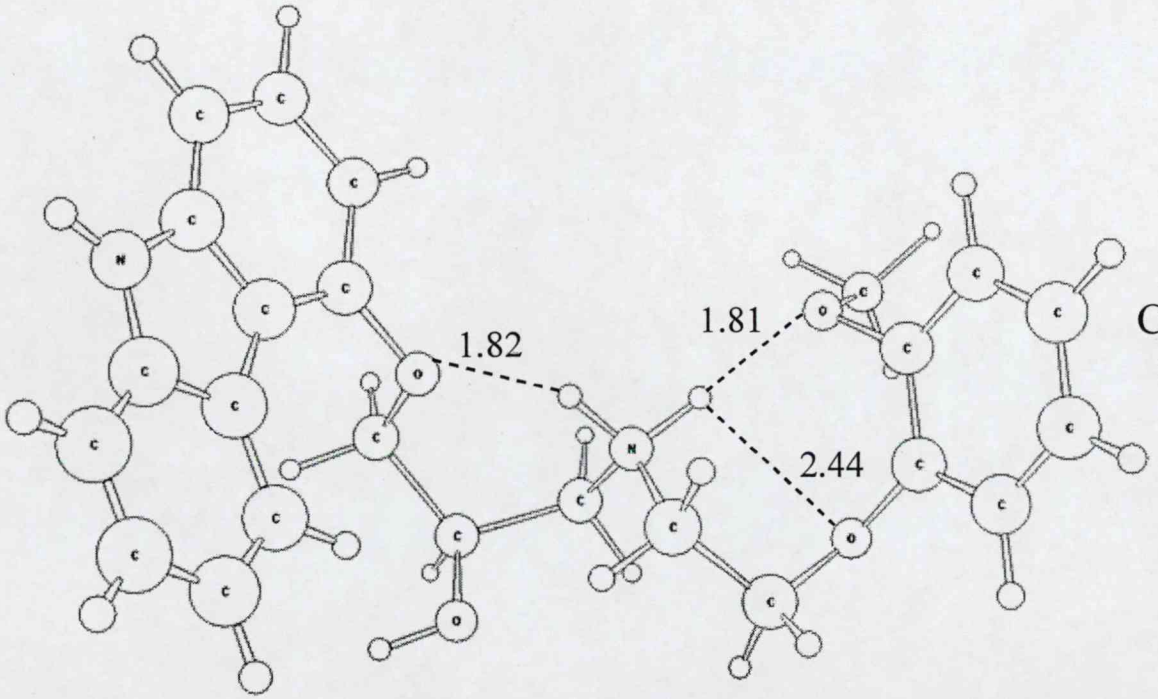

C-*R*-272
(1.55)

Figure 4 cont'd

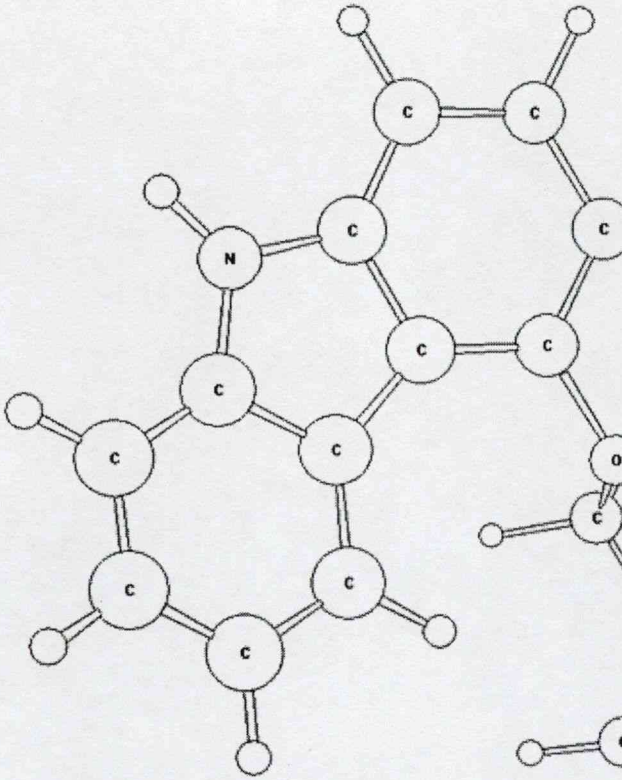

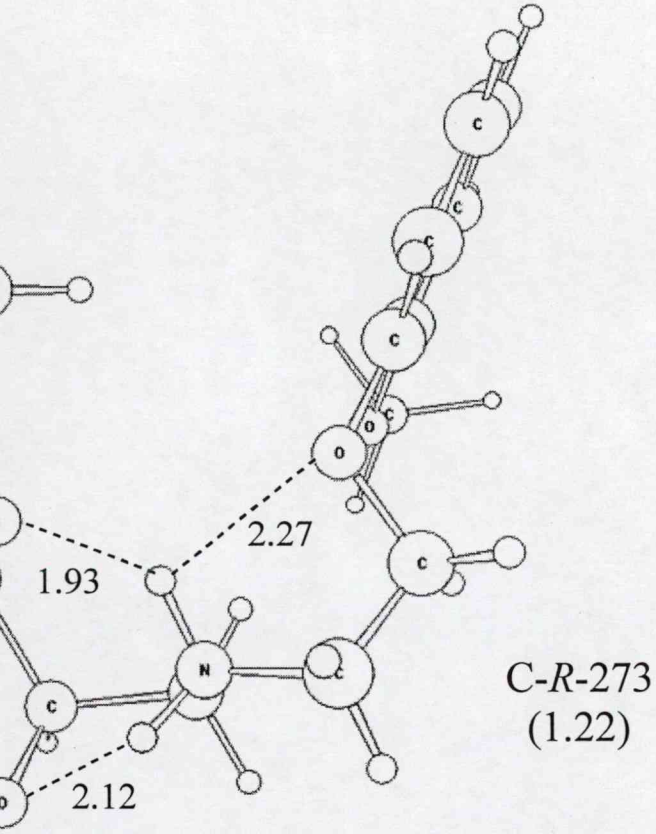

Figure 4 cont'd

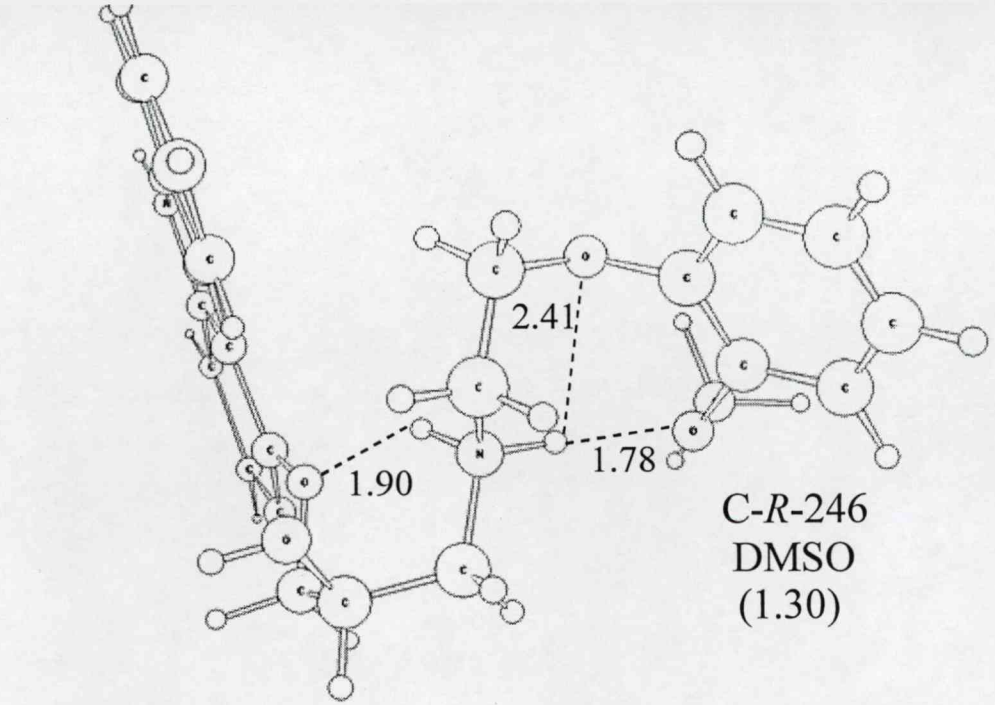

C-*R*-246
DMSO
(1.30)

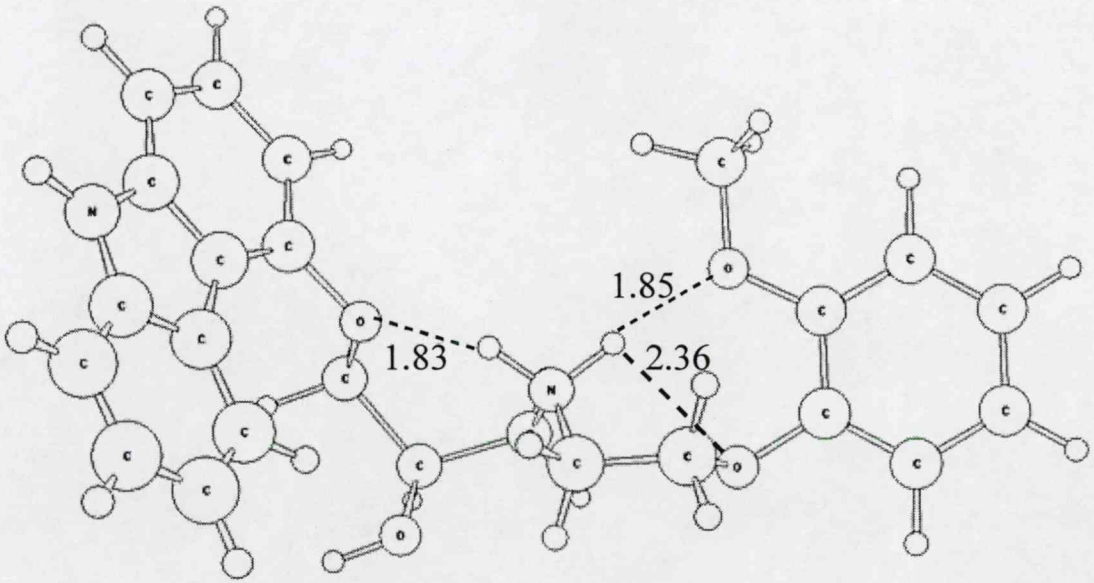

C-*R*-247
DMSO
(2.82)

Figure 5

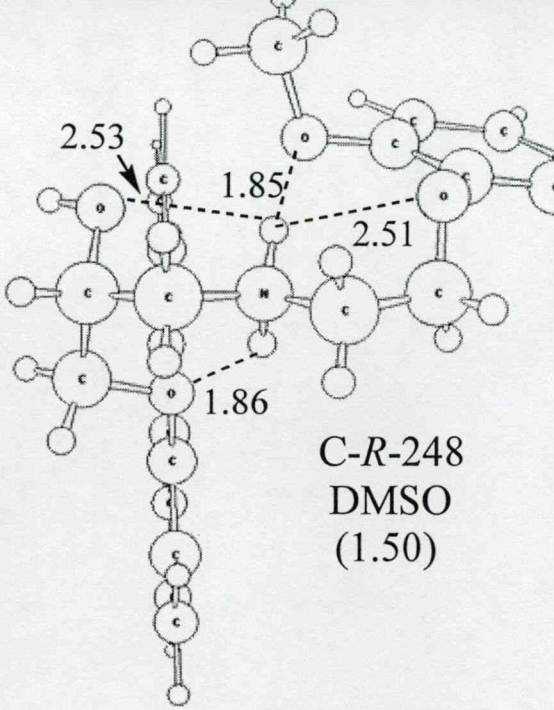

C-*R*-248
DMSO
(1.50)

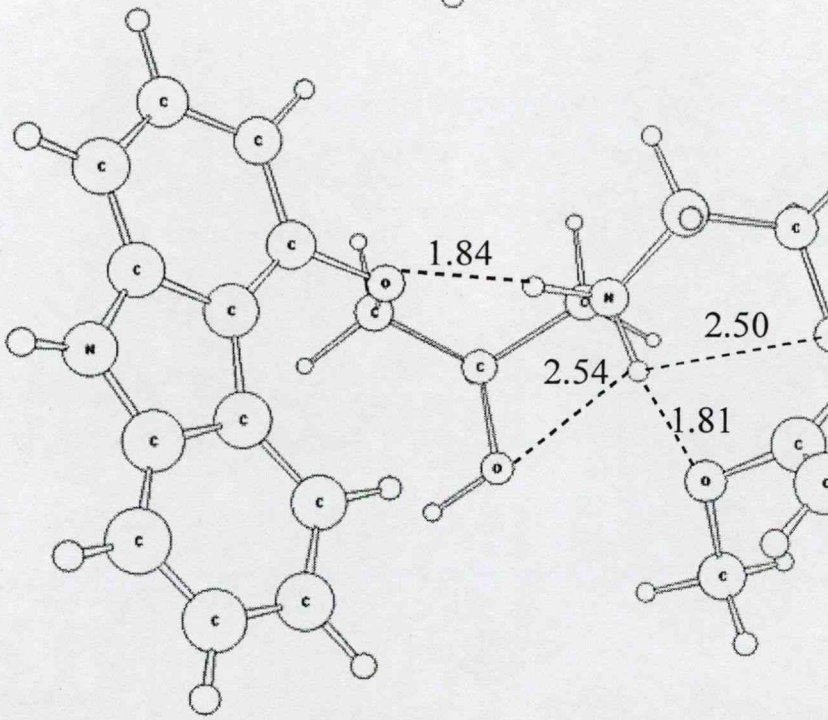

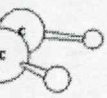

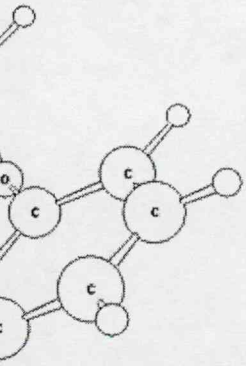

C-*R*-249
DMSO
(1.04)

Figure 5 cont'd

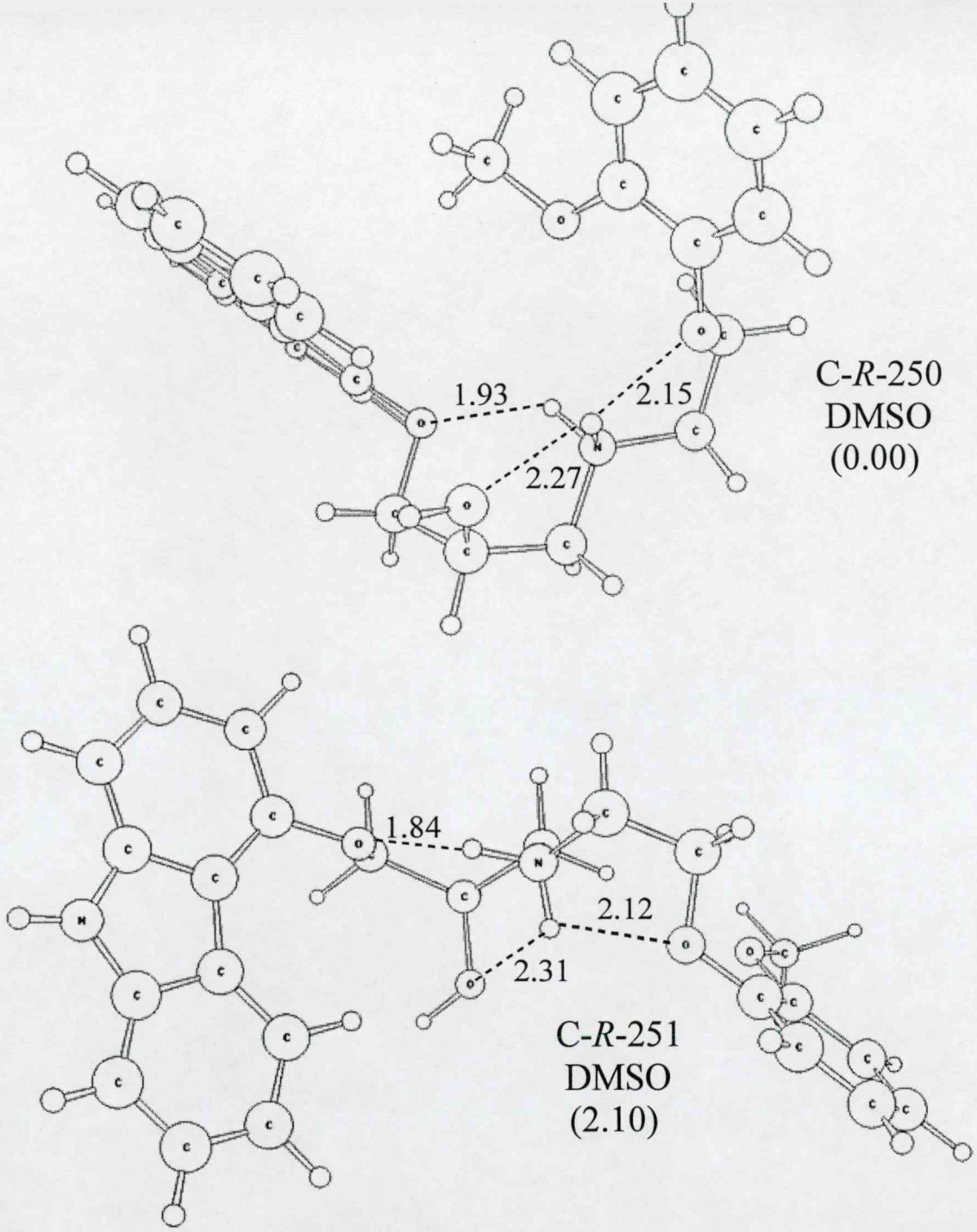

Figure 5 cont'd

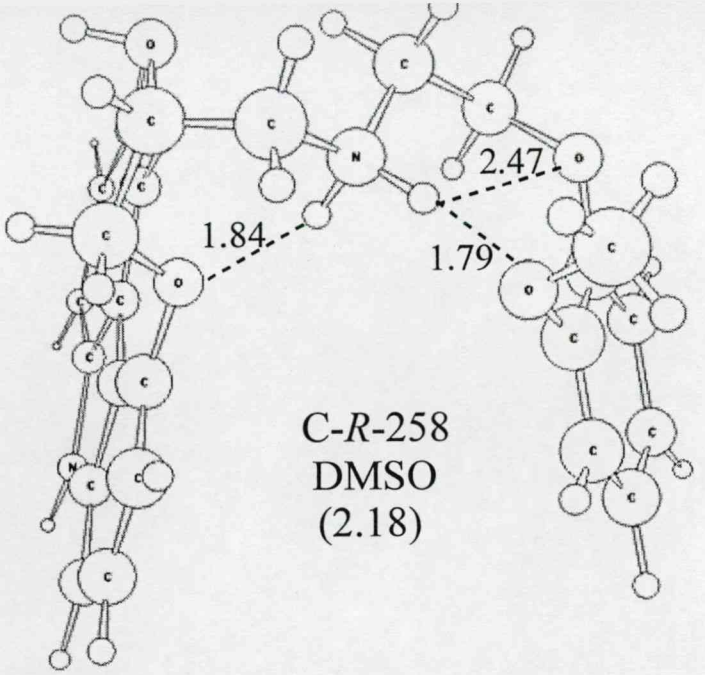

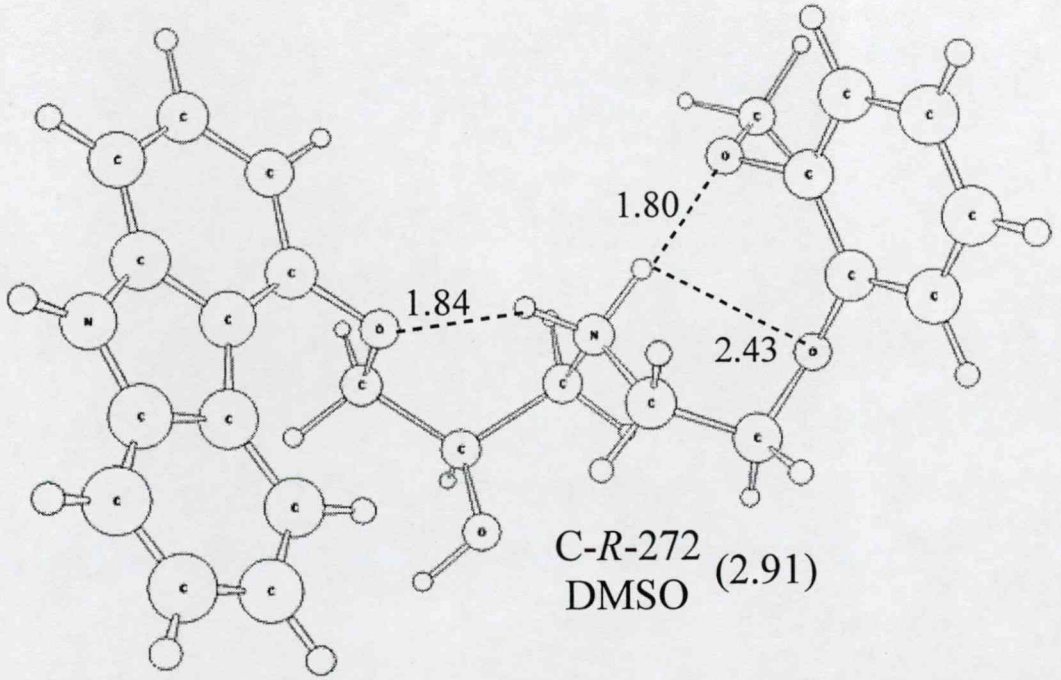

Figure 5 cont'd

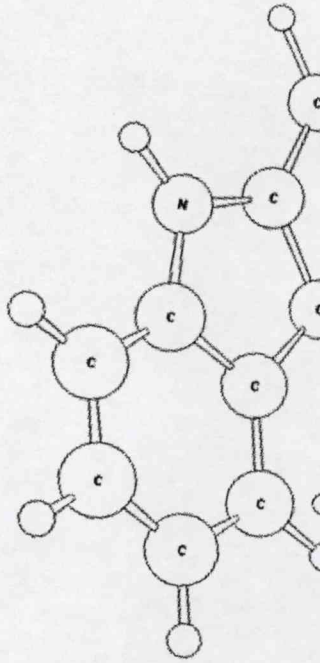
N
C
C
C
C
C
C
C
C

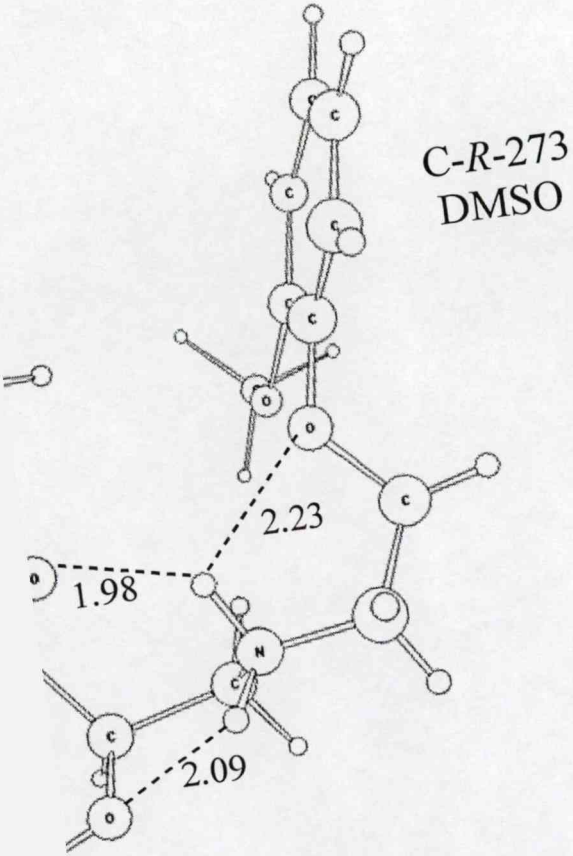

Figure 5 cont'd

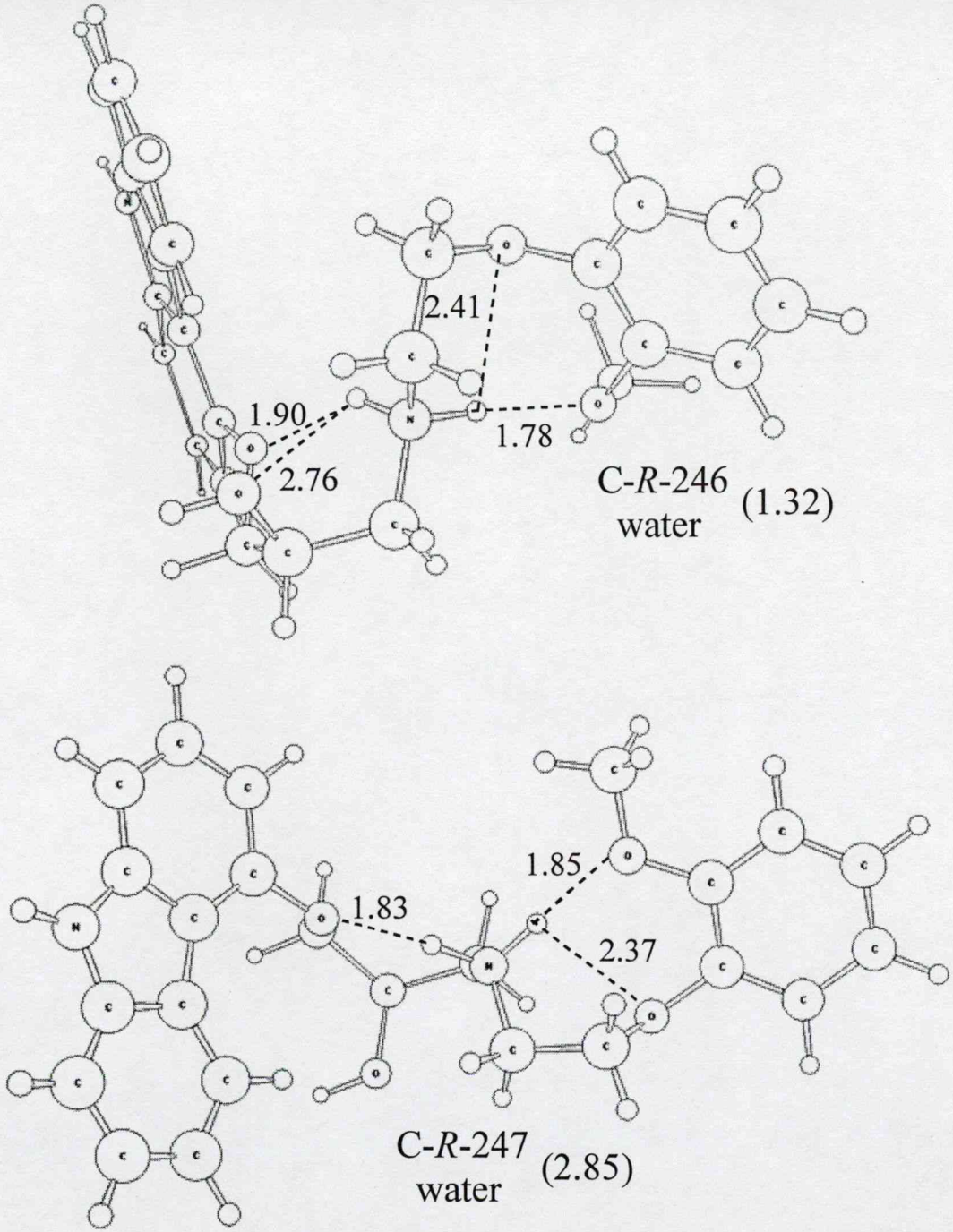

Figure 6

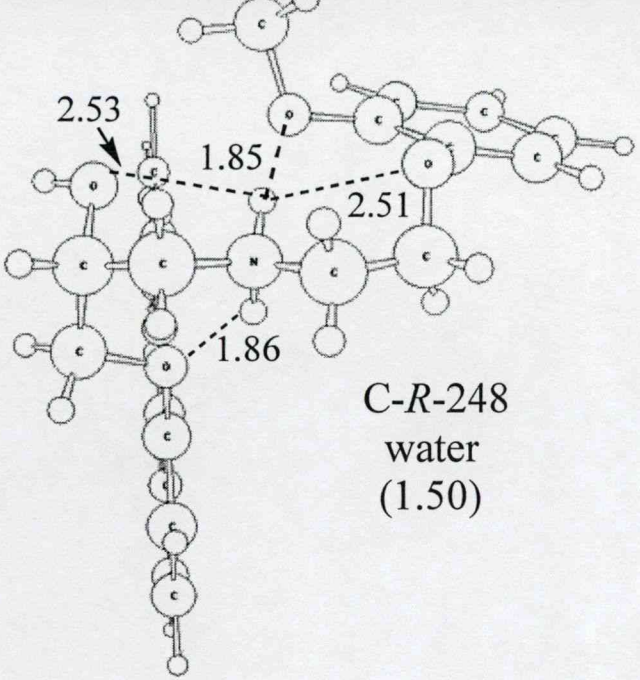

C-*R*-248
water
(1.50)

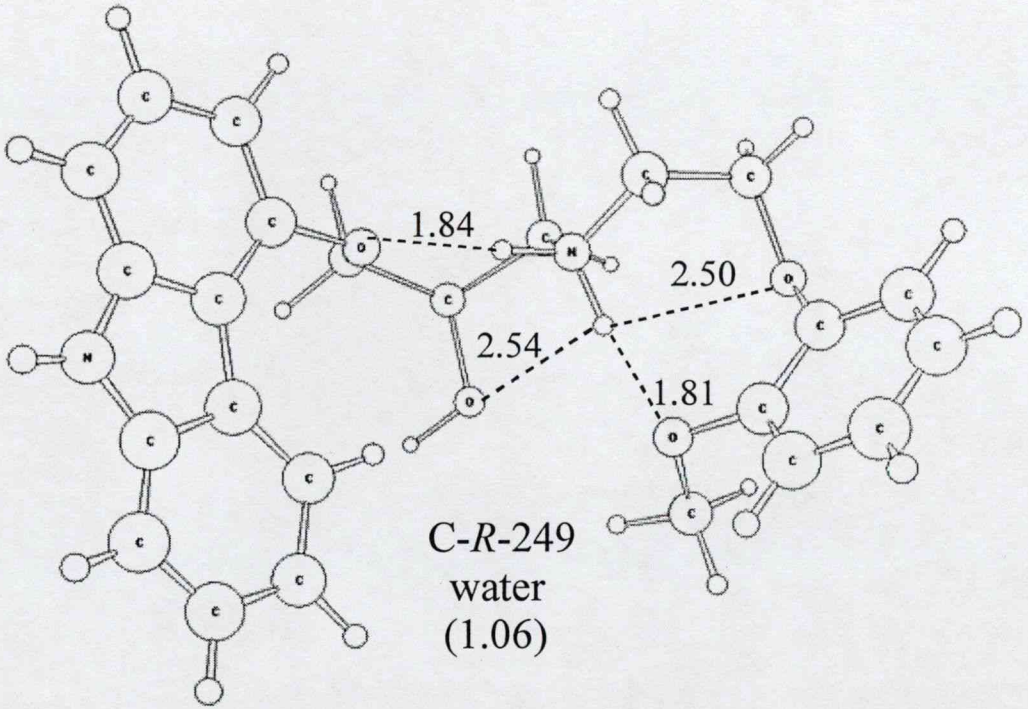

C-*R*-249
water
(1.06)

Figure 6 cont'd

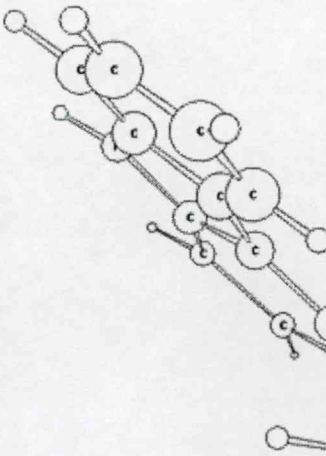

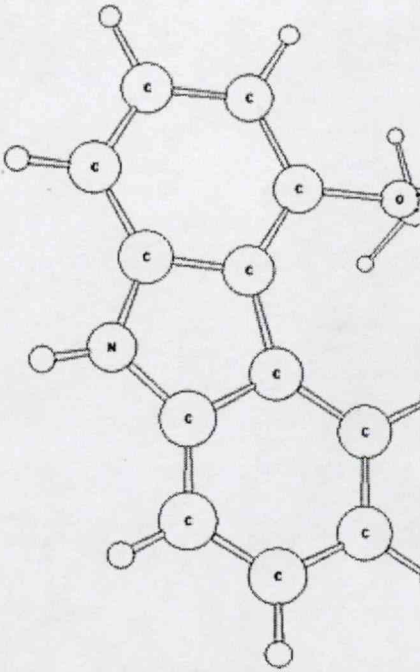

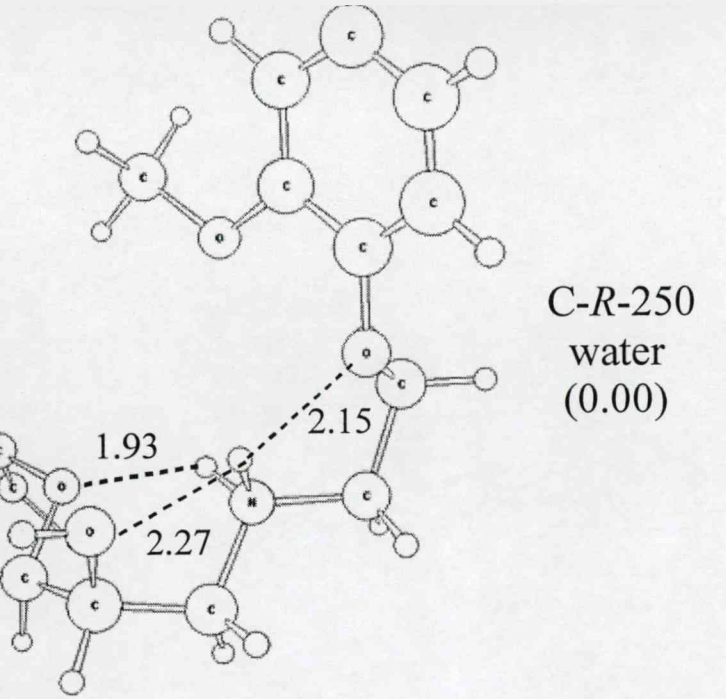

C-*R*-250
water
(0.00)

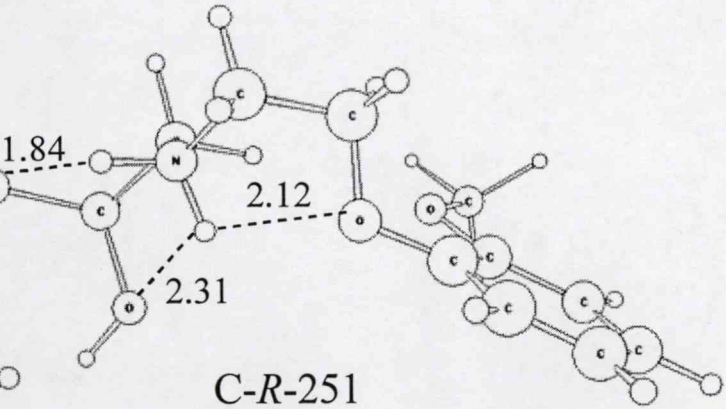

C-*R*-251
water
(2.12)

Figure 6 cont'd

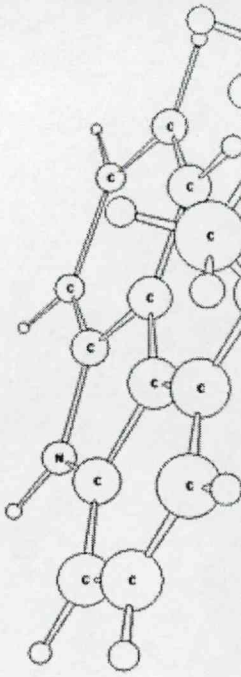
C
C
C
C
C
C
C
C
C
C
N
C
C
C
C

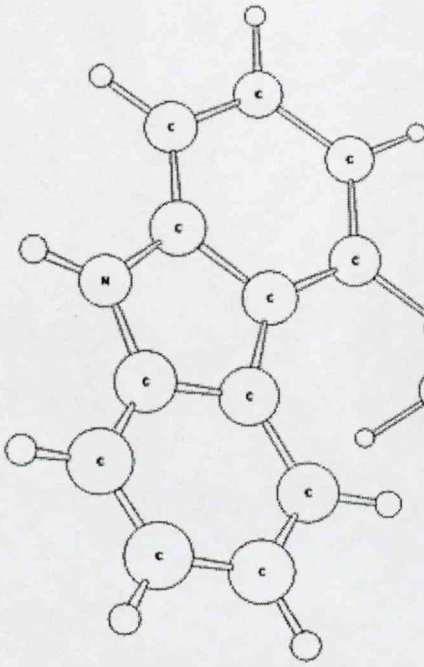
C
C
C
C
C
N
C
C
C
C
C
C
C
C

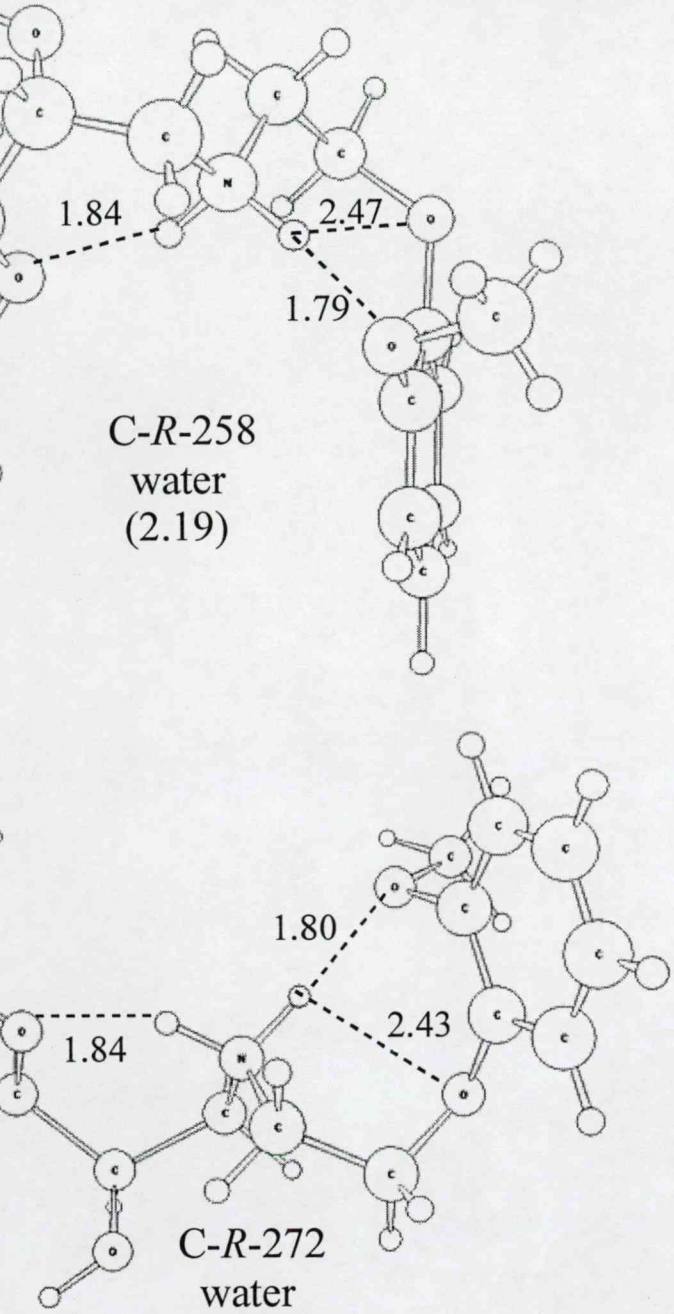

Figure 6 cont'd

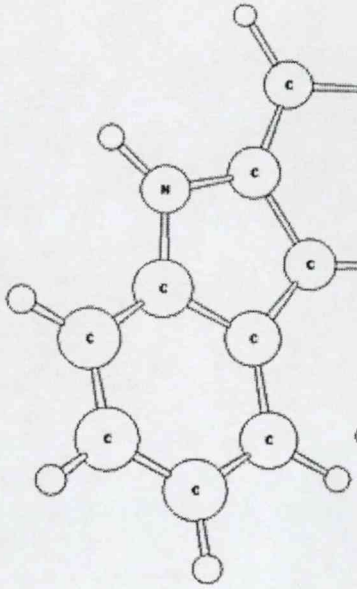
C
C
N
C
C
C
C
C
C
C
C

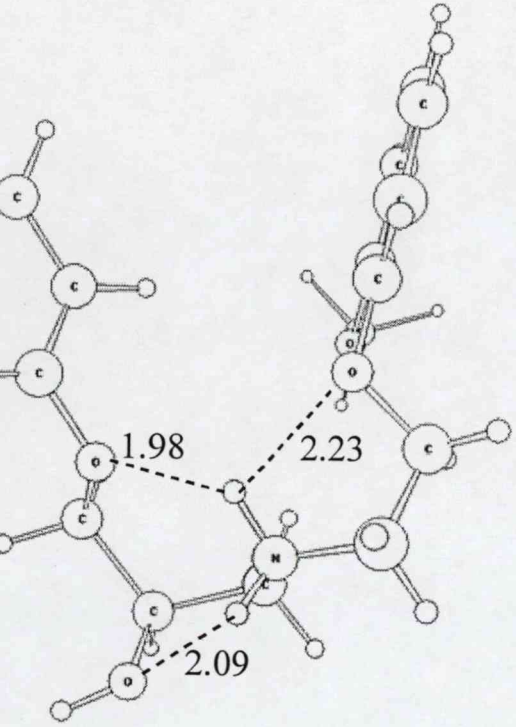

C-*R*-273
water
(1.44)

Figure 6 cont'd

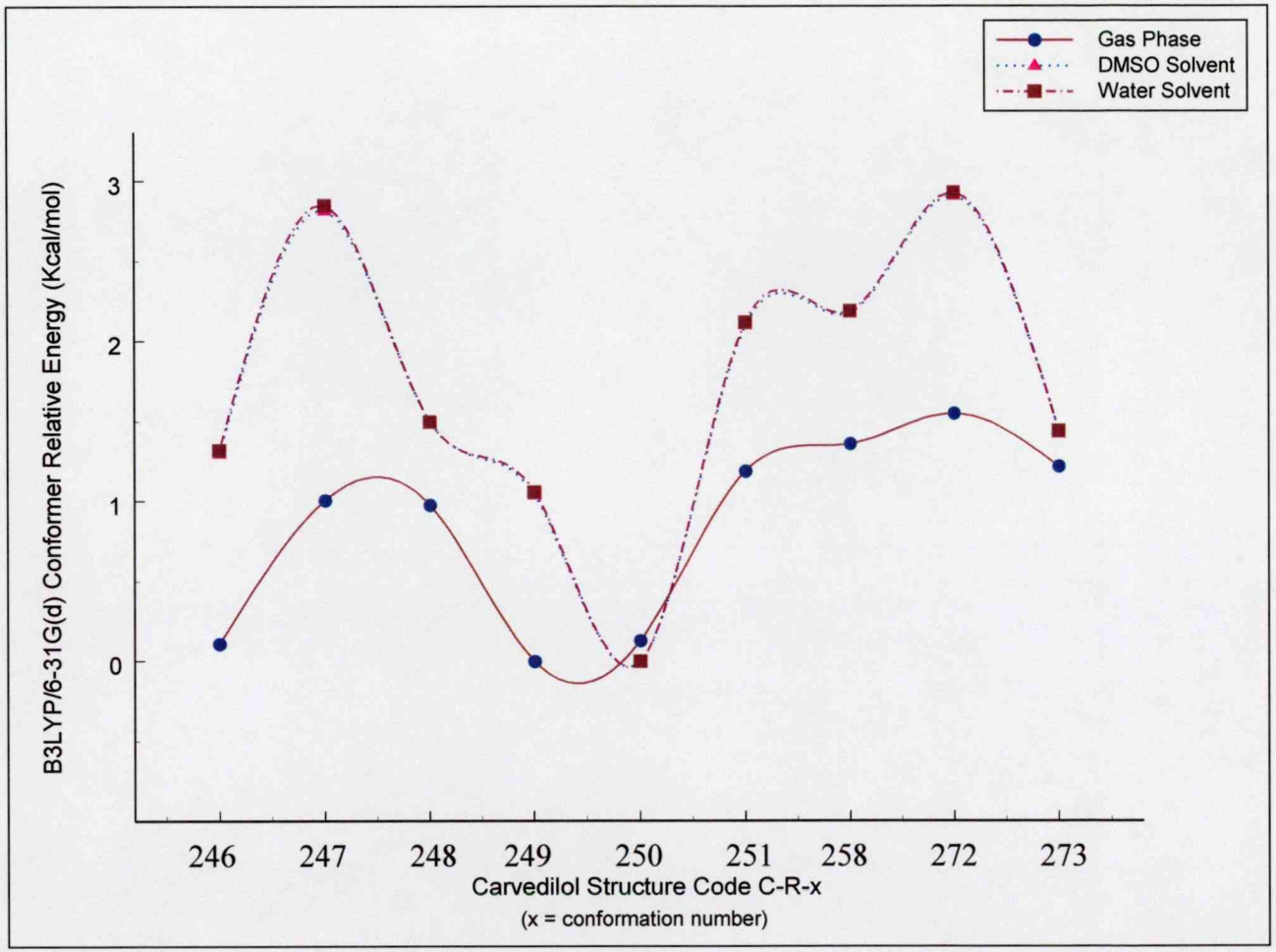
Gas Phase
DMSO Solvent
Water Solvent
B3LYP/6-31G(d) Conformer Relative Energy (Kcal/mol)
3
2
1
0
246
247
248
249
250
251
258
272
273
Carvedilol Structure Code C-R-x
(x = conformation number)

Figure 7

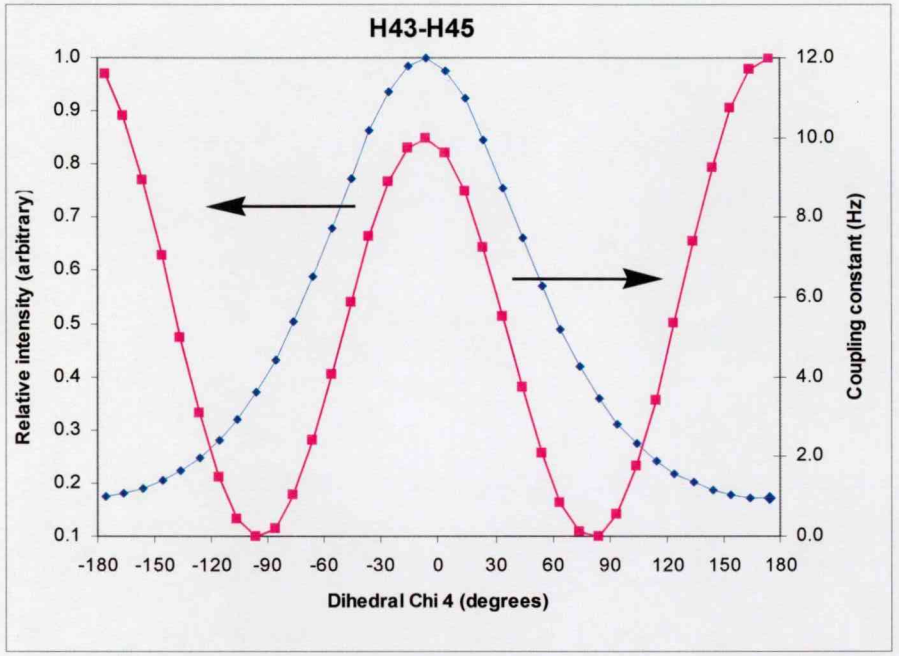
H43-H45
Relative intensity (arbitrary)
Coupling constant (Hz)
Dihedral Chi 4 (degrees)
1.0
0.9
0.8
0.7
0.6
0.5
0.4
0.3
0.2
0.1
12.0
10.0
8.0
6.0
4.0
2.0
0.0
-180 -150 -120 -90 -60 -30 0 30 60 90 120 150 180

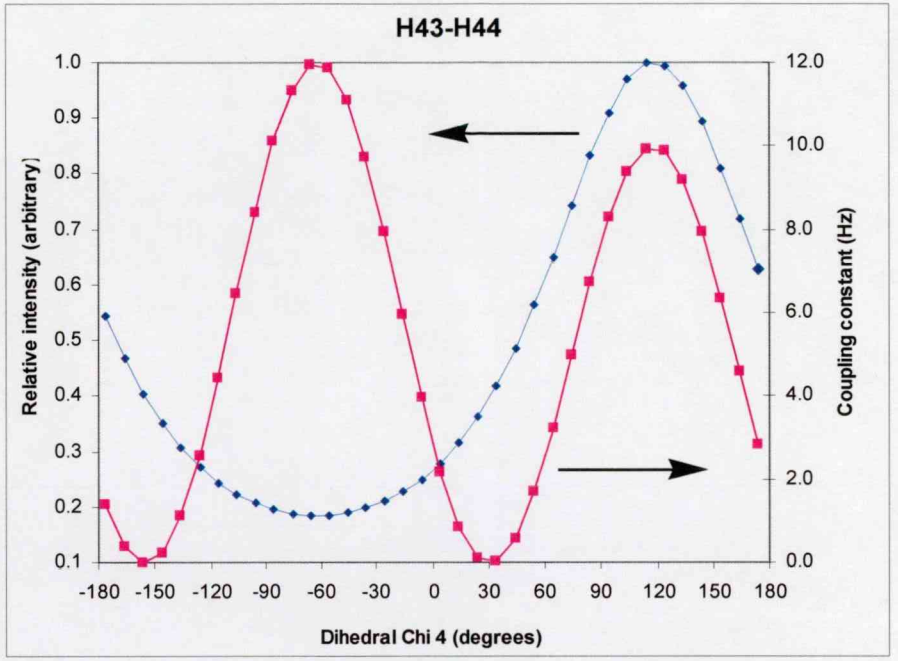
H43-H44
Relative intensity (arbitrary)
Coupling constant (Hz)
Dihedral Chi 4 (degrees)
1.0
0.9
0.8
0.7
0.6
0.5
0.4
0.3
0.2
0.1
12.0
10.0
8.0
6.0
4.0
2.0
0.0
-180 -150 -120 -90 -60 -30 0 30 60 90 120 150 180

Figure 8

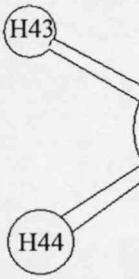
H43
H44

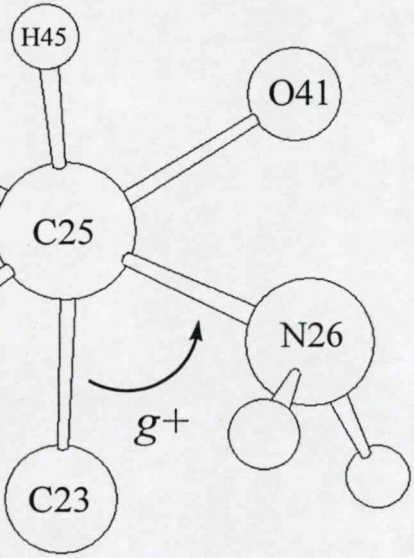

Figure 9

Table 1: Optimized torsional angle orientations of the carvedilol structures evaluated in the current study. Molecular conformation is displayed as [input torsional angle geometry‡/gas phase B3LYP/6-31G(d) optimized torsional angle geometry/DMSO solvent phase B3LYP/6-31G(d) optimized torsional angle geometry/water solvent phase B3LYP/6-31G(d) optimized torsional angle geometry]. (Explicit values of torsional angles are found in **Tables 2-4**.)

Structure Code	Torsional Angle Conformation										
	χ_1	χ_2	χ_3	χ_4	χ_5	χ_6	χ_7	χ_8	χ_9	χ_{10}	χ_{11}
C-*R*-246	[g+/a/a/a]	[a/a/a/a]	[g-/g-/g-/g-]	[g+/g+/g+/g+]	[g+/g+/g+/g+]	[a/a/a/a]	[g-/g-/g-/g-]	[g-/g-/g-/g-]	[g-/g-/g-/g-]	[g+/g+/g+/g+]	[g+/g+/g+/g+]
C-*R*-247	[g+/g+/g+/g+]	[a/a/a/a]	[g-/g-/g-/g-]	[g+/g+/g+/g+]	[g+/g+/g+/g+]	[g+/g+/g+/g+]	[g-/g-/g-/g-]	[a/a/a/a]	[g+/g+/g+/g+]	[g+/g+/g+/g+]	[a/a/a/a]
C-*R*-248	[g+/g+/g+/g+]	[a/a/a/a]	[g-/g-/g-/g-]	[g+/g+/g+/g+]	[a/a/a/a]	[a/a/a/a]	[g+/g+/g+/g+]	[a/a/a/a]	[g-/g-/g-/g-]	[g+/g+/g+/g+]	[g+/g+/g+/g+]
C-*R*-249	[g+/g+/g+/g+]	[a/a/a/a]	[g-/g-/g-/g-]	[g+/g+/g+/g+]	[a/a/a/a]	[g-/g-/g-/g-]	[g-/g-/g-/g-]	[g-/g-/g-/g-]	[g-/g-/g-/g-]	[g+/g+/g+/g+]	[g+/g+/g+/g+]
C-*R*-250	[g+/g+/g+/g+]	[a/a/a/a]	[g-/g-/g-/g-]	[g+/g+/g+/g+]	[a/a/a/a]	[g-/g-/a/a]	[g+/g+/g+/g+]	[a/a/a/a]	[g-/g-/g-/g-]	[g+/g+/g+/g+]	[a/a/a/a]
C-*R*-251	[g+/g+/g+/g+]	[a/a/a/a]	[g-/g-/g-/g-]	[g+/g+/g+/g+]	[a/a/a/a]	[g-/g-/g-/g-]	[g-/g-/g-/g-]	[a/a/a/a]	[g+/g+/g+/g+]	[g+/g+/g+/g+]	[a/a/a/a]
C-*R*-258	[g+/g+/g+/g+]	[a/a/a/a]	[g-/g-/g-/g-]	[g+/g+/g+/g+]	[g+/g+/g+/g+]	[a/a/a/a]	[g-/g-/g-/g-]	[g+/g+/g+/g+]	[g+/g+/g+/g+]	[g+/g+/g+/g+]	[g-/g-/g-/g-]
C-*R*-272	[g+/g+/g+/g+]	[a/a/a/a]	[g-/g-/g-/g-]	[g+/g+/g+/g+]	[g+/g+/g+/g+]	[g+/g+/g+/g+]	[g+/g+/g+/g+]	[g+/g+/g+/g+]	[g+/g+/g+/g+]	[g+/g+/g+/g+]	[g-/g-/g-/g-]
C-*R*-273	[g+/g+/g+/g+]	[a/a/a/a]	[g-/g-/g-/g-]	[g+/g+/g+/g+]	[a/a/a/a]	[g+/g+/g+/g+]	[g+/g+/g+/g+]	[a/a/a/a]	[g-/g-/g-/g-]	[g+/g+/g+/g+]	[a/a/a/a]

‡Torsional angle geometries have been previously optimized at the RHF/3-21G level of theory (taken reference **17**) and are used here as input structures for DFT optimizations.

Table 2: Gas phase (ε = 0.0) optimized values and energies for the converged conformers of the protonated *R*-carvedilol surface at the B3LYP/6-31G(d) level of theory.

Structure Code	Torsional Angle (degrees)											Energy (Hartree)	Relative Energy (Kcal•mol^{-1})
	χ_1	χ_2	χ_3	χ_4	χ_5	χ_6	χ_7	χ_8	χ_9	χ_{10}	χ_{11}		
C-*R*-246	147.66	-178.59	-61.82	67.01	92.56	179.24	-47.81	-68.16	-68.34	54.30	90.60	-1340.99055043	0.11
C-*R*-247	107.44	-171.16	-53.41	67.92	85.46	108.38	-51.47	146.95	106.47	56.63	177.53	-1340.98911556	1.01
C-*R*-248	100.13	-169.42	-51.87	67.66	-167.27	-168.85	65.24	-129.63	-77.61	49.02	106.78	-1340.98917601	0.98
C-*R*-249	98.69	-171.84	-51.36	71.22	-162.18	-59.94	-47.41	-71.17	-70.95	51.53	96.98	-1340.99072989	**0.00**
C-*R*-250	97.94	-174.38	-51.60	71.66	-170.02	-108.22	51.08	-145.73	-113.20	61.69	178.99	-1340.99052227	0.13
C-*R*-251	97.63	-172.97	-49.97	72.69	-173.97	-66.19	-46.46	175.94	112.05	55.44	179.71	-1340.98883102	1.19
C-*R*-258	97.47	-174.15	-55.86	63.28	83.88	175.26	-60.45	116.50	69.38	57.43	-88.53	-1340.98857046	1.36
C-*R*-272	92.99	-175.06	-54.27	63.77	80.27	63.58	44.88	71.86	68.43	57.95	-94.63	-1340.98826529	1.55
C-*R*-273	91.74	-177.88	-52.41	72.27	171.03	63.65	47.12	-177.41	-110.11	51.57	-177.05	-1340.98879141	1.22

Table 3: DMSO optimized values and energies for the converged conformers of the protonated *R*-carvedilol surface. Structures were optimized using the Onsager (dipole) reaction field calculation model in DMSO ($\varepsilon = 46.7$) at the B3LYP/6-31G(d) level of theory (c.f. **Table S1** for respective solute radii used in Onsager calculations).

Structure Code	Torsional Angle (degrees)											Energy (Hartree)	Relative Energy (Kcal•mol^{-1})
	χ_1	χ_2	χ_3	χ_4	χ_5	χ_6	χ_7	χ_8	χ_9	χ_{10}	χ_{11}		
C-*R*-246	150.88	179.18	-63.08	67.55	92.89	-179.91	-48.08	-68.00	-69.15	60.25	92.98	-1340.99216696	1.30
C-*R*-247	108.63	-171.72	-55.13	66.64	84.64	108.06	-51.95	146.85	106.26	58.67	178.65	-1340.98974697	2.82
C-*R*-248	101.74	-171.19	-54.11	66.06	-172.30	-172.33	63.79	-126.92	-74.53	56.40	98.42	-1340.99185150	1.50
C-*R*-249	102.46	-172.21	-53.76	69.78	-162.90	-61.65	-47.65	-70.57	-69.72	54.54	92.88	-1340.99258309	1.04
C-*R*-250	91.13	-175.76	-51.32	73.87	177.54	-166.65	52.18	-162.59	-111.58	67.08	-176.93	-1340.99423903	**0.00**
C-*R*-251	104.99	-172.30	-52.94	71.61	-175.19	-71.24	-46.43	174.18	113.01	58.03	177.65	-1340.99089225	2.10
C-*R*-258	115.34	-174.34	-57.00	66.15	87.38	178.29	-60.89	114.39	70.11	65.18	-88.62	-1340.99075953	2.18
C-*R*-272	96.58	-175.49	-55.15	63.87	80.29	64.83	44.94	71.61	68.40	62.88	-94.46	-1340.98960067	2.91
C-*R*-273	98.22	177.38	-52.43	74.93	170.96	68.11	48.42	-177.80	-108.48	65.23	-172.71	-1340.99194603	1.44

Table 4: Water optimized values and energies for the converged conformers of the protonated *R*-carvedilol surface. Structures were optimized using the Onsager (dipole) reaction field calculation model in water ($\varepsilon = 78.39$) at the B3LYP/6-31G(d) level of theory (c.f. **Table S1** for respective solute radii used in Onsager calculations).

Structure Code	Torsional Angle (degrees)											Energy (Hartree)	Relative Energy (Kcal•mol^{-1})
	χ_1	χ_2	χ_3	χ_4	χ_5	χ_6	χ_7	χ_8	χ_9	χ_{10}	χ_{11}		
C-*R*-246	150.84	179.18	-63.08	67.55	92.88	-179.87	-48.08	-68.01	-69.16	60.35	93.04	-1340.99219535	1.32
C-*R*-247	108.23	-171.74	-55.21	66.48	84.80	107.04	-51.55	146.70	106.37	58.30	178.53	-1340.98976077	2.85
C-*R*-248	101.82	-171.19	-53.92	66.10	-172.10	-171.98	63.68	-126.97	-74.48	56.51	98.38	-1340.99190386	1.50
C-*R*-249	102.19	-172.53	-53.48	69.90	-163.21	-62.04	-47.86	-70.22	-69.67	56.39	92.20	-1340.99261927	1.06
C-*R*-250	91.26	-175.77	-51.35	73.87	177.49	-166.72	52.19	-162.67	-111.57	67.18	-176.89	-1340.99430184	**0.00**
C-*R*-251	105.11	-172.31	-52.99	71.60	-175.21	-71.30	-46.43	174.16	113.05	58.12	177.61	-1340.99093123	2.12
C-*R*-258	114.80	-174.65	-57.11	66.04	86.98	178.26	-60.87	114.42	70.10	65.88	-88.43	-1340.99081121	2.19
C-*R*-272	96.56	-175.39	-55.28	63.90	80.69	64.73	44.89	71.69	68.43	62.40	-94.42	-1340.98962465	2.93
C-*R*-273	98.46	177.28	-52.58	74.95	170.94	68.52	48.46	-177.73	-108.50	65.62	-172.58	-1340.99200916	1.44

Table 5: NMR proton chemical shifts and assignments for carvedilol in DMSO (DMSO-d_6).

Proton Chemical Shift (θ, ppm)	**Proton Assignment**	**Relevant Section of Carvedilol**
8.27	H15[§]	Carbazole Aromatic Ring
7.14	H16[§]	
7.35	H17[§]	
7.46	H18[§]	
11.26	H19	
7.1	H20[§]	
7.3	H21[§]	
6.7	H22[§]	
5.2	H42	Stereocentre
4.19	H43	
4.15	H39[§] & H40[§]	Connecting Backbone
2.88	H44	
2.83	H45	
2.95	H47 & H48	
4.01	H49[§] & H50[§]	
3.73	H38, H55, & H56	Methoxy Group
Unresolved ~ 6.8-6.9	H51, H52, H53, & H54	Aromatic Benzene Ring

[§]Cross-checked with reference **30**.

Supplementary Tables

Table S1: Solute radius values used for *R*-carvedilol conformer optimizations with the Onsager (dipole) reaction field model. Respective solute radii were calculated with B3LYP/6-31G(d) molecular volume calculations for each of the DFT-converged conformers found in **Table 2**. (Calculations were performed with the scf=tight option for a more accurate integration.)

Structure Code	Solute Radius (Å)
C-*R*-246	6.12
C-*R*-247	5.99
C-*R*-248	5.94
C-*R*-249	5.86
C-*R*-250	5.72
C-*R*-251	5.93
C-*R*-258	5.72
C-*R*-272	5.82
C-*R*-273	5.97